PB85-233369

Proceedings of the Cryocooler Conference (3rd) Held at Boulder, Colorado on September 17-18, 1984

(U.S.) National Bureau of Standards, Boulder, CO

Prepared for

National Aeronautics and Space Administration
Greenbelt, MD.

May 85

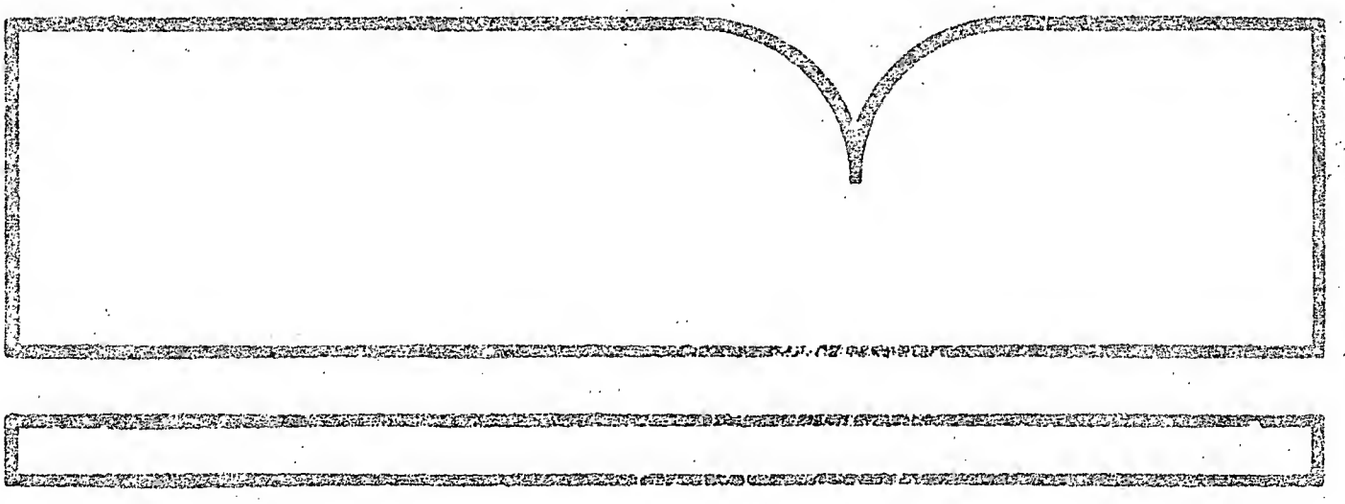

NBS-114A (REV. 2-8C)

PB85 233697AS

U.S. DEPT. OF COMM. BIBLIOGRAPHIC DATA SHEET (See instructions)	1. PUBLICATION OR REPORT NO. NBS/SP-698	2. Performing Organ. Report No.	3. Publication Date May 1985

4. TITLE AND SUBTITLE

Proceedings of the Third Cryocooler Conference

5. AUTHOR(S)

Ray Radebaugh, Beverly Louie, and Sandy McCarthy

6. PERFORMING ORGANIZATION (If joint or other than NBS, see instructions)

National Bureau of Standards
U.S. Department of Commerce
Gaithersburg, MD 20899

7. Contract/Grant No.

8. Type of Report & Period Covered

Final

9. SPONSORING ORGANIZATION NAME AND COMPLETE ADDRESS (Street, City, State, ZIP)

Same as Item 6.

NBS Category No.
NBS-280

10. SUPPLEMENTARY NOTES

Library of Congress Catalog Card Number: 85-600544

Also Available from GPO as SN003-003-02662-0

[ ] Document describes a computer program; SF-185, FIPS Software Summary, is attached.

11. ABSTRACT (A 200-word or less factual summary of most significant information. If document includes a significant bibliography or literature survey, mention it here)

This document contains the proceedings of the Third Cryocooler Conference, held at the National Bureau of Standards, Boulder, CO, on Sept. 17-18, 1984. About 140 people from 10 countries attended the conference and represented industry, government, and academia. A total of 26 papers were presented orally at the conference and all appear in written form in this document. The emphasis in this conference was on small cryocoolers in the temperature range of 4 - 80 K. Mechanical and non-mechanical types were discussed in the various papers. Applications of these small cryocoolers include the cooling of infrared detectors, cryopumps, small superconducting devices and magnets, and electronic devices.

12. KEY WORDS (Six to twelve entries; alphabetical order; capitalize only proper names; and separate key words by semicolons)

conference; cryocoolers; cryogenics, cryopumps, helium, infrared detectors, refrigeration; superconductors.

13. AVAILABILITY

[X] Unlimited

[ ] For Official Distribution. Do Not Release to NTIS

[X] Order From Superintendent of Documents, U.S. Government Printing Office, Washington, D.C. 20402.

[ ] Order From National Technical Information Service (NTIS), Springfield, VA. 22161

14. NO. OF PRINTED PAGES

279

15. Price

☆ U.S. GOVERNMENT PRINTING OFFICE: 1985-461-105/20125

USCOMM-DC 6043-P80

PB85-233369

NBS SPECIAL PUBLICATION 698

U.S. DEPARTMENT OF COMMERCE National Bureau of Standards

Proceedings of the Third Cryocooler Conference

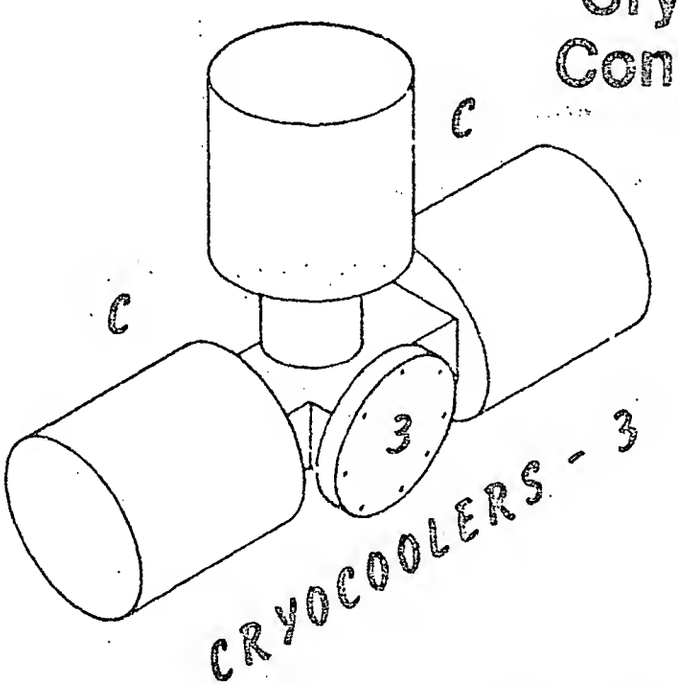

National Bureau of Standards
Boulder, Colorado
September 17-18, 1984

The National Bureau of Standards[1] was established by an act of Congress on March 3, 1901. The Bureau's overall goal is to strengthen and advance the nation's science and technology and facilitate their effective application for public benefit. To this end, the Bureau conducts research and provides: (1) a basis for the nation's physical measurement system, (2) scientific and technological services for industry and government, (3) a technical basis for equity in trade, and (4) technical services to promote public safety. The Bureau's technical work is performed by the National Measurement Laboratory, the National Engineering Laboratory, the Institute for Computer Sciences and Technology, and the Center for Materials Science.

The National Measurement Laboratory

Provides the national system of physical and chemical measurement; coordinates the system with measurement systems of other nations and furnishes essential services leading to accurate and uniform physical and chemical measurement throughout the Nation's scientific community, industry, and commerce; provides advisory and research services to other Government agencies; conducts physical and chemical research; develops, produces, and distributes Standard Reference Materials; and provides calibration services. The Laboratory consists of the following centers:

- Basic Standards[2]
- Radiation Research
- Chemical Physics
- Analytical Chemistry

The National Engineering Laboratory

Provides technology and technical services to the public and private sectors to address national needs and to solve national problems; conducts research in engineering and applied science in support of these efforts; builds and maintains competence in the necessary disciplines required to carry out this research and technical service; develops engineering data and measurement capabilities; provides engineering measurement traceability services; develops test methods and proposes engineering standards and code changes; develops and proposes new engineering practices; and develops and improves mechanisms to transfer results of its research to the ultimate user. The Laboratory consists of the following centers:

- Applied Mathematics
- Electronics and Electrical Engineering[2]
- Manufacturing Engineering
- Building Technology
- Fire Research
- Chemical Engineering[3]

The Institute for Computer Sciences and Technology

Conducts research and provides scientific and technical services to aid Federal agencies in the selection, acquisition, application, and use of computer technology to improve effectiveness and economy in Government operations in accordance with Public Law 89-306 (40 U.S.C. 759), relevant Executive Orders, and other directives; carries out this mission by managing the Federal Information Processing Standards Program, developing Federal ADP standards guidelines, and managing Federal participation in ADP voluntary standardization activities; provides scientific and technological advisory services and assistance to Federal agencies; and provides the technical foundation for computer-related policies of the Federal Government. The Institute consists of the following centers:

- Programming Science and Technology
- Computer Systems Engineering

The Center for Materials Science

Conducts research and provides measurements, data, standards, reference materials, quantitative understanding and other technical information fundamental to the processing, structure, properties and performance of materials; addresses the scientific basis for new advanced materials technologies; plans research around cross-country scientific themes such as nondestructive evaluation and phase diagram development; oversees Bureau-wide technical programs in nuclear reactor radiation research and nondestructive evaluation; and broadly disseminates generic technical information resulting from its programs. The Center consists of the following Divisions:

- Inorganic Materials
- Fracture and Deformation[3]
- Polymers
- Metallurgy
- Reactor Radiation

[1]Headquarters and Laboratories at Gaithersburg, MD, unless otherwise noted; mailing address Gaithersburg, MD 20899.
[2]Some divisions within the center are located at Boulder, CO 80303.
[3]Located at Boulder, CO, with some elements at Gaithersburg, MD.

Proceedings of the Third Cryocooler Conference

National Bureau of Standards
Boulder, Colorado
September 17-18, 1984

Edited by:

Ray Radebaugh, Beverly Louie, and Sandy McCarthy
National Bureau of Standards
Boulder, Colorado 80303

Sponsored by:

Cryogenic Engineering Conference
International Institute of Refrigeration–Commission A 1/2
NASA/Goddard Space Flight Center
National Bureau of Standards
Naval Research Laboratory
Office of Naval Research

U.S. DEPARTMENT OF COMMERCE, Malcolm Baldrige, Secretary
NATIONAL BUREAU OF STANDARDS, Ernest Ambler, Director

Issued May 1985

Library of Congress Catalog Card Number: 85-600544

National Bureau of Standards Special Publication 698
Natl. Bur. Stand. (U.S.), Spec. Publ. 698, 279 pages (May 1985)
CODEN: XNBSAV

U.S. GOVERNMENT PRINTING OFFICE
WASHINGTON: 1985

For sale by the Superintendent of Documents, U.S. Government Printing Office, Washington, DC 20402

ABSTRACT

This document contains the proceedings of the Third Cryocooler Conference, held at the National Bureau of Standards, Boulder, Colorado, on September 17-18, 1984. About 140 people from 10 countries attended the conference and represented industry, government, and academia. A total of 26 papers were presented orally at the conference and all appear in written form in this document. The emphasis in this conference was on small cryocoolers in the temperature range of 4 - 80 K. Mechanical and nonmechanical types were discussed in the various papers. Applications of these small cryocoolers include the cooling of infrared detectors, cryopumps, small superconducting devices and magnets, and electronic devices.

Key words: conference; cryocoolers; cryogenics, cryopumps; helium; infrared detectors; refrigeration; superconductors.

DEDICATION TO THE MEMORY OF PROFESSOR WILLIAM E. GIFFORD

The 3rd Cryocooler Conference on Refrigeration for Cryogenic Sensors and Electronic Systems is dedicated to our late colleague, Professor William E. Gifford of Syracuse University, for his valuable contributions to the field of cryorefrigeration. He was one of our pinneers, an inventor of practical systems, a dedicated teacher who inspired his students, and founder of an organization to carry on the development and manufacturing of cryorefrigeration machinery.

SPONSORS

National Bureau of Standards

Office of Naval Research

Naval Research Laboratory

International Institute of Refrigeration - Commission A1/2

Cryogenic Engineering Conference

NASA/Goddard Space Flight Center

CHAIRMAN

Ray Radebaugh - National Bureau of Standards

ADMINISTRATOR

Sandy McCarthy - National Bureau of Standards

ADVISORY COMMITTEE

Edgar A. Edelsack - Office of Naval Research

Max Gasser - NASA/Goddard

Peter J. Kerney - CTI Cryogenics

Paul Lindquist - Wright-Patterson AFB

Ralph Longsworth - Air Products and Chemicals

Martin Nisenoff - Naval Research Laboratory

Allan Sherman - NASA/Goddard

Klaus D. Timmerhaus - University of Colorado

Graham Walker - General Pneumatics Corp.

James E. Zimmerman - National Bureau of Standards

LOCAL COMMITTEE

Beverly Louie - National Bureau of Standards

Ray Radebaugh - National Bureau of Standards

James E. Zimmerman - National Bureau of Standards

CONTENTS

omit

INTRODUCTION AND SUMMARY

This document contains the proceedings of the Third Cryocooler Conference, which was held at the National Bureau of Standards, Boulder, Colorado, on September 17-18, 1984.

This series of conferences began in 1977 when about 40 invited speakers and participants assembled at the National Bureau of Standards in Boulder to discuss cryocoolers for small superconducting devices. Proceedings of that meeting are available from the Superintendent of Documents, U. S. Government Printing Office, Washington, D. C. as NBS Special Publication 508, entitled "Applications of Closed-Cycle Cryocoolers to Small Superconducting Devices". Since it was open only to invited participants, it may be considered conference number zero.

Because the scientific and engineering community showed great interest in a conference on cryocoolers, the first open conference, consisting mostly of contributed papers, was held in 1980 at the National Bureau of Standards, Boulder, with about 115 in attendance. The emphasis in that First Cryocooler Conference still was on the temperature range below 20 K. Proceedings of that conference are available from the U. S. Government Printing Office as NBS Special Publication 607, entitled "Refrigeration for Cryogenic Sensors and Electronic Systems". In response to a questionnaire, participants favored holding such a conference every two years and that trend has been followed.

The Second Cryocooler Conference was held in 1982 at NASA Goddard Space Flight Center, Greenbelt, Maryland. At that time the scope of the conference was expanded by considering temperatures up to 80 K, but it still emphasized small cryocoolers. The broadened scope brought in more participants and it was found that many concepts and techniques used at 80 K were common to lower temperature coolers as well. It was here that the scope of these series of conferences seemed to jell.

The scope of this Third Cryocooler Conference was the same as the second - small cryocoolers of about 10 W or less and temperatures below 80 K. However, any studies on devices or concepts outside this range that would have applications within the range were still considered. About 140 participants from 10 countries attended the conference. The two-year interval for the Cryocooler Conferences has meshed well with the Cryogenic Engineering Conference held on the alternate years. Sessions on small cryocoolers at the Cryogenic Engineering Conference are attended by the general cryogenic engineering community. The Cryocooler Conferences attended by specialists allow for a more in depth focus on cryocoolers.

Twenty-six papers were presented at the Third Cryocooler Conference and the written versions of all appear in this document. Three invited review papers were given on areas of widespread interest. A survey of the papers presented here as well as those in past conferences shows considerable progress in this area of high reliability as indicated by the papers on the Stirling cryocooler with magnetic bearings. The split Stirling cryocooler is well represented and shows advances in the area of a more reproducible drive for the displacer. Interest and progress in non-mechanical refrigeration techniques, such as magnetic refrigeration and absorption compressors for Joule-Thomson coolers, are evident from the number of papers in that session. Significant advances were made in the modeling of cryocoolers and in the understanding of regenerator behavior. Considerable work on cryocoolers is now being done in China and we are pleased to have had for the first time at these Cryocooler Conferences two papers from Chinese authors.

Applications of cryogenics depend intimately on the development of efficient, reliable, and inexpensive cryocoolers. We feel that the cryocooler progress represented by the papers that follow will have a significant impact on the development of cryogenics.

The Editors

D1

DESIGN OF CRYOCOOLERS FOR MICROWATT SUPERCONDUCTING DEVICES

J. E. Zimmerman

National Bureau of Standards
Electromagnetic Technology Division
Boulder, CO 80303

The primary applications of the cryocoolers considered here are for cooling various Josephson devices such as SQUID magnetometers and amplifiers, voltage standards, and microwave mixers and detectors. The common feature of these devices is their extremely low inherent bias power requirement, of the order of 10^{-7} W (or sometimes much less) per junction. This provides the possibility, not yet fully exploited of designing compact, low-power cryocoolers for these applications, the design criteria being totally different from those of any cryocoolers presently available. Several concepts have been explored and a number of laboratory model cryocoolers have been built. These include low-power non-magnetic regenerative machines of the Stirling or Gifford-McMahon type, three- or four-stage Joule-Thomson machines, liquid-helium dewars with integral small cryocoolers to reduce the evaporation rate, and liquid-helium dewars with integral continuously or intermittently operated small helium liquefiers to permit operation of cryogenic devices for indefinite time periods.

Key words: Cryocooler; cryogenics; refrigeration; superconducting devices; SQUID.

1. Introduction

A workshop on "Applications of Closed-Cycle Cryocoolers to Small Superconducting Devices"[1] was held at the National Bureau of Standards Boulder Laboratories in October 1977, out of which came the present series of conferences, more broadly conceived, on refrigeration for cryogenic sensors and electronic systems. The intent of this paper is to return to the narrower theme of the first workshop, to emphasize again the nature of the problem and to give at least the rudiments of a design philosophy which is appropriate to the needs of Josephson and other very low-power superconducting devices. This paper is presented in the conviction that the practical potential of superconducting devices, primarily SQUIDs and other Josephson devices, is largely unrealized precisely because of the lack of a compatible, low-cost cryocooler. The commercial viability of systems consisting of these devices and integral cryocoolers can hardly be judged from the market for the devices themselves, currently estimated to be of the order of a hundred per year, since the cost and inconvenience of the present cryogenic support systems greatly inhibits their use.

2. Small Superconducting Devices

For the past 20 years most cryoelectronic systems have been built around superconducting tunnel junctions or microbridges exhibiting the Josephson effect, commonly known as Josephson junctions. Bias power is typically in the range of a few microwatts (the order of 1 mA at 1 mV) down to a few picowatts per junction. Arrays of up to 1000 Josephson junctions should have bias power requirements of a milliwatt or less. While most Josephson devices are specifically designed for operation in the neighborhood of 4 K (that is, in liquid helium at atmospheric pressure or below), research and development continues on higher-temperature materials. Many niobium devices have been made which operate at temperatures of 8 to 9 K, and a double-junction Nb-Al-Ge SQUID

(the SQUID, or superconducting quantum interference device, used primarily as an ultra-sensitive magnetic sensor but also as memory element, counter, and for other purposes, consists of a low-inductance superconducting loop with one or two Josephson junctions appropriately biased for the application) has been demonstrated to operate at a temperature above 20 K [2].

Room-temperature transistors when used at low temperatures typically require much greater bias power than Josephson junctions. GaAs FETs which have been used as low-noise preamplifiers for SQUIDs require 20 to 50 mW, so that an array of these could require a considerable refrigeration capacity. However, these are not cryogenic devices, and their noise performance does not improve below 50 K or so, at which temperature refrigeration is at least 12 times cheaper, so to speak, than at 4 K. It has been suggested that a true cryogenic transistor is one of the prime requirements, along with reliable and convenient miniature cryocoolers, for the widespread acceptance of cryogenic instrumentation in general. A number of cryogenic transistors have been suggested [3,4].

There is considerable interest in arrays of cooled infrared sensors both for astronomical studies, and more extensively, for military applications. Both the scale of the arrays and the requirement of an infrared window to the outside world may impose relatively large heat loads on the cooling mechanism. In any case, this application will not be considered in this paper, although some of the design principles discussed may be applicable.

3. Refrigeration Requirements

Since Josephson devices require virtually no bias power, the essential function of a cryocooler reduces to that of intercepting radiation and conduction heat leaks along electrical connections and mechanical supports from the room-temperature environment. Elementary arguments show that it is much more efficient, and also easier, to provide for these heat leaks by some optimum distribution of cooling capacity at several discrete temperatures, or by a continuous distribution of refrigeration, than by simply providing a large cooling capacity at the low-temperature end. This principle is well-known, and yet it is common practice to specify the cold-end cooling capacity of cryocoolers and to mention the refrigeration at higher temperatures almost as an afterthought, if at all, rather than the other way around. Lending weight to the argument is the fact that heat conduction in all the commonly used materials, both metallic alloys and non-metals, but excluding copper and other pure metals, increases monotonically with temperature (see figure 1) [5]. The fourth-power law of radiation is a more dramatic example of the same tendency.

Some typical magnitudes of low-temperature heat leaks are instructive. Radiant energy from a low-emissivity (0.1) surface of a radiation shield at 20 K is about 0.9 mW/m^2. As an example of heat leaks through support structures, it can be shown that a mass of 1 kg at a temperature of 10 K can be kinematically supported at 10 G loading inside a radiation shield at 20 K by cords or wires 10 cm long with heat leaks of 9 μW for nylon or 60 μW for stainless steel (these heat leaks were calculated using thermal conductivities from figure 1 and tensile strengths of 900 MPa for nylon and 1800 MPa for stainless steel). Thus, the heat leaks would still be small for shorter and thicker support structures, and most cryoelectronic devices have much less than 1 kg mass. The case of electrical leads is slightly more complicated. For bias power in the range of milliwatts or less, negligible heat leak can be achieved by the use of fine wires of low-conductivity alloy. Signal lines, on the other hand, may have to have low electrical resistance, and relatively high thermal conductance, to avoid degrading the signal-to-noise ratio. Nominally pure copper is widely used for this purpose, but since its conductivity may be 1000 times that of most alloys at low temperatures, it may introduce unnecessarily large heat leaks to the cryogenic device to which the signal lines are connected. We will return to the subject of signal lines after a discussion of refrigeration mechanisms.

4. Liquid Helium As a Refrigeration Mechanism

A liquid-helium bath provides a relatively small cooling capacity at the boiling point (the heat of vaporization, 83 J/mol at 4.2 K). The cold vapor provides additional cooling capacity, the specific heat at constant pressure, which is nearly uniformly distributed in temperature above 8 or 10 K (~ 21 J/mol·K). The total cooling capacity of the vapor, ~ 6000 J/mol, is more than 70 times the heat of vaporization. In general, liquid helium does not provide an ideal distribution of refrigeration. As shown below and elsewhere, ideal cryogenic refrigeration systems for small superconducting devices will usually require monotonically increasing cooling capacity vs temperature, and only in rather special applications (perhaps to absorb the ohmic heat generated in high-current leads to a superconducting magnet) would the temperature-independent cooling capacity of helium provide an efficient refrigeration mechanism. This may be the essential reason for using liquid nitrogen or some other mechanism (see example below), along with liquid helium as a low-temperature cryogen, to provide additional cooling capacity at higher temperature.

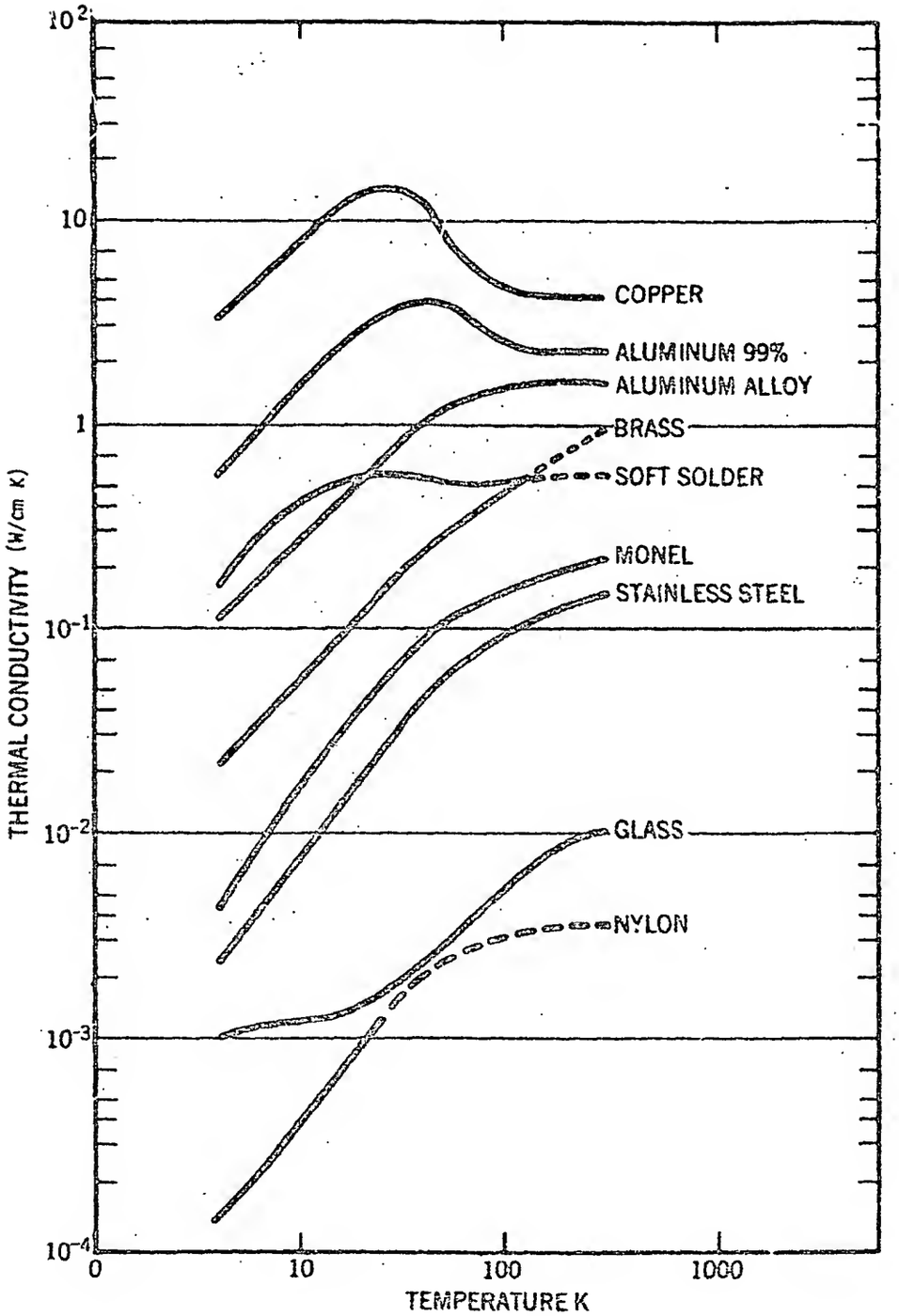

Figure 1. Thermal conductivity of some materials commonly used in cryogenic design.

5. Cryocoolers

Two types of cryocooler are under development for small superconducting devices, Joule-Thomson (J-T) and regenerative (Stirling, Gifford-McMahon, Vuilleumier). Joule-Thomson cryocoolers are highly attractive for very low-power applications because of their simplicity of construction and, more importantly, for having no solid moving parts in the cryogenic part of the system, so they generate essentially no magnetic interference or vibration (there may be high-frequency noise or hiss due to turbulent flow of the working fluid). Let us see how their qualitative features compare with the those of the heat leaks through various materials as noted above, and of thermal radiation. The following table gives the gross cooling capacities of a hypothetical four-stage Joule-Thomson cryocooler, with gas flow rates of 10 mL/s (standard temperature and pressure) per stage:

Working Fluid	CF_4	N_2	H_2	H_e
Temperature (K)	160	84	23	4.2
Low/high Pressures (MPa)	0.2/10	0.2/10	0.2/10	0.1/2
Gross Cooling Capacity (W)	3.3	1.1	0.13	0.012

The gross cooling capacities for a multi-stage reversible machine (Stirling, Carnot, etc.) with the same gas flows per stage are similar to the Joule-Thomson case. Here the cooling capacity, in the perfect-gas approximation, is of the form $PV(T2/T1)\ln(P1/P2)$, where the pressure-volume product PV is at standard temperature and pressure, P1/P2 is the compression ratio, and T2/T1 is the ratio of temperature of the stage to ambient temperature. Thus for P = 0.1 MPa (atmospheric pressure), V = 10 cm^3/s (per stage), T1 = 300 K, $\ln(P1/P2) = 1.0$, the gross cooling capacities for a hypothetical four-stage machine are:

Temperature (K)	150	50	15	5
Gross cooling capacity (W)	0.5	0.17	0.05	0.017

Using ordinary helium as the working fluid, the cooling capacity of the bottom stage may be considerably less than 0.017 W, since the perfect-gas approximation is quite inadequate at 5 K. These cooling capacities are roughly comparable to those of the Joule-Thomson example with the same flow rates, but note that Stirling and similar regenerative machines typically operate at much lower pressures and compression ratios than Joule-Thomson machines.

The point to be noted here is that in an intuitively "balanced" design (that is, comparable gas flows in all stages), the refrigeration capacities of the successive stages increase with increasing temperature, qualitatively matching the heat leaks that are expected from the low-conductivity materials commonly used in cryogenic design.

6. Electrical Connections

Copper, the most widely used material for electrical connections, may be a poor choice from the point of view of cryocooler design and thermal (Nyquist) noise generated in the lead resistance. The thermal conductivity of copper peaks at a temperature in the neighborhood of 20 K before dropping off linearly to zero at 0 K. Thus, the use of copper leads may result in large heat leaks just in the low-temperature region where cooling capacity is inherently small. The electrical resistivity of pure copper is small at low temperatures, so that the high-temperature portion of the leads will dominate the total lead resistance, and also the Nyquist noise. For most alloys, on the other hand, the thermal conductivity decreases more or less linearly below room temperature. It is easy to show that wires of practically any alloy such as brass, copper-nickel, or beryllium-copper, of the appropriate diameter for a specified total lead resistance, will reduce the heat leak at the low-temperature end by a factor of 100 or more, relative to copper, with only a moderate increase in the heat leak at the high-temperature end. The use of such alloys should provide a much better match to a "balanced" cryocooler design (as defined above) than pure copper. In addition, Nyquist noise generated in the leads will be lower in the alloy than in copper, since a relatively larger part of the electrical resistance will be at low temperature. The spectral density of total Nyquist noise power is proportional to the integral over the length of the wire of the product of Boltzmann's constant, the temperature, and the differential resistance, that is, the integral of $k_b T dR(T)$.

High-frequency and microwave leads can give large heat leaks if not specifically designed for cryogenic use. The above principles still apply, but since high-frequency currents flow only in a thin surface layer (less than 1 μm at 10 GHz in copper at room temperature), electrical losses and

heat leaks can both be reduced by using thin layers of low-resistivity metal on high-resistivity or insulating substrates, rather than using thick self-supporting conductors of low-resistivity metal. Furthermore, waveguides for very high frequency radiation can incorporate vacuum gaps to eliminate heat conduction entirely.

In a previous paper [6], we derived the optimum (minimum input power) distribution of refrigeration for cooling an electrical lead or a mechanical support of constant cross section, extending from ambient temperature T_{amb} to a low temperature T_o, whose thermal conductivity K could be expressed as a power of the temperature T: $K=K_nT^n$. The analysis was based on the Wiedemann-Franz Law for the relationship between thermal conductivity K and electrical resistivity ρ, that is, $K\rho/T \sim 2.4 \times 10^{-8}$ W-Ω/K^2. Applying this analysis to the case of temperature-independent conductivity gives an optimum temperature distribution (see Appendix for a summary of the mathematical analysis)

$$T = T_o \exp(az), \text{ where } a = \ln(T_{amb}/T_o),$$

and z is the reduced distance measured from the cold end. For the case where the conductivity is proportional to temperature ($K = K_1T$), the optimum temperature distribution is

$$T = ((1-z)T_o^{1/2} + zT_{amb}^{1/2})^2.$$

It turns out that in all cases the optimum distribution of refrigeration has the same z-dependence as the temperature. In the earlier paper we gave, as an example, the ideal minimum input power required to refrigerate an electrical lead (or set of leads) with temperature-independent thermal conductivity and net electrical resistance of .023 Ω. The result was 315 mW for the distributed refrigeration plus 93 mW for the heat flow remaining at the cold end of the leads, a total of 408 mW of mechanical power to produce the required refrigeration. In the case of thermal conductivity proportional to temperature (and the same electrical resistance), the ideal minimum input power works out to be 280 mW for the distributed refrigeration and only 19 mW for the cold end, a total of 299 mW. Although the difference in total power for the two cases is hardly significant, the factor of five difference in the cold end term could be very significant for cryocoolers where the performance at the cold end is limited by regenerator losses and non-ideal gas properties. This numerical example provides some quantitative support for the qualitative arguments given above for choosing the right kind of materials for electrical connections.

The optimum temperature distribution of refrigeration is the quantity of interest in designing a cryocooler. The optimum distribution is temperature-independent for the case of constant conductivity and proportional to $T^{1/2}$ for the case of conductivity proportional to temperature. Thus, liquid helium would provide essentially ideal refrigeration for the improbable example where it is necessary to use only materials of constant conductivity (probably no such materials exist) and constant cross section. An additional degree of freedom available to the designer is to vary the cross section of the electrical wires or wave guides in some optimum way as a function of position within the cryocooler. In fact, deviations from the Wiedemann-Franz Law (see above) are such as to be favorable to the use of copper or other pure metals such as silver and unfavorable to the use of high-resistivity alloys such as stainless steel, provided the cross-section is varied in some more-or-less optimum way. Materials of moderate electrical resistivity such as brass obey the Wiedemann-Franz Law more closely. Consideration of all the options can make the optimum design a difficult analytical problem, but it can be asserted with some confidence (based partly on experience) that the casual use of pure copper for electrical leads in the low-temperature end of low-power cryoelectronic systems can be disastrous.

7. Examples

One notable example of the use of a cryocooler with small superconducting devices is the hybrid cryostat recently reported by Archer [7]. He incorporated a two-stage commercial cryocooler with a 4.5-liter helium reservoir to achieve better than a five-day operating time for a pair of 100-120 GHz receivers at 2.5 K. The receivers consist of superconducting (tunnel junction) mixers at 2.5 K and GaAs FET IF preamplifiers at 20 K. Estimated heat leaks (actual heat leaks were slightly greater) to the 2.5 K helium bath include radiation (∿1.5 mW) and conduction (∿12 mW) through fill tube, dc leads, IF coaxial lines, 3-mm waveguides, four mechanical tuning rods, and massive solid supports for the helium reservoir and the receivers. Direct-current and microwave-bias-power levels were not mentioned in the paper and can be assumed to be negligible. Heat leaks at higher temperatures are intercepted by the cryocooler, which provides heat sinks and radiation shields at 20 K and at 65 K. Heat conduction through electrical connections was minimized by using design principles and materials already described (see above): unplated stainless steel waveguides for local-oscillator power, vacuum gaps in the low-loss signal waveguides, copper-beryllium alloy for the coaxial lines, and brass wire for dc connections.

This example demonstrates the small magnitude of total heat leak that can be achieved by careful design in a rather difficult application. It should be noted that this impressive performance was obtained without taking advantage of two mechanisms which, in principle, might further reduce the 13.5 mW heat leak by a considerable factor. First, by thermally linking the evaporating helium vapor to the various conducting members listed above, most of the heat leak from 20 K could be intercepted before reaching the 2.5 K bath. Second, if optimally loaded support members in tension were substituted for the massive supports, much of the heat conduction could be eliminated, although this substitution might be inconvenient to put into practice. It is curious to note that with this system as described (or any similar system), the cryocooler can easily provide all of the refrigeration required at higher temperatures, so that only about 1% of the total cooling capacity of the liquid helium, namely the heat of vaporization at 2.5 K, is actually essential to the operation of the system. One percent is not as bad as it seems, however, since one must apply the Carnot factor in calculating the work necessary to perform this refrigeration. Needless to say, any mechanism which leads to reducing the required mass and size of the cold components (the helium reservoir, for example) has a synergistic effect of reducing heat leak through reduction or elimination of support structure and surface area. This might be significant if the helium reservoir were eliminated in favor of a microminiature Joule-Thomson or Stirling stage, perhaps using helium-3 as the working fluid, to provide continuous cooling at 2.5 K.

There are other examples of small superconducting devices being operated in hybrid cryostats or in cryocoolers, but few which illustrate so nicely the variety of design problems that may be encountered. One problem not encountered in this example is that of magnetic interference, which is of overriding concern in designing cryocoolers for SQUIDs and certain other Josephson devices. The problem of scaling Joule-Thomson refrigeration systems down to "microminiature" size, as needed for Josephson and similar devices, has been addressed by Little in previous conferences of this series. His work has resulted in the commercial production of a remarkable series of tiny J-T cryocoolers whose gas-flow channels are etched into the surface of glass plates which are then bonded to cover plates, giving milliwatt cooling capacities at 80 K when supplied with nitrogen at 10 or 20 MPa [8]. Multi-stage units capable of maintaining cryogenic temperatures required for superconducting devices have not yet been demonstrated, but such a development would be extremely interesting because of the possibility of integrating the superconducting circuits on the same substrate.

A four-stage J-T cryocooler using more conventional materials and techniques, and specifically intended for a SQUID biomedical gradiometer, is under development by Tward. It is described in another paper in these proceedings [9]. J-T systems are highly attractive for low-level magnetic-measurement devices because there are no solid moving parts in the cryogenic system itself, and so magnetic interference is inherently low or non-existent. Simple Stirling or Gifford-McMahon cryocoolers with gap regenerators, for temperatures in the range of 7 to 9 K, have been under development for several years in the author's laboratory and elsewhere [10 to 15]. These typically have four or five discrete stages or else a tapered displacer to provide a continuous distribution of refrigeration as anticipated by the discussion above. In either case, the available refrigeration capacity is very small by the usual standards, but sufficient for the purpose of cooling microwatt superconducting devices and their associated electrical connections and support structure, as anticipated by the discussion above. The problem of compressor contamination is inherently less serious with these machines than with Joule-Thomson machines, but nevertheless there is a similar need for extremely clean compressors or pressure-wave generators with the appropriate pressures and compression ratios. Temperatures as low as 4 K have not been achieved with regenerative machines operating at the same pressure throughout. However, the possibility of maintaining temperatures below 4 K has been demonstrated using a separate cold-end stage operating at sub-atmospheric pressure [16]. A J-T stage operating at the same peak pressure as the regenerative machine with which it is incorporated, so that only one compressor is required, has also been reported [17].

Perhaps the greatest challenge facing the designer of a practical miniature J-T cryocooler is to build a set of almost perfectly clean compressors to provide the necessary high pressures and high compression ratios for the different stages. Both Tward and Little (private communication), and others, are currently working on solutions to the problem. Metal bellows or diaphragms are attractive in principle, but not easy in practice, since the slightest plastic deformation of the metal (at the valve ports, for example) will cause almost immediate failure. Gas-lubricated or magnetically suspended clearance seals between piston and cylinder, and unlubricated sliding seals of glass or graphite-filled teflon on hardened metal, and "hard-on-hard" clearance seals where both piston and cylinder are made of hard materials like ceramic or metal carbides and nitrides have all been demonstrated, in various applications, with varying degrees of success and reliability. Yet another approach is to demand less in the way of cleanliness of the compressor and to effectively purify the gases after compression (see paper by Tward in these proceedings).

8. Discussion

Several laboratory cryocoolers for microwatt superconducting devices, based more or less on the refrigeration mechanisms and design principles summarized above, have been developed during the last few years. These have demonstrated significant advances in construction methods, use of materials, computer analysis, miniaturization, interference reduction, and efficiency. Although a completely satisfactory machine has not yet been produced, it is likely that this goal will be realized during the next year or two. Work in the immediate future will surely concentrate on the design of miniature, ultra-clean compressors. One or more of the current experimental cryocoolers will be used with SQUID magnetometers and gradiometers to determine levels of vibration and magnetic interference. Further miniaturization of Joule-Thomson systems and new concepts for integrating these with superconducting microcircuits will certainly inspire active interest.

9. References

[1] Zimmerman, J. E., and Flynn, T. M., eds."Applications of Closed-Cycle Cryocoolers to Small Superconducting Devices, NBS Special Publication 508, April 1978.

[2] Rogalla, H., University of Giessen, private communication.

[3] Van Zeghbroeck, B. J., "Superconducting Current Injection Transistor", Appl. Phys. Lett. 42, April 15, 1983, p. 736.

[4] Frank, D. J., Brady, M. J., and Davidson, A., "A New Superconducting-Base Transister", 1984 Applied Superconductivity Conference, Sept. 9-13, 1984, San Diego, CA.

[5] Goodall, D. H., Cryogenic Data. A. P. T. Division, Culham Laboratory, March 1970.

[6] Sullivan, D. B., Daney, D., Radebaugh, R., and Zimmerman, J. E., "An Approach to Optimization of Low-Power Stirling Cryocoolers", in Refrigeration for Cryogenic Sensors, Max Gasser, ed., NASA Conference Publication 2287, December 1983, p. 107. We regret that a page of text was omitted from the published version of this paper. The missing page should follow page 109 of the proceedings. Also the references were missing. There should be a plus sign (+) between the two terms of equation 7, not minus (-), and the words "Bottom and top radii for the displacer and" should be deleted from the captions of figures 4 to 7. A corrected copy of this paper is available from the authors.

[7] Archer, J. W., "A High-Performance 2.5 K Cryostat Incorporating a 100-120 GHz Dual Polarization Receiver", Rev. Sci. Inst. To be published, 1985.

[8] Little, W., Microminiature Refrigeration, Rev. Sci. Instr. 55, 1984, p. 61.

[9] Tward, E., these proceedings.

[10] Chen Guobang, Zhejiang University, private communication.

[11] Heiden, C. University of Giessen, private communication.

[12] Lambert, N. these proceedings.

[13] Matsubara, Y., and Yasukochi, K., "An Application of Gap Regenerator/Expander Precooled by Two Stage G-M Refrigerator", in Refrigeration for Cryogenic Sensors, Max Gasser, ed., NASA Conference Publication 2287, December 1983, p. 157.

[14] Myrtle, K., Gygax, S., Plateel, C., and Winter, C., "Regeneration Efficiency, Shuttle Heat Loss and Thermal Conductivity in Epoxy-composite Annular Gap Regenerators From 4 K to 80 K", in Refrigeration for Cryogenic Sensors, Max Gasser, ed., NASA Conference Publication 2287, December 1983, p. 131.

[15] Sager, R. E., and Paulson, D. N., "Regeneration Experiments below 10 K in a Regenerative-cycle Cryocooler", in Refrigeration for Cryogenic Sensors, Max Gasser, ed., NASA Conference Publication 2287, December 1983, p. 81.

[16] Sullivan, D.B., and Zimmerman, J. E., "Very Low-Power Cryocoolers Using Plastic and Composite Materials", Int. J. Refrigeration, 1979, p. 211.

[17] Zimmerman, J. E., "Recent Developments in Self-contained Cryocoolers for SQUIDs and Other Low-power Cryoelectronic Devices", Proc. ICEC10 (Helsinki), Collan, H., Berglund, P., and Krusius, M., eds. Butterworth, 1984, p. 13.

10. Appendix

Following are the results (from the analysis of reference 6) of the optimization of the refrigeration distribution along a cryogenic member (a wire or support post), of constant cross section A and length a, with one end at ambient temperature T_{amb} and the other end at a low temperature T_o, whose thermal conductivity can be expressed as a power of the temperature, $K = K_n T^n$. Here z is the fractional distance measured from the cold end, Q(z) is the heat flow rate, dQ/dz and dQ/dT are the optimum distributions of refrigeration in z and in T, respectively, required to achieve the minimum ideal mechanical input power W expended on the working fluid, and T(z) is the corresponding temperature distribution:

CASE 1: $K = \text{constant}, (n = 0)$

$$T(z) = T_o e^{z \ln(T_{amb}/T_o)}$$

$$dQ/dz = (KA/a) T \ln^2(T_{amb}/T_o)$$

$$dQ/dT = (KA/a) \ln(T_{amb}/T_o)$$

$$W = (KA/a) T_o \ln^2(T_{amb}/T_o)$$

CASE 2: $K = K_n T^n, (n \neq 0)$

$$T(z) = (T_o^{n/2} + \alpha z)^{2/n} \quad \text{where } \alpha = T_{amb}^{n/2} - T_o^{n/2}$$

$$dQ/dz = 2\alpha^2 (2 + n) K_n AT/an^2$$

$$dQ/dT = \alpha (2 + n) K_n AT^{n/2}/an$$

$$W = 4K_n A\alpha^2 T_{amb}/an^2$$

D2

RECENT CRYOCOOLER PROGRESS IN JAPAN

Yoichi Matsubara

Atomic Energy Research Institute
Nihon University
Tokyo 101, Japan

This paper reviews the recent progress of cryocoolers and its related devices in Japan. Part of the research and development of cryogenic technology including small scale cryocoolers is supported by a number of national projects. The Japanese National Railways has been developing the light weight 4 K on-board refrigerators since 1977 as part of the MAGLEV train program. An investigation of superconducting and cryogenic fundamental technology has been conducted by the Science and Technology Agency since 1982, including high performance cryocooler (related to Stirling cycle), magnetic refrigerator and superfluid refrigeration. A study of space cryogenics such as the cooling systems of IR-detectors was started by the Ministry of International Trade and Industry in 1984. In addition to these national projects, several companies also have done their own activities on cryocooler investigation, for special applications such as cryopump, NMR-CT and JJ devices. Compact heat exchangers, high performance regenerators and reliable compressors are also being investigated as a critical component technology.

Key words: Cryocoolers; heat exchangers; helium; low temperature; refrigerators; regenerators.

1. Introduction

The research and development scheme of cryocoolers can be classified into two categories. The first one is related to the investigation of reliability, compactness and cutting costs of the well known cryocooler systems. Stirling or Gifford-McMahon cryocoolers with a JT loop and small scale Claude cycle also belong in this category. The second one is a fundamental approach to the novel refrigeration systems such as a magnetic refrigerator or regenerative cryocoolers which can be cooled down to liquid helium temperature without a JT loop. As a critical component, compact heat exchangers, high performance regenerators and reliable compressors are also important. With this in mind, the recent progress of the relatively small cryocoolers, operated at liquid helium temperature are reviewed.

2. Claude Cycle Cryocooler

The Claude cycle has been used for rather high capacity helium liquefiers, however, two on-board Claude cycle cryocoolers with a capacity of 30 watts at 4.4 K and 5 watts at 4.5 K have been fabricated for the MAGLEV project of JNR since 1978 [1, 2]. In this particular case, the following considerations were taken:

(1) The automatic inlet and exhaust valves of the expanders and cylindrical cam for the piston were employed for the compactness of the crosshead.

(2) A direct coupling system of the high speed flywheel was employed as an energy absorber of the expander. This energy absorber system makes the expander unit compact and light weight.

(3) The laminated metal heat exchangers made of aluminum perforated plates and plastic separators were employed for the 5 watt systems.

In the field of industrial electronics, the need for cryocoolers to cool superconducting magnets in such systems as magnetic resonance imaging or the control of the single crystal drawing furnaces has gradually increased. To meet these requirements, the Toshiba Co. developed 4.4 K 5 watt Claude cycle cryocooler, as shown in figure 1. Figure 2 shows the available energy balance of this system. It is reported that the JT valve loss is limited, although the losses due to the heat exchangers and expanders could be decreased.

The research activity for developing smaller Claude cycle cryocoolers has been continuing, however, there are almost no reports about the long term operation to date, and it has remained as a problem for the future.

3. G-M Cycle Cryocooler with JT Loop

The G-M cycle or modified Solvay cycle has been developed mainly as a 20 K cryocooler for the cryopump applications. Recently, several companies have been investigating the relatively high power G-M cycle cryocooler as a precooler for the JT loop for the recondensor of liquid helium.

Most of the cooling systems for superconducting magnets require simultaneous cooling of the radiation shield and liquid helium bath. Figure 3 shows the flow diagram of a 4.5 K cryocooler with 77 K additional cooling loop developed by Hitachi Ltd.. This work has been supported by MITI since 1982. The typical cooling power of the G-M cooler is 18 watts at 20 K and 60 watts at 80 K, respectively. The expander efficiency is reported as 44% at first stage and 38% at second stage. The details are shown in figure 4. The layered heat exchangers with perforated aluminum plates are used for the JT loop. It has a scroll type cross section as shown in figure 5. Figure 6 shows the cooling power at 4.5 K and 77 K where the JT flow rate was maintained at 10 Nm^3/hr. Indications shows that this system can be applied to both the large cryostat with low heat load at 4.5 K (such as superconducting NMR-CT) and the small cryostat with high heat load at 4.5 K (such as J-J devices).

The Mitsubishi Electric Co. investigated the 4.3 K 5 watt system, where a G-M cooler was used as a precooler developed by Osaka Oxygen Industries in 1981. They reported the effect of the different ambient temperature on the cooling power of the system. Figure 7 shows that the cooling capacities of G-M cooler decreased about 30% when the ambient temperature was increased to 40°C and the inlet helium gas temperature was increased to 50°C, (line B in figure 7), compared to the capacities operating at 20°C (line A). Figure 8 shows the cooling capacities for the 4.3 K J-T stage. It should be noted that the degradation of cooling capacities, 5.8 to 4.9 watts, is only about 16%. They also studied the effect of the ambient magnetic field on the valve motor up to 1 kGauss.

Sumitomo Heavy Industries Ltd. investigated 4.3 K 3 watts (max. 3.65 watts) cryocooler. The typical cooling capacity of their G-M cooler is 8 watts at 20 K and 20 watts at 77 K. One of their interests is related to the development of a reliable compressor. Three rotary compressors were used at the operating pressure of 1-20 atm for the JT loop (9 $Nm^3/hr.$) and 7-20 atm for the G-M cycle as shown in figure 9. The total input power is about 7 kW. The amount of lubrication oil for each compressor is successfully controlled by the overflow at a constant level which feeds it back to the intake port of the lower pressure stage. The dew point of the working helium gas is initially controlled below -70°C, although the pressure drop within the first heat exchanger increased 0.6 -0.84 Kg/cm^2 during 1660 hr. operations.

4. Fundamental Approach to the Novel Refrigeration Systems

Most of the cryocoolers being commercially used at liquid helium temperature have a JT loop as a final stage of the cooling system. However, a couple of attractive methods are now being investigated. An investigation of superconducting and cryogenic technology was conducted by the Science and Technology Agency in 1982. In this program, studies of high performance cryocoolers (related to Stirling cycle) and magnetic refrigerators were included.

4.1 Stirling Cycle

In the development of the Stirling cycle, there are some similarities between the prime mover and cryocooler. Figure 10 is presented by Ishizaki (ECTI). As a prime mover, he oeveloped the miscellaneous Stirling engines of output power below 50 kW ((a) of figure 10), the cold energy application system of LNG (b), and a hybrid system using LOX and liquid hydrogen (c) [3, 4]. As for the cryocooler, the most popular two stage cycle (d) were used for several applications where the cooling temperature was above 10 K. He also investigated a cryocooler operating at the liquid phase of helium (e).

According to the program of the Science and Technology Agency, the R & D of high performance Stirling cryocooler is now in progress at JNR, in cooperation with the Aisin Seiki Co. and ECTI. Figure 11 shows the single stage Stirling cycle operating below 15 K. The hot end temperature of the regenerator was maintained at a constant, using the evaporating gas from the liquid helium. The relation between the hot and cold end temperature is shown in figure 12. These figures indicate that the rare earth compounds (Gd-Er-Rh) when used as regenerator material improve the regenerator efficiency when it works below 15 K. The lowest temperature achieved in this experiment on the rare earth compounds was 3.74 K at the lower limit of temperature oscillation, when the mean operating pressure was about 0.7 atm and the hot end temperature was about 8K. They also confirmed that the cooling system can obtain near 4 K by using the two stage Stirling cycle when the hot end temperature maintained near 30 K.

4.2 Magnetic Refrigerator

The study of the magnetic refrigerator according to the Science and Technology Agency program is divided into three groups, a fundamental study of working materials (Institute of Metallic Material), a fundamental study of the refrigeration cycle (Tokyo Institute of Technology) and magnetic refrigeration systems (Toshiba Co.).

Figure 13 shows a schematic of the reciprocating magnetic refrigerator developed by the Toshiba Co. through this program. It consists of two sets of superconducting DC magnets and pistons with working materials (GGG). A two stage G-M cycle cryocooler (Air Products and Chemicals), USA) was used for the precooler of the working materials. The distance between the maximum and zero magnetic field is about 100 mm, which corresponds to the piston displacement, and is realized using field correcting magnets. All of the magnets are connected in series and operated at a permanent current mode after the initial excitation using detachable current leads. The experimental results of the test run are shown in figure 14 at the excitation current of 80 A and the maximum field of the working material of 4 Tesla. It indicates the increasing liquid helium level within the refrigeration space at each heat absorption process.

Hitachi Ltd. is also investigating a magnetic refrigerator which is operating between 20 K and 4 K, using a G-M cycle precooler and rotary moving method. Details may be obtained at the end of this year.

4.3 Component Technology

A study of regenerators below 20 K is now in progress at Nihon University and is supported by the program of the Science and Technology Agency. Thermal properties of regenerative materials which have a high specific heat below 20 K such as GdRh have been measured. To evaluate the effectiveness of the regenerator, a simple Vuilleumier cycle cryocooler was used. The minimum temperature of 5.4 - 6.5 K was obtained with this VM cooler. The details of these results will be given later in this proceedings.

Most of the compact heat exchangers, which can be used for a small Claude cycle cryocooler or JT loop precooled by a regenerative cryocooler, have been made by the perforated aluminum plates and plastic separators, however, Hitachi Ltd. recently developed a new heat exchanger made by a diffusion bonding method using perforated cooper plate and SUS304 separators, which has a similar cross section shown in figure 5. They reported that the axial conduction loss of this heat exchanger is greater th an that of epoxy bonding type, although the total heat transfer effectiveness is not decreased significantly when it is used at high Re number.

Showa Seiki Industries, in cocperation with Tohoku University and ECTI, developed a small oil free compressor, constructed by three stage reciprocal pistons and swash plate mechanism with a diaphragm for separating oil. Input power is 750 watts and the helium gas pressure at the inlet and outlet are 0.1 and 2.0 MPa with the flow rate of 2 Nm^3/hr. This compressor can be applied to the JT loop of the small cryocooler system for SQUID or other JJ devices.

5. Summary

Most of the cryocooler activities in Japan, at this time, seems to be aimed at the development of a compact and reliable cryocooler having several watts at liquid helium temperature. It will depend on the progress of the small superconducting magnet applications such as super LSI pattern printing devices, the single crystal drawing controller and the superconducting NMR-CT. Due to the improvement of the superconducting materials, the allowable cooling temperature is nearly 10 K, however, in considering the cooling temperature stability, the latent heat of the liquid helium is still attractive.

Miniature cryocoolers for the IR-detector, SQUID or other JJ devices are not being investigated in Japan, except for some fundamental research. However, a conceptual study of the sensor technology for unexplored spectrum has been started by the Ministry of International Trade and Industry this year, which includes the study of IR-detector cooling system for space application. Research will be conducted next year at the Electrotechnical Laboratory.

I wish to acknowledge to Y. Ishizaki, T. Koisumi, T. Horigami, N. Matsuda, A. Obara, K. Sawada and H. Wada for their useful information.

6. References

[1] Ohtsuka, T. and Iguchi, M., Proceedings of the Second International Seminar on Superconductive Magnetic Levitated Train, (Nov. 1982).

[2] Fujita, T. et al. Japanese Activities in Refrigeration Technology (Refrigeration for Cryogenic Sensors, NASA CP-2287, 33-46, (Dec. 1982).

[3] Ishizaki, Y., Stirling Engine Technology in Japan, (Intersociety Energy Conversion Engineering Conference), Boston (1979).

[4] Oshima, K. et al, The Utilization of LH_2 and LNG Cold for Generation of Electric Power by a Cryogenic-type Stirling Engine, ICEC 7, 310-317, London (1978).

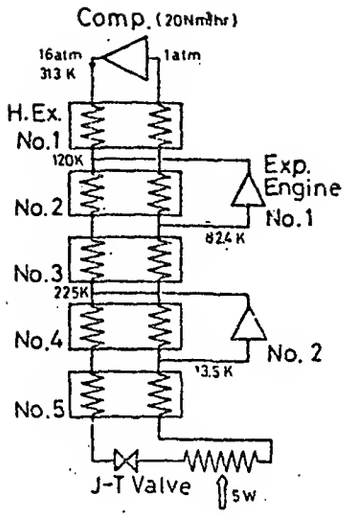

Fig. 1 Flow diagram of 4.5 K 5 watt Claude cycle

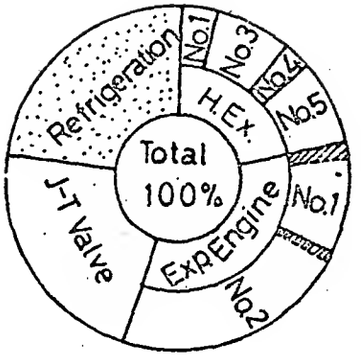

Fig. 2 Energy balance of the Claude cycle

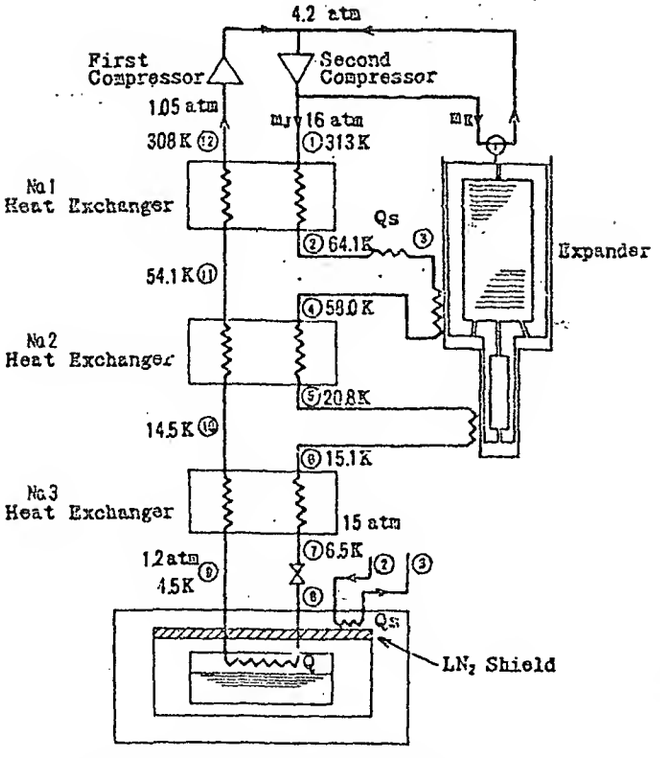

Fig. 3 4.5 K 6.5 watt cryocooler with JT loop precooled by G-M cycle

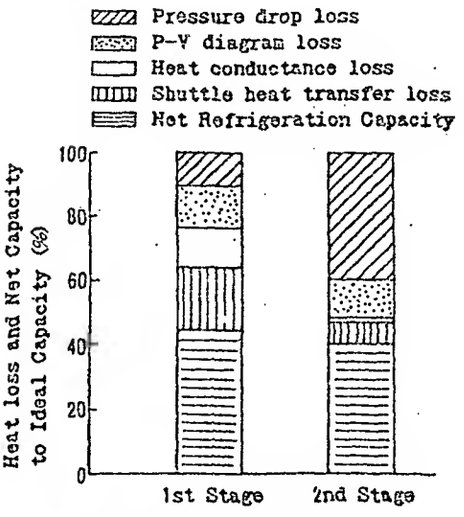

Fig. 4 Expander loss analysis of G-M cycle

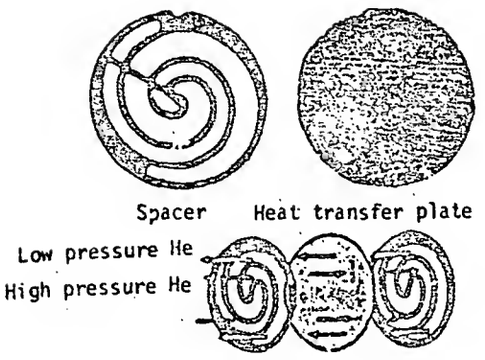

Fig.5 Cross section of scroll type heat exchanger

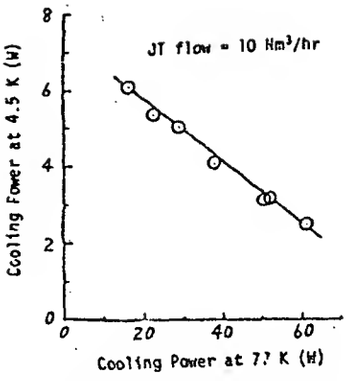

Fig.6 Cooling power dependency of 4.5 K and 77 K

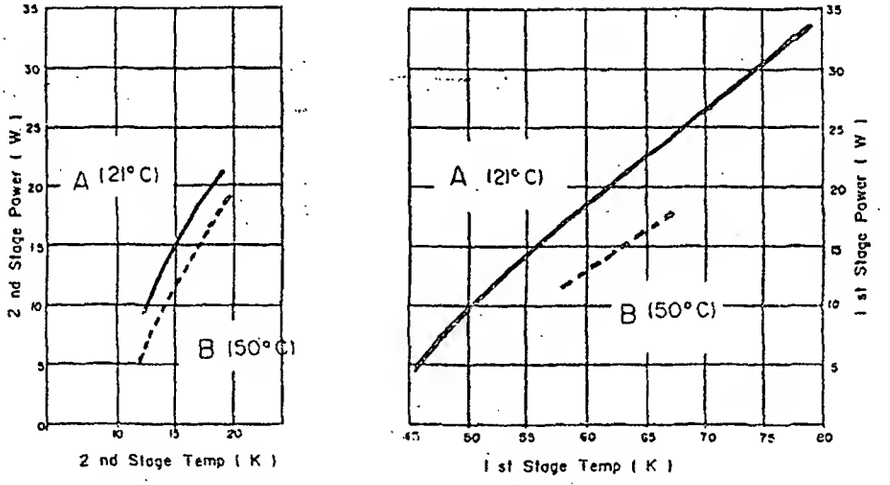

Fig.7 Ambient temperature effect of the G-M cooler performance

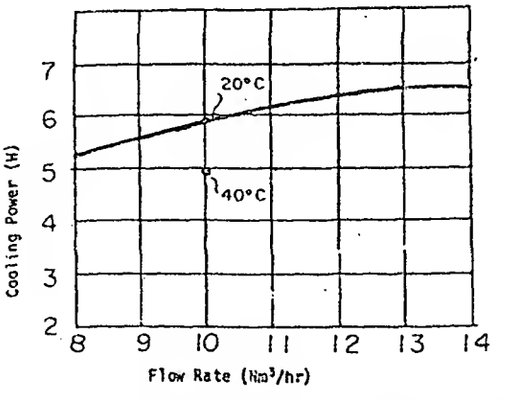

Fig. 8 Performance of 4.5 K cooler with JT loop precooled by G-M cycle

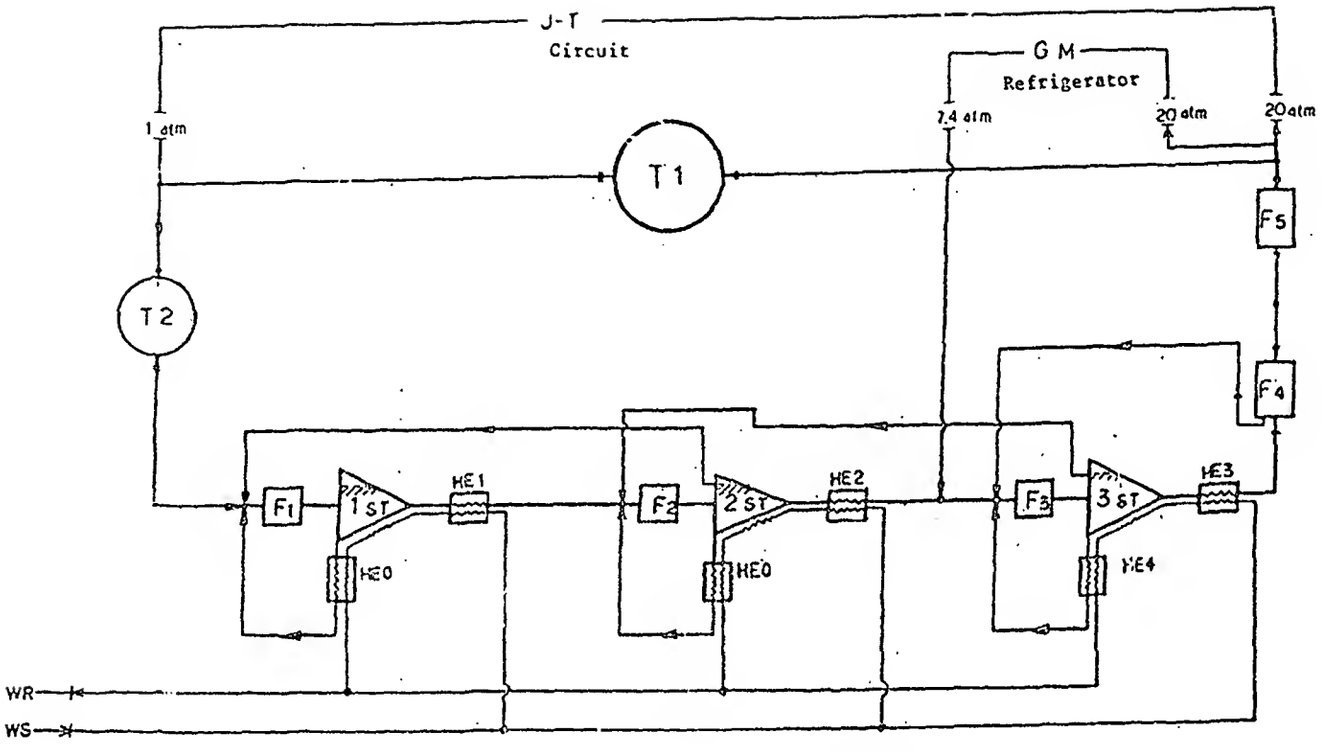

1ST.2ST.3ST; Compressor
HE; Heat Exchanger
F ; Filter
T ; Tank

WR; Water return
WS; Water supply

Fig.9 Flow diagram of three stage compressors

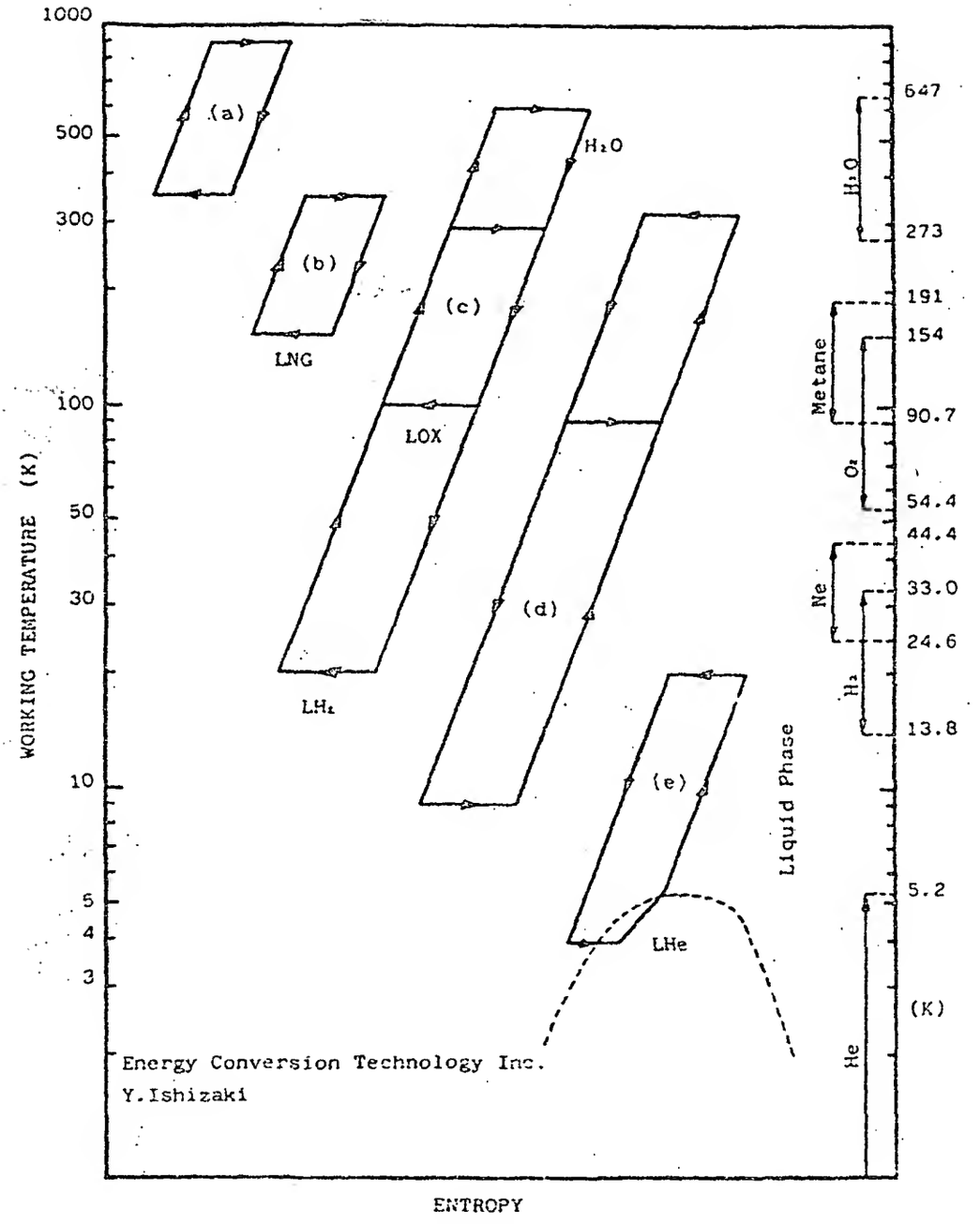

Fig.10 Schematic T-S diagrams of the Stirling cycle machines

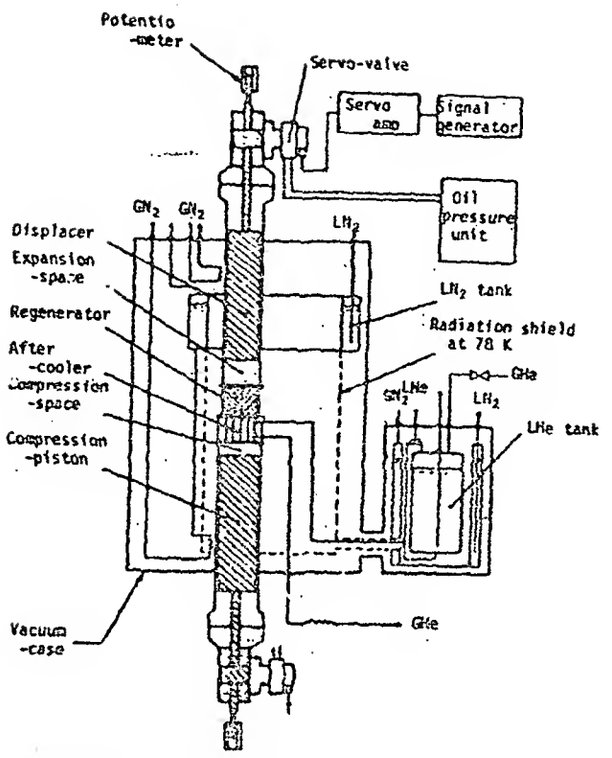

Fig.11 Single stage Stirling cycle operating below 15 K

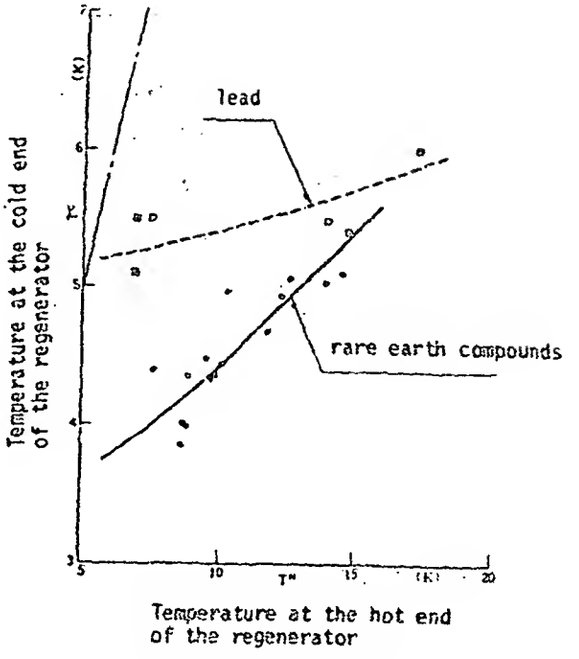

Fig.12 Test result of the Stirling cycle

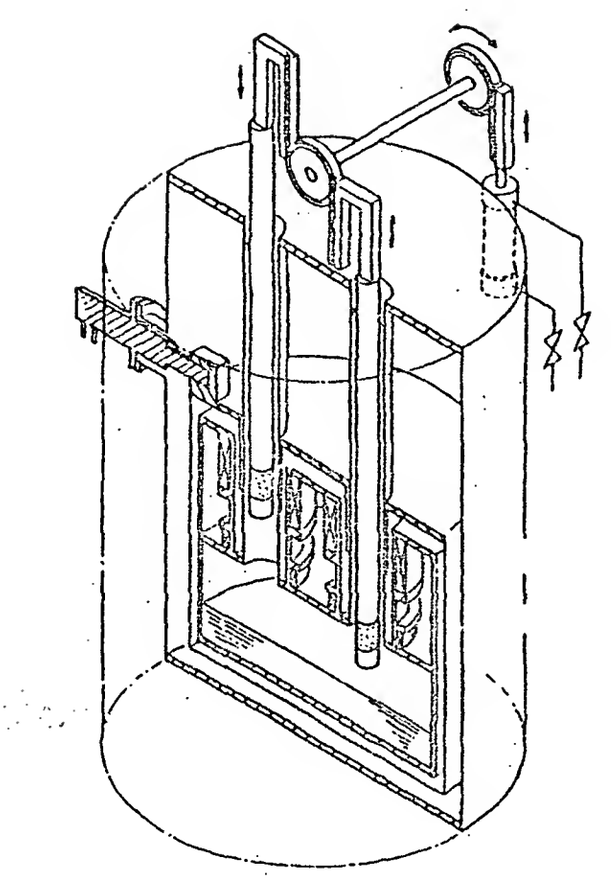

Fig.13 Schematic of the reciprocating magnetic refrigerator

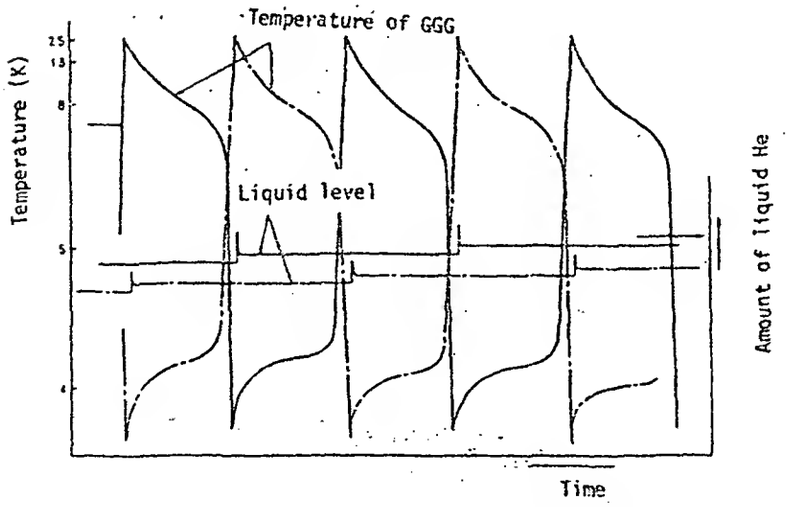

Fig.14 Test result of the magnetic refrigerator

D3

MAGNETIC REFRIGERATION FOR LOW-TEMPERATURE APPLICATIONS

J. A. Barclay

Gp. P-10, MS-K764
Los Alamos National Laboratory
Los Alamos, New Mexico 87545

An increasing number of applications require refrigeration at low temperatures ranging from production of liquid helium for medical imaging systems to cooling of infrared sensors on surveillance satellites. Cooling below about 15 K with regenerative refrigerators is difficult because of the decreasing thermal mass of the regenerator compared to that of the working material. In order to overcome this difficulty with helium gas as the working material, a heat exchanger plus a Joule-Thomson or other expander is used. Regenerative magnetic refrigerators with magnetic solids as the working material have the same regenerator problem as gas refrigerators. This problem provides motivation for the development of non-regenerative magnetic refrigerators that span ~4 K to ~20 K. Several laboratories around the world have magnetic-refrigeration programs underway; some are working on 4 - 20 K refrigerators. In the development efforts, particular emphasis has been placed on high reliability and high efficiency. Detailed calculations indicate considerable promise in this area, but several key problems have been identified in each of several possible devices. The principles, the potential, the problems, and the progress towards development of successful 4 - 20 K magnetic refrigerators are discussed.

Key words: Carnot cycle; low temperature; magnetic; non-regenerative; refrigerator; review.

I. INTRODUCTION

Magnetic resonance tomography and magnetic-field-gradient ore separation are two examples of developing commercial applications of superconducting magnets.[1,2] Many other potential users for superconducting magnet systems exist.[3] All of the superconducting magnet systems will require liquid helium or closed-cycle refrigeration near 4 K. Long wavelength infrared (LWIR) sensors need to be cooled to 8 - 10 K to obtain an adequate signal-to-noise ratio for high sensititivity.[4] Small helium liquefiers and some LWIR systems require approximately 1 W of cooling power. At this size, the efficiency of conventional refrigeration systems is typically a few percent of Carnot efficiency for heat rejection near room temprature.[5] Mean periods between failures or major maintenance are several thousand hours.

Regenerative gas refrigerators typically cease operation near 15 K because of decreasing thermal mass of the regenerator material. Hence both regenerative and recuperative gas refrigerators have a recuperative low-temperature stage plus an expander, such as a Joule-Thomson (J-T) device.[6] The efficiency of the bottom heat exchanger and J-T expander operating from 15 - 20 K down to ~4 K is 50-60% of Carnot if carefully designed.[7] The J-T loop suffers from poor reliability and requires a high-pressure compressor for operation.

If a simple, non-regenerative, non-recuperative 20 - 4 K refrigerator with high reliability and high efficiency (greater than 60% of Carnot) could be developed, it would offer significant improvements to existing refrigerator systems by eliminating the J-T loop and its associated problems. Refrigerators based on the magnetocaloric effect that execute a magnetic Carnot cycle between ~15 - 20 K and ~4 K can potentially satisfy these requirements. This conceptual

review paper will try to illustrate the development of magnetic refrigerators for the 20 - 4 K temperature region. The reference list is not complete but is representative.

II. PRINCIPLES

A. Materials

All refrigeration processes require an entropy change to absorb heat from a cold thermal source and deliver it to a higher temperature sink. Therefore, the entropy-temperature (S-T) diagrams for the working magnetic materials are essential to understanding the operation of magnetic refrigerators. In the 4 - 20 K region several types of magnetic materials can be used; the most obvious ones are paramagnets. There are many criteria for selection of suitable refrigerants including low lattice specific heat and a large magnetic moment. A survey of existing and potential paramagnetic materials has been published. [8] This and other work [9,10,11,12] have shown that gadolinium gallium garnet (GGG) is an excellent initial choice for 4- 20 K magnetic refrigerator design. Figure 1 shows the S-T curves for GGG as a function of aplied magnetic field.

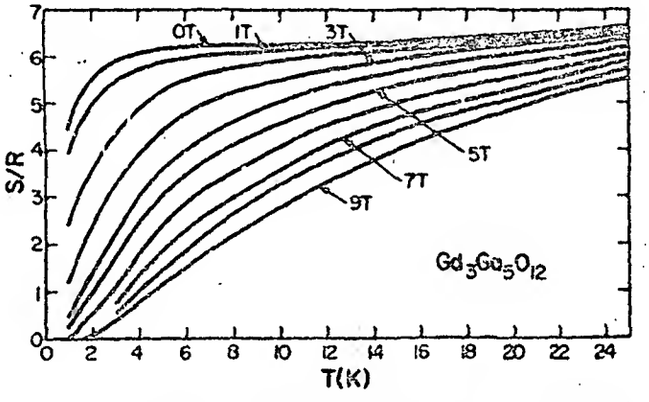

Figure 1: The entropy of gadolinium gallium garnet as a function of temperature and magnetic field.

It is also possible to consider composites of paramagnets such as D_yVO_4-GGG as suggested by the Grenoble group.[13] Physical mixing of materials allows some freedom in shaping the entropy-temperature diagrams which, in turn, allows cycles other than the Carnot cycle to be considered. Figure 2, taken from reference 13, shows the S-T curves for a 50-50% composition of the materials. As will be explained in the next section, this composite would be unsuitable for a magnetic Carnot cycle but is well suited to a magnetic Ericsson cycle, as was suggested in reference 13. The entropy change at 20 K in the composite is comparable to that in GGG alone, but the parallel nature of the S-T curves is essential for effective regeneration if a good regenerator material is used.

Finally, ferromagnetic materials can also be considered as working materials in this temperature range. An example is EuS whose calculated S-T curves [14] are shown in Fig. 3. Other ferromagnets such as GdRh [15] could be used although rhodium is extremely expensive. GdRh has a Curie temperature near 20 K but lower Curie temperature materials are available. For example, the ErRh-GdRh series has Curie temperatures ranging from ~6 K to ~20 K.[16]

B. Cycles

The only non-regenerative, non-recuperative cycle that exists for use in the 4-20 K range is the magnetic Carnot cycle. This consists of two isothermal stages and two adiabatic stages while magnetizing or or demagnetizing. Characteristics of this cycle are that the magnetic field is

continously changing and excellent heat transfer is required during the isothermal parts of the cycle. Because the lattice entropy of many paramagnets becomes comparable to the field-induced entropy change near 20 K, the upper operational limit of the Carnot cycle is near 20 K, depending upon the magnetic field strength and the magnitude of the lattice entropy.

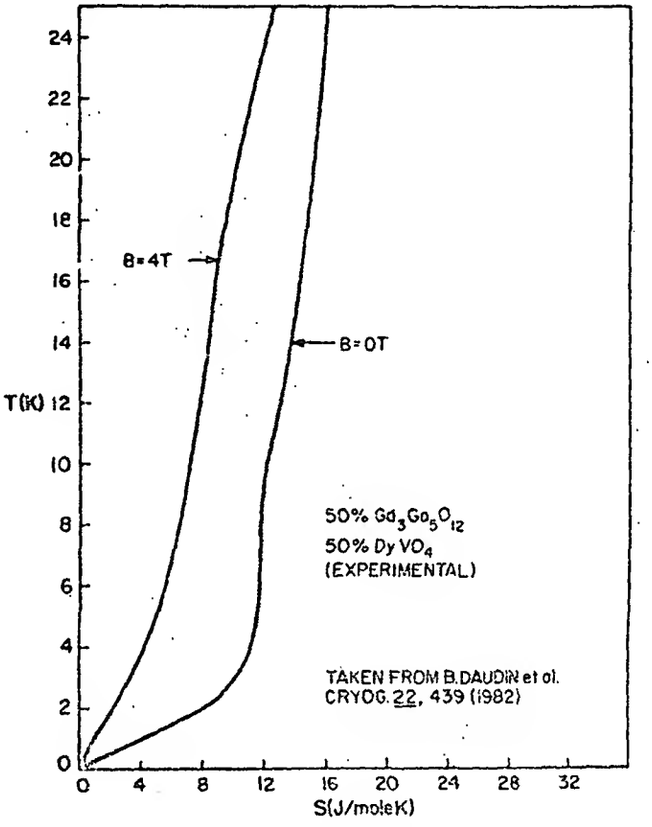

Figure 2: The entropy of 50% gadolinium gallium garnet and 50% Dyprosium Vanadate as a function of temperature and magnetic field.

Other cycles besides the Carnot cycle have possibilities if regeneration or recuperation can be effectively added. The magnetic Stirling cycle (two isomagnetization stages and two isothermals); magnetic Ericsson cycle (two isofield stages and two isothermals) and the magnetic Brayton cycle (two isofield stages and two isentropes are all possible in the 4-20 K range. These cycles are illustrated in Fig. 4 using the entropy temperature diagram of a paramagnetic material. Each cycle has different field-temperature changes required at different parts of the cycle. These requirements will be reflected in the designs of actual refrigerators. The magnetic Stirling cycle using a paramagnet such as GGG is probably a good choice because the amount of regeneration is minimal, as is shown in Fig. 4.

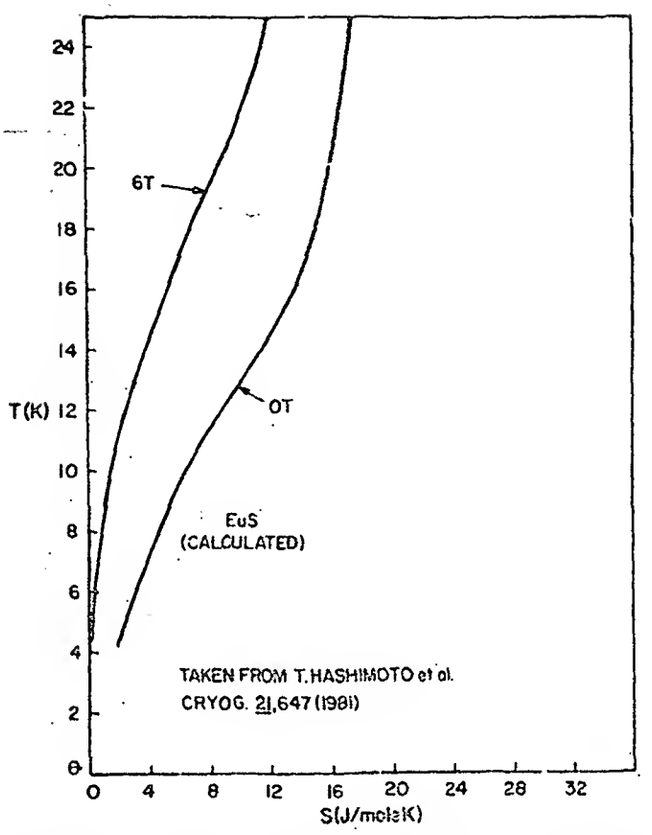

Figure 3: The calculated entropy of europium sulfide as a function of temperature and magnetic field.

Figure 4 also shows that the Brayton and Ericsson cycles are not feasible with a single paramagnetic material because the regenerative heat flows will be completely unbalanced. Composites or ferromagnets will be required for successful implementation of these cycles.

The entropy changes in the various cycles can be obtained from

$$dS = \left(\frac{C_B}{T}\right) dT + \left(\frac{\partial M}{\partial T}\right)_B dB \ . \qquad (1)$$

Knowledge of C_B and M as a function of B and T allows calculation of the heat and work flows during the idealized cycles. Real cycles, of course, are polytropic and require detailed knowledge of many additional sources of irreversible entropy and heat capacities of thermal addenda in order to be correctly modelled.

III. Potential

A. Designs

A series of ~2 - 4 K magnetic refrigerators have already been built and tested with varying degrees of success.[17,18,19,10] The Grenoble group has reported efficiencies as high as 79% of

Carnot [17] for a 2 - 4 K reciprocating design using GGG. In the 4 - 20 K range there is a large variety of magnetic refrigerator design possibilities. Table I presents an attempt at classification of the possibilities and includes location of groups working on devices of the various types.

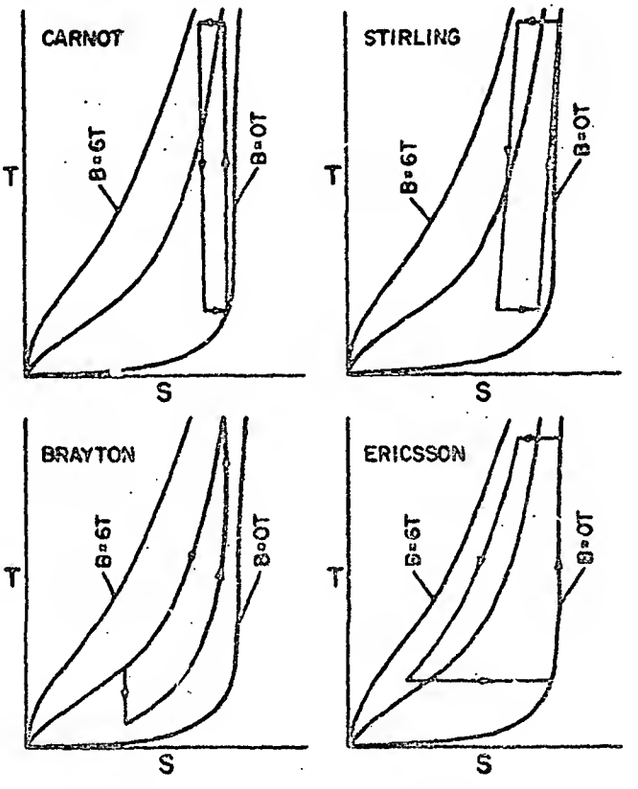

Figure 4: The magnetic cycles illustrated on the entropy-temperature diagram of a paramagnetic material.

Table I. Possible 4 - 20 K Magnetic Refrigerator Designs

	Non-Regenerative Non-Recuperative	Regenerative	Recuperative	Hybrid
Rotational	*LANL, **HAC	Grenoble		
Reciprocating	***J.P.L., Tokyo	LANL		(LANL)
Other	****Tokyo	MIT		(MIT)

*LANL - Los Alamos
**HAC - Hughes Aircraft Co.
***J.P.L. - Jet Propulsion Laboratory
****Tokyo - Japanese groups at Tokyo Institute of Technology, Hatachi-Research Laboratories, and other interacting laboratories.

The majority of devices underdevelopment appear to be non-regenerative, non-recuperative. Both rotating and reciprocating designs have been chosen. The details on most of these devices are not fully known because the various groups have not yet published reports. There are pros and cons to each design. Some of these design choices will become apparent in the discussion of the problems in the next major section.

B. Second-law analysis[21]

The efficiency of a refrigerator executing a thermodynamic cycle between hot and cold temperature, T_H and T_C, respectively, can be written as

$$\eta = \frac{\dot{Q}_C}{\dot{W}_{TOTAL}} \left(\frac{T_H}{T_C} - 1 \right) . \qquad (2)$$

where $\dot{Q}_C$ is the reversible cooling power and $\dot{W}_{total}$ is net work flow into the refrigerator. This total work rate includes the pump power, magnet supply power, etc., in addition to the work rate from the refrigerator itself. The refrigerator work rate can be calculated from the Second Law according to

$$\dot{W} = \dot{Q}_C \left(\frac{T_H}{T_C} - 1 \right) + \frac{T_H \int \dot{W}_I \left(\frac{1}{T} - \frac{1}{T_H} \right) dT}{\int dT} + \frac{T_H \int \dot{q}_J \left(\frac{1}{T} - \frac{1}{T_H} \right) dT}{\int dT} + \frac{T_H \int \Delta \dot{S}_{IRR}\, dT}{\int dT} , \qquad (3)$$

where $\dot{W}_I$ is the power added externally that the refrigerator must remove, e.g., friction, $\dot{q}_J$ is the power introduced through heat conduction from the surroundings; and $\Delta \dot{S}_{IRR}$ is the rate of irreversible entropy production from different mechanisms. Once a specific design is chosen, a detailed analysis of the device can be done and a projected efficiency obtained. For example, in a Carnot-cycle rotational device designed at Los Alamos, the work rates from each mechanism were calculated and are presented in Table II.

Assuming good heat exchangers, pump efficiencies of 50%, and drive motor efficiency of 90%, the overall projected efficiency for the wheel device was 65% when rotating at 0.2 Hz through a 6-T field to pump 0.67 W from 4.3 K to 15 K. This is an excellent efficiency but only slightly greater than a very well designed J-T loop. However, the low rotational frequency suggests it may have a long lifetime and good reliability.

Table II. WORK RATES FROM VARIOUS MECHANISMS FOR A CARNOT-CYCLE WHEEL REFRIGERATOR

Item		$\dot{W}$ (watts)
$\dot{W}$	reversible	1.64
$\dot{W}_H$	conduction	0.046
$\dot{W}_H$	heat transfer	0.012
$\dot{W}_H$	pressure drop	0.011
$\dot{W}_C$	conduction	0.016
$\dot{W}_C$	heat transfer	0.012
$\dot{W}_C$	pressure drop	0.0001
$\dot{W}$	4-15 K conduction	0.18
$\dot{W}$	friction	0.10
$\dot{W}$	parasitic heat leak	0.10
$\dot{W}_H$	heat exchanger	0.060
$\dot{W}_C$	heat exchanger	0.060

IV. Problems

A. Isothermal Stages

The importance of the need for "isothermal" stages in efficient low-temperature cycles was realized by Jacob [22] some years ago for a Brayton cycle. The isothermal stages are essential for all efficient low temperature cycles for the following reasons. In order to transfer heat to and from magnetic material to a single-phase heat-transfer gas, a temperature difference between the cold magnetic material and the gas (ΔT_C) and hot magnetic material and gas (ΔT_H) must exist. The direct effect of ΔT_C and ΔT_H on efficiency can be calculated from Eqs (2) and (3) by integrating from $T_C - \Delta T_C$ to T_C at the cold stage and T_H to $T + \Delta T_H$ at the hot stage. The total expression is complex, but for only the reversible cooling power component to the efficiency, we obtain

$$\eta = \frac{(T_H - T_C)}{T_C \left[\dfrac{\ln \left(\dfrac{T_C}{T_C - \Delta T_C} \right) \Delta T_H}{\ln \left(\dfrac{T_H + \Delta T_H}{T_H} \right) \Delta T_C} - 1 \right]} \quad . \tag{4}$$

For example, between 4 and 20 K, if $\Delta T_C \sim 0.3$ K and $\Delta T_H \sim 1$ K, the efficiency drops from 100% (reversible) to 92.5% from this effect alone. This clearly indicates that magnetic Brayton cycles in the 4-20 K range will be less efficient than the other cycles. While this effect is probably obvious, it is important to remember for operation at very low temperatures.

B. Addenda

The major effect of additional thermal mass from various sources is to reduce the cooling power of a magnetic refrigerator. This is particularly important in non-regenerative designs using the magnetic Carnot cycle because many of the addenda items have temperature-dependent thermal masses that tend to contribute more entropy near 20 K than near 4 K. There are several ways to account for the effects of addenda on the refrigerator, but the total entropy approach is one of the more useful ways. In this approach, the entropy of each item in the refrigerator and that of the magnetic materials are totaled. The change in total entropy caused by the magnetic field is easily obtained.

Some of the addenda items common to many 4 -20 K designs are containers, forms, supports, etc. which must be present to support or contain the paramagnetic material. Because excellent heat transfer between the working material and heat-transfer gas is required, a porous magnetic-material of some geometry along with convected helium gas are used. The porosity of the material can lead to entrained helium gas, which causes an internal thermal load and gas movement during the cycle. The housing around the moving working material doesn't contribute to the addenda once thermal equilibrium is attained, but thermal conduction from hot to cold sections adds a thermal load equivalent to thermal addenda. Figure 5 shows the relative magnitudes of the entropy of the addenda for a particular design. These effects are a severe problem in non-regenerative designs.

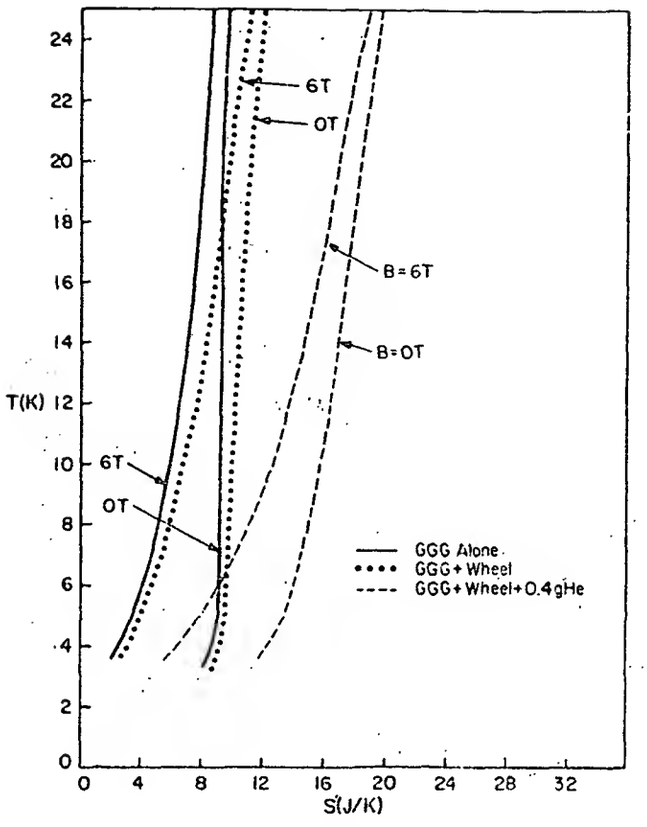

Figure 5: The total entropy of a particular design that shows the effects of various contributions of thermal addenda.

C. Flow Control

In any 4 -20 K refrigerator that uses convective heat transfer between helium gas and the magnetic solid, there will be a flow-control problem. The problem is caused in part by the temperature differences in the refrigerator and in part by the motion of the working material. In a rotating design, either crossflow or counterflow gas motion in sections of the wheel is possible and heat transfer occurs continously. The hot and cold section must be separated by some sealing mechanism, such as clearance or labyrinth seals. Rubbing seals of various designs are possible, but careful attention must be paid to clogging due to small particles from abrasion. Because of the close tolerances in highly effective porous beds, performance could degrade rapidly with clogging. Friction must also be kept to a minimum, especially when it occurs at the cold part of the refrigerator.

Reciprocating designs need flow during the motion of the piston of working material in order to achieve an isothermal stage in a cycle. Clever designs are needed to establish flow through the piston in some fashion and at the same time have isolated hot and cold sections in the refrigerator cylinder.

Pumps are essential to flow control. The pumping power must be fairly small compared to the cooling power in order to attain high efficiency. Efficient, reliable, long-lifetime pumps

operating at low temperatures are a real problem area. The small pressure differences and modest volume flow rates are different requirements from most previous low-temperature pump work [23]

D. External Heat Exchangers

High performance heat exchangers are very important for high efficiency because the temperature differences allowed on each end of the refrigerator must be relatively small according to Eq. 4. The heat exchanger heat-transfer irreversibility for single-coil heat exchangers in a pot of boiling or condensing cryogen, such as liquid hydrogen or helium, can be shown to be given by [24]

$$\frac{\dot{S}_{IRR}}{\dot{m}C_p} = \left(\frac{T_{in} - T_o}{T_o}\right)\left(1 - e^{-N_{tu}}\right) + \ln\left(\frac{T_o + \left(T_{in} - T_o\right)e^{-N_{tu}}}{T_{in}}\right) \quad . \tag{5}$$

where $\dot{S}_{IRR}$ is the entropy generation rate, C_p is the fluid thermal mass flow rate, T_{in} is the gas inlet temperature, T_o is the cryogen bath temperature, and N_{tu} is the number of heat transfer units characterizing the heat exchanger. For N_{tu} greater than about 10, Eq. (5) reduces to

$$\dot{S}_{IRR} \cong \frac{1}{2}\,\dot{m}C_p\left(\frac{\Delta T}{T_o}\right)^2 \quad . \tag{6}$$

where ΔT is defined by $T_{in} = T_o + \Delta T$. Equation (6) clearly shows that a small ΔT is important for efficient heat exchangers if the N_{tu} is reasonably high. Exchangers with $N_{tu} > 10$ are readily achieveable.[25]

E. Magnetic Field

1. Forces

The forces between the magnetic material and the magnet can be substantial if high fields and large volumes of material are combined. For example, in a simple axial case where dB/dz might be 70 T/m, 100 cm^3 of saturated GGG in a cylindrical piston will experience a force of ~5400 N (1200 lbs_f). Clearly, forces of this magnitude must be carefully considered in any design. Reciprocating devices have the possibility of partially cancelling the forces by using two opposing pistons, but these designs must have supports for the large compressive stress between magnetic pistons. Rotating devices have natural cancellation of forces but have a large load on the drive shaft bearing because the entire wheel is attracted into the magnet.

2. Profile

Reciprocating devices use solenoidal magnets which are rather straight forward but do require some field shaping depending upon the desired cycle. Non-regenerative Carnot cycles require approximately linear field profiles which are readily approximated. Rotating devices allow several possible ways for production of the magnetic field such, as Helmholtz pairs, racetrack coils, and solenoids or bent solenoids. The first two allow axial drive while the latter requires rim drive. The difficulty in all these cases in that the ratio of field at the magnetic material to the field in the magnet windings is large, i.e., 1: 1.2-1.4. This restricts the maximum field easily obtainable at the magnetic material when the coils are wound with NbTi superconducting wire.[26] If Nb_3Sn is used to wind the magnets, higher fields are possible but only at higher costs.

V. PROGRESS

There are several magnetic-refrigeration development projects around the world. The comments here are restricted to those with immediate interests in ~4 to ~20 K prototypes.

A. Hughes Aircraft Corporation

As indicated in Table I, HAC has started a magnetic refrigerator development program on low-temperature devices for applications as spacecraft coolers.[27]

B. Jet Propulsion Laboratory

The deep-space communications network uses a series of antennaes with cooled maser amplifiers. The present Gifford-McMahon plus J-T loop coolers have worked for many years, but there is a desire to see if the J-T loop could be replaced by a magnetic stage that would increase efficiency and improve reliability. A report on this project is included in another session of this conference.[28]

C. Massachusetts Institute of Technology

This is a fairly new program working on a magnetic regenerative concept and on hybrid gas-magnetic devices.[29]

D. Grenoble Group

Following the outstanding success of their 2-4 K reciprocating magnetic refrigerator, the French group have started work on a 4-20 K rotational magnetic refrigerator.[30]

E. Tokyo Group

The Japanese group represents several industrial research laboratories in collaboration with Professor Hashimoto's group in the Department of Applied Physics at Tokoyo Insititute of Technology. Their general interest is in low-temperature refrigerators for cryogen liquefaction. They have reported several results on their use of GGG to liquefy helium [31] with a charge/discharge magnet cycle. We understand that they are now modifying their apparatus to operate in a reciprocating mode between ~4 and 20 K.

F. Los Alamos National Laboratory

The 4-20 K rotational refrigerator under development at Los Alamos is part of a broad magnetic refrigeration program. The objectives include basic research to provide a data base for design and prototype development to prove the potential of this technology by constructing and testing working devices. The 4-20 K device is described below in more detail.

1. Description. The rotational concept has several desirable features, such as balanced magnetic forces and continuous refrigeration. The Carnot cycle is also the easiest of the cycles to execute, although the entrained fluid problem must be carefully handled. A magnetic wheel designed to execute a Carnot cycle is shown in Fig. 6. The GGG used in this design is contained in small rectangular compartments on the rim of the wheel. The GGG is in the form of approximately spherical chunks. The wheel is made from stainless steel, and stainless steel screen is used to enclose the inside and outside of each compartment.

The wheel rotates inside a stationary housing that has two duct regions such that helium gas can pass radially through the GGG. The ducts are located at positions where the GGG reaches 20 K as it is magnetized and where the GGG reaches > 4.2 K as it is demagnetized. The external heat exchangers are connected to the ducts and form part of a hermetic system around the wheel that contains the helium gas. Two pumps circulate the helium gas through the wheel and external heat exchangers. The wheel can be driven inside the housing by a magnetic coupling to avoid any cold seals to a rotating shaft. The fabrication tolerances on the wheel and the housing need to be very close, so that clearance seals are formed between the moving wheel and the fixed housing. Because the entire housing contains helium gas, there should be very little movement of helium past these clearance seals.

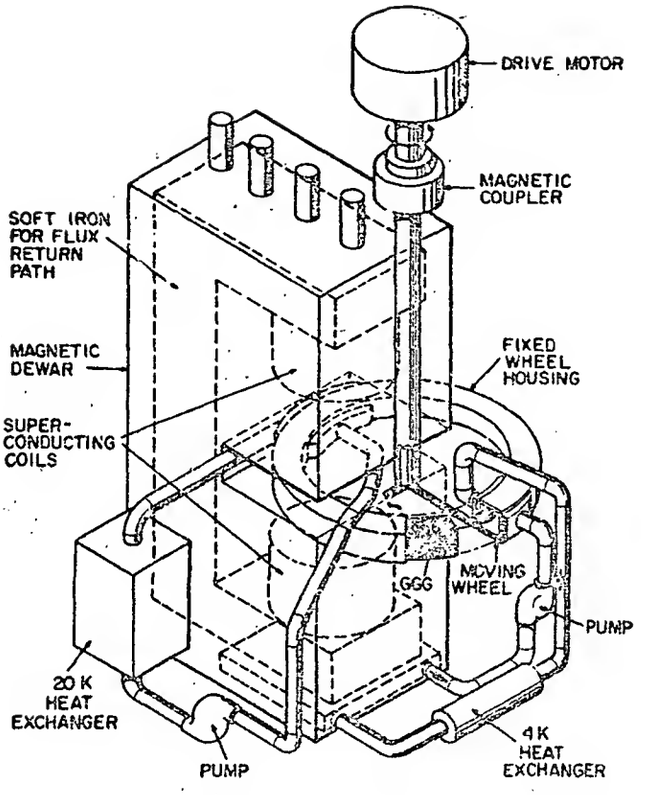

Figure 6: A schematic diagram of a Carnot-cycle, wheel-type magnetic refrigerator for operation between 4.5 and 20 K.

The magnet consists of a pair of solenoids wound on iron cores and supported by an iron yoke for flux return. The resultant c-shaped magnet is designed for a maximum field of ~ 6T in the gap of 2 cm. The leads can be removable so that after the magnet is charged and put in persistent mode, the power supply can be turned down and the leads removed. The magnet is kept at ~ 4.2 K by liquid helium in the dewar surrounding the magnet. Because the whole magnetic refrigerator operates in a vacuum chamber, the liquid helium dewar need only be single-walled and have no superinsulation directly on it.

2. Results

The magnet works well in persistent-mode and produces 6T in the gap where wheel is located. The flow of helium through the wheel is about as expected with respect to the pressure drops, but there is significantly more leakage from duct to duct than expected. There is substantial loading on the central shaft bushing and early versions of the wheel jammed when the field was increased from zero. As an example of the performance, Fig. 7 shows an early curve of the cooling power as a function of temperature span.

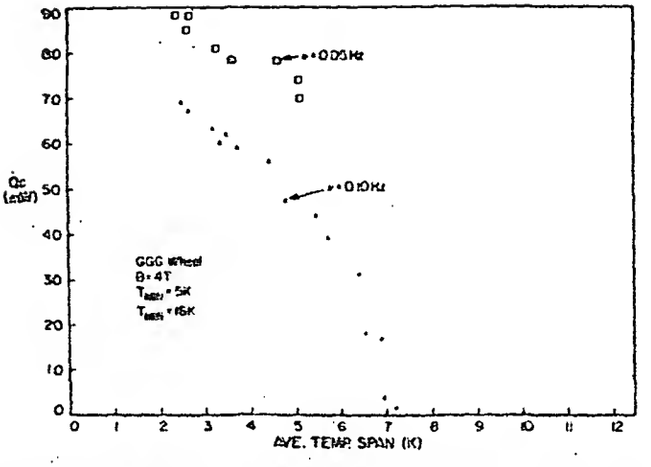

Figure 7: The cooling power as a function of average temperature span for the Carnot-cycle rotational refrigerator.

So far the results indicate that gas movement is the dominant problem, as might have been expected. The efficiency of the overall refrigerator, including drive motor, gear reducers, friction, etc., is low, typically 1% of Carnot but the efficiency of the refrigerator excluding these contributions is ~20% of Carnot. Obviously much more work needs to be done to achieve the design goals but these early results are very encouraging, and we expect they are the beginning of a series of successful devices from the several existing programs.

Acknowlegements

This work was performed under the auspices of the U.S. Department of Energy. Funding support from DOE (BES), DARPA, and NASA (KSC) are gratefully acknowledged.

References

1. Manatt, S. L., Some Potential Application of Nuclear Magnetic Resonance, NASA Jet Propulsion Laboratory, Report 0-902, June 1983.
2. Selvaggi, J., 5 Tesla, Iron Clad, Fast Field, Superconducting MRMS, paper to be presented at ASME winter meeting, Dec. 10-14, 1984, New Orleans, LA
3. See, for example, the proceedings of any applied Superconductivity Conference or Cryogenic Engineering Conference, such as Adv. in Cryog. Eng. 29, 29-255 (1984).
4. Mas'lin, W. L., Cryogenics in Space Systems; Presented at the meeting of the IRIS Speciality Group on Infrared Detectors, Boulder, CO., Aug. 2-4, 1983.
5. Strobridge, T. R., Cryogenic Refrigerators - an Updated Survey, NBS-TN-655 (1974).
6. Barron, R. F., Liquefaction cycles for Cryogens, Adv. in Cryog. Eng. 17, 20 (1972).
7. Dean, J. W. and Mann, D. B., The Joule-Thomson Process in Cryogenic Refrigeration Systems, NBS-TN-227 (1965).
8. Barclay, J.A. and Steyert, W. A., Materials for Magnetic Refrigeration Between 2 K and 20 K, Cryogenics 22, 73 (1082).
9. Daudin, B., Lagnier, R. and Salce, B., Thermodynamic Properties of the Gadolinium Gallium Garnet, $Gd_3Ga_5O_{12}$ Between 0.5 and 25 K, J. Mag, and Mag. Mat. 27, 315(1982).
10. Numazawa, T., Watanabe, Y., Hashimoto, T., Sato, A., Nakagome, H., Horigami, O., Takayama, S. and Watanabe, M., The Magnetic Refrigeration Characteristics of Several Magnetic Refrigerants below 20 K, II:Thermal Properties, Proc. Int'l Cryog. Eng. Conf., Kobe, Japan, May, 1982.
11. Hakuraku, Y., Kapitza conductance of the gadolinium gallium garnet, $Gd_3Ga_5O_{12}$ between 1.4 K and 2.1 K.

12. Hornung, E. W., Fisher, R. A., Brodale, G. E., and Giauque, W. F. Magnetothermodynamics of Gadolinium Gallium Garnet. II. Heat Capacity, Entropy, Magnetic Moment from 0.5 to 4.2 K, with Fields of 90 kG, Along the [111] axis, J. Phys. Chem. 61, 282(1974). See also J. Chem Phys. 59, 4652 (1973).
13. Daudin, B., Lacaze, A. A., and Salce, B., D_yVO_4-$Gd_3Ga_5O_{12}$: A Composite material to Achieve Magnetic Refrigeration Using a Cycle with Internal Heat Transfer, Cryogenics 22, 439 (1982).
14. Hashimoto, T., Numazawa, T., Shino, M., and Okada, T., Magnetic Refrigeration in the Temperature Range from 10 K to Room Temperature: the Ferromagnetic Refrigerants, Cryog. 21, 647 (1981).
15. Azhar, A. A., Mitescu, C. D., Johansen, H. R., Zima, C. B., and Barclay, J. A., Specific Heat of GdRh, paper accepted to be presented at the 30th Annual Conf. on Magnetism and Magnetic Materials, San Diego, Nov. 1984.
16. Buschow, K. H. J., Clyhock, J. F., and Nieuwenhuys, A. R., Extremely Large Heat Capacities between 4 and 10 K, Cryogenics 15, 261(1975).
17. Lacaze, A. F., Beranger, R., Bon Mardion, G., Claudet, G., and Lacaze, A. A. Double Acting Reciprcating Magnetic Refrigerator: Recent Improvements, Adv. Cryog. Eng. 29, 573 (1984).
18. Hashimoto, T., Numazawa, T., and Naro, T., The Carnot type Magnetic Refrigeration Below 4.2 K: Computer Simulation, Adv. Cryog. Eng. 29, 589 (1984).
19. Pratt, W. P., Jr., Rosenblum, S. S., Steyert, W. A., and Barclay, J. A., A Continuous Demagnetization Refrigerator Operating near 2 K and a Study of Magnetic Refrigerants, Cryo. 17, 689 (1977).
20. Barclay, J. A., Hoze, O., and Paterson, L., A Reciprocating Magnetic Refrigerator from 2-4K Operation: Initial Results, J. Appl. Phys. 50, 5870 (1979).
21. Tolman, R. C., and Fine, P. C., On the Irreversible Production of Entropy, Rev. Mod. Phys. 20, 51 (1948).
22. Jacobs, R. B., The Efficiency of an Ideal Refrigerator, Adv. in Cryog. Eng. 7, 567 (1962).
23. McConnell, P. M., Liquid Helium Pumps, NBSIR 73-316 (AFAPL-TR-73-72) June, 1973.
24. Bejan, A., Second Law Analysis in Heat Transfer and Thermal Design, in Adv. in Heat Transfer, 15, 1 (1982)
25. Kadi, F. J., and Longsworth, R. C., An Assessment and Study of Existing Concepts and Methods of Cryogenic Refrigeration for Superconducting Transmission Cables, Air Pdts. and Chem. Inc. Report COO-0255206.
26. See, for example, the critical current vs field curves from I.G.C. 1875 Thomston Ave., Waterbury, CT. 06704.
27. Private Communication - O. Weinstein, Hughes Aircraft Corporation
28. Private Communication - B. Johnson, Jet Propulsion Laboratory
29. Private Communication - J. L. Smith Jr., M.I.T.
30. Private Communication - A. Lacaze, Grenoble
31. Nakagome, H., Tanji, M., Horigami, O., Ogivara, M., Numazawa, T., Watanabe, Y., and Hashimoto, T., The Helium Refrigerator I.: Development and Experimental Results, Adv. Cryog. Eng. 29, 581 (1984).

D4

RECIPROCATING MAGNETIC REFRIGERATOR

Dean L. Johnson

Jet Propulsion Laboratory,
California Institute of Technology,
Pasadena, CA, USA

The Jet Propulsion Laboratory is developing a 4-15 K magnetic refrigerator to test as an alternative to the Joule-Thomson circuit as the low temperature stage of a 4-300 K closed-cycle refrigerator. The reciprocating magnetic refrigerator consists of two matrices of gadolinium gallium garnet spheres located in tandem on a single piston which alternately moves each matrix into a 7 tesla magnetic field. A separate helium gas circuit is used as the heat exchange mechanism for the low and the high temperature extremes of the magnetic refrigerator. Details of the design and results of the initial refrigerator component tests are presented.

Key words: Closed cycle refrigerators; expansion engine; gadolinium gallium garnet; gas pumps; magnetic refrigeration.

1. Introduction

In the past few years a lot of interest has been generated towards designing and developing a continuously operating 4 K magnetic refrigeration stage for a closed cycle refrigerator (CCR) [1-4]. Its potential for high efficiency performance makes magnetic refrigeration a likely alternative to the passively operating, but highly inefficient Joule-Thomson circuit. The success of the magnetic refrigerator for this temperature range will depend on the development of suitable design approaches to answer questions of heat transfer effectiveness, helium gas movement, wear rates of materials and expected life cycles of the refrigerator components.

The Jet Propulsion Laboratory (JPL) has initiated the development of a 4-15 K magnetic refrigerator to assess its potential as a replacement to the Joule-Thomson circuit of a closed cycle refrigerator [5]. JPL has been using 1 Watt at 4.5 K closed cycle refrigerators since 1965 for cooling the low-noise maser amplifiers required to receive very weak signals from spacecraft in deep space. Up to 30 CCRs are in near continuous operation in the Deep Space Communications Network that JPL operates for the National Aeronautics and Space Administration. These CCRs log approximately one quarter of a million hours annually. The successful development of a magnetic refrigerator would reduce the overall life-cycle costs of the CCR by reducing the electrical power consumption of the CCR and by insuring a longer MTBF for the operating refrigerator.

The design of the engineering model 4-15 K magnetic refrigerator under development at JPL addresses the basic requirements of refrigeration power, DC field stability, reliability and efficiency. It is the objective of this paper to describe the design of the magnetic refrigerator, discuss the component test results, and provide a status of the development effort.

2. Experimental design

Choice of the magnetic refrigerator design must depend ultimately on the device it is to cool, in this case the maser, an ultrasensitive microwave signal amplifier whose performance depends critically on a stable DC magnetic field, and on a low operating temperature having milliKelvin stability. The refrigerator package for the maser must be orientation independent since it is located in the feedcone of a large tracking antenna which points anywhere from horizon to zenith. The design requirements for the magnetic refrigeration system is therefore quite stringent. The design of the engineering model presently under development addresses only the basic requirements of refrigeration capacity, DC field stability, reliability and efficiency. The reciprocating design has been selected for its relative' simpler fabrication requirements and the greater ease with which the experimental results could be verified theoretically.

The schematic of the magnetic refrigerator design is shown in figure 1. All components have been fabricated at JPL. The major components are shown in figure 2. The CTI Model 1020 expansion engine provides the high temperature heat sink for the magnetic refrigerator and is capable of producing better than 9 W of refrigeration at 15 K. This refrigeration capacity is a major determining factor in the final 4 K cooling power of the magnetic refrigerator. The hydrogen heat switch is used during initial cooldowns to precool the helium dewar and magnet assembly to 20 K before liquid helium is transferred into the dewar. This experimental design presently calls for the external transfer of liquid helium to cool the magnet; future designs will require the magnetic refrigerator stage to provide the parasitic refrigeration requirements of the magnet.

The 7 T magnetic field is supplied by a 10.2 cm NbTi solenoid having a 6.3 cm bore. The magnet is operated in persistent mode. When the magnet is fully charged, the current leads will be detached at the magnet to minimize heat leak into the liquid helium bath. Quench protection of the magnet is provided by a short length of stainless tubing attached across the magnet leads and immersed in the liquid helium bath. The magnet is encased with a magnetically soft material, Hiperco (Carpenter Technology Corp., Reading, PA), having a saturation induction of 2.4 T. The Hiperco is used to entrap much of the magnetic flux exiting from the bore of the magnet.

The piston is driven with a 185 W (1/4 H-P) speed-controllable gearmotor. This rotational motion is converted to reciprocating motion by means of a "ball reverser" (Norco, Inc., Georgetown, CT), a nut with ball bearings that run in a cross-hatched track cut into the drive shaft. The track has a set stroke length of 9.2 cm and provides a displacement of $3.175\ \text{cm}/2\pi$ rad. A 10 rad/s rotation rate for the gearmotor translates to a 5.1 cm/s linear speed for the GGG piston and to a cycle frequency of 0.28 Hz. A turn-around in the ends of the track automatically reverse the direction of travel of the nut to provide smooth reciprocating motion without reversing the direction of rotation of the drive motor. A rotary ferrofluidic feedthrough (Ferrofluidics Corp., Nashua, NH) couples the gearmotor to the ball reverser, which is housed in the helium gas of the magnetic piston circuit. This eliminates the requirement for reciprocating vacuum seals on the piston drive shaft.

The key components of the 4-15 K magnetic refrigerator are the cylinder assembly and the piston containing the paramagnetic material. The cylinder assembly is made of thin-wall stainless steel and provides the ducts through which the heat exchange fluid flows (Fig. 2). The ducts are made from thin-wall rectangular waveguide to minimize the annular gap between the piston and the magnet. The phenolic piston is machined in three parts -- two thin-wall cups to contain the porous $Gd_3Ga_5O_{12}$ (GGG) matrices and a solid center section to separate the matrices (Fig. 2). Threads were cut into each piece to facilitate both the assembly of the piston and the modifications to the matrices. Each compartment is 33 mm long and 38 mm in diameter and is filled with 160 gm of 1.1 mm diameter GGG spheres for a fill factor of about 60%. Stainless screens are inserted in each end of the compartment to prevent the GGG from migrating out the holes in the piston.

The use of the two matrices doubles the heat removal capacity per cycle of the piston and provides a more continuous transfer of heat to help reduce temperature fluctuations. The 4.2 K cooling power of the magnetic stage operating ideally in a Carnot cycle can be given as

$$\dot{Q}_C = nT_C v \Delta S \eta$$

where n is the number of moles of Gd^{3+} in the matrices, T_C is the refrigeration temperature, ν is the frequency of operation and ΔS is the change in entropy during the isothermal demagnetization, and η is the fraction of Carnot efficiency at which the magnetic refrigeration stage operates. In this design there is 0.948 moles of Gd^{3+}, and if the matrix cycles between 0.5 T and 6.5 T over the temperature span of 4 K and 16 K we can assume ΔS is 0.3R (which takes into account the entropy change of the GGG minus the entropy change of the entrained helium gas), then the refrigeration power at 4.2 K is

$$\dot{Q}_C = 9.9 \nu \eta \text{ W}.$$

Some of the factors effecting the efficiency are the thermal heat leaks along the cylinder wall and the drive shaft, the heat capacities of the piston and cylinder, and the heat transfer between the gas and the GGG matrices. These factors ccontributing to the loss of cooling power of the refrigerator will be identified and minimized during refrigerator testing. No attempt will be made to calculate these effects here. To minimize the internal heat load due to the entrained helium, the helium gas pressure will need to be kept below about 0.1 MPa.

Helium gas provides the heat transfer between either matrix and the low-temperature source and the high-temperature sink. When the GGG matrix is positioned adjacent to a gas duct in the cylinder, helium gas is forced through the holes on one end of the matrix compartment, through the porous matrix, and out the set of holes on the other end of the compartment (fig. 3). The ridge in the center prevents gas leakage along the outside of the piston. The indents in the outer surface of the piston allow the gas to flow through the matrices while the displacer is still in motion so that gas flow need not be limited to the time the piston is positioned at the ends of the stroke. The placement of the gas ports in the cylinder and the geometry of the piston eliminate the need for mechanical valves at these low temperatures. During this portion of the cycle the refrigerator operates in an isothermal fashion. As the piston is then moved from one end of the stroke to the other, the outer ridges of the piston act as close tolerance seals to prevent the gas from either circuit from passing along the cylinder wall and thermally short-circuiting the matrices. The low-friction fiberglass-impregnated teflon seals further insure that the gas leakage is minimized. This allows the matrices to magnetize or demagnetize in an adiabatic fashion. Thus the cycle of the piston should approximate the Carnot cycle.

Heat exchangers filled with phosphor-bronze screens are used to transfer heat between the helium gas in the circuits and the heat source or the heat sink. Fluid flow through the gas circuits is produced by separate linear-induction, positive-displacement pumps in both the low- and high-temperature gas circuits. The two gas pumps are driven back and forth in phase relation to the motion of the GGG piston. The pumps easily develop the low pressure head required to overcome the pressure drop through the GGG matrices and the heat exchangers. These pumps have been operated successfully at low temperatures but their long-term performance has not yet been determined.

3. Component Test Results

The use of the Hiperco surrounding the magnet provides a more rapid transition between the high field and low field regions enabling a shortened stroke length for the GGG piston. Figure 4 compares the measured axial magnetic field profile of the solenoid with and without the Hiperco and shows the position of the piston at the end of the stroke. At either end of the stroke, the axial field at the position of the center of the two GGG matrices is 0.5 T and 6.5 T, with a maximum ±7% change in the measured axial field over the length of the GGG matrix in both the high-field and the low-field regions.

The magnetic field pulls both GGG matrices towards the center of the magnet. The magnitude of this attractive force depends on both the magnitude and gradient of the magnetic field which, for cylindrical symmetry, may be approximated by $F_z = m_z (\partial B_z / \partial z)$, where F_z, m_z, and B_z are the axial components of the force, the GGG magnetization and the magnetic field, respectively. The use of the Hiperco to shape the 7 T field has generated a magnetic field gradient of 105 T/m which produces a force as high as 1550 N on each of the 160 gm GGG matrices at 4.2 K. This large force dictates the need for careful positioning of the matrices to provide adequate force balancing. From the force equation the first choice made was to position the matrices so as to coincide with

the distance between the maxima in the field gradient. Figure 5 shows the measured force required to move the 4.2 K piston through the magnetic field, with the maximum net force being measured as 630 N. This force could be reduced by decreasing the separation distance between the two matrices. This reduction in force is desirable to reduce the power needed to drive the piston. However the matrices then move through a different portion of the magnetic field profile which will have an unknown effect on the refrigerator performance. These effects will be examined during testing of the magnetic refrigerator. Additional force compensation, if needed, may be provided by imbedding small slugs of GGG in the center section of the piston so as to be thermally isolated and not a part of the refrigeration process.

4. Conclusion

The high reliability of the individual components should result in a high reliability for the magnetic refrigerator as well. The gearmotor has been overdesigned to handle the anticipated large loads for smooth operation at slow speeds. Operation at these slow speeds will minimize the wear rate on the low-temperature sliding seals. The magnetic refrigerator has been designed to minimize the problems associated with gas contamination. The magnetic refrigerator stage is a closed gas loop system; the gas circuit is sealed after the initial charge of helium gas. The internal gas displacers eliminate the need for an external compressor to provide the gas flow. The external and internal portions of the piston drive train are coupled together with a rotary seal to prevent gas contamination entering the circuit along the drive shaft. The magnetic refrigerator also requires no small orifices as with the Joule-Thomson valve, further minimizing the problems associated with gas contamination. Elimination of the Joule-Thomson circuit can reduce the input power requirements for the compressor by about a third.

The design of the reciprocating magnetic refrigerator to pump heat from 4 K to 15 K has been presented. Initial tests to examine the field shaping ability of the Hiperco and to measure the resulting magnetic forces on the GGG piston have been made in an open-cycle dewar. Further testing to reduce the magnetic force through field shaping will be made in the assembled refrigerator so that the refrigerator performance may be measured as well. The magnetic refrigerator is currently being assembled.

The research described in this paper was performed by the Jet Propulsion Laboratory, California Institute of Technology, under contract with the National Aeronautics and Space Administration.

5. References

[1] Van Geuns, J.R., A study of a new magnetic refrigerating cycle. Philips Res. Rep. Suppl. 6:1 (1966).

[2] Nakagome, H., Tanji, N., Horigami, O., Numazawa, T., Watanabe, Y., and Hashimoto, T., The helium magnetic refrigerator I: Development and experimental results. Advances in Cryogenic Engineering Vol. 29, Plenum Press, New York (1984).

[3] Barclay, J.A., Overton, Jr., W.C., Stewart, W.F. and Steyert, W.A., Magnetic refrigeration for 4-20 K applications'. Technical Report AFWAL-TR-83-3120 (Dec. 1983).

[4] Lacaze, A.F., Claudet, G., Lacaze, A.A., and Seyfert, P., Prospects in Magnetic Refrigeration Proceedings of the ICEC10: Paper A1-2, Helsinki (1984).

[5] Deardorff, D.D. and Johnson, D.L., Magnetic refrigeration development. The Telecommunications and Data Aquisition, Progress Report 42-78, pp 49-58, Jet Propulsion Laboratory, Pasadena, CA (July 84).

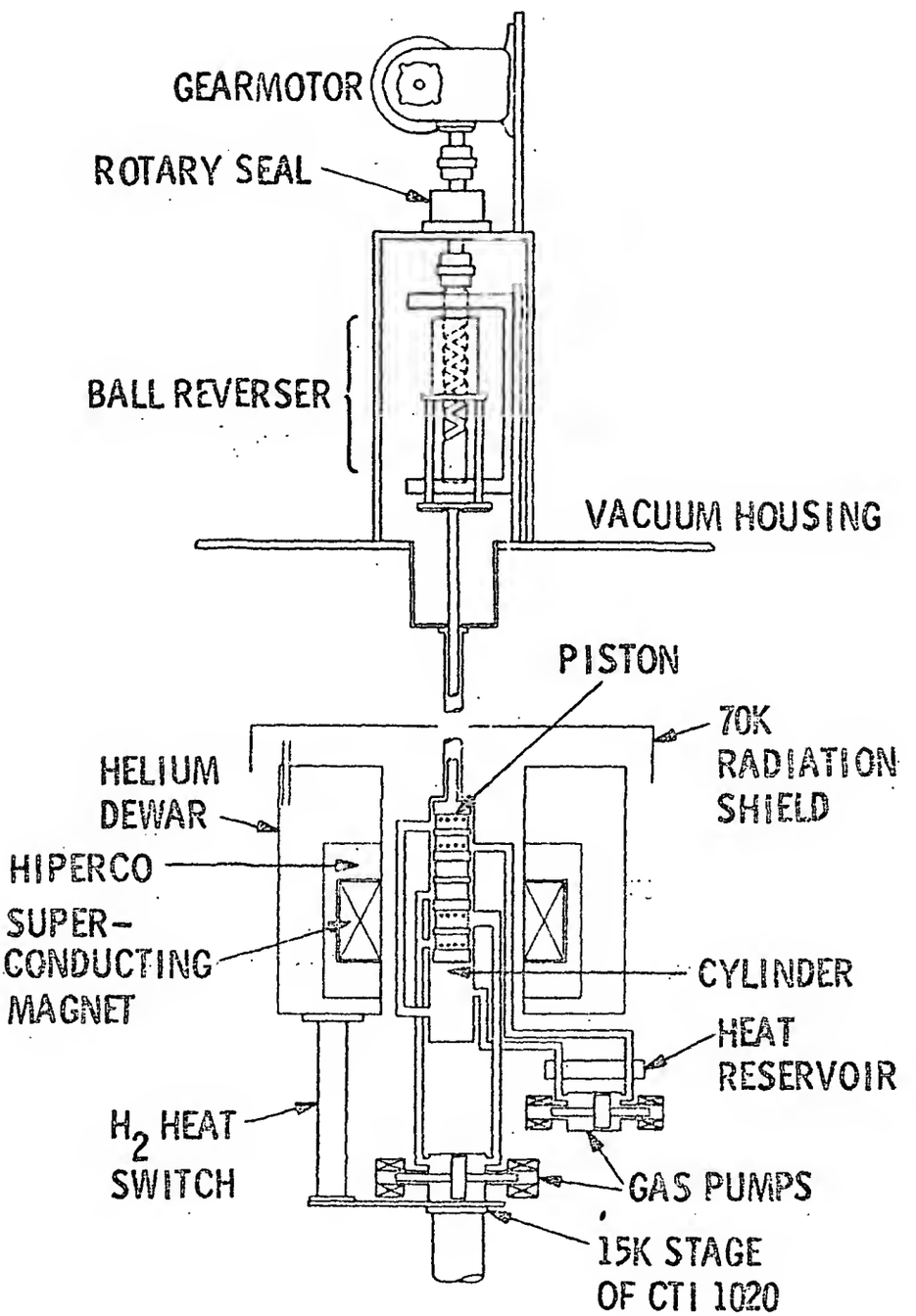

Fig. 1 Schematic of the magnetic refrigerator.

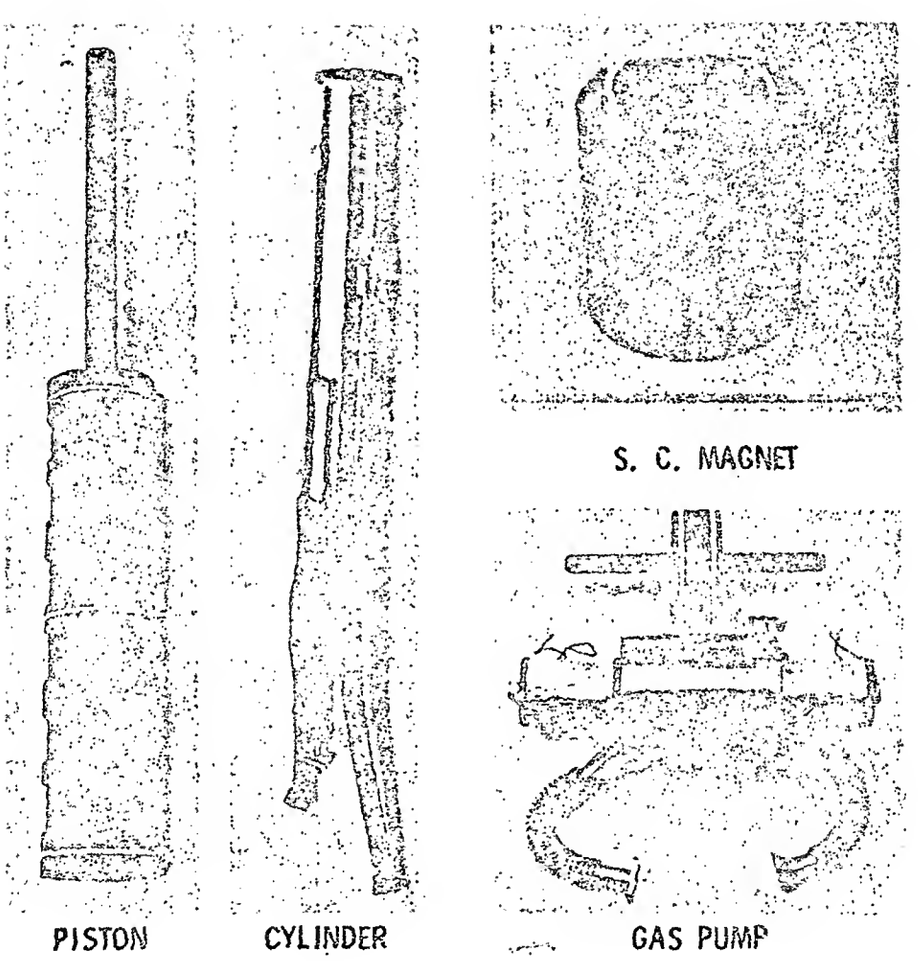

Fig. 2 Magnetic refrigerator components.

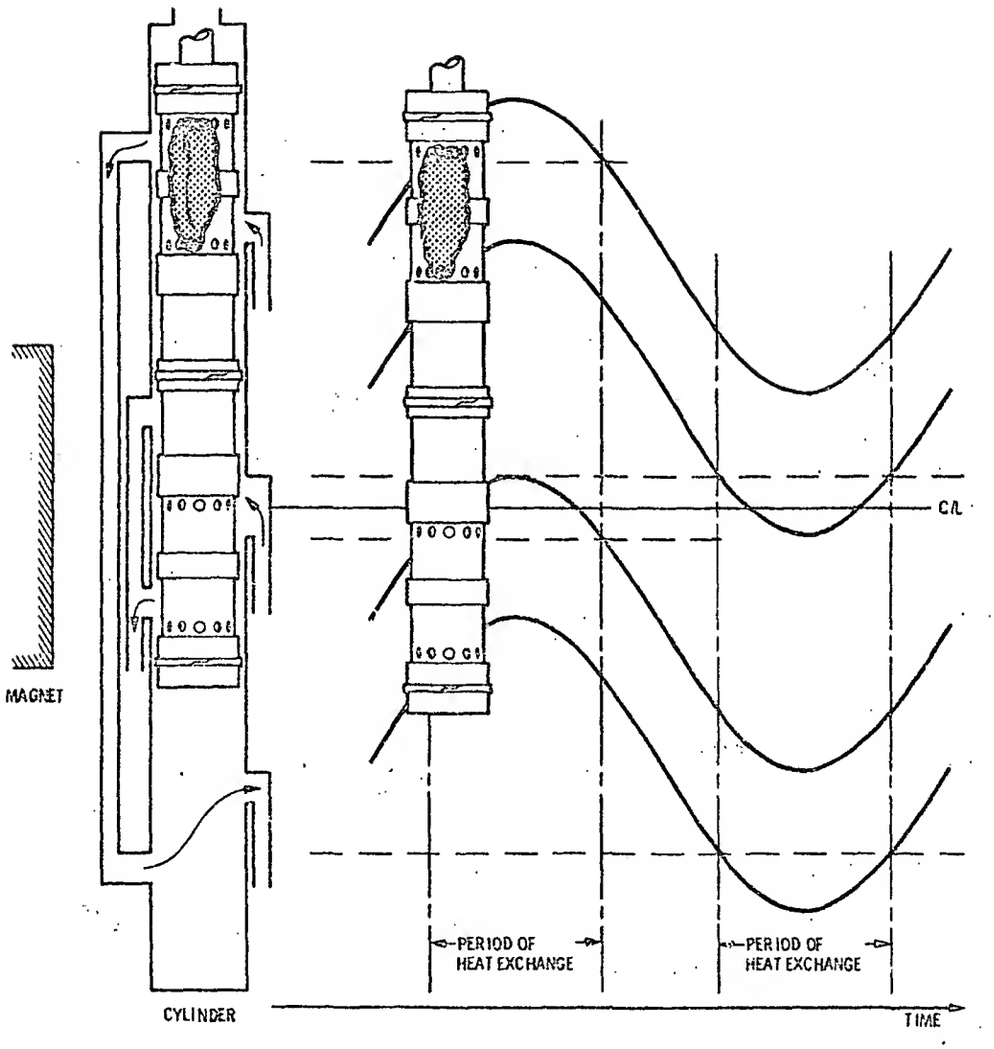

Fig. 3 Schematic showing the time during one cycle of the piston when the indents align with the gas ducts to allow the heat exchange gas to flow through the GGG matrices.

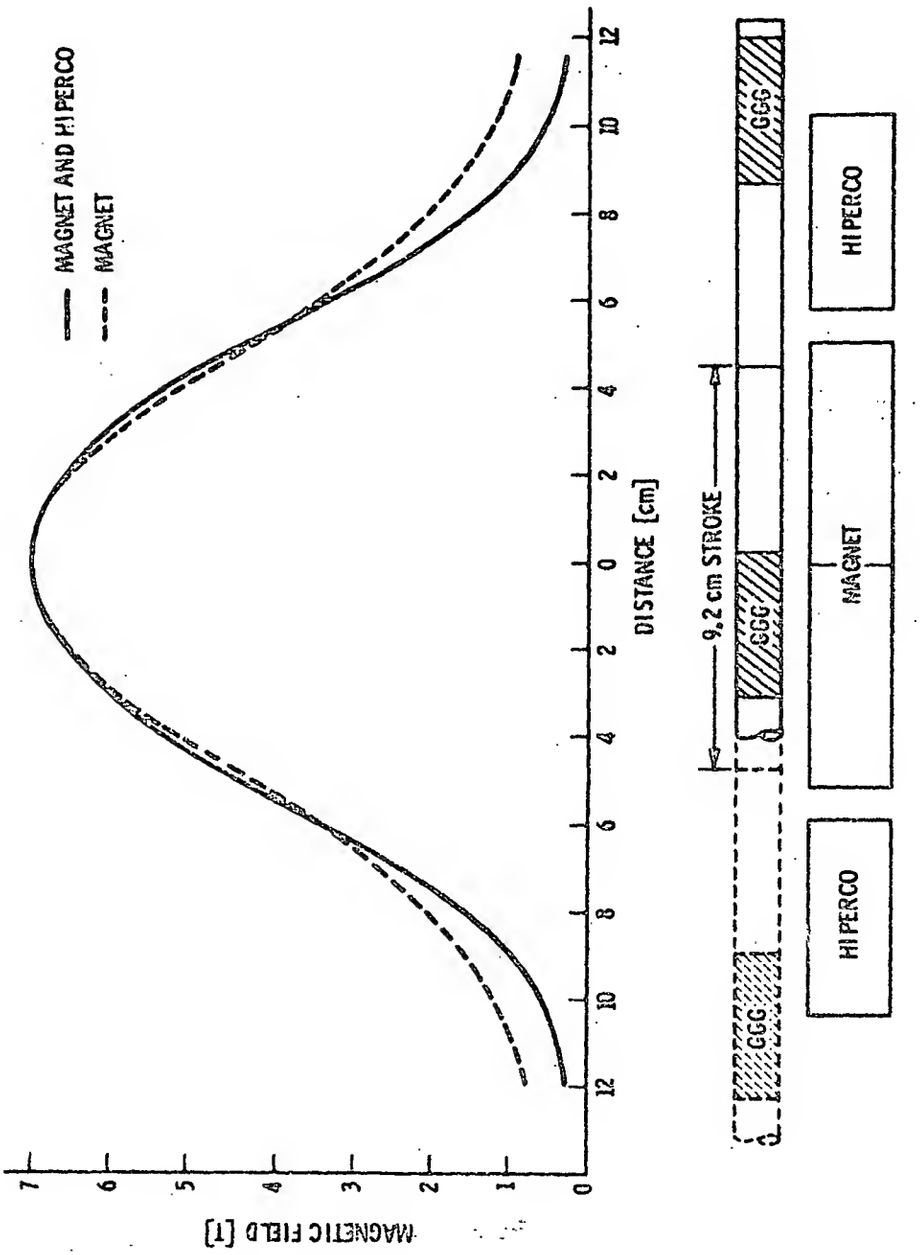

Fig. 4 Comparison of the measured axial magnetic field profiles with and without the Hiperco material. The extreme positions of the piston are shown with respect to the field profiles.

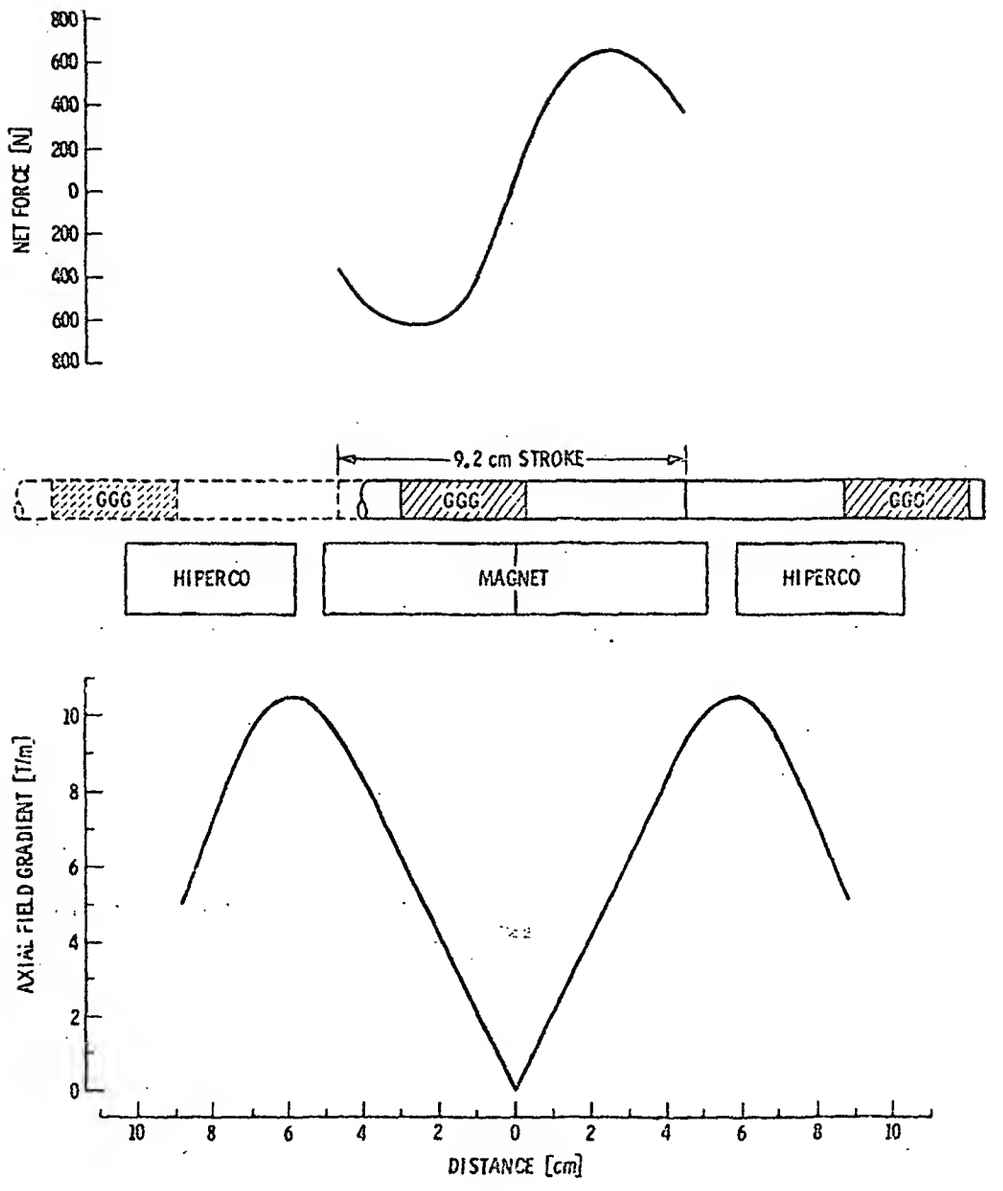

Fig. 5 a) The measured net force required to move the piston through the magnetic field. b) The magnitude of the axial field gradient for the magnet/Hiperco assembly. The extreme positions of the piston are shown with respect to these curves.

IMPROVED HEAT SWITCH FOR GAS SORPTION COMPRESSOR

Chung K. Chan

Jet Propulsion Laboratory
California Institute of Technology
4800 Oak Grove Drive
Pasadena, California 91109

Thermal conductivities of the charcoal bed and the copper matrix for the gas adsorption compressor were measured by the concentric-cylinder method. The presence of the copper matrix in the charcoal bed enhanced the bed conductance by at least an order of magnitude. Thermal capacities of the adsorbent cell as well as the heat leaks of two compressor designs were measured by the transient method. The new gas adsorption compressor had a heat switch that could transfer eight times more heat than the previous one. Because of this, the cycle time for the new prototype compressor was also improved by a factor of eight to within the minute range.

Key words: Charcoal bed; copper foam; gas adsorption; gas heat switch; heat capacitance; refrigerator; switch ratio; thermal conductance.

1. Introduction

In the gas sorption refrigeration cycle, whether it is the gas adsorption system [1,2] or the gas absorption system [3,4], the sorption (adsorbent or absorbent) bed must be cycled between the temperature of the heat source and the temperature of the reservoir to which heat is being rejected. Thus, making and breaking thermal contacts of the sorption bed with the reservoirs are essential operations. A similar situation exists for the salt bed of the magnetic refrigerator. Heat switches based upon different physical mechanisms have been developed. Mechanically actuated heat switches [5] have been proved unreliable at cryogenic temperatures, and require large contact force. Magnetoresistive heat switches [6] are, except at very low temperatures, of very low efficiency and require a magnetic field. Gaseous thermal switches [7,8] which are probably the oldest idea, depend on the switching action resulting from the presence or absence of the gas. Efficient gaseous switches require a small gas gap but large heat transfer areas which are sometimes hard to achieve. Since the primary goal of the sorption refrigerators is one of lifetime and reliability, it was decided to use a reliable gas heat switch for the adsorption compressor [9].

Since the switching function in the gaseous heat switch is accomplished by the presence and absence of the gas between two surfaces, gas supply and a suction pump are required. These functions are provided by an adsorption pump connected to the switch. In our earlier gas adsorption compressor (GAR-I) [9] the heat switch in each compressor unit was controlled by a miniature pump. In our current modular design (GAR-II), each compressor unit has one heat switch but four heat switches are controlled by one pump [10].

One majc difficulty in the gas adsorption or desorption process is to transport heat into and out of the porous media rapidly. In the GAR-I design, because of this limitation, the cycle time of the gas sorption refrigerator was in the range of six to fifteen minutes. This time was too long for a practical refrigerator. As an ongoing development effort of nonmechanical (gas adsorption or absorption) refrigerators for spaceborne instruments, research has been performed to study the heat transfer characteristics of the porous charcoal medium, the porous medium enhanced by a metal matrix, and the gas heat switch. This paper presents the results of these research efforts that lead to the construct :n of the rapidly cycled compressor [10].

2. Thermal conductance and gas adsorption compressor designs

The thermal properties of charcoal beds with heat transfer enhancement element are essential data for compressor design and performance analyses. The thermal conductivity of a bed of charc · was measured in the temperature range between 20C and 475C, using a conventional steady-state method, the so-called concentric-cylinder method, with the inner cylinder being a heater. The charcoal particles (200 μm - 400 μm in size) were filled into the space between the heater and an outer stainless steel cylinder. The heat flow was radial as the length of the cylinder (L) was large (5.1 cm) compared to the distance between the cylindrical shells (0.85 cm). The temperature gradient due to the radial heat flow was measured by two thermocouples located at radii r_i and r_o, close to the mid-point of the cylinder. The thermal conductance k of the bed was calculated from the following relation:

$$k = \frac{\dot{Q}\ln(r_o/r_i)}{2\pi L(T_i - T_o)} \qquad (1)$$

where k = thermal conductance (W/cmK)
$\dot{Q}$ = power of the central heater (Watt)
T_i, T_o = temperatures measured at radii r_i, r_o, respectively

With r_i = 0.31 cm and r_o = 1.17 cm, the results for the thermal conductivities k of the charcoal bed are listed in Table 1. Thermal conductivities between 1.17×10^{-3} W/cmK and 1.26×10^{-3} W/cmK are found. These values are in the same order of magnitude as those of the zeolite bed reported in the literature [11].

Table 1. Thermal conductance of charcoal bed

T_i(C)	T_o(C)	$\dot{Q}$(W)	$k\left(\frac{W}{cmK}\right)$
229	59	4.45	1.17×10^{-3}
295	78	6.24	1.17×10^{-3}
365	90	8.19	1.22×10^{-3}
420	104	9.49	1.23×10^{-3}
475	116	11.12	1.26×10^{-3}

The thermal conductivity of a copper foam (3% by volume) was determined by the similar method and the value was listed in Table 2. It was observed that the copper foam had thermal conductivity an order of magnitude better than the charcoal bed. Hence, when the charcoal was packed into the copper foam matrix, the thermal conductance of the bed would be increased by an order of magnitude. Because of this heat enhancement, in our earlier adsorption compressor (GAR-I), as shown in Fig. 1, 7.38 gm of charcoal which was confined within a stainless steel cylinder of volume 14.35 cm^3, was packed into the open foam copper matrix. The temperature of the adsorbent cell was controlled by a 40 W heater and a gas heat switch gap to a 77 K heat sink. The presence and absence of the gas in the gap are controlled by a miniature adsorption pump containing a small amount of charcoal. A schematic of the adsorbent bed, the heat switch and the miniature pump is shown in Fig. 1.

Table 2. Thermal conductance of copper foam

T_i(C)	T_o(C)	$\dot{Q}$(W)	$k\left(\frac{W}{cmK}\right)$
46	44	2.15	0.040
76	69	4.66	0.026
144	130	11.28	0.033
195	170	16.7	0.027
274	227	28.1	0.024

The heat path from the adsorbent bed to the 77 K heat sink passes through the porous bed and the stainless steel wall and is interrupted by the 0.18 mm annular gap between the inner stainless steel cylinder and the outer brass cylinder before it reaches the 77 K heat sink. The gap may be vacuum or filled with hydrogen gas through the stainless-steel capillary tube C, depending on the temperature of the miniature adsorption pump. The pump is maintained in weak thermal contact with the heat sink through an appropriately sized wire. A heater and a silicon diode were attached to the pump chamber.

The pump chamber was leak tested, vacuum outgassed and backfilled with hydrogen at 77 K and 200 torr. At that temperature all the gas was adsorbed onto the charcoal and there was no gas in the heat switch gap, i.e., the heat switch was off. When the pump was heated to about 110 K, the gas was released and the pressure built up. Hydrogen began to flow from the pump to the gas gap, i.e., the switch was on. Hydrogen was chosen because of its relative high thermal conductivity. The test results are presented in the next session.

The new refrigerator design (GAR-II) of 250 mW at 20 K consists of banks of individual compressor modules. A schematic of a modular design is shown in Fig. 2. This design involves four banks (A, B, C and D) containing sixteen compressor modules in total. Each compressor module is a double walled cylindrical unit as shown in Fig. 3. The charcoal, confined within the stainless steel inner pressure vessel, is packed into an open copper matrix foam. The gap between the inner and the outer cylinders is the gas heat switch. The heat switches of four compressors are controlled by one miniature adsorption pump of charcoal which when heated supplies gas to the switch, turning it on and when cooled, removing gas from the switch, turning it off. Each bank has one such miniature adsorption pump, so all the compressors in each bank are cooled at the same time.

3. Transient experimental measurements and results

Transient thermal tests were performed for the GAR-I compressor (Fig. 1) and the GAR-II compressor module (Fig. 3) to determine the heat capacity of the adsorbent bed, the heat leak, and the switching capacity of the heat switch.

In the tests involving the heat capacity, both the adsorbent cell and the heat switch pump were evacuated. The adsorbent cell was then heated, and the transient temperature was recorded. As the first iteration, the heat leak was ignored and the heat capacity of the adsorbent cell $(mc_p)_{cell}$ which included the charcoal, the stainless steel vessel and the copper foam was determined by

$$(mc_p)_{cell} = \frac{\dot{Q}}{\left(\frac{dT_a}{dt}\right)} \qquad (2)$$

where $\dot{Q}$ = heat input

$\frac{dT_a}{dt}$ = transient temperature gradient of the cell

The heat leak K_L from the cell was determined by recording the temperature during the cool down of the cell:

$$K_L = \frac{(mc_p)_{cell}}{t_f - t_i} \ln\left(\frac{T_i - T_s}{T_f - T_s}\right) \tag{3}$$

where T_i, T_f are temperatures at times t_i and t_f

T_s is the heat sink temperature

With the knowledge of the heat leak, as a second iteration the heat capacity was recalculated by

$$(mc_p)_{cell} = \frac{Q - K_L(T_a - T_s)}{\left(\frac{dT_a}{dt}\right)} \tag{4}$$

where T_a is the adsorbent cell temperature.

The heat capacities of the GAR-I adsorbent cell calculated by equations (2) and (4) are shown in Fig. 4. A theoretical curve based on the properties of carbon, stainless steel and copper is also shown in the same figure for comparison. It was observed that the experimental data were about 30% higher than the theoretical prediction. Fig. 5 shows the response of the switch to the heating of the charcoal pump. Within 50 seconds the switch is conducting. The value of the conductance K can be determined from the temperature transient by an energy balance of the adsorbent cell:

$$[(mC_p)_a + (mC_p)_{s.s.} + (mC_p)_c] \frac{dT_a}{dt} = -K(T_a - T_s) \tag{5}$$

where m is the mass

C_p is the heat capacity

the subscripts a, s.s. and c represent the adsorbent, the stainless steel vessel and the copper foam, respectively

$\frac{dT_a}{dt}$ is the gradient of the temperature transient

T_s is the heat sink temperature

The thermal conductance K was plotted as a function of the mean temperature, i.e., $(T_a + T_c)/2$ in Fig. 6. The theoretical K was calculated by knowing the heat switch area A, the gap size δ and the thermal conductivity k_g of the gas as

$$K = \frac{k_g A}{\delta} \tag{6}$$

Thus, with hydrogen as the working gas, the switch of GAR-I has a conductance of 0.8W/K when the switch is on and a conductance of 0.14W/K when the switch was off, giving a switch ratio of 5.7.

Similar tests were performed for the GAR-II compressor, and the results are shown in Figs. 7, 8 and 9. The thermal conductance of this new heat switch design was found to be 8 times better than the previous design. The switch of GAR-II has a conductance of 5W/K when the switch was on and a conductance of 0.37W/K when the switch was off, giving a switch ratio of 14.

4. Conclusions

The thermal properties of the adsorbent bed and the heat switch were determined by steady state and transient experiments. Results of these heat transfer studies led to the design and the construction of a new gas sorption compressor which had a heat switch that could transfer 5 W/K of heat from a 6 cm (H) x 2.54 cm (D) cylindrical modular compressor. Because of this, the cycle time for the new prototype compressor was about one minute. Since the system weight is almost inversely proportional to the cycle time, this improvement will no doubt reduce the refrigerator weight in spaceborne missions.

The research described in this paper was carried out by the Jet Propulsion Laboratory, California Institute of Technology, through contract with the National Aeronautics and Space Administration.

5. References

[1] Chan, C. K., Cryogenic refrigeration using a low temperature heat source, Cryogenics 21, 391-399 (1981).

[2] Chan, C. K., Tward, E. and Elleman, D. D., Miniature J-T refrigerators using adsorption compressor, Advances in Cryogenic Eng. 27, 735-743 (1981).

[3] Lehrfeld, D. and Boser, O., Absorption-desorption compressor for spaceborne/airborne cryogenic refrigerators, AFFDL-TR-74-221, AF Flight Dynamics Laboratory, Wright-Patterson AFB.

[4] Jones, J., $LaNi_5$ hydride cryogenic refrigerator test hardware results, Refrigerator for Cryogenic Sensors, NASA Conference Publication 2287, 357-373 (1982).

[5] Siegwarth, J. D., A high conductance helium temperature heat switch, Cryogenics 16, No. 2, 73-76 (1976).

[6] Radebaugh, R., Electrical and thermal magnetoconductivities of single-crystal beryllium at low temperatures and its use as a heat switch, J. of Low Temperature Physics 27, 91-105 (1977).

[7] Torre, J. P. and Chanin, G., Heat switch for liquid helium temperatures, Rev. Sci. Instrum. 55, 213-215 (1984).

[8] Tward, E., Gas heat switches, NBS Special Publication 607, Boulder, CO, 178-187 (1981).

[9] Chan, C. K., Tward, E., and Elleman, D. D., Kinetics of gas adsorption compressor, Advances in Cryogenic Engineering 29, 533-542, (1983).

[10] Chan, C. K., Performance of rapid cycled gas adsorption compressor, paper presented at the 10th International Cryogenic Conference, Helsinki, Finland, July 31-August 3, 1984.

[11] Volkl, J., Heat conduction in zeolite beds, Heat Transfer 1982, 2, C018, 105-108.

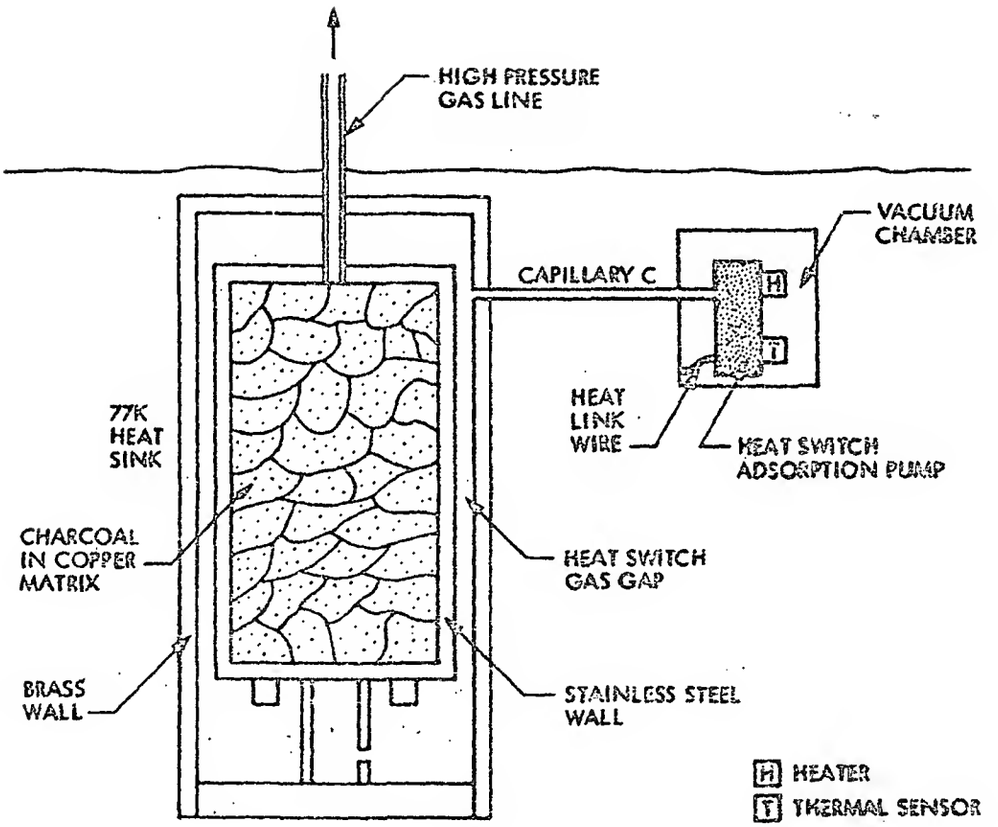

FIG. 1. GAR - I COMPRESSOR

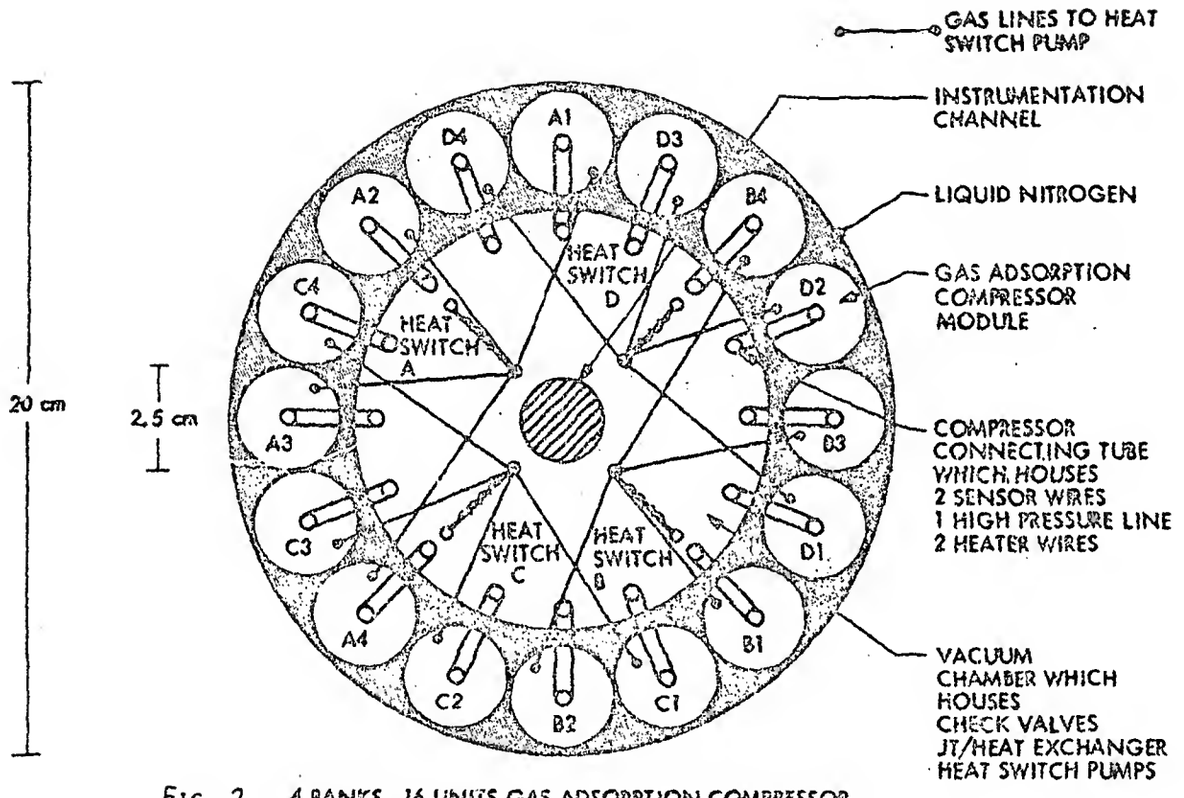

FIG. 2. 4 BANKS, 16 UNITS GAS ADSORPTION COMPRESSOR MODULAR DESIGN

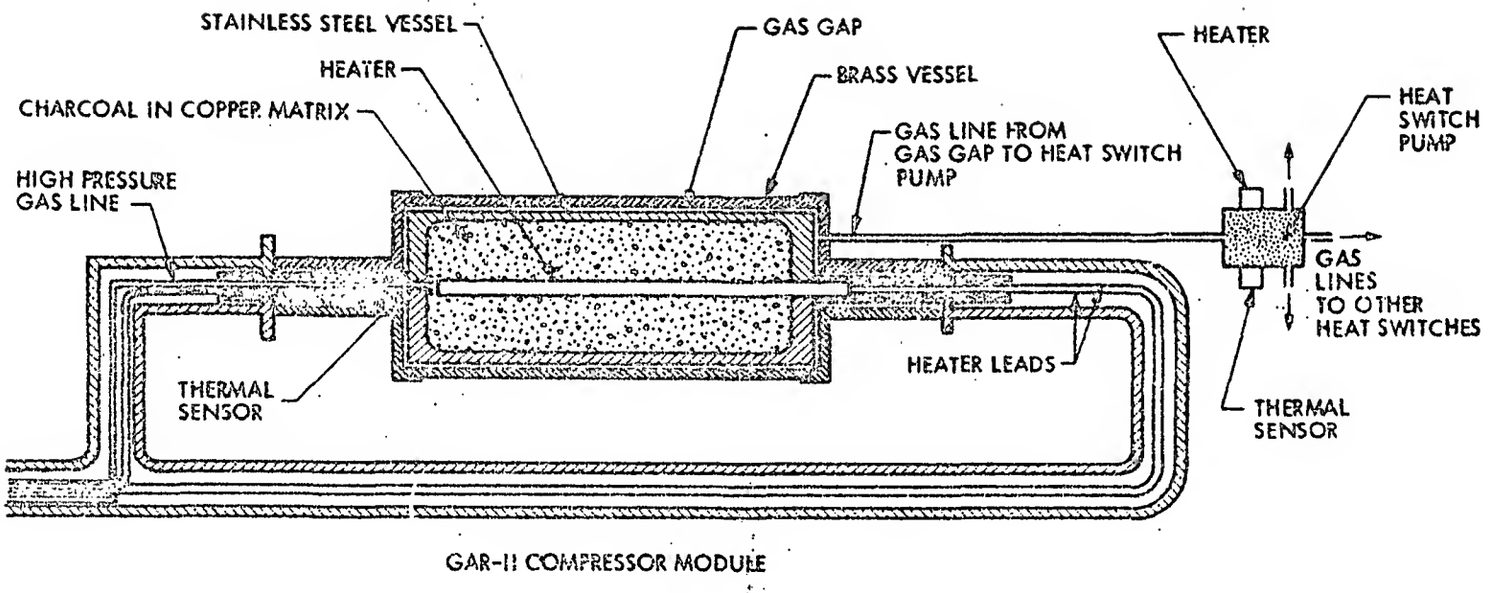

FIG. 3. GAR - II COMPRESSOR MODULE

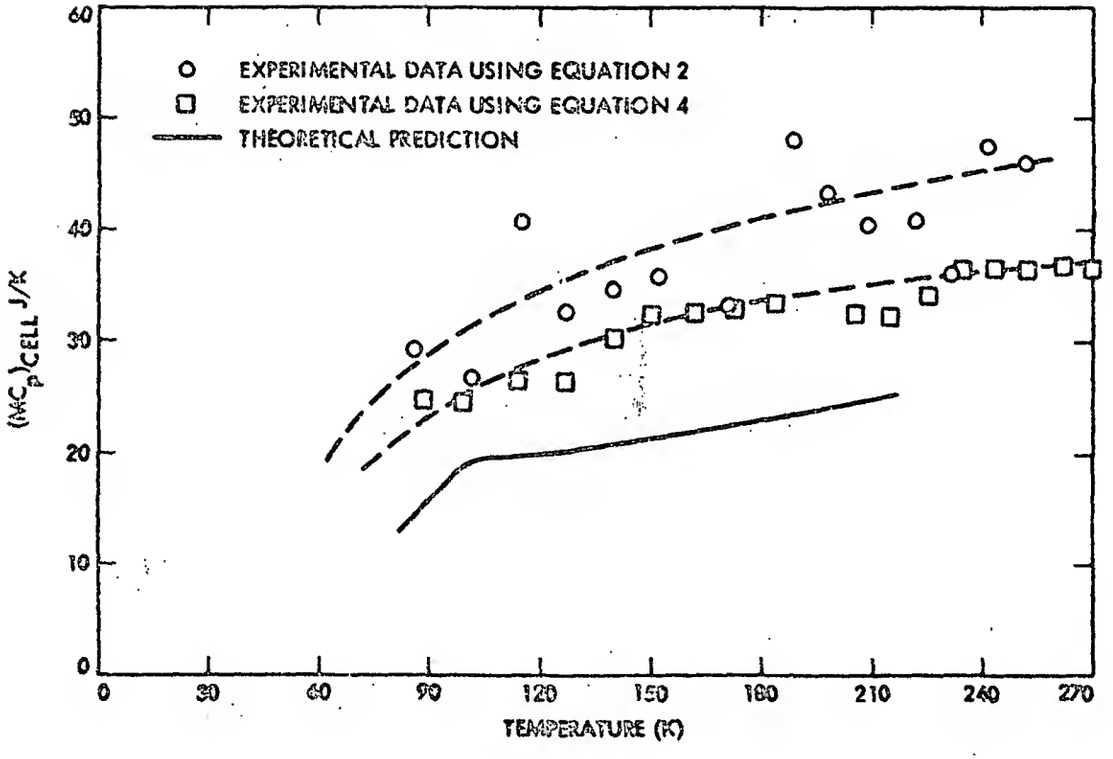

FIG. 4. HEAT CAPACITANCE OF THE GAR-I ADSORPTION CELL

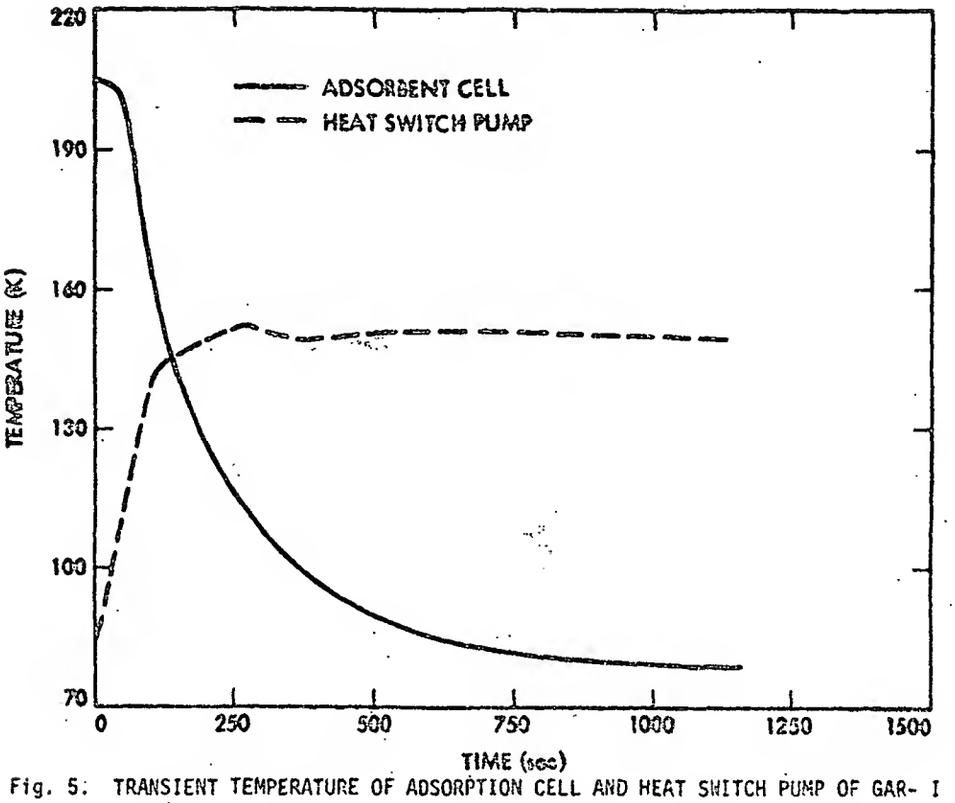

Fig. 5: TRANSIENT TEMPERATURE OF ADSORPTION CELL AND HEAT SWITCH PUMP OF GAR- I

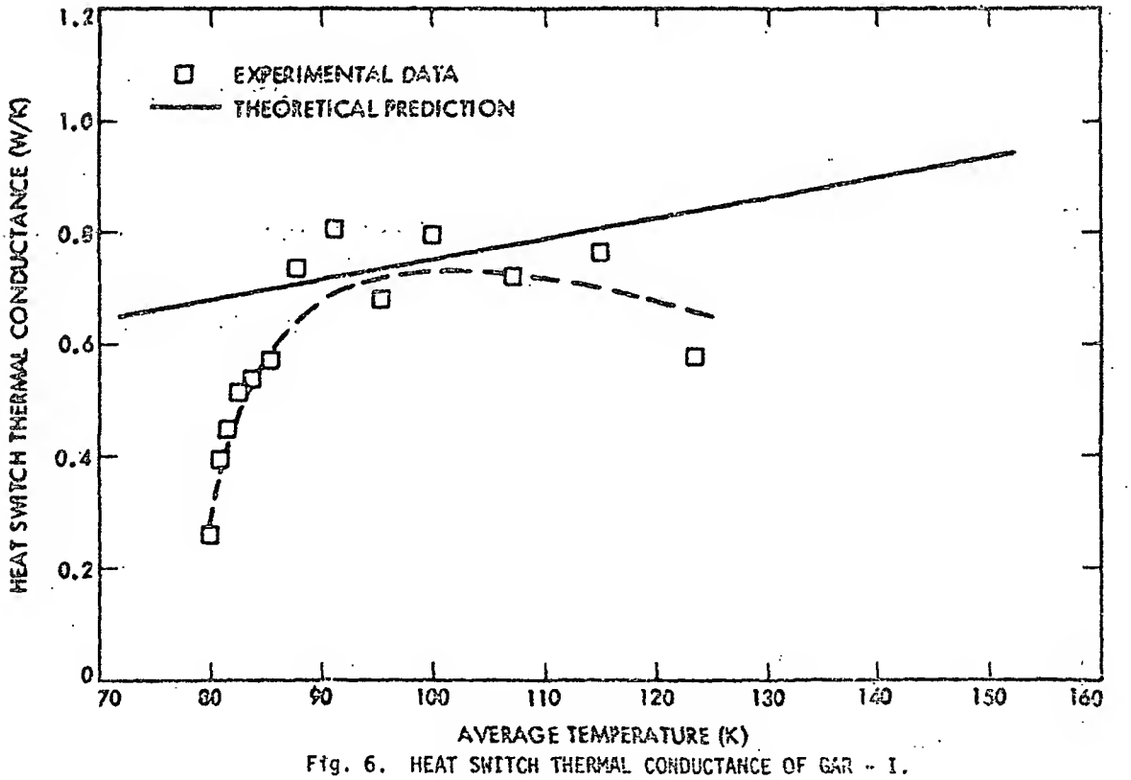

Fig. 6. HEAT SWITCH THERMAL CONDUCTANCE OF GAR - I.

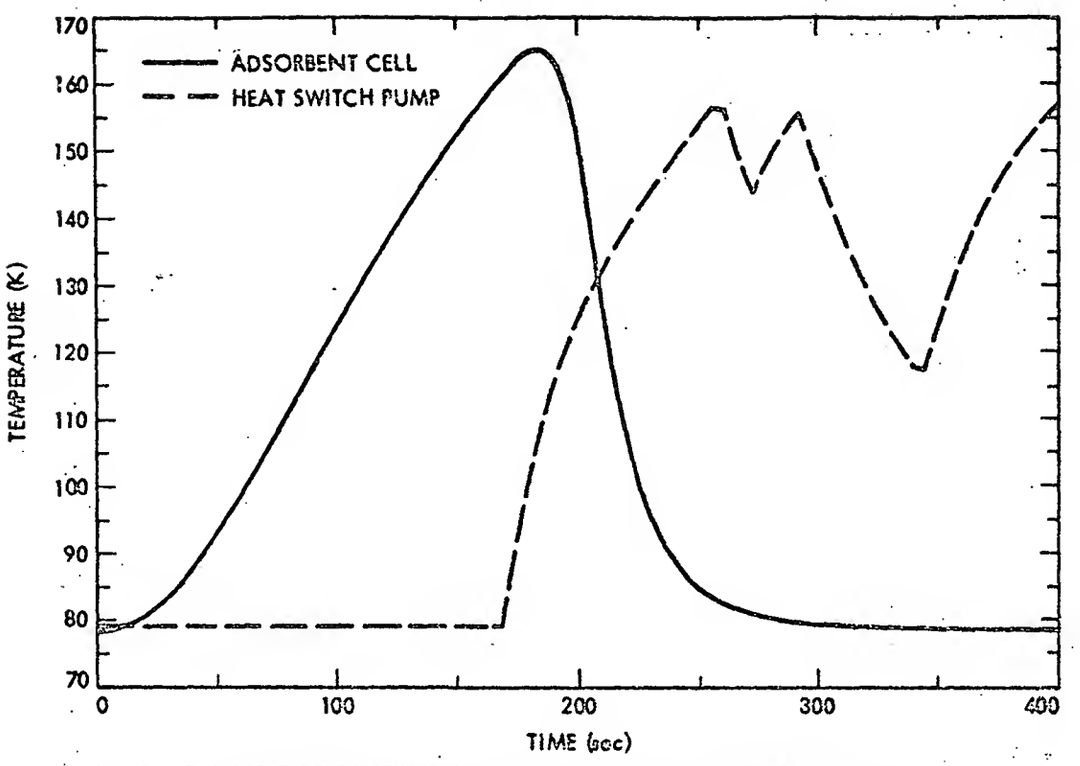

Fig. 7. TRANSIENT TEMPERATURES OF ADSORBENT CELL AND HEAT SWITCH PUMP OF GAR - II.

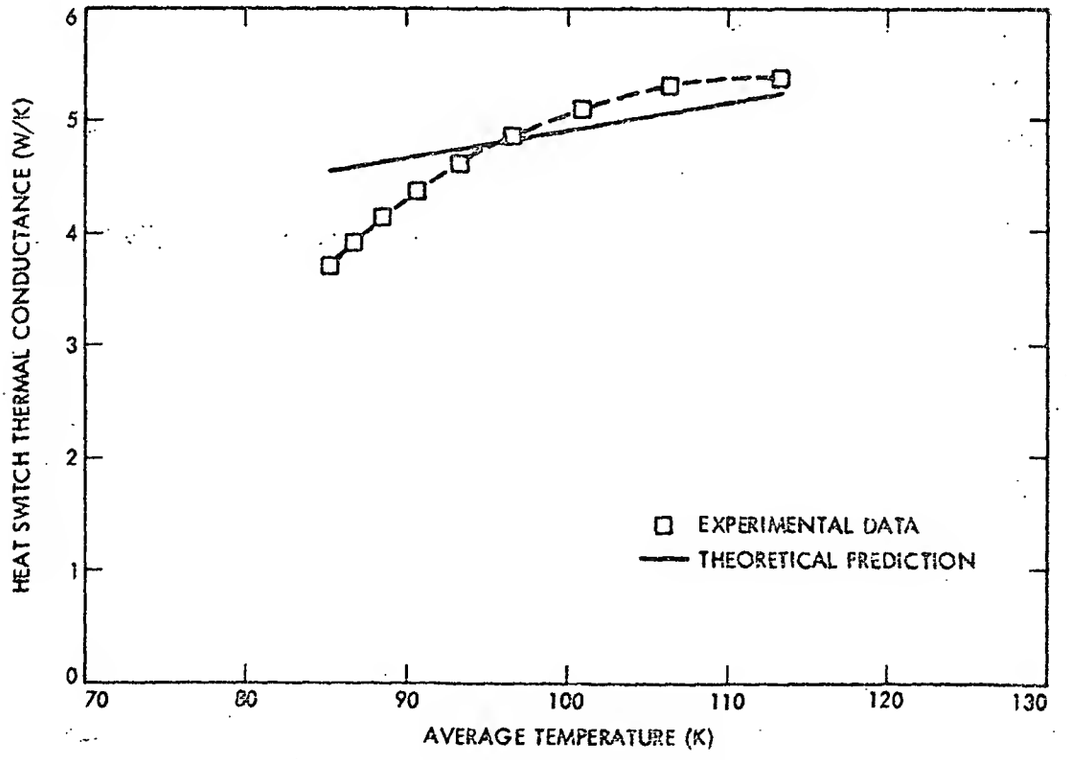

FIG. 8. HEAT SWITCH CONDUCTANCE OF GAR - II.

D6.

HYDRIDE ABSORPTION REFRIGERATOR SYSTEM FOR TEN KELVIN AND BELOW

Jack A. Jones

Applied Mechanics Division
Jet Propulsion Laboratory
California Institute of Technology
Pasadena, California 91109

Recent work at JPL has shown that a very long-life, lightweight and efficient hydride absorption refrigerator system can be built to operate at ten Kelvin and below. The system consists of four basic stages of refrigeration. The first stage can be accomplished by means of an active refrigeration system such as a long-life Gifford-McMahon expander or a charcoal-sorption refrigerator, or even by a passive space radiator operating below 120 K. The second stage is operated by a hydride absorption system, wherein a heated hydride powder drives off high pressure hydrogen through a Joule-Thomson/heat exchanger expansion loop such that the hydrogen is partially liquefied (20 K at 1 atmosphere pressure). In the third stage, the vapor pressure over the collected liquid hydrogen is lowered by means of absorbing the hydrogen vapor onto a different low pressure, warm hydride. With a 1.7 torr partial pressure of hydrogen gas in the hydride, liquid hydrogen is solidified and sublimes at 10 K. Long-life adiabatic demagnetization refrigerators, helium desorption, or helium diaphragm compressors may possibly be used to cool to 4 K or below.

Preliminary analysis shows that the hydride concepts provide an extremely efficient means of refrigeration to 10 K, and that an entire sorption refrigeration process can be accomplished solely by using low grade heat energy at about 150°C. Furthermore, an entire sorption refrigerator system has no moving parts, other than long-life valves, which have been life-tested at JPL to an accelerated life of 500 years. Preliminary tests and analyses of the sorption refrigerators indicates an expected lifetime of at least ten years. Present lightweight Gifford-McMahon expanders have lifetimes greater than 2.3 years, although this can likely be increased by means of redesign and/or redundancy.

Key words: absorption; adiabatic demagnetization; adsorption; cryogenic; Gifford-McMahon; hydride; hydrogen; refrigerator; sublimation.

1. Introduction

There are a number of mechanical cryogenic refrigerator systems that are capable of producing temperatures as low as ten Kelvin and below. These systems, which include various Stirling cycles, Brayton cycles and Vuillcumier cycles, all require the use of wear-related moving parts and/or very complicated electrical equipment. Although much progress has been made in recent years, none of these systems has, to-date, demonstrated extremely long life (five years or greater), primarily because of mechanical failure problems. It was precisely for this reason that the Jet Propulsion Laboratory decided in 1979 [1] to explore the possibility of using non-mechanical sorption refrigeration systems for sensor cooling systems that would eventually explore the outer planets. These missions require lifetimes of ten years and more. With sorption refrigeration systems, there are no wear-related moving parts, and the controlling electronics can consist entirely of simple, long-life, solid state timers.

Recent work at JPL has demonstrated the feasibility of extremely long life (at least ten years) for hydride absorption coolers in the twenty Kelvin range [2, 3], and analyses has proven

that this temperature range can be lowered to ten Kelvin by means of using an additional, non-mechanical solid hydrogen sublimation stage. This extremely efficient stage then opens the door to even lower temperature, long-life systems when used as a preliminary stage for helium sorption systems or for adiabatic demagnetization refrigeraters, both of which will be described later in this paper.

2. Principle of Operation

2.1 20 K Refrigeration

The basic principle of operation for the 20 K hydride refrigerator is that a continuous flow of high pressure hydrogen gas is generated by means of non-mechanical hydride compressors. The high pressure gas is pumped through a series of heat exchangers and a Joule-Thomson (J-T) valve such that the net cooling effect due to expansion of the gas at the J-T valve lowers the hydrogen temperature to its liquefaction point, 20 K at one atmosphere pressure (Figure 1).

The principle of the compressor operation is based on the fact that the intermetallic hydrides such as $LaNi_5$, absorb about six atoms of hydrogen per unit formula with an equilibrium pressure of a few atmospheres at room temperature. The density of the absorbed hydrogen at room temperature is almost twice the density of free liquid hydrogen at cryogenic temperatures.

The equilibrium pressure of the absorbed hydrogen is a very strong function of temperature, and thus the hydrogen static pressure can be increased from 4 atmospheres at 40°C (313 K) to about 60 atmospheres at 120°C (393 K). Cycling can also be achieved with the use of other metallic hydrides, whose temperature-pressure characterisics are different than $LaNi_5$. By alternately heating and cooling a series of hydride containers, a continuous flow of high pressure gas is thus supplied to the Joule-Thomson (J-T) expansion valve in Figure 1. The expansion of the gas causes partial liquefaction which can then absorb heat at liquid hydrogen temperatures.

The basic advantages of this type of system are that it provides considerably lower temperatures (20 K or lower) than those from passive radiator systems (approximately 80 K), and yet it still has no mechanical moving parts, other than self-operating check valves, which have been life-tested at JPL for an accelerated life of 500 years. It is much simpler, and has a much longer life expectancy than present orbiting mechanical refrigeration systems, and it can be operated using low temperature waste heat or direct solar heat.

In order to provide heating and cooling of the hydride compressors, a simple gas-gap thermal switch can be used (Figure 2). For spacecraft application, heating could be obtained by means of a flat plate solar collector (or possibly a radioactive thermal energy source), and the heat could be transferred to the hydride by injecting a gas into the gold-plated gap between the solar plate collar and the hydride. To cool the compressor, the solar plate thermal switch gap would be evacuated, and gas would be injected into the gap between the compressor and the cooler radiator heat pipe. Low pressure hydrogen, e.g. 1 torr, gas could be used as the thermal switch actuator gas, and this could be stored in a cooled hydride material for very long-life and light-weight storage.

2.2 10 K Refrigeration

In order to produce temperatures as low as 10 K, the vapor pressure over collected liquid hydrogen is lowered by means of absorbing the hydrogen vapor onto a very low pressure, warm hydride. With a 1.7 torr partial pressure of hydrogen (corresponding to a hydride temperature of about 0°C), the hydrogen is solidified and sublimes at 10 K (Figure 3). A cryogenic sensor can be continuously maintained at 10 K by means of providing two dewars of hydrogen. While one is being liquified, the other is sublimated. The cryogenic sensor can be attached to both dewars by means of a thermal switch, thus being continuously maintained at 10 K.

Another design for the 10 K stage involves liquefying hydrogen at 20 K by means of a hydride liquifier stage, and then expanding the liquid directly to a low pressure 10 K solid hydrogen "snow". Blockage of the J-T valve could be prevented by means of using a porous copper trap, wherein sensor heat is readily transmitted to the J-T valve itself.

3. Overall Cycle Possibilities

3.1 Multi Stage Sorption Refrigeration System

In order to produce an entire spacecraft refrigeration system, a number of possibilities exist in terms of refrigerator staging. Although some spacecraft applications (such as sun-synchronous polar orbits, geosynchronous orbits, and interplanetary missions) adapt themselves well for very low temperature passive radiator stages in the 80 K to 120 K region, most low earth orbit applications cannot readily achieve radiator temperatures below about 150 K. Since this results in relatively high specific power requirements for the hydride system, a number of alternate colder upper stage refrigeration systems have been studied.

For one type of system, solar heat could be collected at 425 K, and used to power four sorption stages (Figure 4), while a small amount of electrical power is used for a thermoelectric cooler (TEC) stage. For the charcoal/methane and charcoal/nitrogen sorption stages, large quantities of gas are absorbed onto charcoal at low pressure and 225 K. The gas is then released at high pressure when the charcoal is heated to 425 K. The process is similar to the hydride system, except that the gases are physically adsorbed onto the surface of the charcoal, while the hydrogen is chemically bonded to the metal hydride powder. The charcoal sorption stages and the TEC are cooled by a 225 K radiator, a temperature which is readily obtainable for radiators facing away from earth, with or without solar light, in low earth orbit. The TEC provides cooling to 175 K, which liquifies methane at high pressure (26.5 atm). When the liquid methane is expanded to 1.8 atm, it cools to 120 K. This 120 K stage is then used to liquefy nitrogen at 24.8 atmospheres. When the nitrogen expands to 1.4 atm, it cools to 80 K, which is then staged to a rare earth, misch metal hydride compressor to reach 18 K for liquid hydrogen. The refrigerator system then cools to 10 K for the solid hydrogen sublimation stage.

A sorption system design to obtain one watt of cooling at 10 K requires a total estimated power of only 600 watts, most of which is supplied directly as solar heat. This is therefore the most efficient 10 K refrigeration system presently possible, primarily because it does not require the use of a very inefficient helium refrigeration cycle. Prior to the hydride sublimation stage design, it simply had not been possible to achieve such low hydrogen pressures for extended periods in a closed-cycle operation. It should also be mentioned that the entire refrigeration system uses absolutely no wear-related moving parts, other than extremely long-life, room-temperature valves. All calculations are based on actual empirical absorption/adsorption data for the respective gases.

A charcoal/helium sorption refrigeration stage, similar to the methane and nitrogen stages, may be possible to obtain temperatures of about 4K, but preliminary calculations have shown that is likely to take many kilowatts of charcoal sorption heating to produce enough helium flow to generate one watt of liquid helium J-T cooling. A likely alternative to a charcoal/helium sorption compressor, however, is an oil-free helium diaphragm compressor, although much development work is necessary in order to obtain a contamination-free life of ten years. Another lower stage alternative is to desorb helium from a saturated 10 K charcoal bed. The heat of desorption is relatively high compared to the very low charcoal specific heat at this temperature, and substantial cooling can result. Although temperatures below 4 K have been obtained with this method [4], much development is still needed in this area also.

3.2 Gifford-McMahon Pre-Cooling

Another extremely efficient means to achieve first stage cooling for the hydride system is to use a Gifford-McMahon (G-M) refrigeration cycle [5], which is powered by compressed hydrogen from a hydride system. In the G-M cycle, gas is compressed in a cylinder to a high pressure and the heat of compression is rejected at some temperature, typically room temperature. The gas is then forced through a piston-type cold regenerator that has a low cycle rate and low pressure drop seals. The gas is then allowed to expand to a very low pressure while flowing back through the regenerator and into the low pressure end of the compressor. The isentropic expansion of the gas precools the regenerator for the next cycle. Although not as efficient as some other refrigeration cycles, one of the big advantages of this system is that the primary friction-related part is a piston seal, which has a low cycle rate and a very low pressure drop across it. In fact, present Cryogenic Technology Incorporated (CTI) Gifford-McMahon refrigerators have expansion cooler mean-time-between- failure (MTBF) lifetimes in excess of 20,000 hours [6]. Since present CTI expansion coolers are run at about 72 RPM, if lower speeds or stronger, multiple seals are used, even greater MTBFs can be expected. Also, since a 9 kg expander can provide about 15 watts of cooling at 70 K, multiple expanders could be used and valved off, if the low pressure drop expansion seal begins to show signs of degraded life.

At present, the major problem with G-M upper stage refrigerators is that oil-lubricated compressors are used. Although elaborate oil cleaning systems have been devised, eventually the oil will freeze out and contaminate the cryogenic portions of the system. This requires periodic maintenance every 2000 to 5000 hours. With a hydride compressor, however, there is absolutely no oil present, and the entire system can operate free of contamination, essentially forever.

A sketch of a G-M upper stage expander and a lower stage adiabatic demagnetization refrigerator, discussed in the next section, appears in Figure 5. Pre-cooling of the hydrogen gas at about 70 K can be accomplished with the G-M expander. The overall specific power, i.e. power required per cooling watt, of this system is relatively good, and in fact, approaches approximately 300 for 20 K cooling, and is about 400 for 10 K when combined with a hydride sublimation cooler. This compares with about 1000 or higher for most other mechanical systems at 10 K.

3.3 Adiabatic Demagnetization Lower Stage

An adiabatic demagnetization (ADM) stage, which purportedly achieves 80% of carnot efficiency [7, 8] can be used to reach temperatures of 4 K or lower. For ADM, a wheel of paramagnetic material is rotated partly inside an extremely high superconducting magnetic field. typically about 7 Tesla. The application of the magnetic field causes heat to be generated in the paramagnetic material. This heat can then be removed at some elevated temperature, e.g. 10 K. When the wheel is rotated away from the 10 K heat sink, it rotates out of the high magnetic field, and its temperature is lowered a tremendous amount, typically to 4 K or below. The entire cycle can be designed to use no moving parts, other then a slowly rotating wheel and possibly some low pressure drop helium circulators to enhance heat transfer into and out of the paramagnetic material.

The 10 K or 14 K hydride stage can be of great advantage for the ADM refrigerator, since ADM requires extremely strong super conducting magnets in order to operate. Since 14 K is just within the superconducting magnet temperature region, the system may be able to "bootstrap" itself from 14 K to lower temperatures by progressively increasing superconductive magnetic field strength with decreasing temperature.

4. Experimental Results

4.1 Charcoal Sorption Refrigeration

Recent work at JPL has confirmed the use of charcoal sorption to produce a continuous flow of high pressure nitrogen. By alternately heating and cooling from cannisters of charcoal between 250 K and 400 K, a continuous flow of 50 atmospheres (750 psi) nitrogen has been produced. By flowing the gas through a J-T/heat exchanger assembly, a total cooling power of approximately 1/2 watt has been generated.

Although the total average power required for this proof-of-principle test was approximately 200 watts, much lower LN_2 specific powers are predicted with methane-staged sorption refrigeration, as previously described and shown in Figure 4.

4.2 Liquid Hydrogen Refrigeration

Most of the experimental results regarding liquid hydrogen hydride refrigeration life testing are available in [3, 9], and are summarized for convenience below:

In particular, a complete heated hydride compressor system has been thus far successfully tested at ERGENICS Corporation to 6000 hours of continuous operation, and the JPL cryogenic J-T system has accumulated over 1,000 hours of successful operation between 14 K and 29 K, without any evidence of wear. It should be noted that the ERGENICS compressor that operated for 6000 hours weighed only about 10 kg and yet delivered a hydrogen flow which would have been equivalent to about 3 watts of cooling at 25 K if a J-T/heat exchanger loop were used. With a lower cycle speed, it can be said that it survived at least 18000 hours of 1 watt equivalent cooling and yet still performed close to original specifications. Preliminary third-stage experiments have confirmed the sublimation of hydrogen at 13.8 K, although a reduced pressure drop heat exchanger system is required to reach lower temperatures. Furthermore, the only moving parts in the system, room-temperature check valves, have been life-tested at JPL to an accelerated life of 500 years [10].

Life tests on hydride particle size have confirmed that the hydride particles break down after repeated cycling, but the average particle size reaches a final spherical equivalent diameter of about 1 micron after about 5000 cycles. Although some binary hydride alloys, such as $LaNi_5$, have shown a significant loss of capacity when subjected to many cycles at elevated temperatures [11], small additions of aluminum to rare earth, nickel-type alloys make the alloy greatly resistant to disproportionation. [12]. ERGENICS Corporation has estimated effective hydride disproportionation as approximately 1% per year, based on aluminized misch-metal hydride alloys. For expansion cooling, Joule-Thomson (J-T) valves have long proven their inherent reliability, as evidenced by well over one million hours of accumulated life for the JPL Deep Space Network Maser receivers [13]. Although simple decontamination thaws are recommended every six to twelve months for the JPL maser fixed-orfice, J-T valves, it is likely that no thaws would ever be needed for the new JPL design of non-clogging, spring-loaded, J-T valves [3]. Furthermore, the hydride system has absolutely no oil-contaminated vapors, as are present on the JPL mechanical refrigeration Maser compressors and thus overall contamination can be substantially reduced if proper initial decontamination steps are taken.

4.3 Solid Hydrogen Sublimation

There has been considerable work done on solid hydrogen sublimation by Lockheed Corporation [14]. Although hydrogen solidifies at about 14 K and 1 psi pressure, its temperature has been readily lowered to as low as 7 K by means of evacuating the vapor space above the hydrogen, thereby causing it to sublimate directly from the solid phase to the gaseous phase. Since the transition heat from gas to liquid is very high (190 BTU/lbm) and the solid latent heat is relatively low (25 BTU/lbm), the amount of cooling energy required to go from liquid to solid is quite low, although the heat of sublimation, which is approximately 190 + 25 = 215 BTU/lbm, is very high.

That is to say, once liquid hydrogen has been made, it takes very little extra power to produce solid hydrogen. This in fact, has been confirmed by analysis using a specialized JPL sorption computer program [15], using $LaNi_5$ to produce liquid hydrogen and a low pressure hydride to further reduce the vapor pressure, and thus its temperature.

5. Summary and Conclusions

Recent work at JPL has shown the possibility of achieving extremely long-life (10 years or greater), efficient, and relatively simple refrigeration systems for obtaining 10 K temperatures and below. The various possible stages are described below:

1. The first stages of refrigeration can be obtained by either passive radiation (80 K to 120 K for high orbits or interplanetary missions), charcoal/methane sorption (120 K) combined with charcoal/nitrogen sorption (80 K), or by a Gifford-McMahon refrigeration system (40 K minimum) powered by a hydride compressor.

2. The next stage of refrigeration to 20 K can be accomplished by a standard hydride J/T compressor system, such as the compressor unit recently life tested for 6000 hours [3].

3. The ten Kelvin temperature stage is obtained by low pressure hydride sublimation evacuation of the vapor space above hydrogen to 1.7 torr pressure. This can be accomplished by batch processing the liquid hydrogen and then reducing the hydrogen pressure by absorption onto the hydride or by direct expansion of liquid hydrogen through a J/T valve to produce solid hydrogen "snow".

4. Temperatures of 4 K or below may possibly be obtained by adiabatic demagnetization refrigeration, helium desorption, or by an oil-less diaphragm helium compressor.

All of the sorption refrigeration stages have life expectancies of at least ten years, since their only moving parts are room-temperature valves that have been life tested to an accelerated equivalent life of 500 years. Although present CTI Gifford-McMahon expanders have a guaranteed life expectancy of 20,000 hours, their extremely light weight allows for multiple unit redundancy and/or stronger seals and lower cycle frequency to achieve 10 year life (88,000 hours). It is quite likely that longer life seal materials can be made, since the G-M expander seal sees only a very low pressure drop which is at low temperatures. Present G-M refrigerators are life-limited primarily due to oil-contamination from mechanical compressors, a problem which is totally absent with hydride compressor systems.

The overall specific power efficiency to reach 10 K by sorption staging is estimated to be about 600 watts per cooling watt at 10 K, while the specific power with G-M staging is about 400 watts per cooling watt. Most of the power for both systems is in the form of low temperature heat, such as 425 K solar heat or RTG waste heat. This compares with values generally greater than 1000 for every other known 10 K helium cycle refrigeration system.

When compared with all other closed-cycle spacecraft mechanical refrigeration systems, sorption refrigeration, and in particular the 10 K hydrogen sublimation hydride sorption system, appears to be the simplest, most efficient, lightest and least interfering (vibrations and magnetics) and to have the longest potential life of any other existing system.

The help of Dr. Dave Elliott of JPL is gratefully appreciated for his suggestion of combining a Gifford McMahon expander as a first stage to a hydride Joule-Thomson hydrogen liquefier system, and the help of Dr. Steven Bard, also of JPL, is appreciated for the design and testing of the charcoal/nitrogen sorption refrigeration system. Furthermore, the original idea of hydrogen sublimation to obtain 10 K cooling is acknowledged and appreciated from Dr. Al Johnson of Aerospace Corporation.

The research described in this paper was carried out by the Jet Propulsion Laboratory/California Institute of Technology under a contract with the National Aeronautics and Space Administration.

REFERENCES

[1] JPL White Paper: "The Status of Cooler Technology in Relation to Future JPL Space Instrument Cooler Requirements," by the Cooler Technology Study Committee (R. Beer, W. Petrick, D. Pidek, J. Plamondon, M. Saffren and J. Wellman), March 22, 1979.

[2] Jack A. Jones, "$LaNi_5$ Hydride Cryogenic Refrigerator Test Results," Second Biennial Conference on Refrigeration for Cryogenic Sensors and Electronic Systems, GSFC, Greenbelt, Maryland, December 7 and 8, 1982.

[3] Jack A. Jones and P. M. Golben, "Life Test Results of Hydride Compressors for Cryogenic Refrigerators," AIAA Paper No. 84-0058, AIAA 22nd Aerospace Sciences Meeting, January 9-12, 1984, Reno, Nevada. Publication pending in Cryogenics Magazine.

[4] J. C. Daunt and C. Z. Rosen, "Desorption Cooling below 12 K using He^4 desorbed from synethetic zeolite," Cryogenics, June, 1972.

[5] W. E. Gifford, "The Gifford McMahon Cycle," Advances in Cryogenic Engineering, Vol. 11, 1966.

[6] Franz Eberth Fred Chellis, "Comparing Closed Cycle Cryocoolers," CTI Cryogenics Publication, Waltham, Massachusetts, 1979.

[7] W. A. Steyart, "Rotating Carnot-Cycle Magnetic Refrigerators for use near 2 K," Journal of Applied Physics 49(3), March 1978,

[8] Dean L. Johnson, "Reciprocating Magnetic Refrigerator", 3rd Cryocooler Conference on Refrigeration for Cryogenic Sensors and Electronic Systems", National Bureau of Standards, Boulder, Colorado, September 17-18, 1984.

[9] Jack A. Jones, "Cryogenic Hydride Refrigeration," 29 Minute Video Presentation, World Hydrogen Conference, Toronto, Canada, July 15-20, 1984.

[10] Emanuel Tward, Jet Propulsion Lab, Low Temperature Physics Group Supervisor, Private Communication, October, 1983.

REFERENCES (CONTINUED)

[11] J. J. Reilly, A. Holtz, and R. H. Wiswall, Jr., "A New Laboratory Pump for Intermediate Pressures," Review of Scientific Instruments, 42 (10), 1485, 1971.

[12] Doug Goodell, "Stability of Rechargeable Hydriding Alloys during Extended Cycling," Publication pending in Journal of Less Common Metals.

[13] M. H. Higa and E. Hiebe, "One Million Hours at 4.5 Kelvin", National Bureau of Standards Cryocooler Applications Conference, Boulder, Colorado, October 1977.

[14] T. C. Nast and D. O. Murray, "Orbital Cryogenic Cooling of Sensor Systems," Systems Design Driven by Sensors AIAA Technical Specialist Conference, Pasadena, California Oct. 19-20, 1976.

[15] Katherine B. Sigurdson, "A General Computer Model for Predicting the Performance of Gas Sorption Refrigerators," Second Biennial Conference on Refrigeration for Cryogenic Sensors and Electronic Systems, GSFC, Greenbelt, Maryland, December 7-8, 1982.

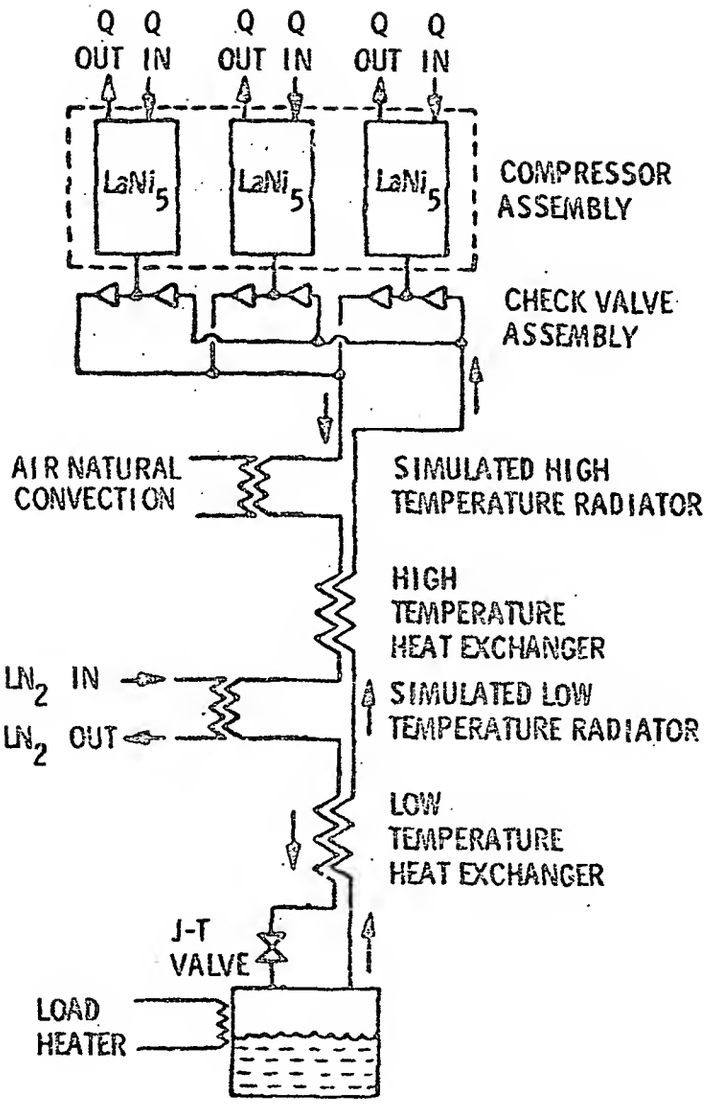

Figure 1 Hydride Refrigerator Operational Schematic

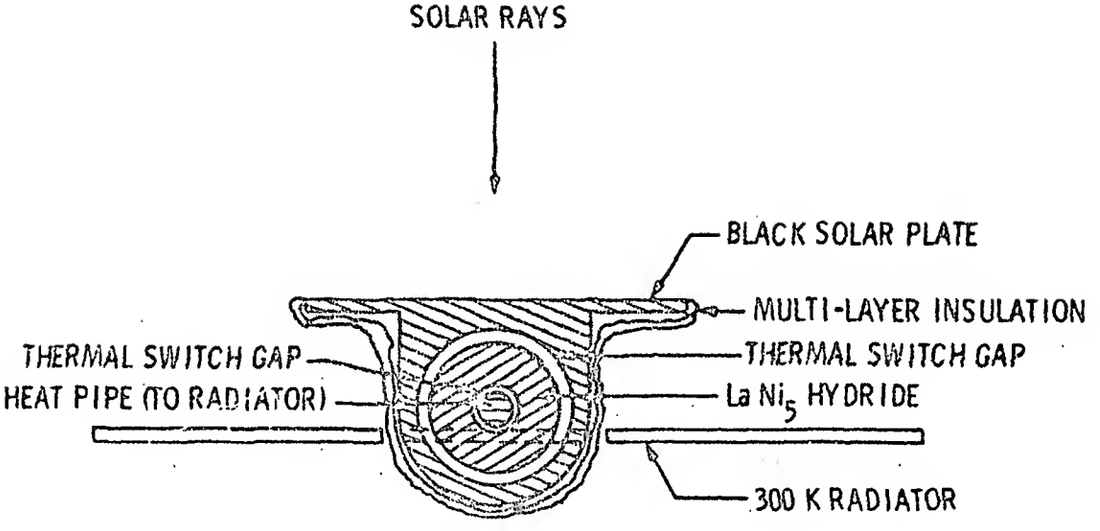

Figure 2 Hydride Compressor Design With Thermal Switches

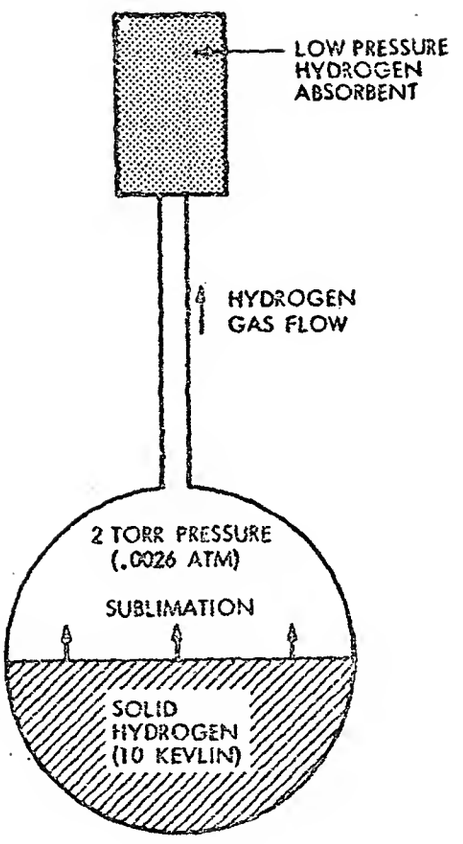

Figure 3 Ten Kelvin Hydrogen Sublimation Refrigerator

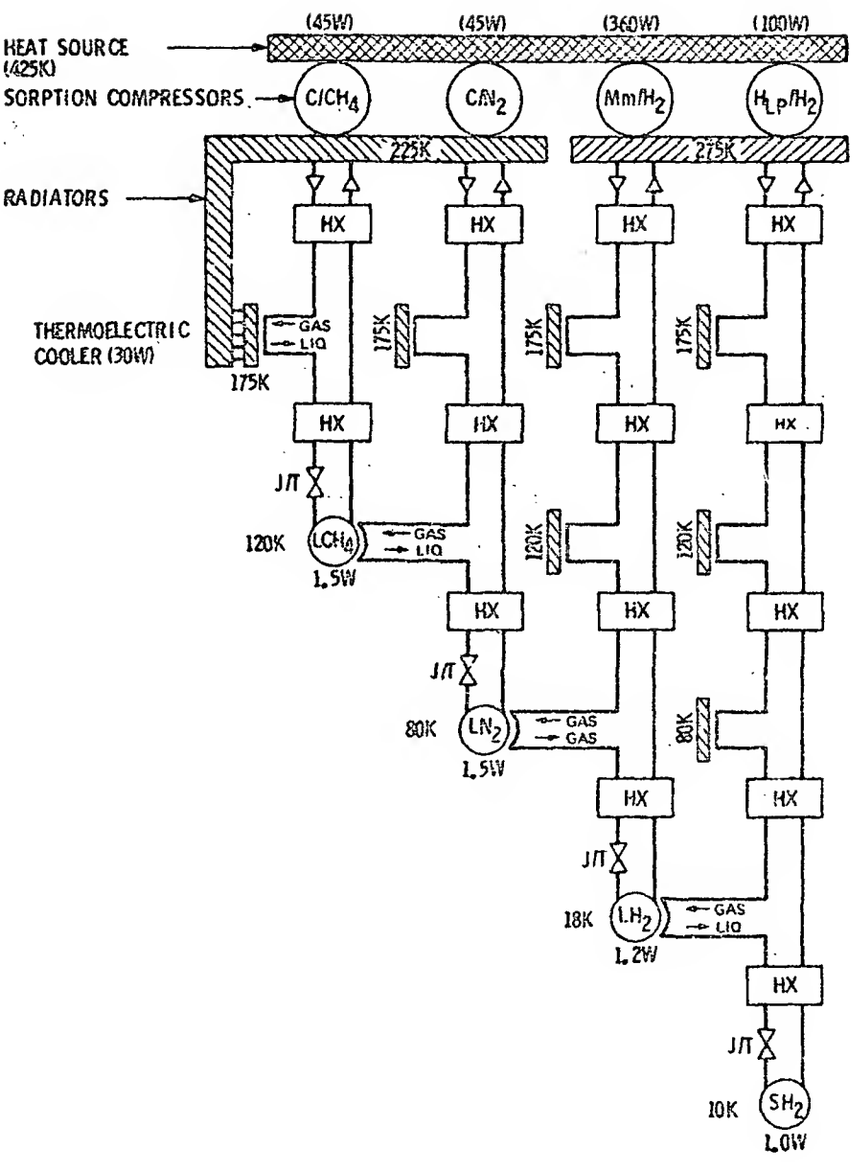

Figure 4 Four Stage Sorption Refrigerator System

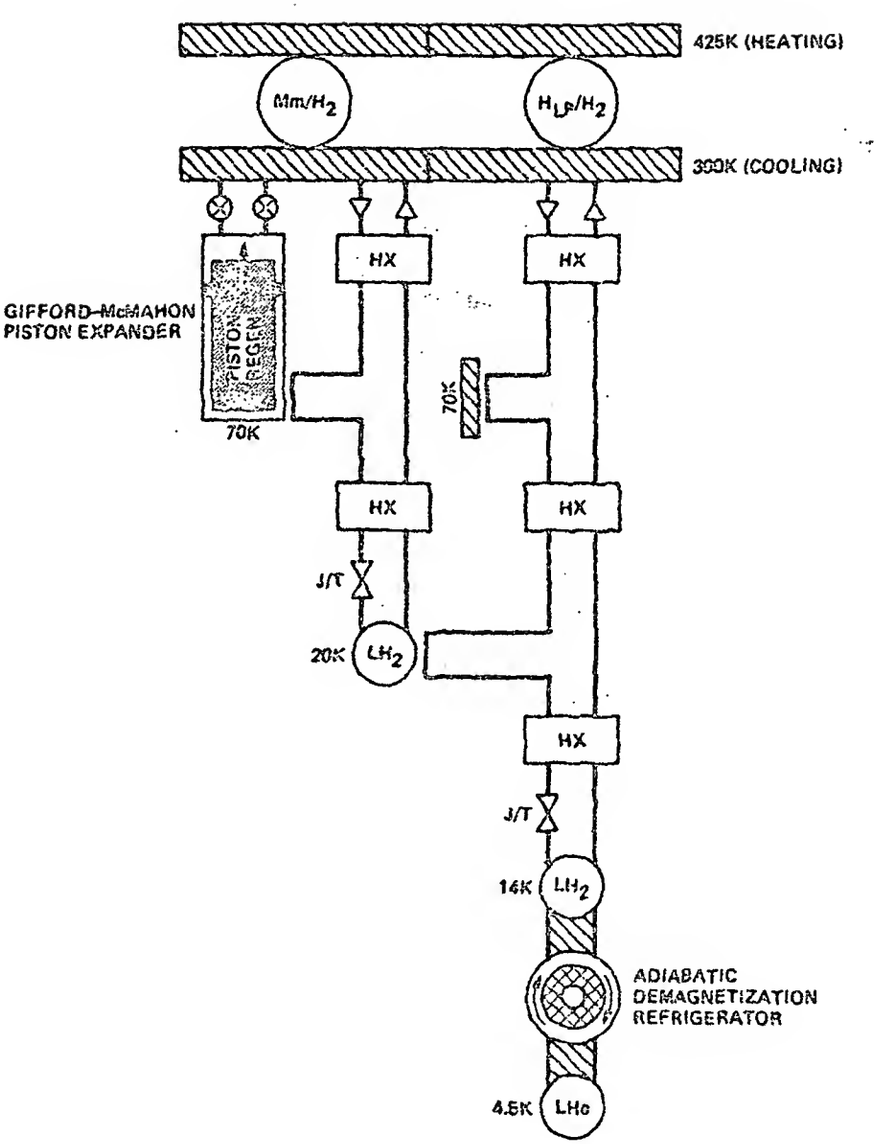

Figure 5 Hydride Refrigerator With G-M Upper Stage and ADR Lower Stage

D7

CLASSIFICATION OF CRYOCOOLERS

G. Walker

General Pneumatics Corporation
Western Research Center
7662 East Gray Rd.
Scottsdale, Arizona 85254

A great diversity of methods and mechanisms have been devised to effect cryogenic refrigeration.

This paper reviews some of the basic parameters and considerations affecting the selection of a particular system.

A classification scheme for mechanical cryocoolers is presented. An important distinguishing feature is the incorporation or not of a regenerative heat exchanger, of valves, and of the method for achieving a pressure variation.

Key words: Cryocoolers; mechanical refrigerators, regenerative heat exchanger.

1. Introduction

A cryocooler is a refrigerating system capable of achieving temperatures in the cryogenic range, generally reckoned to be less than 120K. The word cryogenic is derived from the Greek "icy cold".

Cryocoolers are often rated by their available refrigeration capacity measured in watts. To be meaningful however it is necessary to specify not only the refrigeration capacity but also the temperature at which the refrigeration is available. A cryocooler having a capacity of 1 watt at 4K (liquid helium temperature) is very much different to the cryocooler having a capacity of 1 watt at 80K (liquid nitrogen temperature).

Another important parameter is the power input or work required to achieve refrigeration.

The coefficient of performance of a refrigerator is defined as the ratio:

COP = Refrigeration Capacity/Power Input or Heat Lifted/Work Done

The ideal coefficient of performance is the Carnot value:

$$\text{COP (Carnot)} = T_E/(T_C - T_E)$$

where T_E = minimum cycle temperature (usually the refrigeration temperature)
T_C = maximum cycle temperature (generally the atmosphere temperature)

The ratio of the actual coefficient of performance to the Carnot coefficient of performance is sometimes called the efficiency. It is a useful measure of the way an actual machine measures up to the thermodynamic ideal machine. Thus:

$$\text{Efficiency} = \text{Actual COP/Carnot COP} = \text{Refrig Cap/Power Input} \times (T_C - T_E)/T_E$$

The efficiency of presently available cryocoolers ranges from a minimum of less

than 1 percent to a maximum of near 50 percent. Strobridge (1974) presented "experience" charts for 140 different cryocoolers with the above efficiency variations.

The small machines used for electronic applications have the lowest efficiencies. This is because nearly all the refrigeration generated is consumed in cooling, and maintaining cold, the low temperature region of the machine itself. The surplus or useful refrigeration available from these units is very small; only fractions of a watt are required. Applications requiring a larger useful refrigeration load use systems bigger in size and tending to be more efficient. The highest efficiencies are found in large machines used for liquefiers and range from 20 to 50 percent of the Carnot value.

Other significant parameters for cryocoolers include the total mass and volume of the system and the mass and volume of the cold region. This latter is of particular importance in infra red (I-R) missile guidance or night vision systems with cooled detectors and associated optical/electronic systems mounted in swivelling gimbals. A low mass and volume is necessary to facilitate a fast response with low inerita.

Cooldown time, the period necessary for the machine to achieve stable operation at the design condition following startup is important in some applications of miniature systems, usually weapons related. The combination of a quick cooldown and a slow warmup is a particularly challenging requirement involving mutually opposed high and low 'thermal masses'. Cooldown is sometimes accelerated by operating at a high pressure or speed on startup and later switching to the normal operating mode.

Mechanical vibration and electro-magnetic emissions in the cold region are often important characteristics of cryocoolers. Some applications require the total elimination of any mechanical or electro-magnetic noise. This is best approached by

a) physical separation of the cold region and the compressor unit where large power input and heat transfers take place

b) elimination of moving parts in the cold region

c) the use of plastic, ceramic or other non-magnetic parts in the cold region.

Operating life is another important characteristic often quoted as the mean time before failure (m.t.b.f.) or the mean time before maintenance (m.t.b.m.). This is generally taken to mean the average time of operation before failure (or maintenance) of a number of identical cryocoolers operating under similar conditions. Reliable data for m.t.b.f. and m.t.b.m. based on the accumulated experience of users is very hard to come by. There appears to be no properly organized system for data collection, reduction, rationalization and distribution. Operating life is affected to a large extent by the nature of the system used: Moving parts, sliding seals, bearings, piston rings, etc. wear and generate detritus with deleterious effects on valves, and small passages. Sometimes questions of lubricated versus unlubricated parts involve the balancing in increased wear against the possibilities of contamination of lubricant. Reliability can often be improved by incorporating excess capacity so that operation is intermittent or by the provision of redundant systems.

The shelf life of a cryocooler is frequently important. This is the interval a unit may be required to maintain the capability for operation while standing unused or in occasional intermittent use. Many systems involve mechanical units containing high pressure helium and equipped with a variety of sealed flanges,

shaft seals, screwed fittings etc. Hermetic sealing by seal welding is the best approach to ensure a long shelf life but this of course is not possible for a mechanical unit with dynamic seals.

In split systems where the cold region is separated from the power input unit the nature of the leads connecting the two elements is important. Some systems have flexible leads, others are inflexible. Sometimes they are cold, sometimes at ambient temperature, sometimes a single lead with a cyclic fluctuating pressure, sometimes twin leads with a high pressure feed line and a low pressure return. All these affect the insulation required, the forces and bending moments imposed on gimballed units, the transmission of mechanical, vibration, thermal conduction and pressure attenuation or phasing effects.

Cost, of course, is always important, more so in some cases than others. Separate consideration of capital cost and operating cost including scheduled maintenance and unscheduled maintenance or replacement is necessary. Sometimes the lack of opportunity or possibility for maintenance (space systems) justify increase in the capital cost by the provision of redundant systems or the use of a large, lightly loaded, slow running unit.

The power supplied to drive the cryocooler is eventually degraded to heat and must be rejected from the system. Thus the cooling system to carry the waste heat is an important feature of the cryocooler. Liquid cooling is more efficacious than air or gas cooling because of high heat transfer coefficients and heat capacities achieved with liquids. Air cooling is attractive on grounds of simplicity to almost everyone concerned except those actually responsible for the cooling system. Frequently miniature machines are air cooled but are then located in a pod along with other heat emitting power equipment so the environmental temperature is increased. This complicates the cooling problem. The range of environmental temperature over which the equipment is required to operate ranges from -40°C to as much as 60°C. This in itself presents problems which are compounded in many cases by the further requirement that the refrigeration temperature is a precise value having a tolerance as slight as + or - 0.1°C.

System cooling and heat rejection presents special problems in space applications. All the heat must ultimately be rejected by radiation. The well-known equation:

$$Q = EAST^4$$

where Q = radiation heat flux
E = surface emissivity
A = area of emitter
S = Stefan - Boltzman constant
T = temperature of emitter

clearly dictates a high temperature. However the coefficient of performance equations

$$COP = T_E/(T_C - T_E)$$

dictate the lowest possible maximum cycle temperature, T_C, (corresponding to T in the above radiation equation).

Continuing with the special requirements for aerospace cryocoolers important characteristics are the ability to withstand the high acceleration and vibration spectrum of a rocket launch, the ability to operate in any orientation and in a zero or low gravity regimen. Reliability and long-life assume an importance not found elsewhere.

2. Classification of cryocoolers

There are many military, civil, medical, and scientific applications for cryocoolers in electronic, space, and defense-related systems. These needs, with the multifarous and diverse requirements enumerated above, have, over the past 40

years, attracted the attention of ingenious and resourceful engineers and scientists. The result is an enormous literature and a wide range of different systems and solutions. Walker (1983) has recently summarized the situation and provided an extensive bibliography and a guided introduction to the field.

The ultimate refrigerator has not yet been invented. This would produce whatever refrigeration was required at the appropriate temperature, would be compact, lightweight and run forever with no maintenance on a pennyworth of kerosene without vibration, noise, or smell. All practical machines are essential compromises of conflicting requirements with particular features emphasized as specified by the client for their application.

The classification chart shown in Figure 1 represents one attempt to clarify a confusing situation. The chart is limited to mechanical cryocoolers producing cryogenic refrigeration by compression and expansion of gases including liquefaction of gases at low temperature. It does not include any of the solid state refrigerators or those customarily confined to temperatures below 3K.

2.1 Regenerative heat exchanger

With the above sweeping limitation in mind the first question to ask when confronted with an unknown cryocooler is:

"Does it have a regenerative heat exchanger".

All types of heat exchangers may be broadly classified into regenerative or recuperative heat exchangers. Recuperative exchangers are equipped with separate flow passages for the two or more fluids involved. The passages are usually contained in conduits with solid walls and the fluids flow continuously. Most heat exchangers are the recuperative type. Regenerative exchangers contain a porous matrix of finely divided material, granules, balls, wires, etc. The fluids flow through the matrix in cyclic succession so the cold blow follows the hot blow, etc. The matrix acts as a thermodynamic sponge alternately releasing heat to the cold fluid and receiving heat from the hot fluid.

The unknown cryocooler will almost invariably include one or more recuperative heat exchangers but if there is no regenerative exchanger it will belong to the group of cryocoolers shown in the upper right-hand box of Figure 1. Claude, Linde-Hampson, Joule-Thomson or Joule-Brayton. These are the names of the originators of the thermodynamic cycles on which these various systems work. They all operate with compression of the working fluid at high temperature, expansion at low temperature, and incorporate counter flow, recuperative heat exchangers. Expansion engines are included in the Claude and Joule-Brayton systems.

2.2 Valves

If the specimen cryocooler does include a regenerative exchanger the next question is:

"Does it have any valves to regulate the flow of the working fluid".

If the unit does include valves as well as a regenerator it will be an Ericsson engine of the type shown in the mid-left box, Solvay, Postle and Gifford-McMahon. The distinction between Solvay and Postle machines is that the Solvay unit includes a work-producing low temperature expansion machine. The Postle unit operates with a displacer only. Gifford and McMahon invented the machines carrying their names in the late 1950's but both their inventions were actually reinventions of the Postle and Solvay engines of the previous century.

2.3 Compressor

If the specimen cryocooler contains a regenerative heat exchanger but no valves the next step in classification is the type of device used to achieve a pressure variation.

Stirling engines incorporate a mechanical compressor so the total enclosed volume of the working space varies cyclically usually as the result of the motion of a piston in a cylinder.

In Vuilleumier engines there is no piston but simply a displacer moving working fluid from a hot space to a cold space and vice versa. The machine is said to have a thermal compressor and is sometimes called a thermocompressor. The variation in temperature at constant volume causes a change in pressure, (high when the fluid is in the hot space, low when it is in the cold space). The change in pressure is utilized in a separate but connected cylinder also containing a displacer to achieve refrigeration. The machine was devised by Rudolph Vuilleumier in 1918.

There are innumerable variations of Stirling engines some of which are set out in Figure 1. They involve displacer-piston and two piston versions and multiple piston arrangements and variations.

Vuilleumier engines are also found in a range of variations broadly classified as split systems or integral systems. In both the Stirling and Vuilleumier units a split system has the cold expansion space located in a separate cylinder remote from the hot compression cylinder and coupled to it by a single small-bore lead up to 2 m long.

3. Conclusion

Multiple applications for cryogenic cooling systems have resulted in the development of many different cryocoolers with different characteristics and attributes.

Some of the important requirements and the different types of unit are briefly reviewed.

4. References

[1] Strobridge, T.R., Cryogenic refrigerators - an updated survey, National Bureau of Standards Technical Note 655, (Sup. Docs. U.S. Govt. Printing Office), 12 pp, (1974).

[2] Walker, G., Cryocoolers, (2 volumes), The International Cryogenics Monographs Series, Plenum Publishing Corporation, New York, (1983).

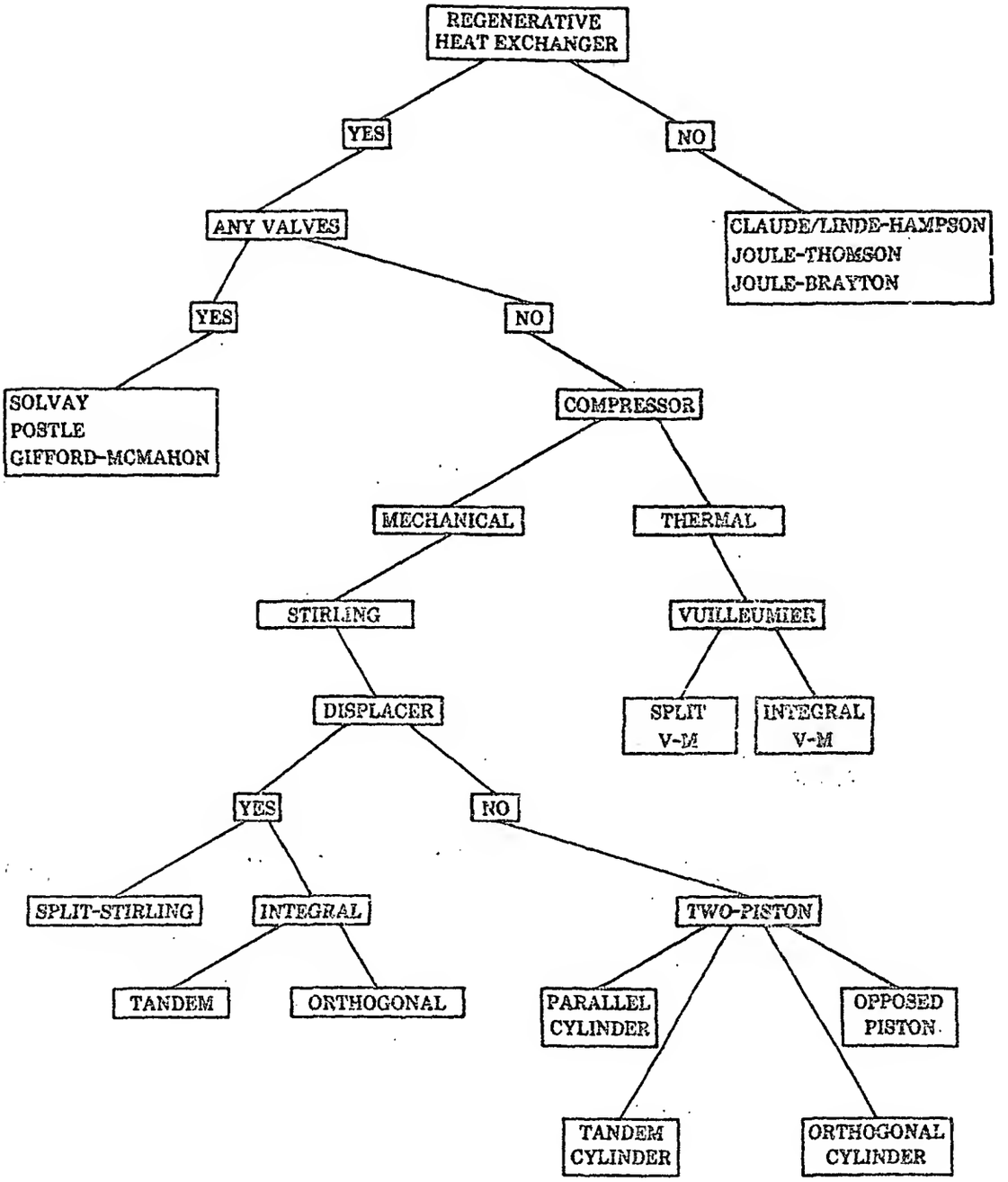

FIGURE 1. CLASSIFICATION OF CRYOCOOLERS

D8

AN EXPERIMENTAL STUDY FOR A MINIATURE STIRLING REFRIGERATOR

Shimo Li and Chen Guobang
Zhixiu Huang Fagao Zhang

Cryogenic Engineering Laboratory
Zhejiang University, China

Cuangji Cui and Jiazhang Li

Low Temperature Physics Laboratory
Beijing University, China

In this paper, experimental results of a miniature two-stage Stirling cryocooler are introduced. The influence of filling gas pressure and refrigeration temperature on the refrigerating capacity along with the relationship between parameters has been measured. The valley pressure corresponding to the lowest refrigeration temperature and the cooldown time versus operating pressure have been discussed. The coefficient of performance and thermodynamic efficiency of the cryocooler have been calculated based on experimental data.

Key words: Cryocooler; cryogenics for infra-red detectors; miniature Stirling refrigerators; refrigeration.

1. Introduction

In recent years, we have studied the thermodynamic characteristics of both types 3Ly-08/194 which is a small single stage refrigerator [1] and A3040 Stirling cycle refrigerator which is a miniature two-stage refrigerator. Measurements have been made of refrigeration temperature, operation pressure, cooling capacity, cooldown time along with the relationship between them. In addition, the influence of surrounding conditions and contamination of the regenerator on the performance of the refrigerator is also considered. In the following, the experimental study on the miniature two-stage Stirling refrigerator will be discussed.

2. Structural Features of the Cryocooler

This miniature two-stage Stirling refrigerator was built in Beijing University in 1972. Its major specifications are listed in Table 1. The device was designed for refrigerating infra-red detectors requiring a refrigeration temperature of about 25-30 K [2]. Most components of the refrigerator are made of stainless steel. The cylinder and displacer define two low temperature expansion spaces. There are two co-axially located regenerators in the displacer. Stacks of stainless steel screen are used as regenerative packing material. A copper shield is installed on the first cold head and there are several layers of Al-coated Mylar outside the shield to reduce radiation loss. During the experiment the insulation space is about 5×10^{-4} mmHg dynamic vacuum. The second stage cold head and the cylinder made of oxygen-free copper, are connected together for better thermal stability. The machine was operated at 1400 rpm. Helium gas is used for working medium. The compressive heat of helium gas is carried away by cooling water.

Table 1. Major specifications of A3040 Refrigerator

Component	Unit	Value
Compressor-cylinder diameter/stroke/volume	mm/mm/cm^3	60/15/42.4
Primary cylinder diameter/stroke/volume	mm/mm/cm^3	23.9/13/3.53
Secondary cylinder diameter/stroke/volume	mm/mm/cm^3	15/13/2.3
Length/diameter of the primary regenerator	mm/mm	40/19
Length/diameter of the secondary regenerator	mm/mm	26/14.3
Structure angle β	degree	60
Volumetric phase angle ϕ	degree	67
Pressure phase angle θ	degree	38
Pressure parameter δ	dimensionless	0.45
Pressure ratio σ	dimensionless	2.67
Filling gas pressure	bar	6.5
1st and 2nd stage temperature T_m/T_e	K/K	95/30
1st and 2nd stage regenerators packing material	mesh	250/300
1st and 2nd theoretical refrigerating capacity Q_m/Q_e	watts/watts	39.4/25.7
Weight of the refrigerator (exclude the motor)	Kg	17

For refrigeration power measurement, 6 m of 0.2 mm constantan wire is coiled on the copper cylinder of the secondary cold head. The electric resistance of the wire is about 50 ohm at room temperature. Power is supplied by an adjustable D.C. supply. The heating power is less than 12 W.

Temperature is measured at three points: T_e is measured with a Ni-Cr-Au-Fe thermocouple at the secondary cold head, while T_m and T_p are measured with Cu-constantan thermocouples at the hot ends of the secondary and the primary cylinder, respectively, (see Fig. 1).

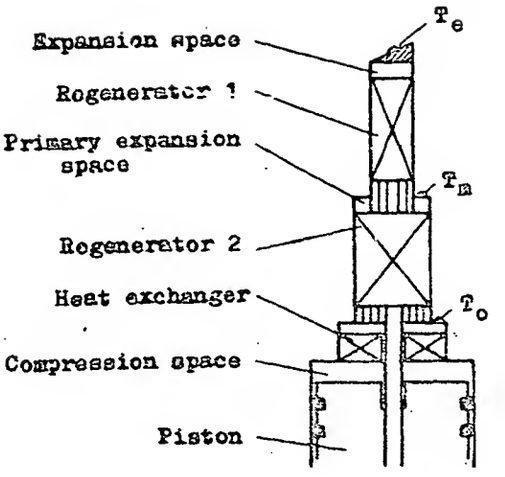

Figure 1. Arrangement for temperature measurement.

Type UJ-26 electric potential meters (with a precision of 0.1 μV) and PZ26b direct digital voltage meters are used in measuring. Good thermal contact of the thermometer with cold head is provided.

3. Experimental Results

The relationship of the lowest refrigeration temperature, cooldown time and filling gas pressure have been measured. The experiment was made under bad conditions, e. g. the outdoor temperature was about 35°C. The temperature of the cooling water was 30°C, and the room temperature was not lower than 30°C.

3.1 The Lowest Refrigeration Temperature

Under a condition of no heat load, a minimum is found in the lowest refrigeration temperature as a function of filling pressure. The relationship between them is shown in figure 2. The refrigeration temperature will increase when the pressure is either higher or lower than the optimum pressure (in the measurement on 3LV-08/194 refrigerator, two optimum pressures have been observed [1]).

3.2 Cooldown Time

The time required for the temperatures T_m and T_e of first and second stage cold heads to decrease from room temperature to the lowest equilibrium temperature under a given operating pressure is called the cooldown time. Figure 3 shows these temperature-time curves under a filling gas pressure of 7.5 bar. It seems that the cooldown time of the machine on the order of 15 minutes is somewhat longer than that of a normal one under normal operating pressure. Probably this is because of the larger heat capacity of the secondary cold head and the copper block of the 2nd cylinder. The cooling curve takes a similar shape with that of reference [3]. As filling gas pressure increases the unloaded cooldown time is shortened (see Fig. 4). When the filling gas pressure decreases from 7.5 bar to 3.5 bar, the cooldown time almost doubles (from 15 minutes to 34 minutes).

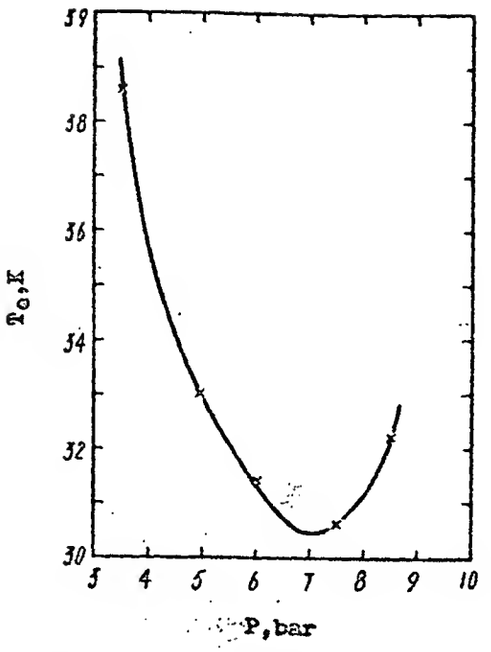

Figure 2. Lowest refrigeration temperature versus operation pressure.

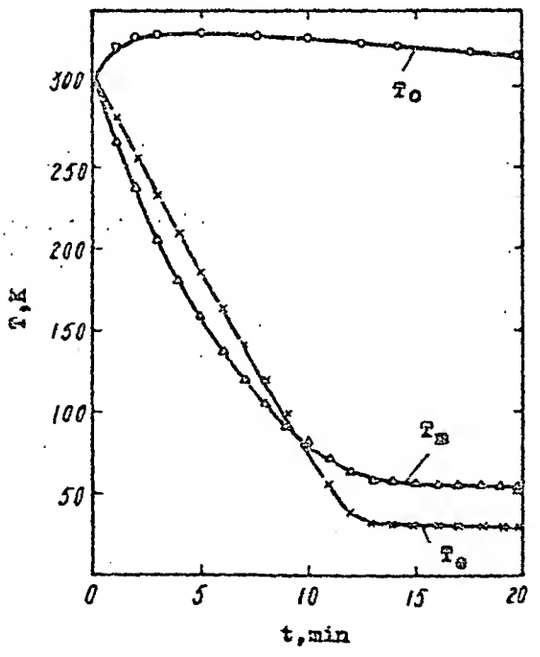

Figure 3. Cooldown curve of miniature two-stage Stirling refrigerator.

Experimental results show that the cooling curves of T_c and T_m are similar to each other. The temperature of the hot end of the 1st cylinder quickly reached a steady state. At the initial stage, the decreasing rate of T_m is greater than that of T_c. Then two cooling curves of T_m and T_e intersect each other. At last, T_m and T_e curves almost reach their equilibrium temperature simultaneously.

3.3 Cooling Capacity

The refrigeration temperature T_e varies approximately linearly with cooling capacity Q_e when the filling pressure is under 9 bar (see Fig. 5). At a given refrigeration temperature T_e, the cooling capacity Q_e increases at the pressure increases. The critical heating power under which the machine is at the full-loaded state is about 3.5 - 10 W when filling gas pressures are 6.5 bar and 7.5 bar (see Fig. 5). While the heating power is increased continually temperatures of the 1st and 2nd stage are reversed, i.e., $T_m<T_e$. Since only a few watts and a temperature just below 40 K are required for practical applications, the cooling capacity required cannot be supercritical. Figure 5 also shows that the variation extent of T_m versus cooling capacity is not great. While the 2nd stage cooling capacity is increased from zero to the critical value, the corresponding difference of the 1st stage temperature is approximately 10 K.

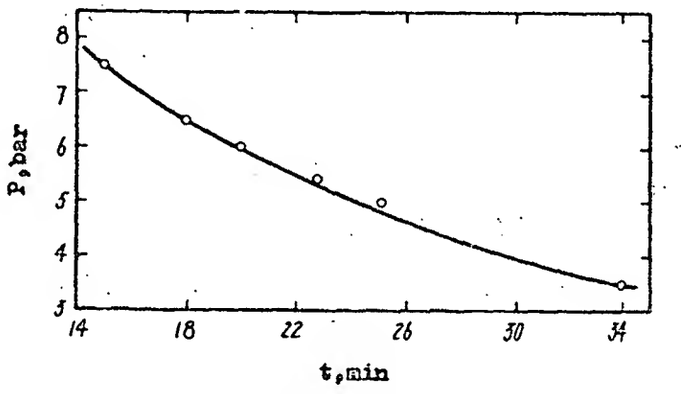

Figure 4. Filling gas pressure versus cooldown time.

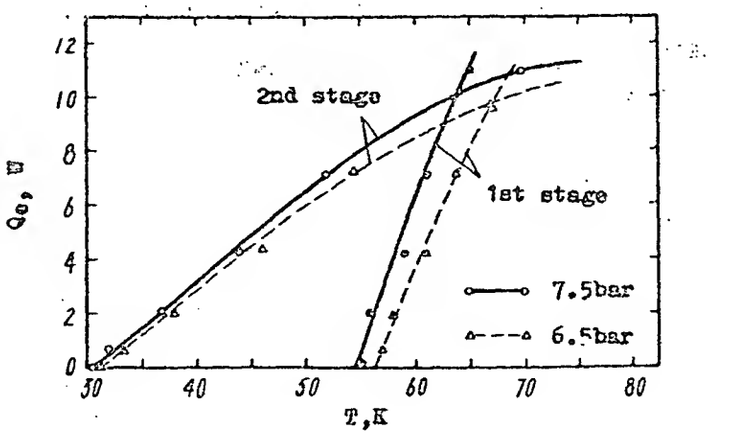

Figure 5. Cooling capacity versus refrigeration temperature.

3.4 Thermodynamic Efficiency

Coefficient of performance ϵ and thermodynamic efficiency η_c are defined as follows

$$\epsilon = Q_e/N \tag{1}$$

$$\eta_c = \epsilon/\epsilon_i = \epsilon \frac{T_o - T_e}{T_e} \tag{2}$$

where Q_e = actual cooling capacity, W
N = actual input power, W
ϵ_i = coefficient of performance for Carnot cycle
T_o = ambient temperature, K

According to thermodynamic principle, the input power increases while the temperature T_e of the expansion space decreases due to the reduction in heat displacement of unit working medium. Thus both of the coefficient of performance and thermodynamic efficiency will be reduced. Figure 6 shows results calculated from experimental data.

Figure 6 shows an optimize-region for the cycle efficiency of the refrigerator correlated to the thermodynamic efficiency η_c of the Carnot cycle, i.e. the efficiency of the machine is highest when operating at corresponding temperatures in this region. However, the coefficient, ϵ, which depends only upon the temperature ratio, increases almost linearly with the refrigeration temperature. On the other hand, it is also learned from studying the effect of dead expansion space S_{ed} on η_c and ϵ, that a temperature increase and a reduction in efficiency η_c take place as S_{ed} increases while ϵ continues to increase. In fact, this shows that it is unreasonable to evaluate cycle efficiency at different refrigeration temperature by using ϵ only.

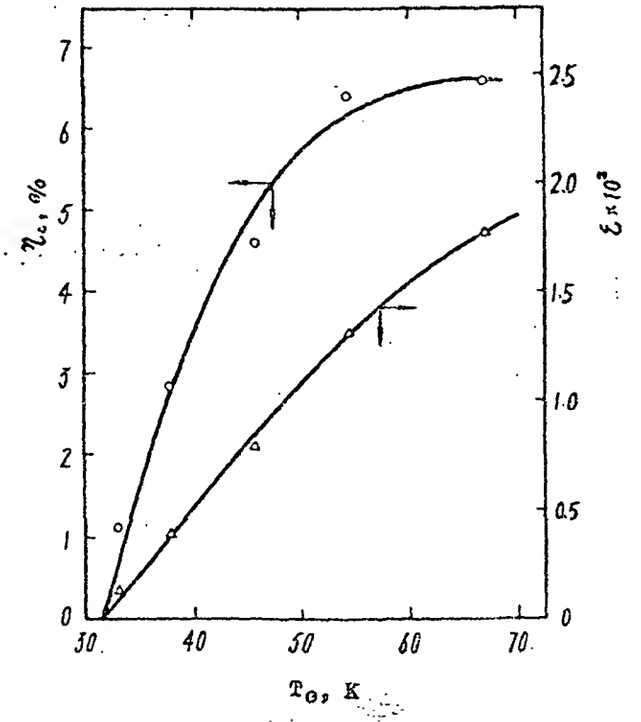

Figure 6. Variation of coefficient ϵ and thermodynamic efficiency η_c with refrigeration temperature T_e.

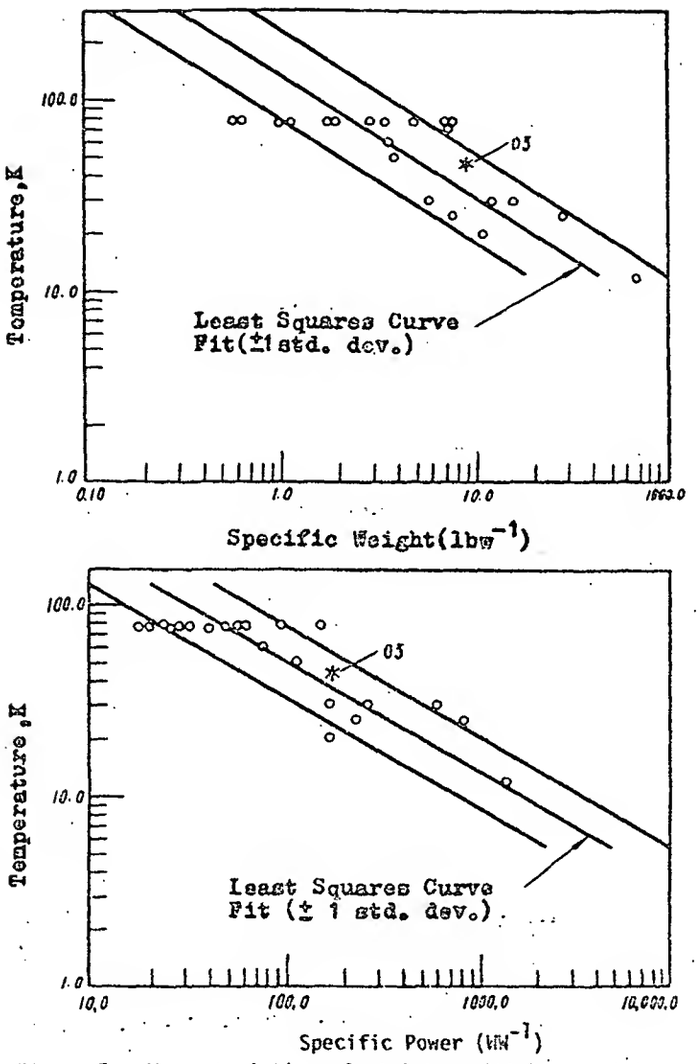

Figure 7. Characteristics of miniature Stirling refrigerator.

Figure 7 shows power and weight characteristics of Stirling refrigerators [4]. Calculated data of our experimental machine are also plotted in the figure (plotted by "*" and numbered 03). From figure 7 it can be seen that specific weight and specific power of our cryocooler are in the middle of the wide band.

4. Discussion

Using experimental data of temperatures and refrigeration powers measured, the different cold losses of the refrigerator are evaluated according to reference [5]. Calculated net cooling capacities are essentially consistent with measured ones. Now the discussion will be made in the following two problems.

4.1 An Optimum Pressure in Figure 2.

A number of experiments on two refrigerators proved that the working pressure has a strong effect on refrigeration temperature and that there is an optimum pressure on pressure versus refrigeration temperature diagram (Fig. 2). It could be explained as follows.

Major cold losses of a refrigerator include shuttle loss, pumping loss, heat conduction loss of the displacer and the cylinder wall, and regenerator inefficiency loss, etc. There are over 30 parameters in all equations which are applied to calculate cold losses. Most of those parameters are structure ones, and only one fourth of those are physical parameters of working medium and operation parameters. Under our operating condition of the machine, the specific heat and thermal conductivity of the working medium undergoes a small change when the pressure changes. The shuttle loss and heat conduction loss are mainly functions of the temperature gradient in the axis direction, but independent of working pressure [6]. The operating temperature of this machine is far away from the critical temperature of the working medium He, so that the enthalpy flow loss caused by the nonideal property of the working as is negligible. Thus the major cold losses which have apparent relations with the pressure are the following three terms:

Pumping loss

$$Q_{pu} = \frac{2(\pi D_c)^{0.6} L_{cy} (P_{max}-P_{min})^{1.6} C_p^{1.6} (T_w-T_e) S^{2.6}}{1.5 Z R^{1.6} K_g^{1.6} (\frac{T_w+T_e}{2})^{1.6}} \tag{3}$$

$$\doteq A\,(P_{max}-P_{min})^{1.6}$$

Friction heat loss in regenerator

$$Q_{rf} = \frac{(P_{max}+P_{min})^3 V_{cm}^3 f L_r}{2(ZRT_e)^3 g_c A_{reg}^2 \rho^2 D_e J} \tag{4}$$

$$\doteq B\,(P_{max}+P_{min})^3$$

Heat load due to limiting value of film coefficient in regenerator

$$Q_{rh} = (1-\eta_r) C_p (T_w-T_e) \frac{(P_{max}+P_{min}) V_{cm} N}{2RT_e Z} \tag{5}$$

$$\doteq C\,(P_{max}+P_{min})$$

The total pressure dependent loss is

$$Q_t \doteq A(P_{max}-P_{min})^{1.6} + B(P_{max}+P_{min})^3 + C(P_{max}+P_{min}) \tag{6}$$

Experimental results and theoretical calculations show [5-7] that these terms account for a major portion of the total loss (over 60% normally) and affect cooling capacity or temperature significantly.

On the other hand the theoretical cooling capacity is proportional to the average operating pressure $P = \sqrt{P_{max} \cdot P_{min}}$ to the first approximation, i.e., it is a linear function of the pressure. But it is known from eq. (6) that the changing rate of the cold loss Q_t increases with the pressure. Therefore, if the changing rate of the cold loss versus pressure is lower than that of theoretical cooling capacity, the net cooling capacity would have increased with pressure, i.e. the limiting refrigeration temperature of the machine could have decreased with pressure. On the contrary, the net cooling capacity should decrease while the pressure increases, i.e. the limiting refrigeration temperature will increase with the pressure. So there must exist an optimum pressure for the refrigerator. Reference [7] discussed the influence of the working pressure of refrigerators on the cooling capacity. As for the case when a possible low refrigeration temperature is required in small power consumption refrigeration, the machine has better operation near the optimum pressure. The advantage of low pressure operation is particularly apparent when the increment in pressure causes a rapid increase in regenerative heat loss.

Incidentally, if the working medium is H_2 instead of He, the corresponding highest pressure Pmax reaches the critical pressure of H_2 when filling gas pressure is greater than 4.5 bar. The lowest refrigeration temperature of the refrigerator cannot be lower than the critical temperature (33 K) of H_2 even though the pressure is increased continuously. Mean while the enthalpy flow loss reaches a considerable large value due to non-ideal property of the working medium.

4.2 Comment

Most of the structure parameters and operation conditions of the refrigerator, such as the gas distribution proportion in the 1st and 2nd stage cold chambers (20% and 80%, respectively) and the relative volume of dead spaces of the 1st and 2nd stage cold chambers corresponding to the largest displacement volume etc. are approaching normal values of practical refrigerators. But why is the refrigeration temperature still higher? First, the length and construction of the secondary regenerator is imperfect, e.g. the dead space of the regenerator is less than 1.5 times the largest volume of the cold space (normal values are 1.5 - 3.5 times). Second, the copper cylinder connected with the cold head of 2nd stage is so close to the 1st stage cold head (about 15 mm) that temperature distribution is unreasonable. The temperature difference $\Delta T = T_m - T_e$ is relatively small. Thirdly, the specific heat of the stainless steel packing material in the secondary regenerator will rapidly decrease and working medium He will increase, when the temperature is further reduced. This phenomenon leads to "thermal saturation" in a regenerator and reduces its efficiency. Besides, the experimental conditions were rather difficult, the temperature of the cooling water which was put into the compressor was too high, and therefore the hot end temperature of the primary regenerator was even higher than 40°C. Therefore, the structure of the 2nd stage regenerator has to be improved and the packing material has to be changed as well.

5. References

[1] Li, S. M., et al. Single Stirling Cycle Refrigerator, to be published. (1984).

[2] Cui, G. J., et al. Oevelopment Introduction of A3040 Miniature Stirling Refrigerator, (1972).

[3] Daniels, A. and du Pre, F. K., Advances in Cryogenic Engineering 16, 178-184, (1971).

[4] Wolfe, W. L. and Zissis, G. J., The Infrared Handbook, Office of Naval Research, Department of the Navy, Arlington, VA, 15-31, (1978).

[5] AO-A 027055 (1976).

[6] Radebaugh, R., XV International Congress of Refrigeration, A1/2-16, Venice, Italy, (September, 1979).

[7] Walker, G., Cryocoolers, Plenum, (1983).

PARAMETRIC TESTING OF A LINEARLY DRIVEN STIRLING CRYOGENIC REFRIGERATOR

F. R. Stolfi and A. Daniels

PHILIPS LABORATORIES
A Division of North American Philips Corporation
Briarcliff Manor, New York 10510

This paper describes the parametric testing of a novel Stirling cycle cryogenic refrigerator which incorporates electro-magnetic bearings, clearance (i.e., non-contacting) seals and electronically controlled linear motion. The last feature, which involves the use of two linear motors, position transducers and a highly accurate electronic feedback network, produces the system capability which forms the basis for the tests. The test results provide designers with an understanding of the basic operation of the Stirling cycle and give potential users some indication of the capabilities of this refrigerator under off design conditions.

Key Words: Control system performance; cryogenic; linear motors; magnetic bearings; refrigerator; Stirling cycle; test results.

1. Introduction

Philips Laboratories designed, fabricated, and tested a unique Stirling refrigerator which can operate for many years without the need for periodic maintenance and without performance degradation, and which is therefore compatible with spaceborne applications. This was accomplished by suspending the internal moving parts of the refrigerator electro-magnetically, to eliminate contact and the associated wear. The electro-magnetic suspension was further enhanced by the use of a direct (linear) drive and by clearance (rather than contacting) seals.

The testing of the refrigerator went through four phases: subassembly tests of the major components in dedicated test fixtures, performance tests at the design point (5 W at 65°K), parametric tests of the performance sensitivity to changes in various operating parameters and a life test. The first two phases of testing were discussed extensively at a previous conference (1); the third is the subject of this paper. The life test is currently in progress, with over 11,000 hours of maintenance-free and degradation-free operation attained to date. The life test will be discussed briefly at the end of this paper.

Since the purpose of a cryogenic refrigerator is to produce cold at very low temperatures with high efficiency, its performance criteria can be readily defined. Input power, cold production (output power) and operating temperature are obviously very important characteristics. The magnitude of these quantities (e.g., the input required to produce a certain amount of cold) depends on the refrigerator geometry (e.g., the size of the components) and on the operating parameters. Therefore, a measure of any cryogenic refrigerator's capabilities is the way in which the performance criteria - input power, cold production and temperature - vary with the various geometric and operational parameters.

To assess its operational capabilities, a parametric study was performed on the refrigerator system at this stage of its development. Specifically, the study was meant to:

- Establish the optimum operating conditions required to produce the nominal cooling (5 W at 65°K) level.

- Provide potential users with information on how the refrigerator performs under off-design conditions.

- Measure the tolerances of the various predicted design quantities as a step toward initiation of the next design.

The parameters of interest are either characteristic variables of the basic refrigeration cycle or those which will determine the capabilities of the refrigerator for potential users. These parametric tests are considered the first logical step in the design of the next generation of this refrigerator, a design which has already been initiated.

2. The Cycle

The Stirling cycle is based on the linear, reciprocating motion of two elements: the piston and the displacer. The reduction to practice, that is, the mechanization of the piston and displacer motions, has proven to be a difficult task. Three approaches deserve mention: crank drives, free-displacer drives and linearly driven piston and displacer drives.

A crank drive, which converts rotary to reciprocating motion is a complex mechanism. It has a crankshaft, connecting rods (drive linkages) and numerous bearings and pressure seals.

The free-displacer drive, which makes use of the gas compressed by the piston to reciprocate the displacer, requires careful attention to the mass of the displacer and to the magnitude of the gas flow; it also requires adjustment of various parameters once the refrigerator is built.

The linearly driven piston and displacer concept, incorporated into the refrigerator design presented in this paper, is an elegant approach to the mechanization of the Stirling cycle, even though its realization requires the construction of two special-purpose linear motors and an electronic position control system.

Although its mechanization is difficult, such designs are chosen because the Stirling cycle is inherently thermodynamically efficient and is very attractive for applications requiring temperatures in the 8°K - 100°K (-450°F - -280°F) range.

In the refrigerator design presented in this paper, the reciprocation of the piston and displacer is sinusoidal, with the displacer position leading that of the piston by about 70°. The p-v (pressure vs. volume) diagram for an ideal (isothermal) cycle is shown in figure 1b, the approximate position of the piston and displacer at the transitions being noted in figure 1a. The variations in the volume of the expansion space (V_e) and the volume of the compression space (V_c) due to the motions of the piston and displacer are shown in figure 1c.

For the ideal cycle, the cold production Q (Watts) is given by,

$$Q = \omega \oint p \, dV_e = -\omega \, x \, y \, P_m \, A_d \sin \phi_{dr} \qquad (1)$$

where, ω = operating frequency (rad/sec)
p = pressure (N/m^2)
x = amplitude of displacer (m)
y = amplitude of piston (m)
P_m = mean pressure in refrigerator (N/m^2)
A_d = surface area of displacer (m^2)
ϕ_{dr} = phase angle between piston and displacer positions (°).

Similarly, the mechanical power which must be provided to the cycle (Watts) is,

$$W = \omega \oint p \, dV_c = -\omega \, x \, y \, P_m \, A_p \sin \phi_{dr} \qquad (2)$$

where, A_p = surface area of piston (m^2).

For the ideal Stirling cycle, the thermodynamic efficiency is,

$$\eta = \frac{Q}{W} = \frac{T_e}{T_c - T_e} \qquad (3)$$

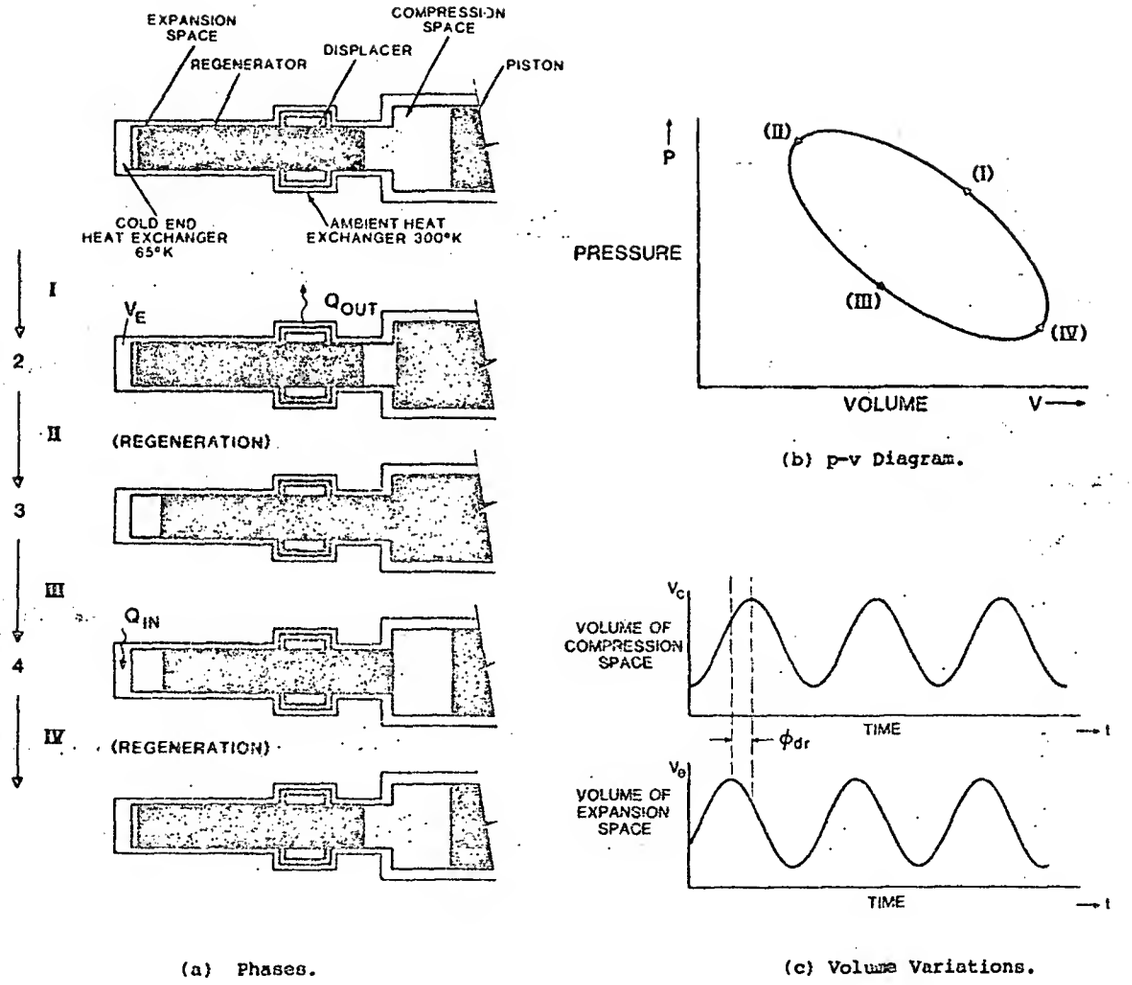

(a) Phases.

(b) p-v Diagram.

(c) Volume Variations.

Figure 1. Phases, p-v diagram and volume variations for ideal Stirling cycle.

where, T_e = temperature of expansion space (cold finger) (°K)
T_c = temperature compression space (ambient heat exchanger) (°K)

which equals that of the Carnot cycle, meaning that the ideal Stirling cycle is completely reversible.

The actual efficiency of the refrigerator is less than the ideal because losses in the cycle cause the input power to increase and the cold production to decrease. Factors which directly effect the input power include mechanical loss (friction) in the drive, flow losses, and adiabatic losses (i.e., where the process differs from the isothermal ideal). Factors which reduce the cold production include flow, insulation and conduction losses, as well as losses due to the non-ideal nature of the regenerator and heat exchanger. The regenerator, often called the heart of a Stirling refrigerator, stores thermal energy in one half cycle to release it in the other half and thereby increase efficiency. In an ideal regenerator (perfect heat transfer), a temperature gradient is established along the regenerator in the direction of flow, which allows the gas to be cooled down and heated reversibly. Also, the pressure drop across an ideal regenerator is zero. In an ideal heat exchanger, the temperature of the gas is constant, exactly equal to the temperature of the heat exchanger walls, regardless of the amount of heat in the gas. All real regenerators and heat exchangers differ from the ideal to some extent.

From the above discussion, it can be seen that the displacer amplitude (x), piston amplitude (y), operating frequency (ω), mean pressure (P_m), and piston/displacer phase (ϕ_{dr}) are important parameters which characterize the operation of a Stirling refrigerator.

3. Description of the Refrigerator

The useful life of a conventional Stirling refrigerator is limited by two major factors: wear and outgassing. Wear is present in most mechanical devices which have moving parts. Bearings and pressure seals wear out; mechanical rubbing and the associated friction generate potentially harmful particles. The other problem is the outgassing products (impurities) of organic materials in the refrigerator working spaces such as lubricants and seals. These impurities are "gettered" (attracted) by the low temperature regions in the machine and eventually clog critical passages. Since both surface wear and the presence of impurities result in thermal degradation, the simplest and perhaps the only road to longevity is to eliminate both.

The Philips refrigerator was designed to produce 5 Watts of refrigeration at 65°K for 5 years or longer (2). Four major features of the unit led to the long life attained: a purely rectilinear drive (with linear motors and with an electronic axial-control system), electro-magnetic bearings, clearance seals, and an all metal/ceramic working-gas envelope. The synergistic combination of these four features has completely eliminated wear and impurities.

A cross sectional view of the rectilinear drive and of the linear motors is shown in figure 2. The drive produces the required linear piston and displacer motions directly, i.e., without the use of a crankshaft or linkages. The motors are of the moving-magnet type, which have the

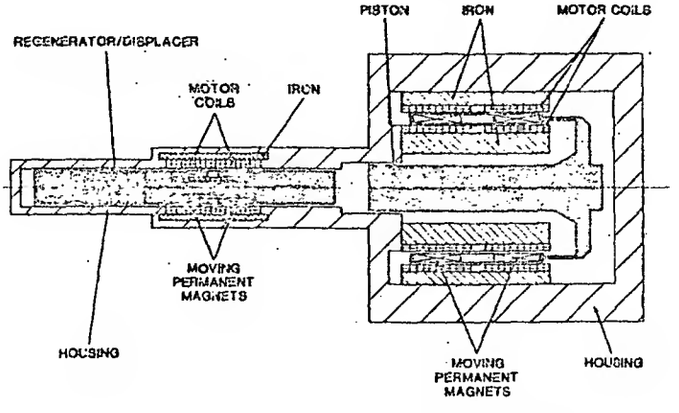

Figure 2. Cross-sectional view of rectilinear drive showing displacer and piston motors.

advantage that no flexing power leads are required. The directly coupled drive eliminates the mechanical drive losses associated with conventional refrigeration devices. Direct coupling requires an axial control system to maintain the proper piston and displacer amplitudes and the phase relationship dictated by the Stirling cycle. The capabilities and versatility of this control are important aspects of this novel refrigerator design and form the system basis which makes the type of testing, described in this paper, possible. The control system is discussed in more detail in section 5.

The electro-magnetic bearings consist of a set of electromagnetic actuators, radial position sensors and an electronic control system. The actuators are small electromagnets, consisting of a coil of wire and iron pole pieces. The radial position sensors are eddy-current type, indicating the radial position by the amount of change in eddy current loss that a radial position change produces in a pick off coil. The radial displacement of the shaft is detected by the sensor which signals the control system to adjust the current in the actuators, thereby suspending and maintaining the reciprocating shaft in the center of its bore. This method permits both the piston and displacer in the refrigerator to be supported without contact and without any bearing friction losses.

The clearance seals are long, narrow, annular passages around the piston and the displacer. Pressure sealing is attained by the flow restriction these passages provide to the oscillating working gas. This method of sealing requires that the piston and displacer reciprocate in close proximity to the adjoining walls. This is made possible by the highly accurate operation of the electro-magnetic bearings.

Since the electro-magnetic suspension, linear drive, and pressure sealing are accomplished without mechanical contact, it was possible to fabricate the working space envelope of the refrigerator (i.e., those internal areas in contact with the working gas) from metal and ceramic only. There are, as a result, no organic compounds of any kind exposed to the working gas. The organic materials required in the construction, such as the insulation of the motor wire or various potting compounds are hermetically sealed in thin-walled envelopes.

A photograph and a cross section of the refrigerator are shown in figure 3. The expander subassembly which houses the displacer is at the left; cold is produced at the far left tip (cold finger). The refrigerator is a single-stage expansion Stirling design (i.e., only one cryogenic temperature, 65°K, is produced) and thus has a single diameter for the displacer bore. The compressor subassembly (in the center of the photograph and right side of cross section) houses the piston and associated parts. The refrigerator has a passive counterbalance, a spring-mass system which significantly reduces the axial vibration of the unit. It is shown at the far right of the photograph and discussed in reference 1.

The moving displacer contains the regenerator, a moving-magnet linear motor, and a non-contacting element for the axial position transducer. The regenerator is fabricated from a phosphor bronze wire mesh which has a high thermal capacity and which remains relatively porous to the reciprocating flow of the helium gas with which the refrigerator is charged. The electro-magnetic bearings which support the displacer (along with the radial position sensors) also form the clearance seals, forcing the gas through the regenerator and through the ambient heat exchanger. The heat exchanger is maintained at ambient temperature by a water jacket; its surface also permits the attachment of a heat pipe instead of the jacket. A vacuum Dewar (partially shown in the cross section and absent in the photograph) lined with super insulation (multi-layers of foil and mesh) thermally isolates the cold finger.

The piston in the compressor subassembly is coupled to its moving-magnet linear motor and to a non-contacting element for its axial position transducer. The electro-magnetic bearing near the compression space forms a clearance seal to the compression pressure; the bearing at the rear of the piston is used for support but forms no seal. All electrical connections are hermetic, using nickel and ceramic feedthroughs.

In the following section, the general procedure for the parametric tests is discussed. Each test involved varying one operating parameter and noting its effect on refrigerator performance (change in the output variables). Section 5 describes the axial control system to provide some understanding of how the parameters can be varied during operation. Finally, section 6, presents test results. It should be noted that all plots and data presented in these sections and section 7 (life testing) represent actual measurements taken on the refrigerator.

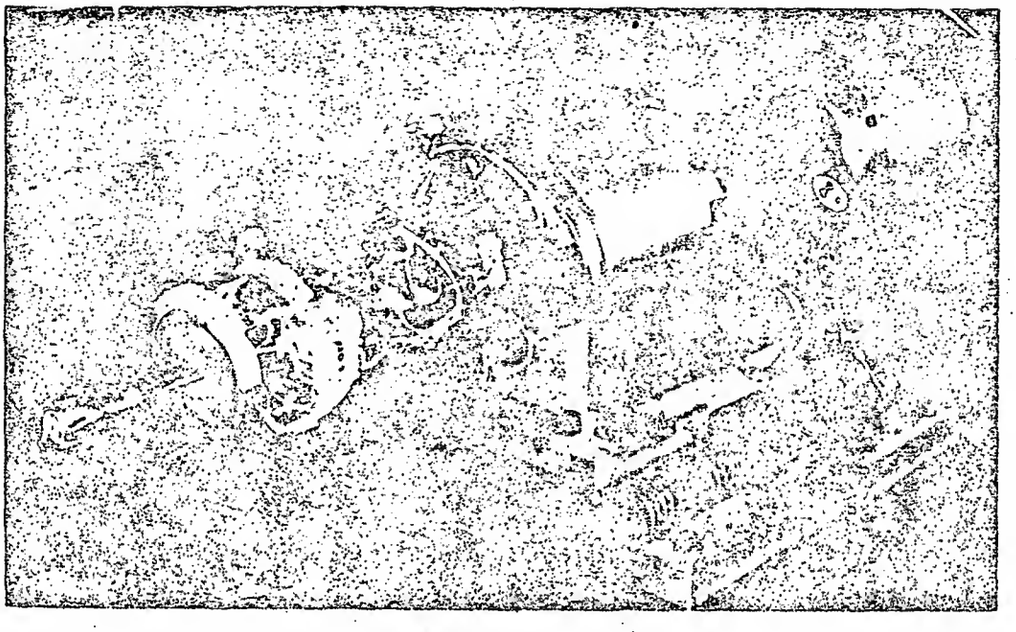

(a) Photograph.

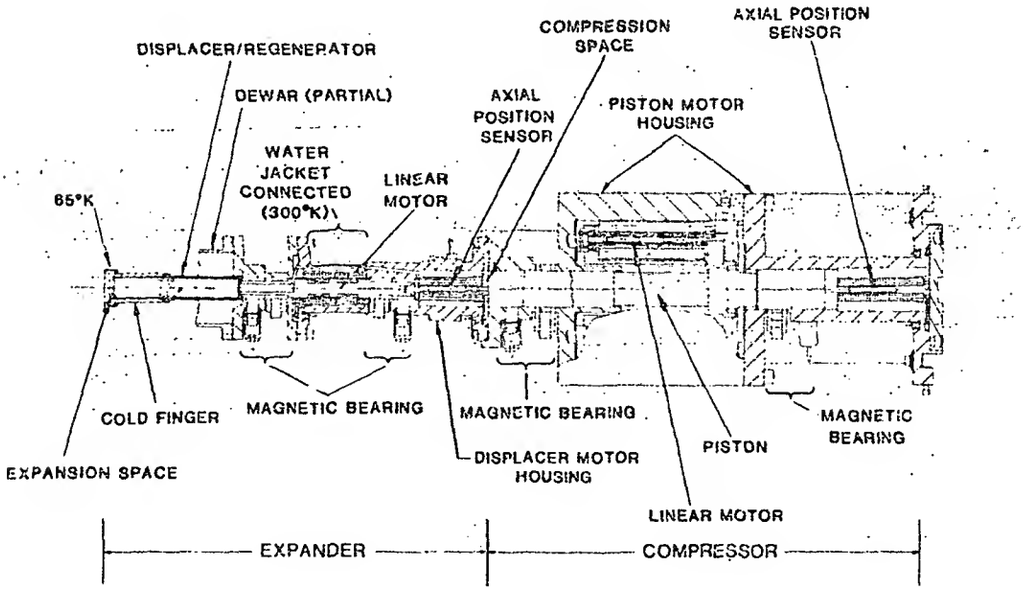

(b) Cross Section.

Figure 3. Photograph and cross section of refrigerator.

4. Overview of the Parametric Testing

The parameters of interest are either characteristic variables of the Stirling cycle (Eqs. 1 and 2) or those which will determine the capabilities of the refrigerator for potential users. Parameters which fall into the first category are piston and displacer amplitudes, operating frequency, mean pressure, and piston/displacer phase. Tests which fall into the second category are output temperature versus cold production and variations in heat-rejection temperature. For simplicity, only one parameter was varied in each test while the others were held constant. The effect of the one parameter on the output variables can then be easily observed. The values at which the other parameters were held constant differ between tests and were chosen so that the parameter which was varied could have a wide excursion. Given this limited scope of the testing, some care must be exercised in the interpretation of results. Even though "optimal" performance was sometimes achieved with only one variable changing, it is possible that a better operating condition exists. The operating parameters are not independent in general and the selection of the operating conditions for performance other than the nominal 5 W at 65°K often involves adjusting several parameters. This also means that if two parameters are varied, the net result on performance may not be the sum of the results of varying each one independently.

A schematic representation of the refrigerator test setup is shown in figure 4. Three pieces of laboratory equipment are required for normal operation: two water coolers and a vacuum station. The water cooler for the ambient heat exchanger removes the heat of compression (thermodynamic cycle) and the ohmic loss of the displacer motor. The water cooler for the piston housing removes only the ohmic loss from the piston motor. (Since this motor is 70% efficient, the power loss is small.) The vacuum station produces the thermally insulating vacuum in the Dewar. The refrigerator was instrumented with transducers to measure temperature, pressure, radial and axial position, coolant flow, and case acceleration (3).

The approach for each test followed a similar procedure. The temperature of the cold tip was first reduced to the nominal 65°K with no heat load applied. This required supporting the piston and displacer with their electro-magnetic bearings, engaging the safety interlock system, and reciprocating the piston and the displacer. The nominal peak displacements for the piston and displacer are 7 mm and 3 mm, respectively, with a nominal phase relationship of 67° (1.17 rad).

Once the desired cold temperature (65°K) was reached, a resistive heater (load) on the cold ti, was turned on, a given parameter was varied and its effect on the other system parameters was measured. The signals measured were either slow-varying dc (e.g., cold temperature) or primarily single-frequency ac (at the operating frequency) with a large amount of noise and higher harmonics (e.g., piston motor current). To measure the former, a dc voltmeter was employed, and the

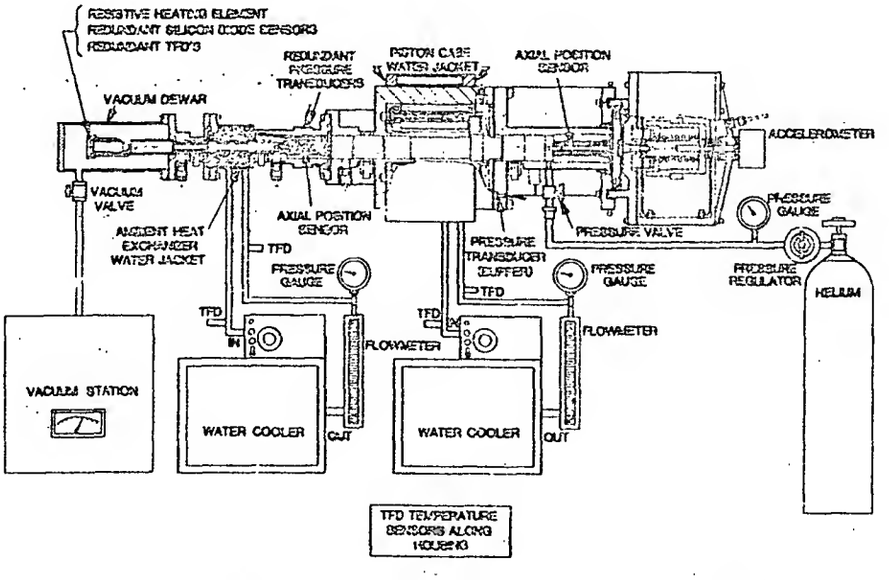

Figure 4. Schematic representation of refrigerator under test.

measured quantity was considered stable when no notable change was observed for about 5 min. The latter was measured with instruments employing one of three standard signal processing techniques: heterodyning with the input reference oscillator used for locking, rms averaging of spectra obtained from a Fast Fourier Transform routine, or time averaging of signals obtained from a high-speed data acquisition system. In this paper, db is defined as 20 log (quantity), the normal mode for the equipment employed. Measured data points are noted; curves are computer-generated using either a linear or polynomial least-squares routine.

5. Axial Control System

As an aid to understanding how parameters can be varied during refrigerator use, the operation and accuracy of the axial control system will be discussed next. A block diagram of the control system is shown in figure 5. The piston amplitude, displacer amplitude, frequency, and piston/displacer phase angle are set with dc voltages which are adjusted at the control panel. The frequency and phase control electronics employ local feedback loops to maintain the accuracy of the reference signals for the displacer and piston closed loop position servomechanisms in spite of component drifts. The reference signals are amplitude-controlled sinusoids with less than 0.1% harmonic distortion. The reference signal to the piston lags the signal to the displacer, producing the desired piston/displacer phase angle. The two closed loop position servomechanisms then control the motions of the piston and displacer with a high degree of accuracy and low harmonic content.

Although the closed-loop position servomechanisms for the piston and displacer look similar in figure 5, they are considerably different because of the extreme dissimilarities in the frequency response of their motor and system dynamics. The displacer, as the measured dynamics of figure 6 indicates, is nearly a pure inertial load. (The additional rolloff which begins at 200 Hz is from filtering the axial position sensor). Principally, the force produced by the motor serves only to accelerate and decelerate the mass. Since the motion is sinusoidal, with the displacer returning to its axial center position after each half cycle, there is no net displacement and no work is done. The mechanical output power is reactive (power factor of 0),

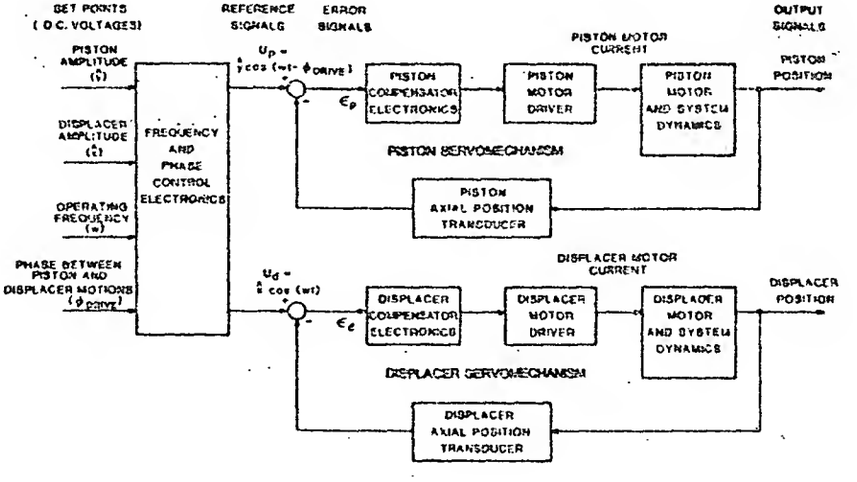

Figure 5. Block diagram of axial control system.

and therefore, the electrical input power to the motor is only the ohmic loss dissipated in having to produce the required force. Ignoring the inductive reactance, therefore,

$$P_d = I_d^2 \; R_d = \omega^4 \; x^2 \; R_d / K_d^2 \qquad (4)$$

where P_d = average electrical input power to displacer motor (W)
I_d = current in displacer motor (A)
R_d = motor armature resistance (Ω)
K_d = motor force constant (N/A) (i.e., Force = $K_d I_d$)

The piston, on the other hand, is designed to resonate on the gas spring of compression (the effective "spring" of gas being compressed in a closed cylinder) which leads to highly efficient electromechanical operation. Its motor and system dynamics, as shown in the measured dynamics in figure 6, has a spring-mass resonance characteristic (along with the position sensor filtering). The reactive inertial force is balanced by the reactive gas spring force, and the motor only produces a real (as opposed to reactive) force term which supplies the required mechanical input power to the thermodynamics (power factor of 1). The electrical input power to this motor can thus be separated into two terms: one resulting from supplying the real mechanical input power to the thermodynamics (Equation 2 above) and one relating to the balanced reactive inertial power and gas spring power. For normal operation, the piston is in resonance and the net reactive power is zero; however, for the parametric tests discussed here, the piston does come out of resonance slightly.

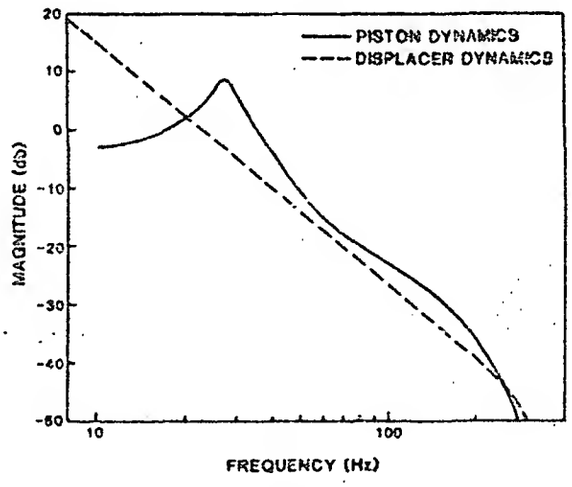

Figure 6. Frequency responses - displacer and piston motor and system dynamics.

The dynamics of a gas spring are different from those of a mechanical spring in two important respects. First, the damping in a gas spring is generally higher than in a mechanical spring. Thus, power is dissipated at resonance which must be supplied by the linear motor, and the quality factor (Q) of the system is low. Second, because of flow losses and leakage past the compression seal, the stiffness of the gas spring is a function of frequency and is slightly nonlinear (i.e., it has some higher harmonic components). These disadvantages of the gas spring are outweighed by the advantage of having a spring for resonance with no mechanical contact, no danger of fatigue failure and no possibility of fracture.

The harmonic operation of the displacer axial control system is illustrated in figure 7a. The system applies current to produce the displacement at the operating frequency (26 Hz) shown in the figure. Power at higher harmonics of the operating frequency is also applied to reduce the harmonic content of the displacement. The amount of rejection of these higher frequencies is determined by the gain of the control system. As discussed in Reference 2, the bandwidth of the displacer control system is 105 Hz, which implies that there is some control system gain at the third harmonic (about 78 Hz). Note in the figure that the second harmonic is 31 dB below the fundamental.

Similarly, the harmonic operation of the piston axial control system is illustrated in figure 7b. The control system bandwidth is 65 Hz, which implies that there is no control system gain and thus no rejection of the third harmonic (the third harmonic content of the displacement is small, however, because of dynamic characteristic of the gas spring). It should be noted that the piston operates at its resonant point with high accuracy (small error in the control loop) because of the high open-loop gain at that frequency (see Ref. 2).

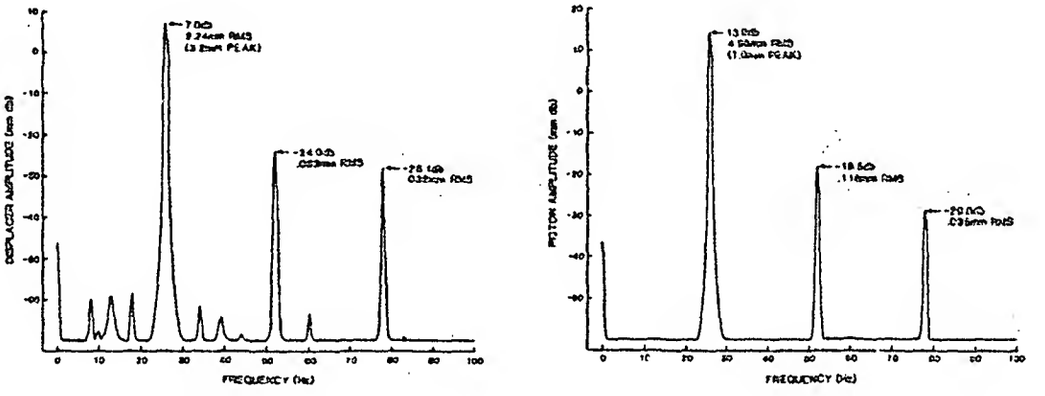

(a) Displacer. (b) Piston.

Figure 7. Frequency spectrum - displacer and piston displacement.

The low harmonic content of the displacements in the figure means that the assumption of sinusoidal volume variations discussed above is valid. For the most part, the variations in input and output power for different operational parameters are therefore approximated well by Equations 1 and 2.

6. Parametric Test Results

6.1 Heat Load

The variations of output (cold) temperature and of electrical input power to the motors with changes in the load power (ie. the power in the resistive heater mounted on the cold finger) are shown in figure 8. The parameter values that were held constant for this test and for all those that follow are listed in appendix A. As expected, as the applied load power increases, so does the cold temperature. It should also be realized that "no applied load" is not the same as zero power output since there are always parasitic loads on the cold finger. Even with the resistive heater off, heat is being radiated from the inner surface of the vacuum Dewar which encloses the cold finger and is being conducted down the wires which connect the temperature sensors and the resistive heating element, as well as down the body of the cold finger itself. These parasitic loads account for the non-linearity of the temperature line at low applied power.

The electrical input power to the linear motors drops as the applied load power increases. This can be explained by referring to Equation 3 above ($\eta = T_e/(T_c - T_e)$) and by examining

several losses. The thermodynamic efficiency of the refrigerator increases as the temperature of the cold finger (T_0) increases. Thus, although the applied load on the cold finger is higher, the refrigerator can cool this load using less electrical input power because of the increased efficiency of the cycle. (The overall measured efficiency -- applied load power/electrical input power to the piston and displacer motors -- is shown versus applied load power in figure 9.) Also, the radiation and conduction losses decrease as the temperature of the cold finger increases (since there is less of a temperature difference between the cold finger and ambient). Finally, the flow losses decrease because the gas density decreases with the increase in average temperature of the refrigerator (flow friction for turbulent flow is a function of density). This last effect is very small.

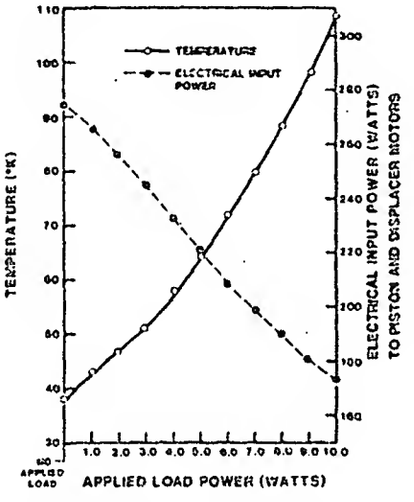

Figure 8. Cold temperature and electric input power to motors vs. applied load power.

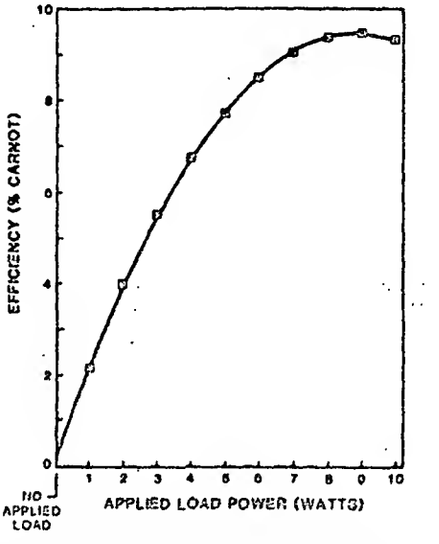

Figure 9. Overall measured efficiency (% of Carnot) vs. applied load power.

It should be noted that the operating parameters of the refrigerator (strokes, frequency, phase, etc.) were not varied for this test. It is possible to produce the off-design cold outputs (i.e., other than 5 W at 65°K) with less electrical input power than given in figure 8 by optimizing these parameters appropriately. Such multi-parameter tests were beyond the scope of this paper. It should also be noted that this test and the heat rejection temperature test which follows are the only ones in which the cold temperature was allowed to vary. In all others, the applied load from the resistive heating element was adjusted to maintain a constant 65°K temperature on the cold finger.

6.2 Operating Frequency

Figure 10 shows the variation of applied load power (cold production) and electrical input power to the motors with changes in the operating frequency. Several effects contribute to the shape of these curves. First, it can be seen from Equations 1 and 2 that both the ideal cold production and the ideal mechanical input power to the Stirling cycle vary linearly with operating frequency (since both are proportional to the number of times that the p-v curve is traversed per unit time). Secondly, many losses such as those due to flow and to imperfect regeneration are functions of gas velocity and therefore of operating frequency. Some losses, such as that caused by the fluid friction of the flowing gas or that resulting from the temperature oscillation of local sections of the regenerator package over a cycle (since the transfer rate between the gas and the regenerator is finite), increase with increasing frequency. Others, such as the clearance seal leakage decrease with increasing frequency. Finally, as discussed, the nature of the displacer and piston motor and system dynamics means that the magnitude and phase of the input power for each are functions of the operating frequency.

For the small range of frequencies considered, the motor and system dynamics produce by far the most significant effect. The displacer motor input power increases as the fourth power of the operating frequency, as noted in Equation 4 and the piston power has a resonant mass-spring characteristic (with some nonlinear effects produced by the gas spring). The sum of these two effects determine the shape of input power variations noted in figure 10. The variation of piston and displacer motor force with operating frequency is shown in figure 11. The displacer motor force varies approximately as the square of the operating frequency as would be true of the purely inertial system, and the piston motor force exhibits the spring-mass characteristic (minimum force at resonance). From this, it is also apparent that the system dynamics dominate the response and any change in the losses is not significant.

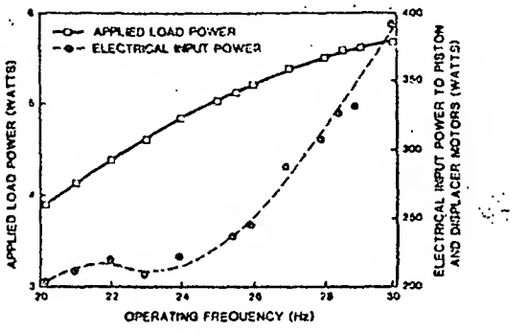

Figure 10. Applied load power and electrical input power to motors vs. operating frequency.

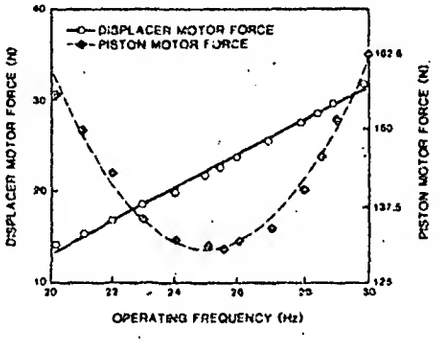

Figure 11. Displacer motor force and piston motor force vs. operating frequency.

Again, some caution should be exercised in interpreting this data. Since this is a test in which only one parameter is varied, conclusions can not be drawn about what is the best frequency at which to operate the refrigerator. Both the mean charge pressure and the piston/displacer phase affect the resonant frequency of the gas spring to some degree. The "optimum" operating frequency must take all such effects into account.

6.3 Piston/Displacer Phase

Figure 12 shows the variations of applied load power and electrical input power to the piston and displacer motors as a function of the piston/displacer phase. For the ideal cycle, the load power and electrical input power should vary as the sine of the phase (see Eqs. 1 and 2). This is the approximate shape of the curves in figure 12. The piston/displacer phase also influences flow losses and the piston gas spring resonance to a lesser degree. These effects are more easily observed in the variations in the piston and displacer motor force shown in figure 13. The

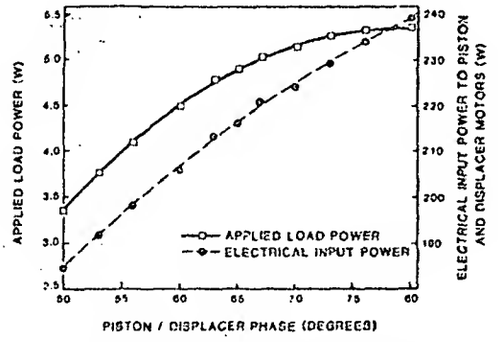

Figure 12. Applied load power and electrical input power to motors vs. piston/displacer phase.

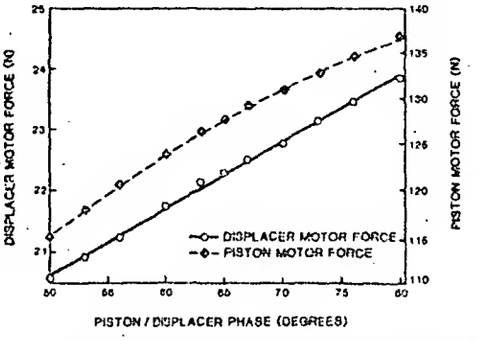

Figure 13. Displacer motor force and piston motor force vs. piston/displacer phase.

displacer motor force shows the effects of the flow losses; the piston force shows the change in resonance. From the figure, it should be noted that the variations in force are less than ± 10%.

6.4 Displacer Amplitude

The variations of applied load power (cold production) and electrical input power to the piston and displacer motors with displacer amplitude are shown in Figure 14. For the ideal cycle, the applied load power is proportional to displacer amplitude (Eq. 1). Several losses, however, are functions of displacer amplitude; the most notable is one associated with the regenerator, referred to as shuttle loss. As the displacer moves, the regenerator passes over different portions of the housing. As a result, there is a mismatch between the temperature gradient along the housing wall and the temperature gradient along the regenerator, and the mismatch increases for increasing amplitudes of oscillation. This mismatch results in heat transfer between the displacer and the housing walls and thus a loss.

Another important effect in this test and in the one which follows relates to the variation in refrigerator dead volume. The designation 'dead volume' is given to those regions in the working space of the refrigerator which do not change in volume as the displacer and piston move (i.e., do not participate in the thermodynamic cycle (Fig. 15)). Dead volume includes the heat exchanger space, connecting passages, and the unfilled space in the regenerator. Relevant to this test, dead volume also includes those regions in the expansion and compression space which are not swept by the peak amplitude of the displacer motion.

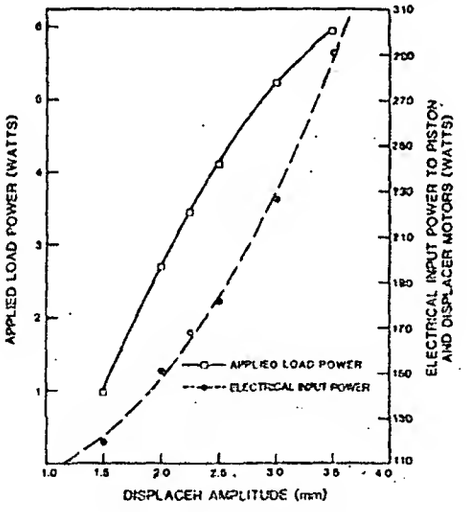

Figure 14. Applied load power and electrical input power to motors vs. displacer amplitude.

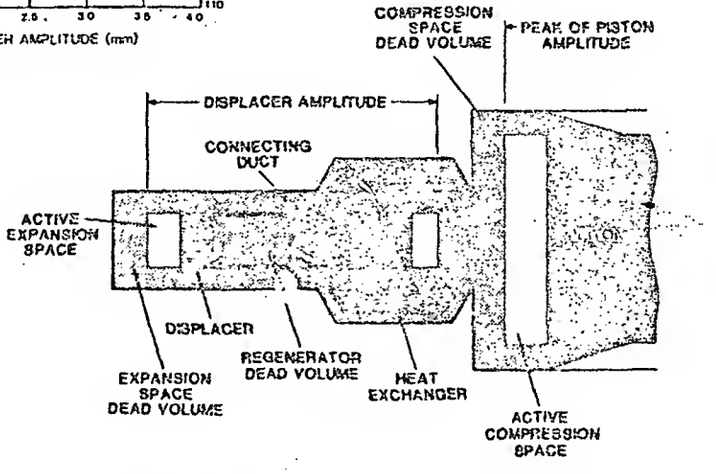

Figure 15. Schematic of dead volume (shaded). (Clearances are out of proportion for clarity).

A discussion of dead volume is given in Appendix B of Reference 2. For this paper, several comments will suffice. In general, dead volume reduces the cold production of a refrigerator. Often, it also reduces the required mechanical input power so that the refrigerator efficiency remains roughly constant. The magnitude of the effect of a given region of dead volume on the cold production or mechanical input power depends on the absolute temperature of that region. The colder the region, the greater the effect.

The electrical input power to the piston motor versus displacer amplitude is shown in figure 16. Since the displacer amplitude has little effect upon the gas spring resonance, the electrical input power to the piston motor is only that which is required to do the thermodynamic work. For the ideal cycle (Eq. 2), the mechanical input power required by the thermodynamics is proportional to displacer amplitude. The piston must also supply the work required to overcome the shuttle loss. Further, from the above discussions about dead volume, the mechanical input power should also be inversely proportional to the displacer amplitude (i.e., the mechanical input power required from the piston should decrease as the displacer amplitude increases because the dead volume decreases and this effect is independent of Eq. 2). In figure 16, the electrical input power to the piston motor varies approximately as the square of displacer amplitude.

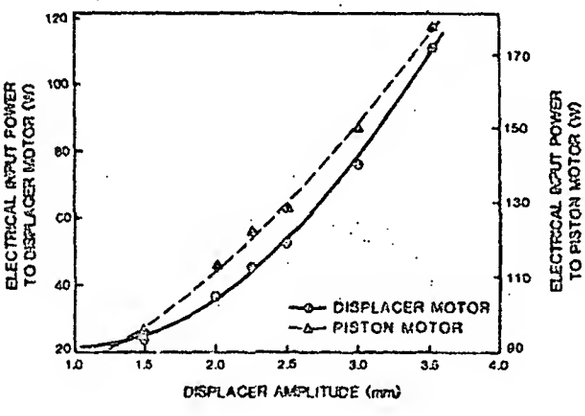

Figure 16. Electrical input power to displacer motor and to piston motor vs. displacer amplitude.

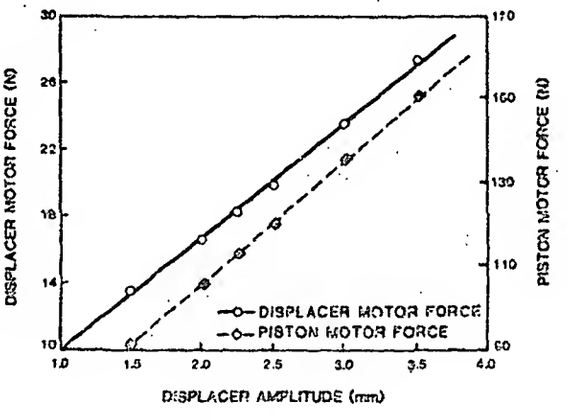

Figure 17. Displacer motor force and piston motor force vs. displacer amplitude

Consider now the electrical input power to the displacer motor versus displacer amplitude in figure 16. Since the displacer is an inertial load, the electrical input power is expected to vary as the square of the displacer amplitude (Eq. 4), as observed. Figure 17 which shows the variation of displacer motor force with displacer amplitude, also varies linearly, as expected for an inertial load.

6.5 Piston Amplitude

The change in applied load power and in electrical input power to the piston and displacer motors with piston amplitude is shown in figure 18. For the ideal cycle (Eqs. 1 and 2), the applied load power and electrical input power are proportional to piston amplitude. This characteristic was indeed observed. Flow losses and the effects of dead volume both change with piston amplitude tending to cancel. The flow losses increase with increasing amplitude because the peak oscillating pressure and volumetric flow rate increase as more volume is displaced by the piston. The dead volume decreases by the amount above the piston in the compression space as the piston amplitude increases (Fig. 15 above). As discussed, this dead volume effect is minimized because the volume is at the temperature of the ambient heat exchanger (warm).

An elegant characteristic for potential users of this refrigerator is illustrated by the linearity shown in Figure 18. If, for any reason, it is desirable to hold the cold temperature constant as the load varies, then piston amplitude provides a very effective means. A control system can be designed to measure cold temperature and adjust piston amplitude to hold the temperature constant (leaving all other operating parameters - displacer stroke, frequency, phase, etc. - fixed). Since the characteristic in Figure 18 is linear over a wide range, such a control system would be trivial to construct.

Figure 19 shows the variations in the force produced by the piston and displacer motors with piston amplitude. It is apparent from the linear nature of the piston force curve that the piston amplitude minimally affects the resonance of the gas spring.

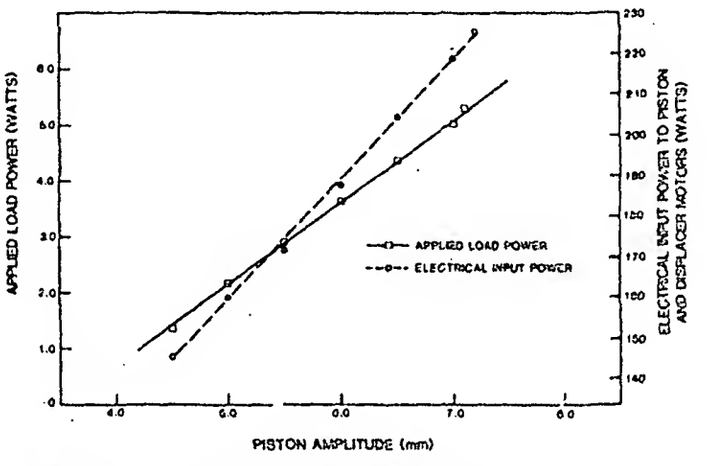

Figure 18. Applied load power and electrical input power to motors vs.piston amplitude.

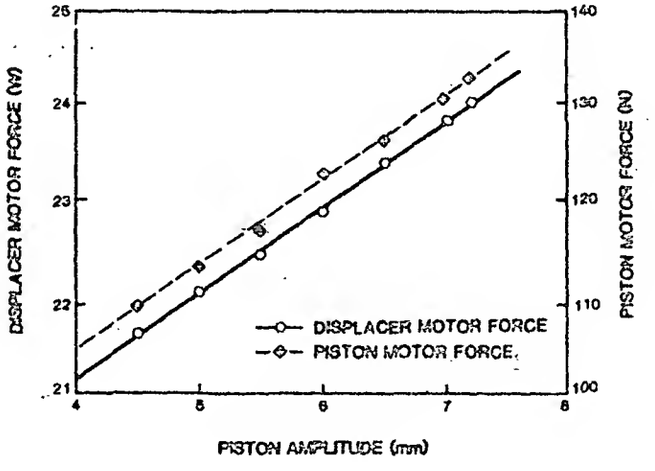

Figure 19. Displacer motor force and piston motor force vs. piston amplitude.

6.6 Mean Pressure

A pressurized bottle of helium was connected to the refrigerator via a pressure regulator and pressure gauge. For the following test, the mean pressure in the refrigerator was varied by adjusting the pressure regulator, while all other operational parameters were held constant (Appendix A). The mean pressure was measured with the pressure gauge, and sufficient time was allowed for the pressure in the refrigerator to stabilize for each measurement data point. The variations of applied load power and electrical input power to the piston and displacer motors with mean pressure are shown in figure 20. For the ideal cycle (Eqs. 1 and 2), these variations are expected to be proportional to mean pressure and, for this small change in pressure (± 'OO), this was observed.

Flow losses and regenerator losses are functions of pressure. Flow losses increase with pressure (density) because the flow is turbulent. This effect is small as shown by the small change in displacer motor force with mean pressure in figure 21. The regenerator becomes less efficient as the heat capacity of the gas increases with pressure (density) but this effect is also small for the small range of pressure variations used in the test and the relatively high cold temperature of this refrigerator (on an absolute scale). The mean charge pressure also

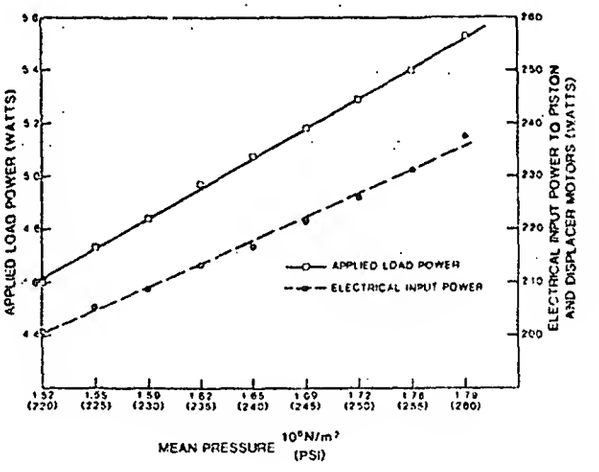

Figure 20. Applied load power and electrical input power to motors vs. mean pressure.

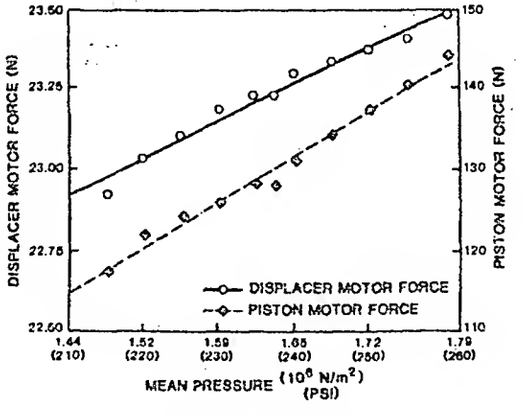

Figure 21. Displacer motor force and piston motor force vs. mean pressure.

determines the resonance of the gas spring and thus affects the electrical input power to the piston motor. The required motor force changes linearly with the mean pressure, again making the effect small for this range of variations tested.

6.7 Heat Exchanger Temperature

As discussed in Section 4 above, the temperature of the ambient heat exchanger is controlled with a closed-cycle water cooler. The water is circulated through a water jacket which surrounds the heat exchanger and returned to the reservoir of the cooler. The cooler has heating and refrigeration capabilities; the temperature of the water in the reservoir is determined by the set point of the thermostat on the water cooler. For the following test, the set point of the water cooler thermostat was varied, and all other operational parameters were held constant. The temperature of the water at the inlet of the water jacket was measured with a thin-film detector (TFD). Since the heat exchanger is not perfect, the temperature of the gas in the heat exchanger was considerably higher than the temperature of the water at the inlet. The gas temperature was not measured directly; however, it has been estimated to be about 15°C higher than the temperature of the water.

The variations in cold temperature and electrical input power to the piston and displacer motors with heat exchanger temperature are shown in figure 22. The cold temperature is proportional to the heat exchanger temperature, with a 3°K [3°C] change in heat exchanger temperature producing an approximate 1°K change in cold temperature.

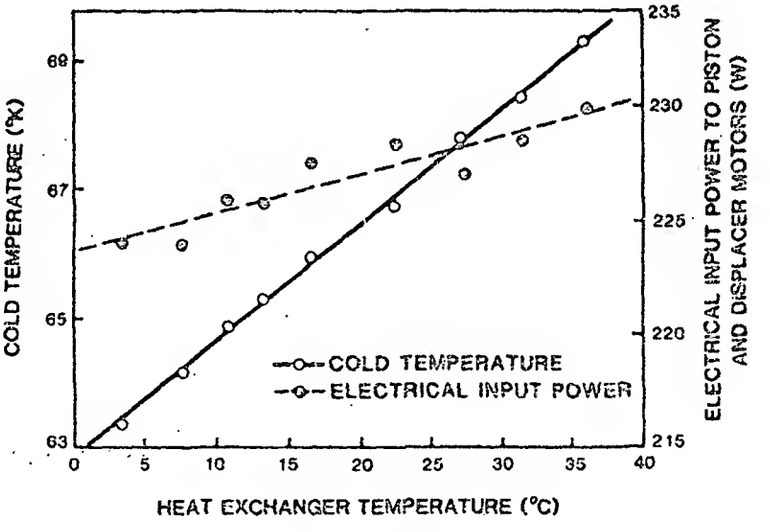

Figure 22. Cold temperature and electrical input power to motors vs. heat exchanger temperature.

The small change in electrical input power to the piston and displacer motors for changes in heat exchanger temperature is to be expected since there is only a negligible change in the efficiency of the refrigerator. Considering the ideal efficiency (Eq. 3), although the numerator increases because the cold temperature (T_c) increases, the denominator ($T_c - T_c$) also increases because of the difference between the cold temperature and heat exchanger temperature increases. There is also some net cancellation in the losses. Insulation losses and conduction losses between the room ambient and the cold finger (such as along the electrical leads to the temperature sensor and to the resistive heating element) decrease because the temperature of the cold finger increases. At the same time, conduction losses between the cold finger and the heat exchanger (i.e., along regenerator and cold finger housing) increase because the temperature difference increases. Also, there is a small decrease in flow losses because the gas density decreases as the average temperature of the refrigerator increases (the flow is turbulent, making the loss a function of density).

7. Life Testing

On August 30, 1984, the refrigerator exceeded 11,000 hours of operation at the nominal operating point of 65°K with a cold production of 5 Watts and continues to operate without problems. During this time, the refrigerator was stopped and restarted over 300 times. The cold temperature (along with several other operational parameters) is being measured with a digital data acquisition system. Measurements are taken every 30 minutes using a sampling frequency of 1 kHz. The samples are averaged over 2 seconds to reduce noise. As of this date, no temperature degradation has been observed to the accuracy of the silicon diode sensors (0.1°K). With the constant cold production, the cold temperature is also measured to be stable within $\pm$ 0.2°K (i.e., temperature fluctuations including noise induced by the silicon diode thermometer are also about 0.1°K). During this period, the refrigerator has never had to be disassembled for maintenance or inspection.

The electro-magnetic bearings along with their radial position sensors are left on continually even if the refrigerator is not operating or is undergoing tests. As of August 30, 1984, the bearings have logged over 21,000 hours of operation.

A small helium leak (approximately 1 psi per day) due to a manufacturing error has developed in one of the housing flanges. A technique to weld the flanges shut, which is proposed for the final version of the refrigerator and which was successfully demonstrated in a test fixture, was not used in this refrigerator. The helium loss is presently being compensated from a helium bottle.

The electronics which control and drive the refrigerator use only commercial parts (instead of space qualified parts) and no redundancy was attempted. Twice during the life test, a commercial electronic part failed. In both cases, the safety interlock system responded correctly and safely shut down the machine. The failed part was replaced and the life test continued. The final version of this refrigerator for actual spaceborne deployment will use space qualified, redundant electronics.

8. Conclusions

A novel feature of this refrigerator, namely full electronic control of the motion of its moving parts, was utilized to characterize its capabilities under parametric changes. The characterization is useful both for designers of the next generation of the refrigerator and for potential users. Designers have both an indication of the accuracy of their "optimal" design point and a determination of the tolerance of the design point to changes in operational parameters. Potential users have an indication of the operation of the refrigerator under off-design conditions which will broaden the range of potential applications.

Some care must be taken in the interpretation of results. In each test only one parameter was varied and its effect was measured. The data shows the quantitative influence of the parameter on the operation of the refrigerator. In general, however, the effect of each parameter is not independent, and thus the combination of two test results will not show the combined effect of varying the two parameters. This also means that more "optimal" off-design operating points than those shown in this paper generally exist. These off-design points are achieved by varying more than one parameter, depending on the operating point desired.

In spite of the limited scope of this work, the versatility of this refrigerator must be appreciated both as a tool for understanding the Stirling cycle and as a general instrument for a wide variety of cryogenic applications. The capability of having parameters electronically controlled and able to be changed in operation, which made this study possible, sets this design apart from refrigerators built in the past.

This work was supported by the NASA Goddard Space Flight Center (Contract No. NAS5-25172).

Appendix A

The following table lists the values for the refrigerator operating parameters which were held constant during each test. As mentioned above, these values were chosen so that the parameter which was varied could have the largest possible excursion.

	Tests						
Parameters	6.1 Load	6.2 Freq.	6.3 Phase	6.4 Disp. Ampl.	6.5 Pist. Ampl.	6.6 Mean Pres.	6.7 Rej. Temp.
Cold Temperature (°K)	var	65	65	65	65	65	var
Load Power (W)	var	var	var	var	var	var	5
Operating Frequency (Hz)	25	var	25	25.5	25.5	25	25.5
Piston/Displ Phase (°)	67	67	var	67	67	67	66
Piston Amplitude (mm)	7.3	7.1	7.3	7.0	var	7.2	7.0
Displacer Amplitude (mm)	3.0	3.0	3.0	var	3.0	3.0	3.0
Mean Pressure (psig)	220	241	220	253	245	var	248
Ambient Heat Exchanger Inlet Temperature (°C)	10.9	9.3	10.9	10.6	10.7	10.0	var
Piston Case Water Jacket Inlet Temperature (°C)	20.3	17	19.1	16	16	15	16

References

[1] A Magnetically Suspended Linearly Driven Cryogenic Refrigerator. by F. Stolfi, M. Goldowsky, J. Ricciardelli and P. Shapiro, Proceedings of the Second Biennial Conference on Refrigeration for Cryogenic Sensors and Electronic Systems, Greenbelt, Md, December 1982.

[2] Philips Laboratories, Division of North American Philips Corp., Design and Fabrication of a Long-Life Stirling Cycle Cooler for Space Applications, Phase I and II - Engineering Model, Final Report: Sept. 1978 - Dec. 1982, by F. Stolfi, M. Goldowsky, C. Keung, L. Knox, E. Lindale, R. Maresca, J. Ricciardelli, P. Shapiro, NASA contract NAS5-25172, Briarcliff Manor, N.Y., March 1983.

[3] Philips Laboratories, Division of North American Philips Corp., Final Report for Parametric Testing of Engineering Model Refrigerator, by F. Stolfi, NASA contract NAS5-26688, Briarcliff Manor, N.Y., February, 1984.

D10

DESIGN OF A FLIGHT QUALIFIED LONG-LIFE CRYOCOOLER

L. Knox, P. Patt, R. Maresca

Philips Laboratories
A Division of North American Philips Corporation
Briarcliff Manor, NY 10510

This paper describes a second generation Stirling cycle cryogenic refrigerator with a linear drive, magnetic bearings, and clearance seals, designed to produce 5 watts of cooling at 65 Kelvin and to meet Space Shuttle mission requirements. The first generation refrigerator (Engineering Model) met all performance specifications, and has operated with no failure for over 12,000 hours. It was not, however, intended to meet launch requirements. Meeting those requirements necessitated improvements in the electromagnetic bearings, the radial position sensors, and in the structural design of the moving elements. As in the first generation refrigerator, organic contamination has been eliminated by the use of all metal and ceramic construction. Reductions in system input power have also been attained by an integral magnetic spring/motor for the displacer and by more efficient linear motors and drive electronics. At the design point, the refrigerator consumes 140 watts, delivered by the system electronics.

Ferrite variable reluctance position sensors reduce the temperature drift of the magnetic bearing system. Additional bearing improvements are realized through increases in gas film damping, ac/dc force capabilities, and structural resonant frequencies. All clearance seal surfaces are specially treated to eliminate potential damage due to contact during launch and system failures. Transmitted vibrations are minimized by a six-degree-of-freedom spring mount.

The work summarized in the paper is being supported by the NASA-Goddard Space Flight Center. (Contract Number NAS5-26668)

Key words: Clearance seal; cryogenics; ferrite sensors; gas film damping; launch vibrations; linear motor; magnetic bearings; magnetic spring; Stirling cycle.

1. Introduction

A long-life refrigerator capable of providing 5 watts of cooling at 65 Kelvin has been successfully designed, fabricated, and tested by Philips Laboratories.[1] Long life was achieved by eliminating wear and working gas contamination. Wear was prevented by use of magnetic bearings and clearance seals. The working gas volume is hermetically sealed from all organic materials used in the construction which prevents degradation due to outgassing. The details of this refrigerator are described in earlier papers; parametric and life test results are presented in a companion paper[2].

A refrigerator of this type is expected to be part of a complete satellite structure which will be launched into space on the Space Shuttle. However, the ability to survive launch

vibrations was not considered in the first generation 'proof of concept' design. Analysis of the expected launch vibrations indicated that the first generation magnetic suspension system could not be modified to accommodate those produced by the shuttle. The second generation design considers these vibrations and is capable of suspending all moving elements during launch and normal operation.

This paper describes the vibration analyses performed and the design revisions which were made to accommodate the vibrations. Several cooler component improvements are also described in this paper.

2. System description

The second generation refrigerator, the Flight Prototype described here, is a single stage, moving regenerator Stirling refrigerator. The piston and displacer/regenerator are linearly reciprocated within a cylindrical housing and radially supported with active magnetic bearings. A brief overview of system construction and operation is presented in this section. A detailed description of the theory of operation of this cooler is available in earlier reports.

The cooler is comprised of a compressor and an expander section (fig. 1). The expander section contains the moving displacer/regenerator and the cold and warm side heat exchangers. The compressor section contains the compressor piston, piston linear motor and gas buffer volume. The piston and displacer are supported by the magnetic bearings, three of which also form clearance seals. Two seals direct the gas flow in the expander section during the cycle; the third seals the compression volume above the piston.

Gas at the cold end expands (i.e. cools) as the piston retracts and increases the total gas working volume. The expanding gas cools the aluminum slit cold end heat exchanger. The heat load is cooled by a thermally conductive cable (not shown) attached to the cold end heat exchanger. The cable minimizes the transmitted mechanical vibrations. The heat exchanger is stationary and supported with a long thin walled tube, or cold finger. In the next phase of the cycle, the displacer moves toward the cold end. The clearance seal forces the gas through the regenerator where it is warmed. As the piston moves toward the cold end, the heat of compression is rejected through another slit heat exchanger in the expander section housing. Finally, the displacer moves toward the compressor end cooling the gas as it flows through the regenerator thus completing the cycle. These discrete motions are approximated by continuous sinusoids, where a phase angle describes the relative timing between the displacer and compressor motion.

The piston (compressor) is reciprocated with a moving magnet linear motor, similar to that used in the Engineering Model. The current to the motor, and therefore the piston motion, is controlled with a low frequency, high efficiency pulse-width-modulated current driver system. The displacer is reciprocated with a novel integrated magnetic spring/linear motor. The phasing is controlled via the system electronics. The displacer spring/motor and the pulse-width-modulated piston motor drive system is described in more detail in a latter section of this paper.

Primary design parameters (such as piston and displacer diameter, strokes, frequency, and radial clearance to the stationary walls) were determined by considering the overall system dynamics. Trade-offs result among system dynamics, thermodynamic losses (primarily conduction), and difficulty of construction (such as clearance seal machining tolerances). The Philips Stirling cycle model was used to develop an optimal design meeting all the design criteria.

Since launch conditions are the primary new considerations in this second generation design, a description of the various vibration analyses is provided in the next section. Other component level improvements such as new reluctance radial position sensors with excellent temperature stability, and an integrally formed aluminum/titanium cold end heat exchanger are described following the vibration section. Finally, primary system design parameters and predicted performance levels are presented in the last section.

3. Vibration considerations

The Engineering Model refrigerator demonstrated the concept of using magnetic bearings and linear drive methods to obtain long-life operation. The Prototype refrigerator described in this paper will demonstrate these concepts in actual space-qualified hardware. As part of this effort, the refrigerator dynamics were modelled to determine the effect of launch vibrations and the design was tailored to achieve an acceptable system response.

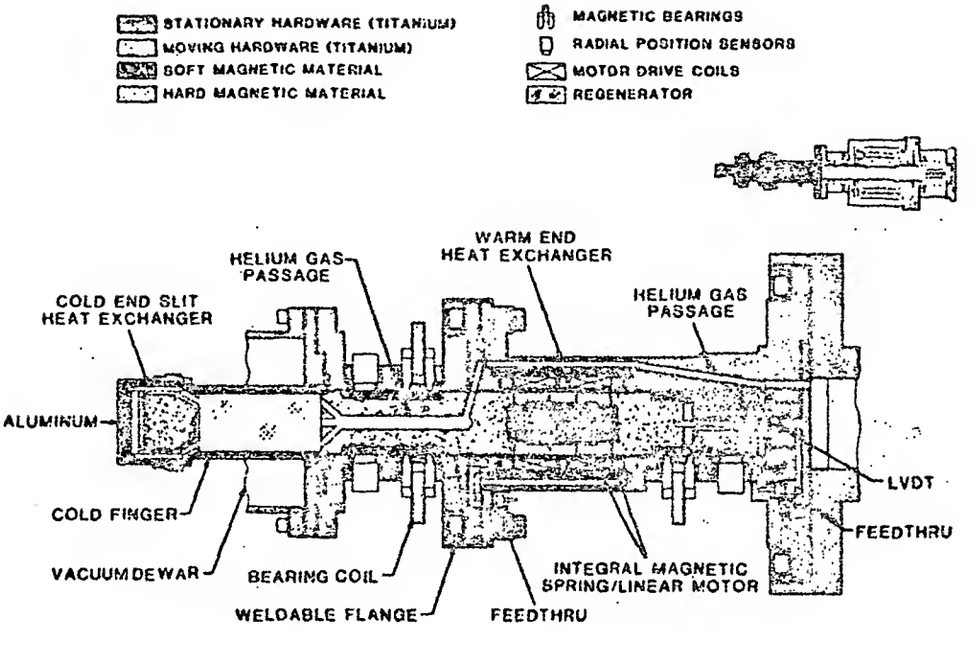

a.

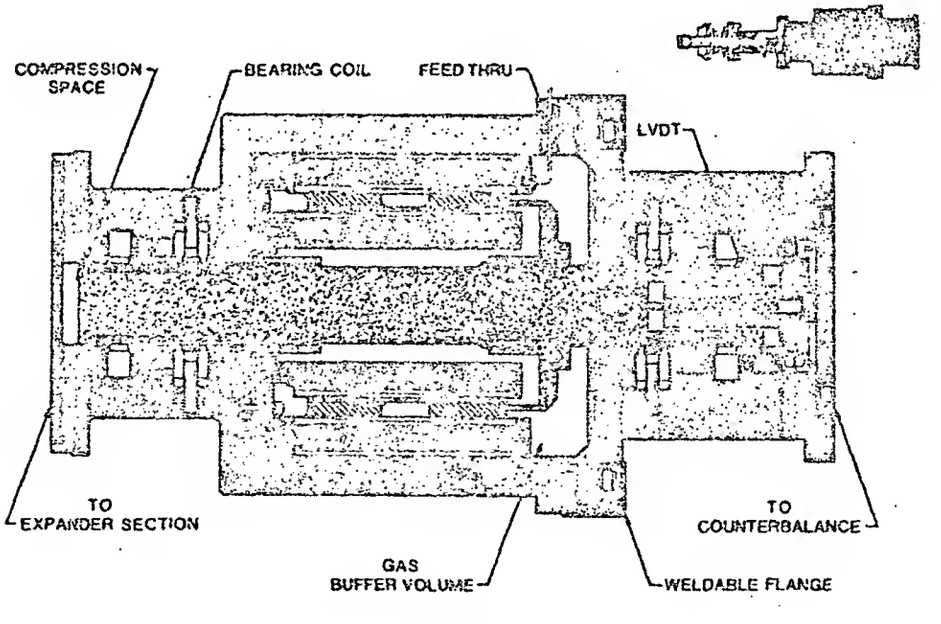

b.

Figure 1. Refrigerator sectional lay-outs
a. Expander (displacer) section
b. Compressor (piston) section

3.1 Refrigerator dynamics

The contiguous surfaces in the clearance seals are the area most susceptible to vibrational damage. If the ultra-clean titanium surfaces of the clearance seals come in contact, potentially catastrophic failure in the form of galling is possible. Magnetic bearings accurately center the shafts within the bores thus maintaining the non-contact operation of the clearance seals. The vibration analyses are focused on determining the bearing performance required to maintain non-contact support during launch. The launch vibrations are described by three independent specifications; random, acoustic, and quasi-static. The analyses for each of these excitations follow.

The bearing performance requirements can be determined from the solid-body vibration amplitudes of the refrigerator. For this purpose, simple first and second order models are sufficient. Forces are transmitted to the refrigerator through the isolation mount (fig. 2) and by acoustic coupling directly to the housing. The vibration amplitudes are calculated assuming a lumped spring-mass system model (fig. 3).

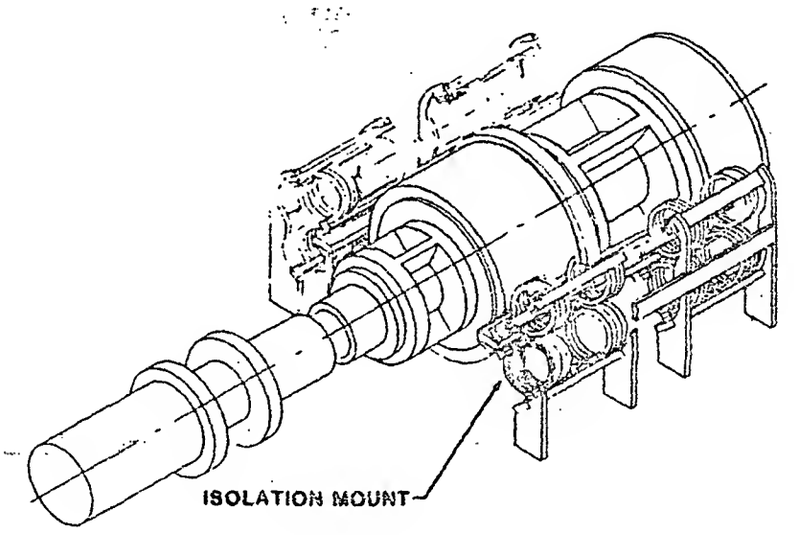

Figure 2. Refrigerator isolation spring mount design

The random vibration specification is a power spectral density (PSD) function describing the random vibrations of the shuttle mount surface. PSD is a statistical method of describing the frequency content of random signals. The vibration amplitude PSD is determined via the given acceleration PSD and the calculated inertial transfer function. The random vibration specifications and the resulting refrigerator vibration PSD function are shown in figure 4. The mounting surface vibrations are effectively filtered by the 7.0 Hz isolation spring mount. The resulting solid-body RMS vibration amplitude is 17 μm with most of the vibration energy contained below 45 Hz.

Acoustic sound energy also induces vibrations in the refrigerator. The pressure difference across the refrigerator produces a net force on the housing. In general, the force on a cylinder perpendicular to a 2-D pressure field is

$$F = A \int_0^{2\pi} P(\theta) \cos(\theta)\, d\theta \qquad (1)$$

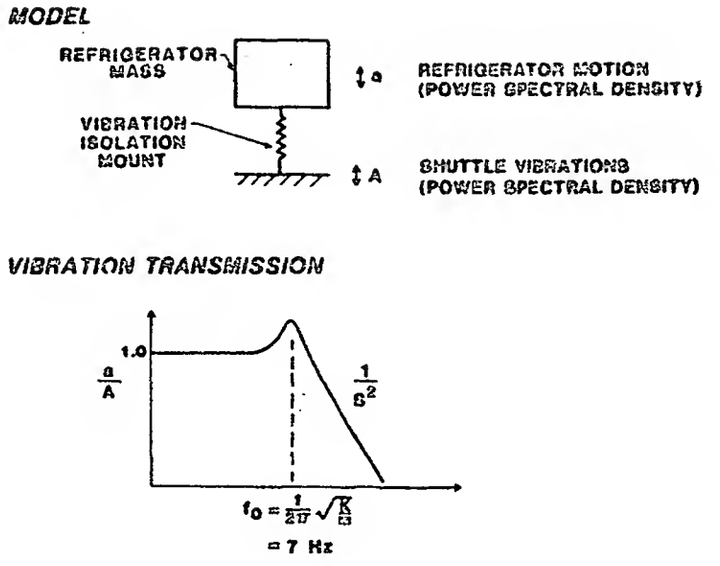

Figure 3. Random vibration lumped spring-mass system model

where A is the cylinder radius and $P(\theta)$ is the pressure distribution over the cylinder surface. Assuming a sinusoidal plane wave, the peak force is

$$\hat{F} = \frac{2 P_0 c}{\omega E} \tag{2}$$

where P_0 is the peak pressure, ω is the angular frequency of the pressure wave, c is the speed of sound in air and E is defined to be

$$E = \frac{1}{2} \left\{ J_0^2(ka) + J_2^2(ka) + Y_0^2(ka) + Y_2^2(ka) - J_0(ka)J_2(ka) - Y_0(ka)\, Y_2(ka) \right\}^{\frac{1}{2}} \tag{3}$$

where $k = 2\pi/\lambda$ and J and Y represent the Bessel functions of the first and second kind respectively.

The acoustic coupling is maximum when the housing diameter is 40% of the sound wavelength. The coupling decreases monotonically at higher and lower acoustic frequencies. Using this model and the acoustic sound pressure specifications shown in figure 5, the refrigerator RMS vibration amplitudes are determined to be less than 2.0 μm. The vibration energy is centered at 40 Hz and is negligible above 100 Hz.

NASA utilizes a third specification to include the effects of shock loads, mount amplification, and launch uncertainty. This specification is termed "Quasi-Static Loading" and is by far the most severe of the three specifications on the refrigerator design. This data was compiled from previous flights and represents the maximum acceleration levels measured on devices with similar isolation mounts.

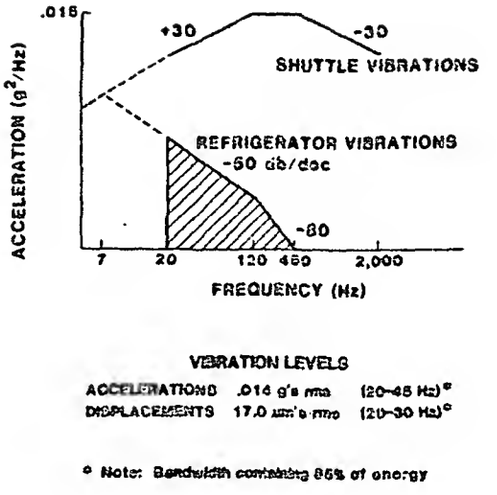

Figure 4. Space shuttle random launch vibrations: specifications and refrigerator vibrations

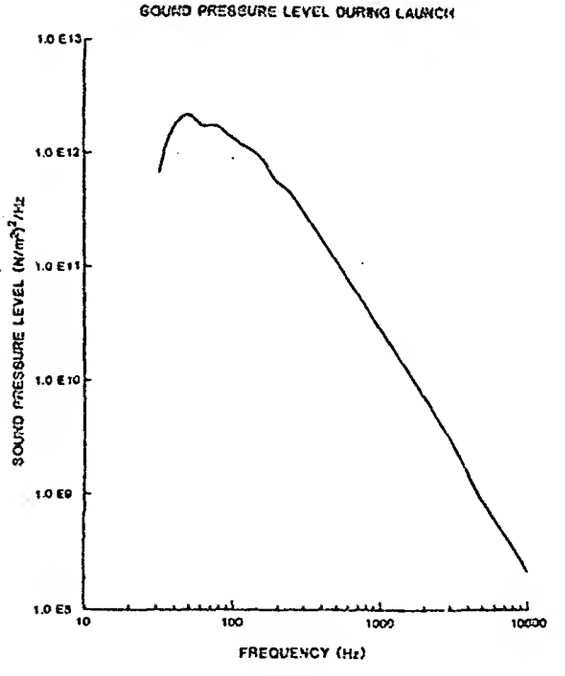

Figure 5. Sound pressure level during launch

The specification describes the vibrations during the three launch phases: lift-off, transonic/maximum aerodynamic pressure, and ascent. Each phase has an ac and dc acceleration component which is applied to the refrigerator simultaneously in three orthogonal axis for a specified duration. The isolation mount frequency determines the ac acceleration specifications; the design frequency of 7.0 Hz yields the specifications presented in table 1.

Table 1. Quasi-static launch vibrations

Occurrence	D.C. Acceleration (g's)	A.C. Acceleration at 7.0 Hz (g's)	Vibration Duration (seconds)
Lift-off	1.5	5.4	20.
Transonic/Maximum Aerodynamic Pressure	3.0	2.7	10.
Ascent	3.2	0.	100.

Meeting these specifications requires either improvements in the magnetic suspension system to totally prevent contact or changes to the titanium surfaces to permit limited contact during launch. The following design changes improve the suspension system performance. In addition, surface treatments will improve the clearance seals to permit limited contact during launch.

3.2 Design changes

The Engineering Model magnetic bearing stiffness must be improved 60-70 dB to avoid contact during launch. The magnetic bearings are controlled by a closed-loop control system which monitors the shaft position and excites the appropriate electromagnets to center the shaft. The achievable open-loop gain of the control system, which determines the apparent bearing stiffness, is limited by the shaft dynamics. The 70 dB gain improvement was demonstrated in a test fixture with a solid (rigid) shaft. Thus, if the shaft dynamics can be improved sufficiently, the refrigerator will withstand the launch vibrations.

The design changes made to improve the shaft dynamics are presented in table 2. The goal is to increase any resonant frequencies beyond the desired control bandwidth and to increase the system damping. The increase in diameters, shorter lengths, and decreased suspended mass all increase the resonant frequencies. The system damping is improved by decreasing the radial clearance in the clearance seal. This cylindrical annulus is filled with the working gas and acts as a viscous dashpot as the shaft moves radially. Decreasing the clearance 25% will double the damping forces. These changes result in the dynamics presented in table 3. These improvements are sufficient to achieve the required bearing stiffness.

Table 2. Design changes to improve shaft dynamics

	Engineering Model	Prototype
• Increase stiffness		
Displacer diameter (cm)	2.0	3.16
Piston diameter (cm)	3.68	4.45
Cold finger diameter (cm)	2.15	3.31
Piston wall thickness (cm)	0.26	0.57
• Increase damping		
Clearance seal gap (μm)	25.	17.
Clearance seal length (cm)		
Piston	4.0	8.0
Displacer	2.5	5.0
• Minimize cold finger suspended mass		
Heat exchanger material	Copper	Aluminum

Table 3. Improved shaft dynamics

	Engineering Model	Prototype
• Squeeze film damping breakpoint (kHz)		
Piston	2.5	50-85
Displacer	0.7	45-155
• First bending resonances (Hz)		
Piston	400	900
Displacer	840	1800

The clearance seal surfaces will be treated with titanium nitride to improve the wear properties. This provides additional protection to the clearance seals and minimizes the chance of catastrophic failure should the surfaces come in contact during launch. Various surface treatments were investigated. Clearance seal samples were coated and subjected to the launch vibrations. The surfaces were analysed microscopically. The samples were subjected to increased vibration amplitudes until excessive wear occurred. The treatments tested and the relative performance data are presented in table 4.

Table 4. Surface treatment evaluation results

Shaft Number	Surface Treatment	Acceleration level (g's) A.C.	D.C.	Results
0	none	3	5	Severe fretting & abrasion
1	TiN plated	3	5	No degradation
1	TiN plated	10	25	Fretting
2	Sn-N implanted	3	5	Minor fretting
2	Sn-N implanted	6	10	Extensive fretting
3	Ag-N vs C implanting	3	5	Light fretting
4	Ti-N plated	3	5	Light abrasion
4	Ti-N plated	6	10	Light abrasion
4	Ti-N plated	9	15	Severe abrasion
5	C implanted	3	5	Moderate fretting
6	C implanted	3	5	Moderate fretting

4. Component improvements

In addition to the work discussed above, several key system components have been improved vis-a-vis the Engineering Model design. Improvements in long term temperature stability and reliability of the bearing control system result from replacing the eddy current sensors in the Engineering Model with ferrite reluctance position sensors. An aluminum slit heat exchanger is used to reduce the cantilevered mass at the end of the cold finger. System efficiency is improved with a magnetic spring integrated in the displacer linear motor and by using a novel low frequency switching driver for the piston motor. Although the thermodynamic efficiency is reduced from the Engineering Model, the overall efficiency (the ratio of cooling to electric input power) has increased as a result of the improved drive systems. Detailed descriptions of each of these improvements follow.

4.1 Aluminum cold end heat exchanger

The Engineering Model refrigerator has a copper annulus cold end heat exchanger. The Flight Prototype uses a slit aluminum heat exchanger. The slits provide an equivalent heat transfer surface area with a shorter heat exchanger length. A reduction in weight results from the reduced material density. The fabrication of the aluminum heat exchanger is outlined in figure 6 [3].

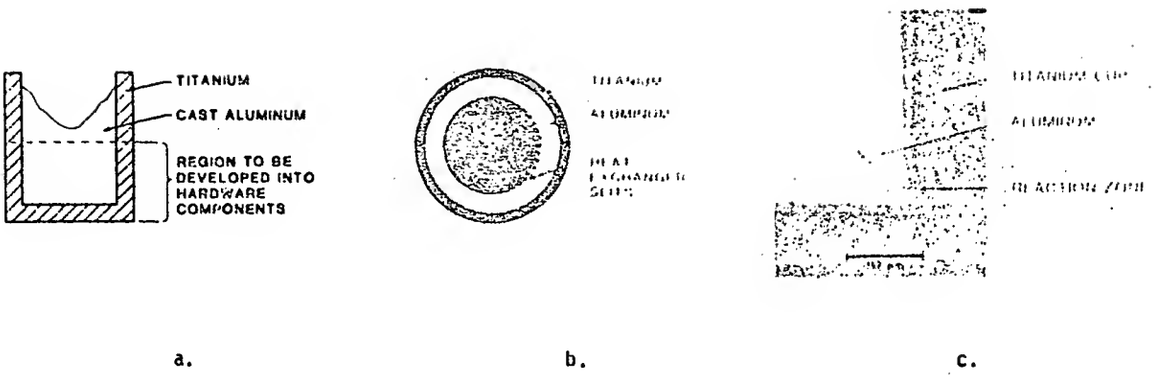

a. b. c.

Figure 6. a. Aluminum-titanium heat exchanger fabrication
b. Heat exchanger photograph
c. SEM photographs of bond interface

A 5 Al-2.5 Sn titanium cup and a mating commercially pure aluminum piece are cleaned and degassed. The assembly is heated in a high vacuum furnace. As the aluminum melts, it wets and adheres to the titanium surface forming a metallurgical joint. The bonded structure is then hipped to remove any voids and improve the structural properties. The center of the aluminum material is removed to form a thick walled composite structure. The heat exchanger slits are electro-discharged-machined (EDM) in the aluminum walls. The outer titanium wall provides the needed strength for pressure vessel containment and is subsequently welded to the cold finger.

A heat exchanger sample has been temperature cycled 1000 times from room temperature to 77 Kelvin and 10 times to 4.2 Kelvin. Metallographic and scanning electron microscopy of the tested sample show good metallurgical bonding. Tensile tests of a cast sample showed that the bond strength exceeds the strength of the aluminum. Figure 6c is a photograph of the aluminum/titanium joint indicative of a superior bond. A heat exchanger sample pressurized to four times the design pressure is currently being cycled from room temperature to 77 Kelvin. To date, 1,000 cycles have been accumulated with no indication of failure.

4.2 Integral magnetic spring/linear motor

During operation, the displacer shuttles gas between the cold and warm ends. The displacer reciprocates at a specified frequency, stroke, and phase relative to the piston motion. The displacer construction includes the regenerator mesh, bearing armature and radial position 'target' material, structural walls, and linear motor. For designs of this type, the fluid damping forces acting on the displacer are small in comparison to inertial forces during operation. Ideally, for compact cooler design, the machine should operate at the highest frequency allowed by the regenerator heat capacity and fluid viscous losses. In addition to the size and weight reduction, the linear compressor motor size decreases with higher speeds, since the output force decreases. However, the displacer motor power loss is proportional to the fourth power of frequency while the cooling capacity is only linearly proportional to frequency. The significance of the displacer motor power has resulted in larger, lower frequency cooler designs.

Due to the large ratio of inertial to damping forces, a resonant displacer/spring system would greatly reduce the required motor power. In fact, 'free displacer' coolers have been made which have no displacer motors. These coolers use the operating pressure wave to drive a resonant displacer/mechanical spring system.

Long life mechanical springs can be designed provided the operating stress levels are sufficiently low. The damping forces for a well mounted mechanical spring are also quite low. However, experience with mechanical spring balancers has shown that small particles are generated during operation. These particles would be catastrophic to the clearance seals. Thus, mechanical

springs could not be used in the design. Gas springs have no wear problems, but do have limited linearity, higher damping than mechanical springs, and do require an additional clearance seal. For these reasons, the gas spring was also not used in this design. Magnetic springs, on the other hand, do not need clearance seals and have no life-limiting properties. As a result of the advances made in permanent magnet material, new, high strength magnets with minimal long term aging and good temperature stability are now available. These improvements have made magnetic springs feasible and the Flight Prototype incorporates one in the displacer design.

One advantage of the Engineering Model's linear motor drive system is the freedom to adjust the displacer and piston strokes independently as well as the phase. In a free displacer design, control and flexibility is lost though fewer components are needed. Thus an adjustable spring or a spring and motor is desirable to maintain operating flexibility.

The Flight Prototype incorporates such an integrated magnetic spring/motor. The motor provides control of the displacer motion. A schematic of the integral spring/motor with the displacer at full stroke is shown in figure 7. The moving magnets act as springs and interact with the stationary coil to produce a force which is proportional to the current in the coils.

The construction of the motor is very similar to the displacer linear motor of the Engineering Model. Radially magnetized magnets are added to the stator at both ends of the coils to provide a self-centering magnetic spring. Good linearity is achieved over the design stroke through proper positioning of the concentric magnets. Another advantage in this design is the single diameter construction. No dead space or void volumes are introduced which would have existed with a conventional face-to-face repulsion magnet spring. The springs reduce the peak force requirements of the motor. Table 5 compares the power requirements of the integral spring/motor design to a conventional linear motor design with equivalent size envelopes. In both cases SmCO5 magnets are used because of their very rigid magnetization and excellent thermal and long term aging stability.

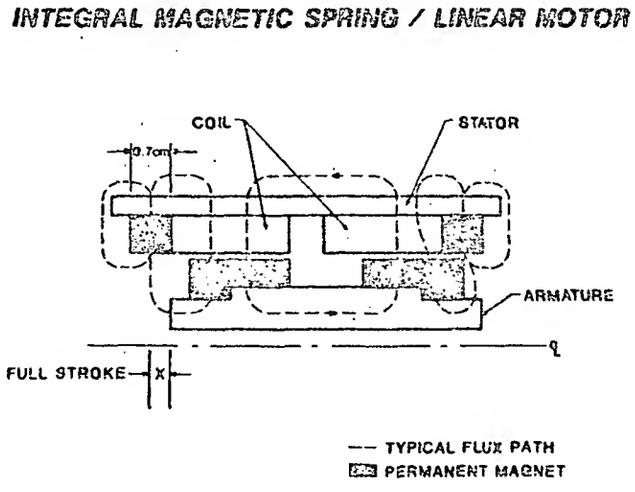

Figure 7. Schematic of integral displacer magnetic spring/linear motor.

Table 5. Power comparison: Integral spring/motor vs. linear motor

	Spring/motor	Conven. linear motor
Peak motor force (N)	12	46
Magnet moving mass (Kg)	.033	.035
Total electric power (W)	5	20

Eddy current damping generated in this magnetic spring is difficult to accurately predict. These eddy currents dissipate stored energy and lower the spring quality factor (Q). Another problem with a magnetic spring of this design is the radial instability and resulting side loads. These side loads occur not only from magnetic eccentricities resulting from mechanical construction, but also from magnet non-uniformity. These side loads have static as well as dynamic components. Because of the difficulty in estimating these effects, tests were performed with a dedicated test fixture.

4.2.1 Static spring test results

Axial springs of this design have a radial instability stiffness which is less than or equal to negative one half the axial stiffness[4,5]. The sign is critical since a 10 N/m axial stiffness PM spring has a radial stiffness ranging from negative 5 N/m to negative infinity. For designs involving no soft magnetic material the inequality qualifier can be removed.

The stiffness of a simple magnet pair (no soft magnetic material) was tested and compared to a finite element analysis of the same geometry (fig. 8). The characteristic geometry of the magnet rings is very close to the spring/motor design. Side load tests were performed by displacing the inner ring toward the outer ring and measuring the radial force. The radial stiffness was measured to be negative one half the axial stiffness. The side loads for zero mechanical eccentricity of various magnet pairs were measured to determine the magnet non-uniformity. Table 6 summarizes the test results. These results indicate that matched magnet segments must be used to produce acceptable performance.

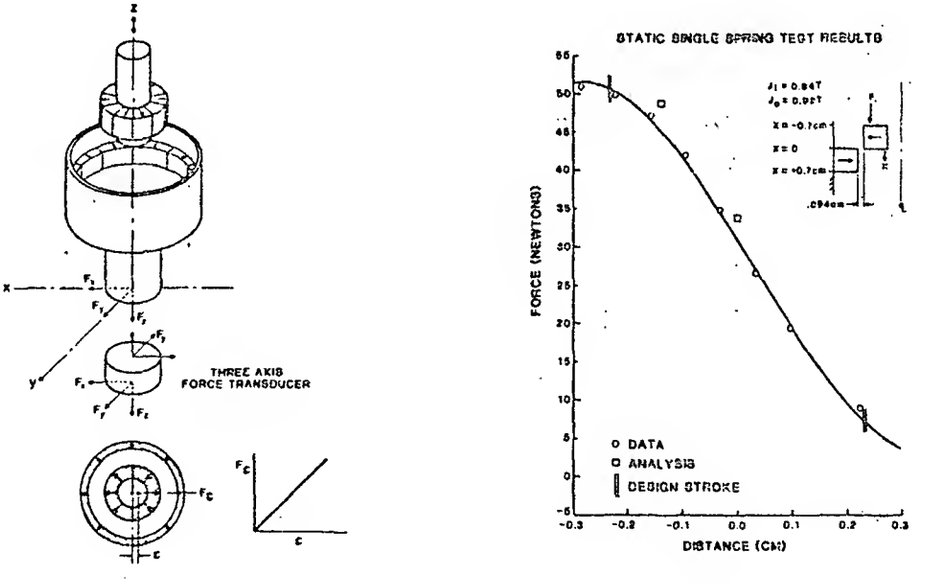

a. b.

Figure 8. Static test of single magnet pair vs. analysis
a. Test set-up
b. Axial test results

Table 6. Static side load test results

Radial instability of single magnetic spring pair

Axial stiffness at mid position	11,000 N/m
Radial instability stiffness	
Theoretical analysis	5,500 N/m
Finite element analysis	5,500 N/m
Measured	5,000 - 7,000 N/m

Magnet non-uniformity

Magnet pair number	1	2	3	4
Peak radial side force (N) (in concentric position)	2.0	1.1	2.6	0.25
Equivalent geometric (cm) eccentricity			0.047	0.005

4.2.2 Dynamic test results

Following these static tests, two sets of springs were mounted to an active radial magnetic bearing test fixture which exhibits no friction and extremely low damping in the axial direction. Figure 9a is a schematic of the test fixture. The integral magnetic spring/motor was in effect split and placed at either end of the bearing test fixture. Figure 9b is a scope trace of the position of the moving mass vs. time resulting from an initial step displacement. The resulting Q of about 70 indicates that there is very little eddy current damping in the magnets. The quality factor, Q, does get lower as additional magnets or magnetic material is placed near the spring indicating that eddy current damping is not negligible.

The test set-up was further modified to test the integral motor/spring concept. An additional small magnet ring was attached to each inner magnet ring as in figure 9c. A coil is placed around each inner magnet ring. This test was performed to verify the analytic procedure used to determine the force constant of the displacer motor. Both dc and ac tests were performed using the motor to excite the moving mass. The dc force constant of the motor agrees well with the predictions. The displacer is driven off-resonance (as it will be in operation) and open-loop and the resulting frequency spectrum of the displacement is recorded. Figure 9d(1) is a force displacement curve of the spring for positive and negative displacements. At low amplitudes, the curves match well, indicating that there should not be any even harmonics in the displacement spectrum. At larger strokes, the curves vary indicating that even harmonics will be present. The resulting frequency spectrum measurement of the displacement is shown in figure 9d(2). These harmonics produce insignificant adverse effects on the thermodynamics.

Through the introduction of bonded high energy product magnets, the damping can be further reduced because of their very high resistivity. In a free displacer design, the motor can be eliminated and axially magnetized springs can be used thus simplifying the fabrication.

4.3 Radial position sensors

The accuracy of the radial position sensors in a magnetic bearing system determines the limit of the achievable accuracy of that system. The Engineering Model cooler which employed magnetic bearings, used eddy current sensors as the means of measuring radial position. These sensors, however, are not without drawbacks: they must be isolated from the helium working gas by a ceramic window and titanium pressure wall, and their extreme temperature drift precludes the use of these sensors in the single-ended mode. Thus, each axis requires two matched sensors, two window assemblies which tend to trap particulates, and high frequency differential electronics to acquire a single position signal (fig. 10).

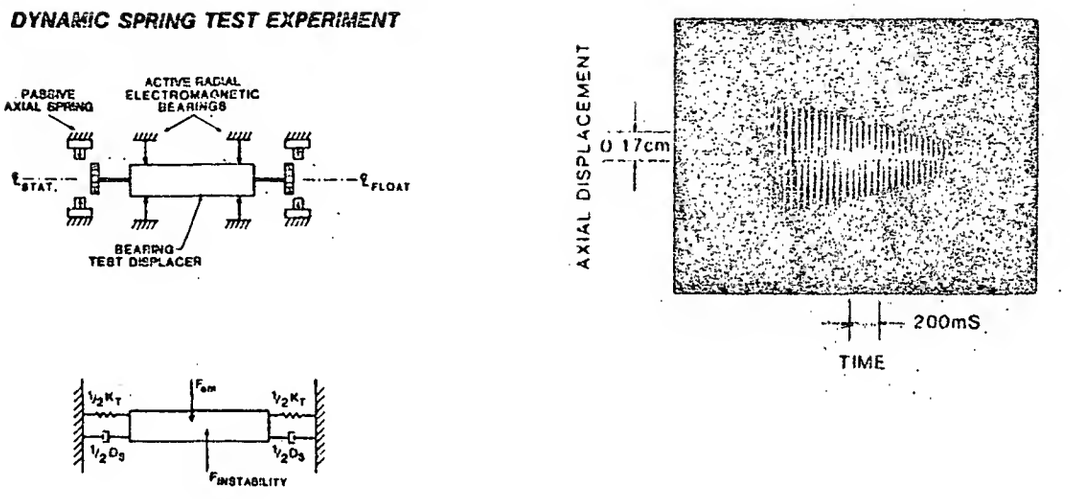

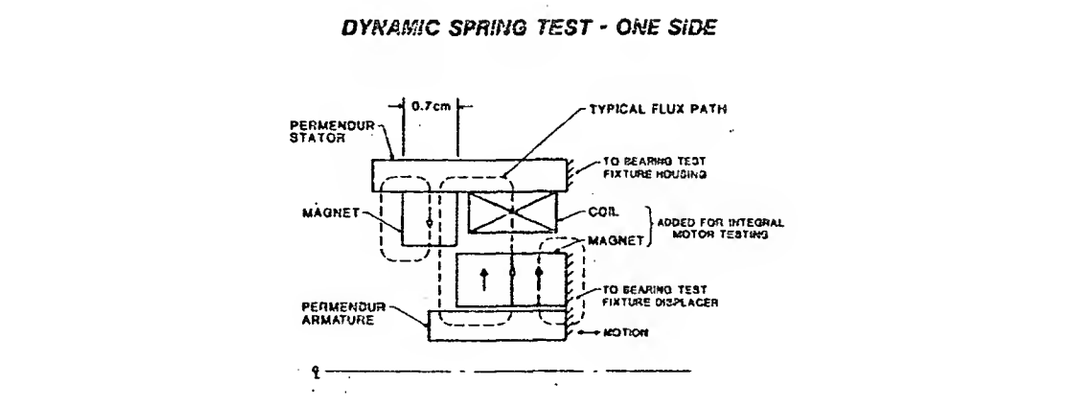

Figure 9. Dynamic test results
a. Dynamic test schematic
b. Damping with permendur backing (Q = 70)
c. Dynamic test fixture with coil and additional magnets
d. Motor test results - displacement spectrum (see next page)

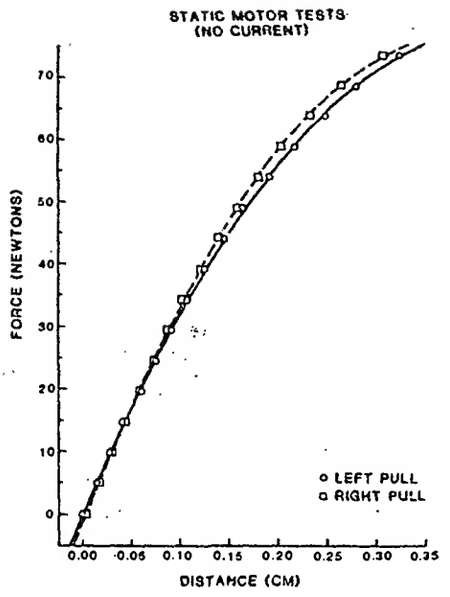

d(1) pull to left and right

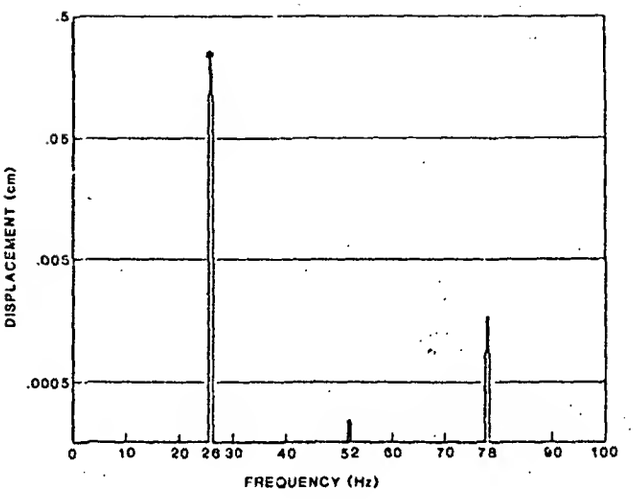

d(2) large stroke

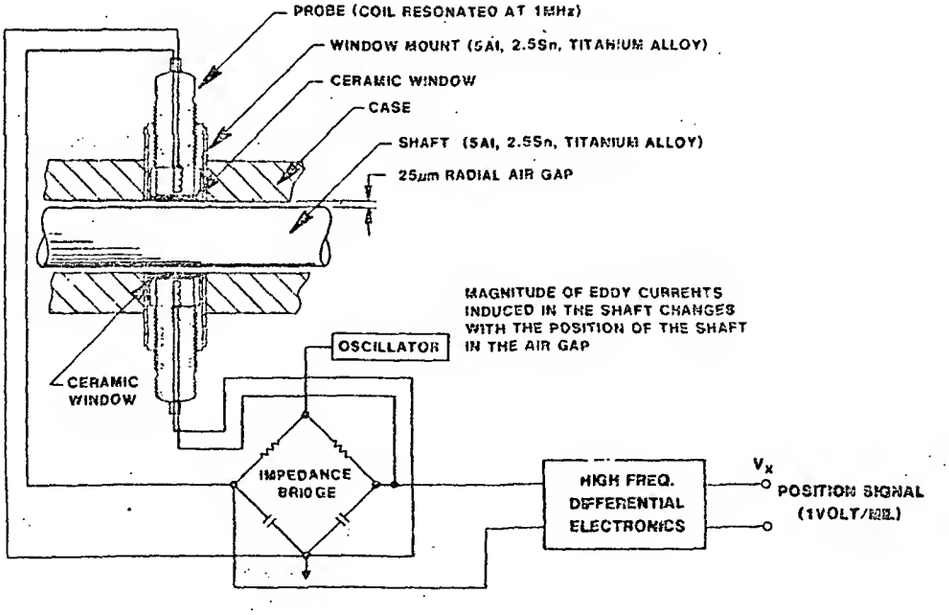

Figure 10. Differential eddy-current sensors

In an effort to simplify both the mechanical and electrical aspects of the radial position sensing, a number of alternative sensing schemes were considered. The major features desired for the new radial position sensor are summarized below:

- Single-ended (to allow redundancy)
- High bandwidth
- Negligible temperature drift
- High signal-to-noise ratio
- Simple electronics (reliability)
- Repeatable, stable, easily cleaned, mechanical assembly

The most promising method, with regard to simplicity of electronics, was that of variable reluctance sensing. Furthermore, with the application of ferrite to a reluctance sensor, eddy currents are eliminated; and thus, high bandwidth is achieved. With appropriate magnetic and electronic design, a reluctance sensor also offers a reasonably linear response with negligible temperature drift in a single-ended configuration. Finally, the reluctance sensor greatly improves the mechanical design if the ferrite sensor itself can penetrate the titanium wall, be ground flush with the wall, and serve as a hermetic barrier. This mechanical design required a hermetic ferrite/ceramic/titanium joint which was the subject of a major effort in materials technology. A functionally representative schematic of the ferrite sensor is shown in figure 11.

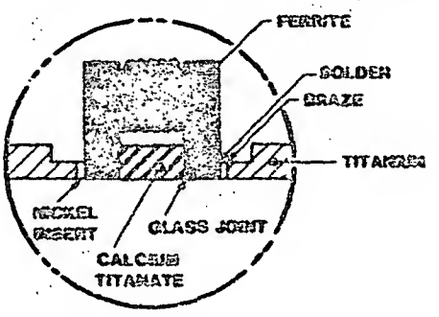

Figure 11. Ferrite radial position sensor

Extensive testing of the ferrite sensor was performed to measure the position sensitivity and the temperature drift in the single-ended mode. Inductance measurements were taken at constant temperature over the range of 0 - 4 mils (fig. 12). The data shows that the inductance, L, is

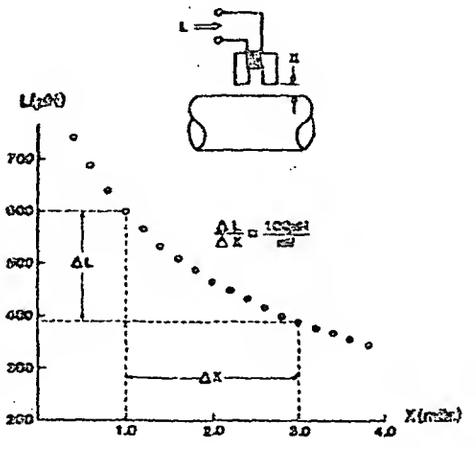

Figure 12. Inductance L vs. position x

inversely proportional to the gap size, x, with a sensitivity, dL/dx, of approximately 100 μH per mil. This represents a change in impedance of 20% per mil of displacement for the ferrite sensor as compared to roughly a 1% change in impedance for existing eddy current sensors.

The relatively high sensitivity to position was one major step towards the minimization of temperature drift; the next criterion to consider was the sensitivity of inductance to temperature.

The temperature sensitivity is measured using a specially designed test fixture which maintains a fixed gap between sensor and target. The fixture is placed in a temperature controlled oven which is cycled from 20 °C to 80 °C repeatedly. The inductance of the sensor is continuously monitored and recorded to quantify any drift in inductance due to a change in temperature.

Figure 13 is a plot of inductance vs. temperature for a fixed 3 mil gap over the range of 20 - 80 °C. The data shows an increase in inductance with temperature from 390 μH at 20 °C to 395 μH at 80 °C. This 5 μH change in inductance translates to a position error of approximately 50 u-inches which represents only 5% of the 1 mil radial clearance between the piston and cylinder.

Previously, the acceptance criterion for matching eddy current probes was expressed in terms of a maximum position error of 200 u-inches or 20% of the 1 mil radial clearance with the probes used in the differential mode. Thus, the ferrite radial position sensor offers much improved temperature stability with the added advantage of operating in the single-ended mode.

Having achieved adequate temperature stability through appropriate choice of materials and geometrical design, the linearity and sensitivity of the electronics was tested. The output voltage as a function of gap size is plotted in figure 14 along with a line describing the ideal linear output.

The close fit of data points to the ideal curve shows a fairly linear relationship between output voltage and position, and a sensitivity of about 10 volts per mil.

In summary, the ferrite radial position sensor has exhibited excellent performance over a wide temperature range. It has demonstrated adequate linearity, good sensitivity, and exceptional temperature stability, while obviating the need for differential sensing and facilitating the incorporation of redundant sensing techniques. Furthermore, it has greatly simplified the electronics design which leads to a lower parts count and, hence, increased reliability. And finally, the mechanical assembly provides a flush bore which is hermetic and can be easily cleaned.

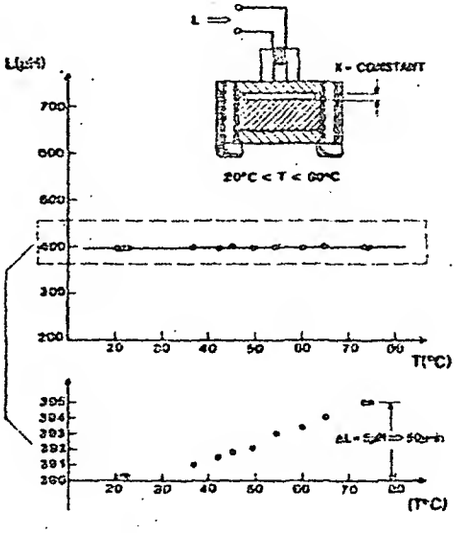

Figure 13. Inductance vs. temperature

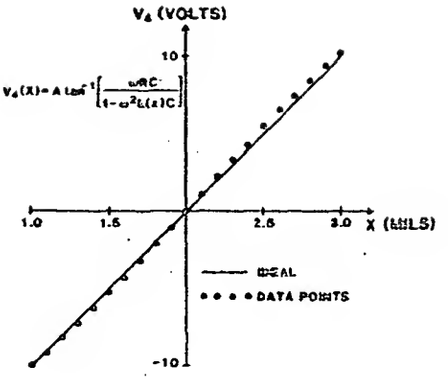

Figure 14. Output voltage (V4) vs. position (x)

4.4 Synchronous linear motor controller

In the Engineering Model cooler, moving magnet linear motors are used in axial control loops to prescribe the reciprocating motions (i.e. amplitude, phase, speed & center position) of the piston and displacer. The axial control is performed with position servo loops employing LVDTs to measure position and linear amplifiers to drive the motors. The linear amplifiers exhibit excellent reliability and high bandwidth, and in general meet all the performance requirements of the original design specifications. However, the poor (~40%) efficiency of the linear drivers precludes their use in a spaceborne system. Therefore, alternative driving methods were investigated, specifically, switching drivers which would provide an axial control system with high reliability and maximum efficiency.

High frequency (100 kHz) switching amplifiers have been used for this application and have achieved efficiencies on the order of 75% with a bandwidth of 1 kHz. Using this type of amplifier, one could directly replace the linear amplifier and use the same control system. However, for high current applications, viz. the piston driver, the high frequency switcher becomes complex and less reliable due to parasitic oscillations associated with the paralleling of power MOSFET transistors and the finite reverse recovery times associated with high current diodes.

A significantly different approach to the axial control provides an alternative driving scheme. Using a nonlinear control system which employs phase lock loop techniques and takes advantage of the electro-mechanical filtering properties of the linear motors. The amplifier used in this system produces a switching waveform at the same frequency as the refrigerator operating frequency. The ac component, the dc component, and the phase of the waveform are controlled by three separate inputs to the amplifier as shown in figure 15.

The amplitude of the fundamental component of the switching waveform is varied by a common mode modulation of the positive and negative pulse widths. The dc component of the waveform is varied by a differential modulation of the positive and negative pulse widths; and the phase and frequency of the switching waveform are prescribed by an ac signal at the third input to the amplifier. These three control lines are used in three distinct control loops to accurately prescribe the amplitude, center position, and phase of a piston or displacer motor (fig. 16).

In the first control loop, a low-pass averaging circuit is used to feedback the dc position of the motor and compare it to a reference signal; the resultant error signal is then compensated and used to adjust the dc component of V_{out} to achieve the desired dc position. A second control loop is realized by using a peak to peak detector to determine the stroke of the reciprocating motor. The stroke amplitude is compared to a reference signal, and the resultant error signal is compensated and used to adjust the ac component of V_{out} to achieve the desired stroke of the motor. Finally, a third control loop is formed to control the phase of the motor.

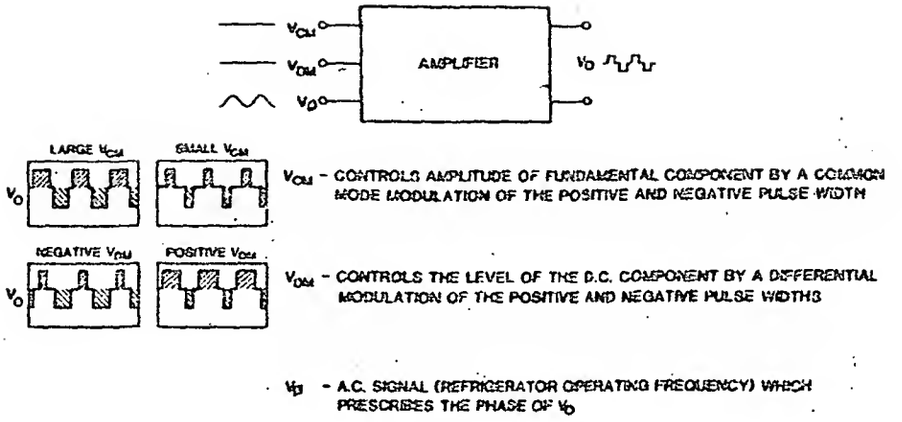

Figure 15. Open loop amplifier

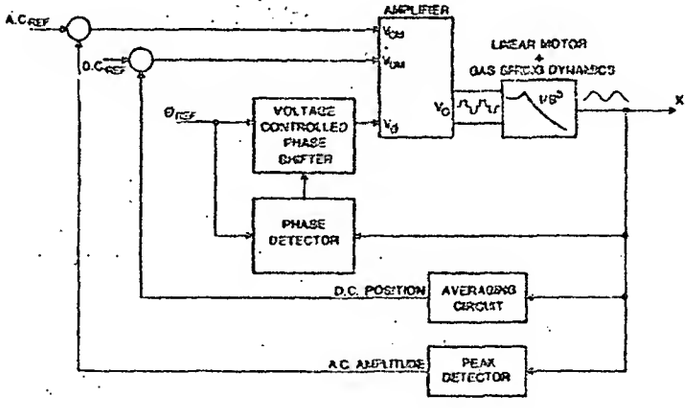

Figure 16. Control scheme showing 3 distinct control loops

A clock signal provides the frequency and phase reference onto which the motor phase is locked via phase locked loop techniques.

A prototype system which can deliver 500 watts of real power to the piston motor with an amplifier efficiency of 95% was designed and fabricated. The system exhibits excellent control of critical operating parameters with negligible distortion of the desired sinusoidal motion (fig. 17) and a surprising tolerance to noise and non-ideal sensor performance.

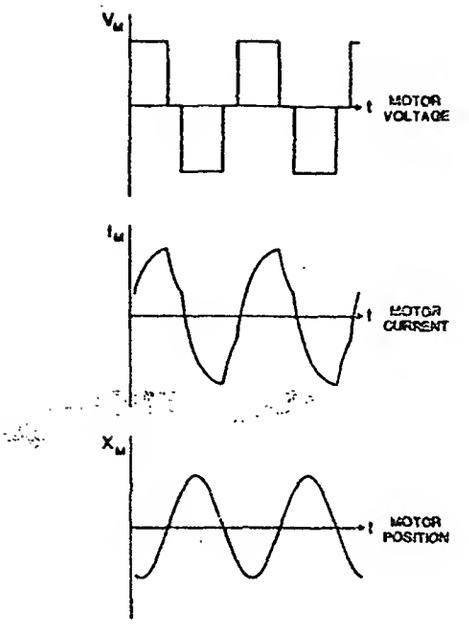

Figure 17. Characteristic waveforms: Voltage, Current, and Position

Since the switching frequency of the amplifier is very low, i.e. the same as the operating frequency of the refrigerator (15 - 25 Hz), the design of the amplifier is greatly simplified, resulting in a lower parts count and hence higher reliability. Furthermore, at these frequencies, switching losses are negligible, and transistors are easily paralleled to achieve very high efficiencies.

In summary, the synchronous motor controller, although exhibiting a slower transient response, provides better efficiency, potentially greater reliability, and better control of steady-state operating parameters than is possible with either a linear amplifier or a high frequency switching amplifier used in a classical position servo loop.

5. System performance

Table 7 is a summary of the key design parameters of the Flight Prototype model. System performance is summarized in Table 8. The thermodynamic efficiency of the design is comparable to the Engineering Model. Overall reduction in system power results from higher efficiency driver systems and the inclusion of the magnetic spring in the displacer motor. The counterbalance design (including power requirements) have not yet been addressed.

Table 7. Flight prototype design parameters

Piston design stroke (mm)	7.4
Piston diameter (cm)	4.45
Displacer design stroke (mm)	2.3
Displacer diameter (cm)	3.155
Operating speed (Hz)	18.9
Charge pressure (N/m^2)	1.69 E6
Regenerator wall thickness (mm)	0.5
Cold finger wall thickness (mm)	0.5
Displacer moving mass (Kg)	0.9
Piston moving mass (Kg)	3.95
Clearance seal gap (μm)	17

Table 7. Flight prototype design parameters (cont.)

Regenerator:	
Material	phosphor bronze
Cross sectional area (cm^2)	7.31
Length (cm)	6.0
Wire diameter (μm)	53.
Fill factor	0.36
Piston motor:	
Motor type	moving magnet linear motor
Yoke material	4% SiFe
Magnet material	SmCo5, BH max = 23 MGOe
Peak motor force (N)	220
Mechanical output power (W)	100
Efficiency (%)	75
I^2R Loss (W)	30

Table 8. Flight prototype system performance

Design cold production (W)	5.
Cold end temperature (K)	65.
Warm end temperature (K)	300.
Thermodynamic shaft input power (W)	100.
Piston motor input power (W)	135.
Displacer motor input power (W)	5.
Total input power to motors (W)	140.

6. Summary

A second generation magnetically suspended, linear Stirling cycle cryogenic refrigerator has been designed to meet the space shuttle launch requirements. The design changes are primarily focused on improving the refrigerator dynamics and thus its capability to withstand the launch vibrations. These include; increased structural resonant frequencies, increased ac/dc bearing force capability, and increased gas film damping. Other improvements, which increase system reliability and efficiency, include an integral displacer magnetic spring/motor, ferrite variable reluctance position sensors, surface treated clearance seals, and an aluminum/titanium cold-end heat exchanger. The work summarized in this paper is being supported by the NASA-Goddard Space Flight Center. (Contract Number NAS5-25688).

References

[1] Philips Laboratories, division of North American Philips Corp., Design and Fabrication of a Long-Life Stirling Cycle Cooler for Space Applications, Phase I and II - Engineering Model, Final Report: Sept. 1978 - Dec. 1982, F. Stolfi, et al, NASA Contract NAS5-25172, Briarcliff Manor, NY, March 1983.

[2] Philips Laboratories, division of North American Philips Corp., Parametric Testing of a Linearly Driven Stirling Cryogenic Refrigerator, F. Stolfi and A. Daniels, 3rd Cryocooler Conference on Refrigeration for Cryogenic Sensors and Electronic Systems; Boulder, CO, Sept. 1984.

[3] Novel Titanium-Aluminum Joints for Cryogenic Cold Finger Structures, H.M. Meehand and R.C. Sweet, Advances in Cryogenic Engineering, Vol 27, Plenum Press, New York, 1981.

[4] Directivity and Stability of Coaxial Permanent Magnet Systems, Th. Gast, A. Mirahmadi and F.E. Wagner, Paper no. V-2 at 5th International Workshop on Rare Earth-Cobalt Permanent Magnets and Their Applications; Roanoke, VA, June 1981. (Book by University of Dayton, KL-365, Dayton, Ohio 45469, USA).

[5] Permanent Magnet Bearings and Couplings, Jean-Paul Yonnet, IEEE Transactions on Magnetics, Vol. MAG-17, No. 1, January 1981, pp 1169-1173.

D11

SIMPLE CONSTRUCTION AND PERFORMANCE OF A CONICAL PLASTIC CRYOCOOLER

N. Lambert

Department of Applied Physics
Delft University of Technology
2628 CJ Delft, The Netherlands

Low power cryocoolers with conical displacers offer several advantages over stepped displacers. The described fabrication process allows quick and reproducible manufacturing of plastic conical displacer units. This could be of commercial interest, but it also makes systematic optimization feasible by constructing a number of different models. The process allows for a wide range of displacer profiles. Low temperature performance as dominated by regenerator losses, as well as several related effects are discussed. In addition a simple device is described which controls gas flow during expansion.

Key words: Composites; conical displacer; cryocooler; flow controller; low power refrigeration; low temperature; plastic; refrigeration; regenerative cooler; Stirling cycle.

1. Introduction

The widespread use of low temperature devices by non-specialists depends heavily on the availability of suitable coolers. Practical solutions to this problem will stimulate research along lines that are presently unattractive. Zimmerman [1] pioneered the development of plastic Stirling coolers with gap regeneration to cool a SQUID device directly. The emphasis is on very low magnetic interference levels (dictating the use of plastics) and very low cooling power. A cooler's performance, as can be shown from elementary principles, improves significantly at low temperatures if multiple stages are used. If one ignores the increase in void volume, adding additional stages is always advantageous. However, all individual stages need separate machining and careful assembly. An attractive alternative is a tapered displacer, which can be considered as consisting of an infinite number of stages. Du Pré and Daniels [2] experimented with such a conical displacer in 1971 and Myrtle et al. [3] successfully built a plastic version suitable for SQUID applications. These units still require a lot of careful machining. In addition, constructing a viable machine from a bare unit is time consuming. We felt the need for a different manufacturing scheme that

- is simple,
- has inherently better reproducibility,
- allowes more design flexibility, and
- reduces the time spent in completing the unit.

2. Conical displacer

In Stirling coolers all losses are distributed along the length of the displacer-regenerator, except for the discrete radiation shields. From the thermodynamic point of view therefore, distributed cooling represents the main advantage of Stirling coolers with a conical displacer compared to their stepped counterparts. The shape of the cone determines the distribution of the cooling power.

There are several more subtle effects however. Cool-down is slightly faster because of the lower mass of the displacer. The gas is expanded within an annular gap, whereby thermal contact during expansion is improved and (the more favourable) isothermal expansion can be achieved even at low temperatures. Several effects depend on the width of the annular gap. At low temperatures the regenerative losses are dominant. Although this loss is mainly due to the plastic, it is still important to keep the thermal resistance of the gas gap low by means of a narrow gap. At higher temperatures shuttle heat transfer losses are more important and a wider gap with corresponding higher thermal resistance becomes attractive. The annular gap of a conical displacer depends on the angle of the taper and varies during a stroke.

A more important issue is the void volume. Zimmerman [1] found that his nylon displacers contracted 1% more than the glass fibre reinforced epoxy cylinder during cool-down. In cylindrical stages it is easy to compensate for axial contraction. However the radial contraction causes an appreciable void volume. At a typical stage length of 150 mm, the annular void volume associated with this 1% differential contraction corresponds to about 3 mm dead stroke - compared to a typical 6 mm active stroke. Since regenerator losses are proportional to the total mass flow squared [4], this effect roughly doubles regenerator losses. Conical displacers have different properties: The gas gap widens during the upgoing stroke and no additional static gap is needed for the gas flow. Axial correction can compensate for radial contraction of a linear cone. However, when either the taper is nonlinear or the contraction is inhomogeneous (temperature gradient) this is impossible and may result in significant void volumes. Therefore in a conical design the sleeve should contract slightly more than the displacer. In that case the void volumes are in the gaps at higher temperatures, where they are less important or even favourable (higher thermal resistance). The only void volume at low temperature is located at the narrow tip, which can be easily filled.

Probably the most important advantage of conical displacers is in construction. When difficult machining can be avoided, this shape clearly favours simple, single step manufacturing processes.

3. Manufacturing

It is not feasible to machine both tapered displacer and sleeve from plastic rods with sufficient accuracy to get a reasonable fit. The obvious solution is to use one of these as a mould for the other; a perfect fit is guaranteed. Myrtle et al. [3] machined the displacer from rods and wrapped glass fabric with epoxy resin around it to obtain the sleeve. However, machining a long narrow displacer from glass fibre epoxy is tedious to say the least. It has to be done by sections, which adds critical aligning steps to the process. We wrapped the sleeve around a brass cone, and tried to cast the displacer in this sleeve afterwards. Uneven distribution of the glass fibres within the epoxy resin made the displacer warp seriously at cryogenic temperatures. This suggested the use of glass powder instead of fibres, but small irregularities in the inner surface of the sleeve prevented a reliable release. Therefore we prepared a special mould from the brass cone. A professional casting rubber contracted about 0.5% (elastically), rendering the mould useless. We obtained good results with unfilled casting wax saturated with fine sand to eliminate contraction (causing cracks) during congealing.

The entire manufacturing scheme is illustrated in figure 1. The critical properties of the cone are sufficient roundness and a straight axis, rather than the precise diameters. The brass cone was machined in about one day on an ordinary lathe, and can be used many times. This garantuees reproducibility.

After coating the brass cone with a parting agent, a layer of glass fibre ribbon is wrapped around it using Stycast 1266 epoxy resin (Emerson & Cuming). Next, a helium diffusion barrier of 5 µm manganin foil and the aluminum tip are secured with a second wrapping. Electrical leads and thermocouples are thermally anchored and protected by the third and final layer. Supports for radiation shields can be built up from glass fibre ribbon or aluminum. Black Stycast 2850 FT (with catalyst 24LV, Emerson & Cuming) is cast in the flange mould attached to the brass cone (fig. 1a). Threaded holes are formed in the plastic by embedding nuts. The entire sleeve is cured at room temperature. Then the brass is released by force, and the supports for radiation shields are machined to the right size.

Figure 1b shows the manufacturing of the displacer mould. The melted wax/sand mixture is cast around the preheated brass cone. After insulating with glass wool, water cooling causes congealing to start from below. An anchor at the bottom prevents an upward shift of the wax during contraction. In this way the contraction can actually be used to force a perfect fit. The brass cone is pulled free at room temperature.

Figure 1c shows casting of the displacer in the wax mould. We use a mixture of fused silica (-200 mesh) and Stycast 1266 epoxy. The ratio of the powder and resin components is 180 powder: 100 component A : 28 component B in parts by weight. Immediately after preparation, the mixture is vacuum treated to remove air bubbles and then injected into the mould. After cure at room temperature the wax is melted. Small surface irregularities are corrected with sandpaper and the displacer is machined to the right length. The glass powder/epoxy mixture is very homogeneous and we found no warp at cryogenic temperatures. However, should the need arise, the displacer can be made flexible by segmenting it and interconnecting the pieces with wire (a single nylon fibre in the casting can be pulled out easily after cure, leaving a convenient channel). With another trivial extension of the moulding process the displacer could be made hollow to decrease thermal conductivity and thermal mass.

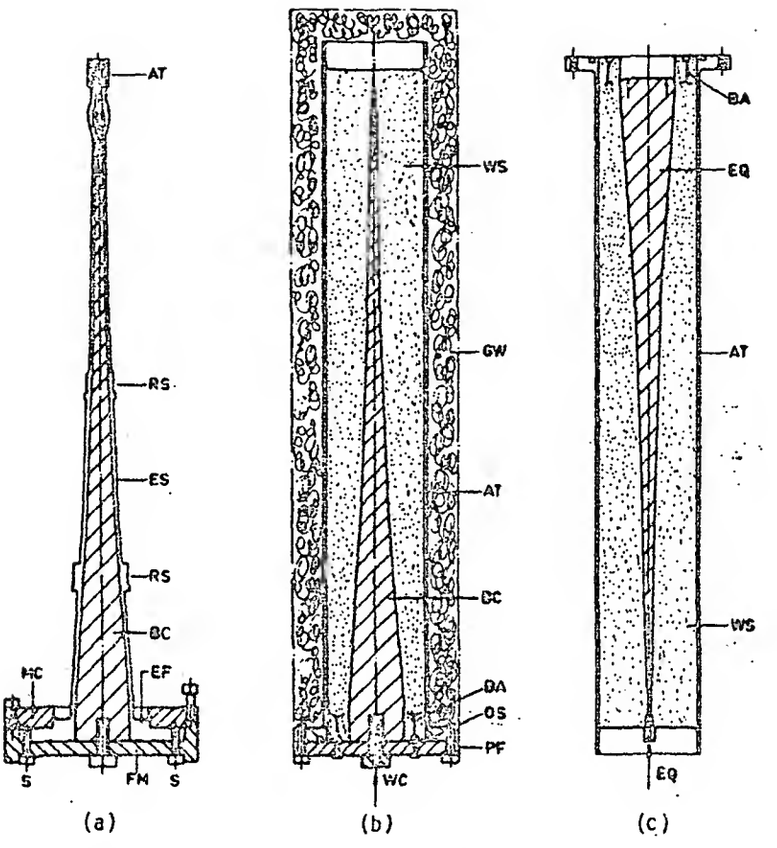

Fig. 1. Manufacturing: (a) The glass fibre epoxy sleeve (ES) is wrapped around the brass cone (BC), with an aluminum tip (AT). An epoxy flange (EF) is cast in a covered (MC) flange mould (FM). Screws (S) may be used to form threaded holes. Supports for radiation shields (RS) are built up and machined after cure. (b) A wax/sand mixture (WS) is cast around the brass cone (BC) within an aluminum tube (AT), and insulated with glass wool (GW). Water cooling (WC) through an insulating flange (PF) determines the direction of congealing. Brass anchors (BA) hold the wax down. (c) Glass powder/epoxy mixture (EQ) is injected into the wax mould.

The photograph (fig. 8) shows the different components. Except for a lathe, no special tools are needed. At the moment the entire process takes about 40 man hours in the laboratory. The main part is consumed by preparation. For a small series a significant gain is possible. A more detailed description of the process can be obtained from the author on request.

4. Results

We compared the dimensions of the plastic displacer and brass cone at room temperature and found the displacer to be about 0.05 mm smaller in diameter along the entire length. The tip of the displacer was shortened until it fitted the sleeve exactly, and this length corresponded to the length of the brass cone within 0.1 mm. Then the tip was lengthened by a 1 mm piece of aluminum. The displacer was now completely free to move in the sleeve. The top of the fully inserted displacer shifted less than 0.1 mm after warming up to room temperature, indicating negligible difference between contraction of sleeve and displacer. At cryogenic temperatures the displacer was still free to move and rotate in the sleeve, indicating negligible warp.

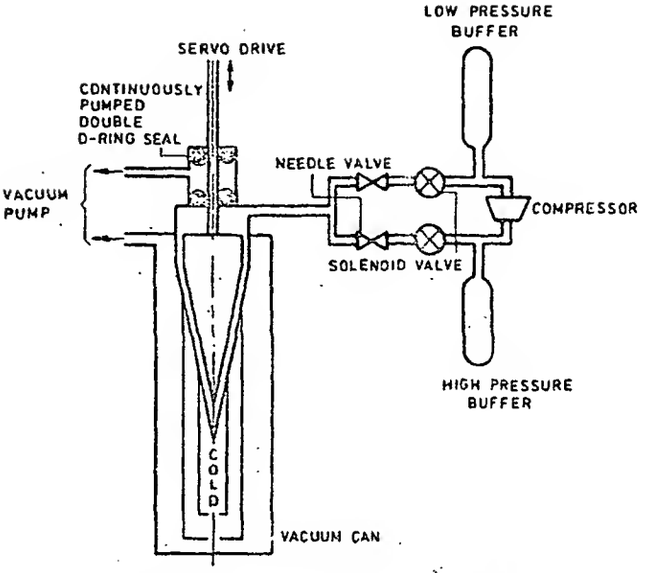

Fig. 2. Experimental setup. The cold space inside the vacuum can is surrounded by radiation shields and superinsulation.

Figure 2 shows a diagram of the experimental setup. The displacer unit with radiation shields and superinsulation is mounted in a continuously pumped vacuum can. For experimental purposes the displacer is driven by a servo motor (electronically controlled) through a vacuum pumped double O-ring seal to avoid contamination of the helium. A small, standard, rubber membrane air compressor is used to compress the helium in a closed circuit. Solenoid valves control compression and expansion in the displacer unit.

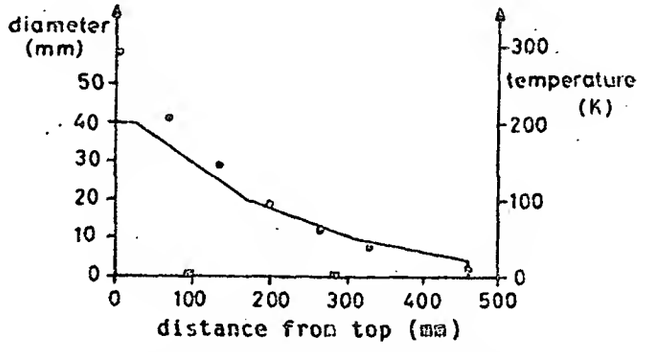

Fig. 3. Diameter (solid line) and temperature (dots) along the length of the cone. Tip temperature measured with germanium resistor, others with thermocouples. Positions of the two radiation shield supports are indicated at horizontal axis.

The first experimental results are promising: At a 1 second period, a 6 mm stroke and a 0.42 to 0.10 MPa (absolute) pressure cycle it cooled down to 10.1 K in 18 hours. Temperature distribution and dimensions of the cone are indicated in figure 3. The temperature at the tip rises 0.4 K with a 1 mW heat load. At present the lowest temperature is limited by the performance of the compressor, and we intend to improve the system in the near future. Although the manganin shield inside the plastic sleeve wall of this unit was damaged during manufacturing, it took about 5 hours before the tip temperature started to rise noticeably due to helium diffusion if pumping was discontinued.

5. Gas pressure and displacement

Several parameters are important in optimizing the operation of a cooler. The gas pressure and displacement waves are of general importance for any regenerative system. At temperatures below about 20 K the regenerator losses are dominant. The gas flows in an axial temperature gradient dT/dz and the heat load on the regenerator is proportional to the thermal capacity of the gas flow mC and the thermal gradient. Heat exchange with the plastic is not perfect. This can be expressed as a thermal impedance Z_T. The temperature difference δT between gas and plastic (reference) is given by

$$\delta T = Z_T \dot{m} C \frac{dT}{dz}$$

The net regenerator loss $\dot{Q}_{reg}$ is a time averaged product

$$\dot{Q}_{reg} = \langle \dot{m} C \delta T \rangle_t = \langle (\dot{m}C)^2 Z_T \rangle_t \frac{dT}{dz}$$

In many textbooks a basic distinction is made between Stirling (piston), Gifford-McMahon (continuous compressor with valves) and Vuilleumier (regenerative thermal compressor) cycle. Indeed the room temperature arrangements and their inherent limitations (high drive forces and sealing, lower efficiency, high temperature construction and low compression ratio, respectively) are quite different, but at the low temperature end the cycles are very similar. The lower regenerator heat load of a constant density cycle (the theoretical Stirling cycle) can in fact be achieved by moving stacked displacer segments down (or up) one by one (analogous to the ripple that passes through a queue of cars waiting at the fast food drive-in). The conventional single displacer system, however, leads to the 5/3 times higher heat load of a pressure controlled system.

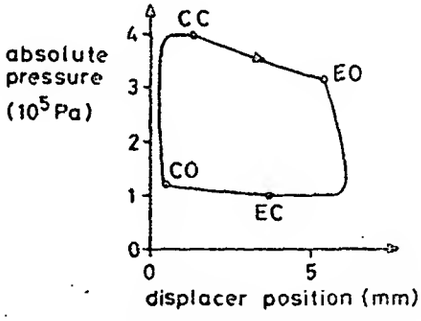

Fig. 4. Pressure - displacement oscilloscope trace. Compression valve opens at CO and closes at CC. Expansion valve opens at EO and closes at EC.

There are still some possibilities left to reduce the regenerator heat loss significantly by manipulating the pressure and displacement cycle. As was pointed out above, it is very important to keep the low temperature void volume low compared to the swept volume. This reduces the unnecessary part of the mass flow. Figure 4 shows the pressure - displacement oscilloscope trace of the actual cycle employed in our machine. The refrigeration power is directly proportional to the area enclosed in the pressure - displacement diagram. The total mass flow corresponds to the difference between maximum and minimum of the product of pressure and displacement (at EO and CO). In a regenerator loss dominated machine like ours, it is important to truncate the rectangular cycle of a typical Gifford-McMahon machine as shown (CC to EO and EC to CO) by timing the valves properly. In this way a small amount of the available refrigeration power is sacrificed, but the regenerator losses are reduced significantly by the decrease in mass flow. Typical numbers are 10% reduction of refrigeration and an improvement of about a factor two in regenerator loss. The ideal case would be truncation along a line of constant amount of gas (hyperbole), i.e. zero mass flow. Unfortunately the unavoidable room temperature volume at the top of the displacer limits the pressure drop between CC and EO.

Another possible improvement involves the time dependence of the mass flow. In the case of a purely resistive thermal impedance (e.g. a narrow gas gap) a square wave is optimal. A sine wave

is only a factor $\pi^2/8$ worse, but peaked functions are clearly less desirable. As indicated by Radebaugh [4] the thermal penetration depth in the plastic will usually dominate at low temperatures. In that case the thermal impedance has an imaginary part. This introduces a 45 degree phase shift and corresponding $1/\sqrt{(\text{frequency})}$ dependence in all Fourier components [5]. The phase shift introduces a extra factor of $1/\pi$ for a sine wave. In this case, determining the optimum wave form involves some mathematics. The optimal solution results in an improvement of only about 20% compared to the sine wave.

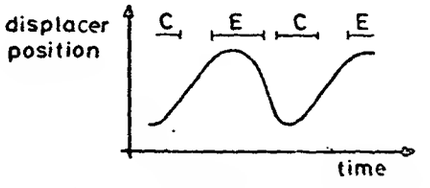

Fig. 5. Displacer movement. C: Compression valve open. E: Expansion valve open.

However, in practical valve operated coolers the mass flow cycle is highly asymmetric and peaked. The performance can be improved significantly by smoothing the gas flow. Our experimental setup allows full electronic control of the displacer movement. Figure 5 shows a typical oscilloscope trace of the non-sinusoidal movement employed in our machine. Most of downward gas transport occurs during the upward displacer movement at high pressure. Most of the upward gas transport occurs during expansion when the displacer is at top position. Therefore more time is spent in raising the displacer and near the top position.

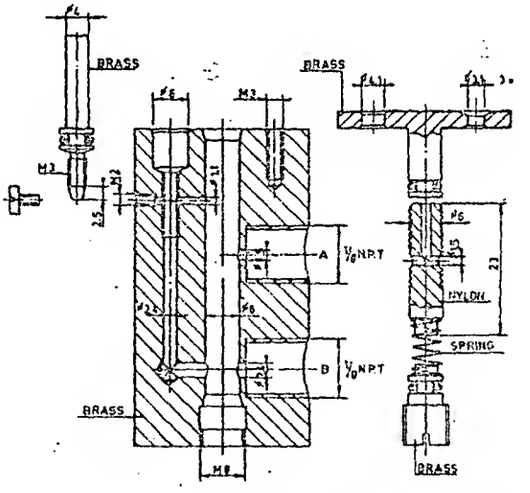

Fig. 6. Gas flow controlling device. Gas flows through needle valve at the left to the outlet port B. The nylon piston at the right stabilizes the pressure difference over the needle valve by closing the inlet port A.

Smoothing of the pressure cycle during expansion and compression is usually achieved by means of a needle valve. The mass flow through such a constriction generally depends on both the pressure difference and the average pressure at inlet and outlet port. This gives rise to a long tail in the pressure decrease as a function of time (a hyperbolic cotangent for laminar flow). The time derivative of the pressure, which represents the mass flow when the displacer is stationary, is highly peaked. A simple solution would be to use a spring-loaded needle valve which opens when the pressure difference over the constriction drops. It is difficult, however, to adjust the flow characteristics of such a device while in operation. Figure 6 shows a more sophisticated device, which essentially consists of a pressure regulator and needle valve in series. Expansion to the low pressure outlet is controlled by the needle valve. The pressure difference over the needle valve is stabilized by a spring-loaded nylon piston which closes the high pressure inlet when necessary. The flow through the device now depends on pressure at the outlet only. In figure 7

the oscilloscope traces of expansion through this device and through an ordinary needle valve can be compared. The lowest temperature in our cooler improved about 0.8 K with this modification, and the effect should be even more important at lower temperatures. Several versions are possible, e.g. a membrane instead of a piston, a stem or needle instead of a poppet valve, an adjustable spring, etc. We suppose that this device can be used in other fields as well. A similar device could be designed for compression, but this is a less critical part of the cycle. Regenerator heat load during compression is low because the displacer is near the bottom position, and compression is inherently more linear than expansion.

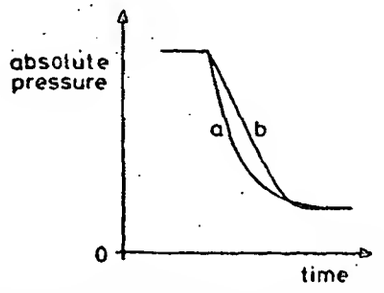

Fig. 7. Expansion through ordinary needle valve (a) and through flow controlling device (b). Note that the time derivative, representing the mass flow, is highly peaked in (a) but almost perfectly constant in (b).

6. Future work

Besides improving the current performance by operating at somewhat higher pressures, we intend to build several different units in the near future. An obvious improvement would be a hollow displacer. This is only relevant at the high temperature section. A significant improvement is expected in low temperature performance by incorporating a higher heat capacitance, e.g. lead particles or He on charcoal, in the plastic. Because the loss from static conduction is negligible at low temperature, regenerator losses can also be reduced by using materials with a higher thermal conductivity. We hope to perform a rather detailed computer analysis including all relevant details, in order to optimize low temperature performance. Another simple extension would be a small, low pressure Joule-Thomson stage using the gas from the regenerative cycle to prevent impurity build up. The gas lines can be embedded in the plastic sleeve. A similar experiment on a stepped cooler [6] indicated that this approach is feasible.

7. Summary

Multiple stage plastic cryocoolers require accurate machining of all separate stages and careful assembly to achieve a close fit of the displacer within the cylinder. Conical displacers are thermodynamically attractive, but were thus far more difficult to make than multiple staged designs. This paper describes a simple process to make both the cold finger and the displacer from a single conical mould. Vacuum flange, cold tip and supports for radiation shields are included. Thermocouples and electric wiring are embedded in the plastic. The first experimental results in low temperature performance are promising. In a laboratory the entire process takes about 40 man-hours, which seems a reasonable starting point for small scale production. The reproducibility of the product allows for systematic performance optimization by constructing a number of different models. The flow controlling device for expansion, and several other improvements concerning regenerator loss may be useful for other projects as well.

This work was initiated during a stay at NBS Boulder Laboratories and carried out at Delft University. We thank Dr J. E. Zimmerman for instructive discussions and advice. The work is sponsored by the Delfts Hogeschoolfonds. We cordially acknowledge the additional support by Prof. H. Postma and Prof. J. E. Mooij, which made the visit to NBS Boulder possible.

8. References

[1] Zimmerman, J. E. and Sullivan, D. B., A Study of Design Principles for Refrigerators for Low-Power Cryoelectronic Devices, 1982, National Bureau of Standards Technical Note 1049 (National Technical Information Service, Springfield, VA 22161).

[2] Du Pré, F. K. and Daniels, A., Gap-regeneration method for Stirling and similar cycles (Proc. XIII Int. Congr. of Refr., Washington D.C., 1971), in Progr. in Refrigeration Science and Technology 1, 137-141 (AVI Publishing Company, Inc. Westport, Connecticut, 1973).

[3] Myrtle, K., Winter, C., and Gygax, S., A 9 K conical Stirling-cycle cryocooler, Cryogenics 22, 139-141 (1982).

[4] Radebaugh, R., Analysis of regenerator inefficiency for Stirling-cycle refrigerators with plastic displacers, XV Intern. Congress of Refrigeration, Venice, Italy, September 1979).

[5] Carslaw, H. S. and Jeager, J. C., Conduction of heat in solids, 64-70 (Oxford at the Clarendon Press, 1959).

[6] Zimmerman, J. E., Recent developments in self-contained cryocoolers for SQUIDs and other low-power cryoelectronic devices (to be published in the Proceedings of the 10th International Cryogenic Engineering Conference, Helsinki, 1984).

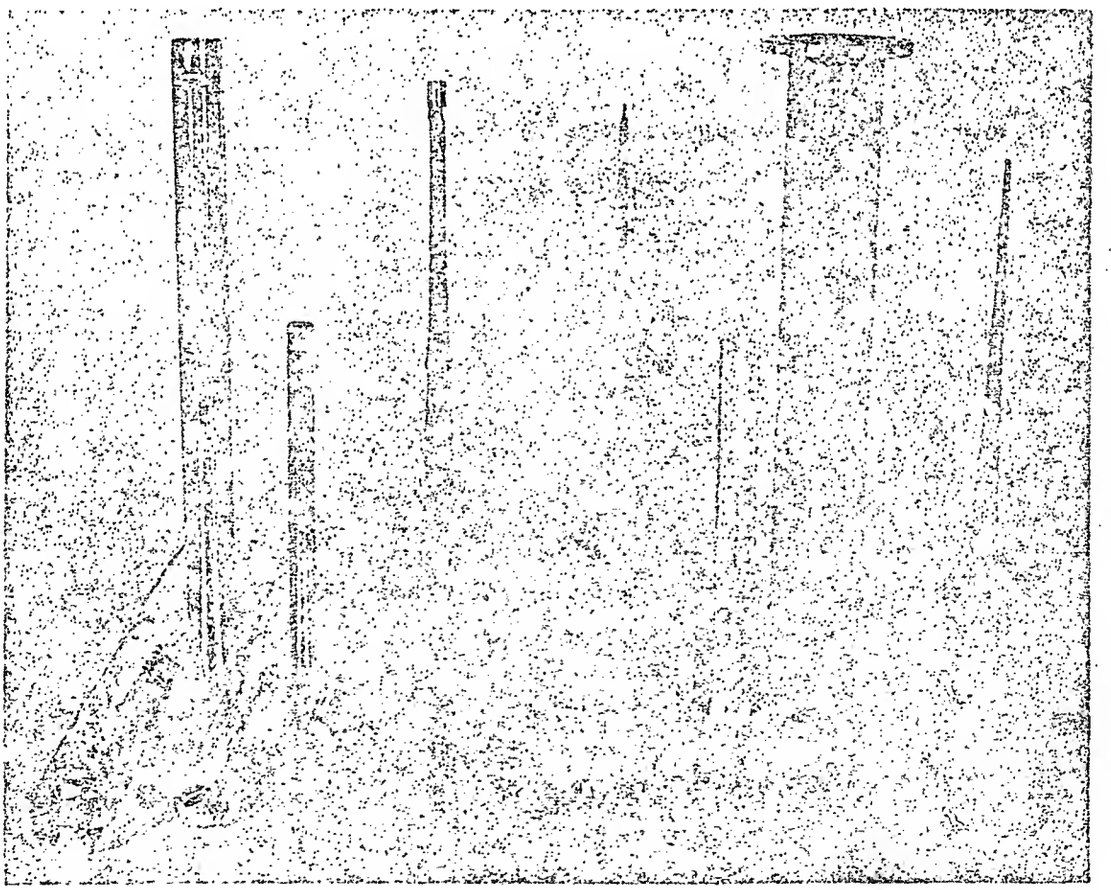

Fig. 8. From left to right: Superinsulation packs and radiation shields, glass fibre epoxy sleeve, brass cone with flange mould and cover, 30 cm scale, wax/sand mould with flange, glass powder/epoxy displacer.

D12

EFFECTS OF LEAKAGE THROUGH CLEARANCE SEALS ON THE PERFORMANCE OF A 10 K STIRLING-CYCLE REFRIGERATOR

C. S. Keung and E. Lindale

Philips Laboratories
A Division of North American Philips Corporation
Briarcliff Manor, NY 10510

The use of clearance seals is essential to achieve long-life, wear-free operation of Stirling-cycle cryogenic refrigerators. This paper describes an experiment which determined the effect of leakage through clearance seals on the performance of such a refrigerator operating at temperatures ranging from 20 K down to 10 K.

The ability of a Stirling-cycle refrigerator to achieve 10 K with clearance seals was successfully demonstrated. Results indicate that the leakage flow undergoes gap regeneration before reaching the cold expansion volume. A simple model of gap regeneration was used to estimate the regeneration loss due to the leakage flow. This regeneration process minimizes the loss in refrigerator performance caused by the clearance-seal leakage. As a result, clearance seals remain effective down to a refrigeration temperature of 10 K.

Key words: clearance seal; cryogenic refrigerator; cryogenics; heat transfer; regenerator; Stirling cycle.

1. Introduction

One of the life-limiting mechanisms in a typical cryogenic refrigerator is the wear of its seal surfaces. Wear of the seal surface not only increases leakage but also generates contaminants. In order to achieve long-life, wear-free operation of cryogenic refrigerators, the use of clearance seal is essential.

A clearance seal is a long, narrow annular gap established between the outside surface of a reciprocating cylinder and the internal surface of a mating cylindrical housing. Sealing is attained by the flow resistance provided by the long narrow gap. Clearance seals were first implemented successfully on a long-life, Stirling-cycle refrigerator operating down to 38 K [1]. In this study, a triple-expansion, Stirling-cycle refrigerator was tested to study the effectiveness of clearance seals to attain temperatures below 20 K. This paper describes the experiment with the three-stage refrigerator and a first order analytical model of the effects of the clearance seal on cold production.

2. Description of refrigerator

The first successful operation of the triple-expansion, Stirling-cycle cryogenic refrigerator used in this study was reported by Daniels and duPré [2] in 1971. In this earlier study, this refrigerator originally reached a temperature of 9 K with a third-stage (coldest) regenerator filled with lead spheres. The refrigerator configuration is typical of conventional Stirling-cycle machines driven by a simple crank-type mechanism (fig. 1). The compression heat is rejected to water through a cooling jacket. The crankshaft is driven externally by a variable-speed motor.

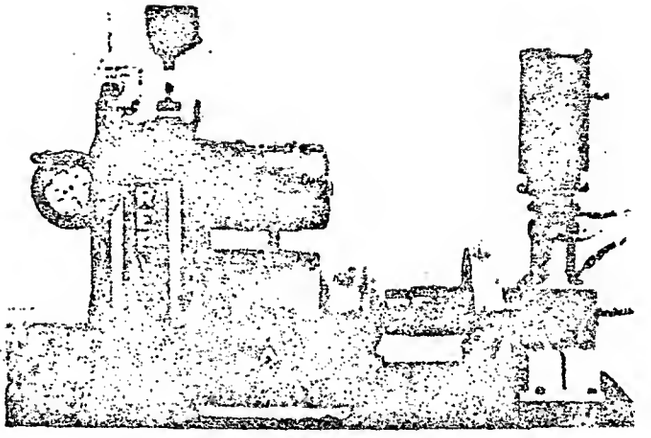

Figure 1. Motor drive and triple expansion refrigerator

The displacer is stepped to three diameters (figs. 2 and 3), with each section containing a regenerator matrix. The first (i.e., warmest) and second stage matrices are made of layers of phosphor-bronze mesh.

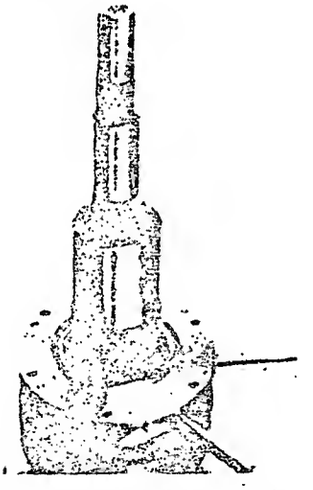

Figure 2. Three stage displacer

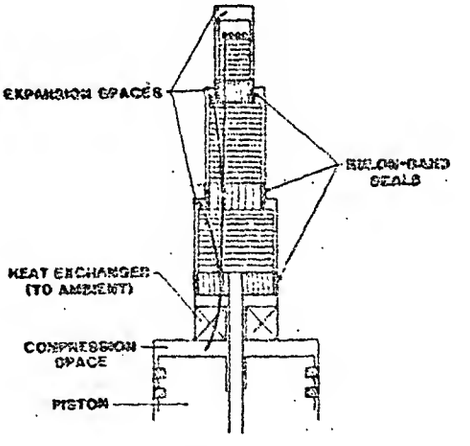

Figure 3. Schematic of triple expansion refrigerator

The original lead spheres were replaced by lead mesh. Lead mesh is made by expanding lead-calcium-tin alloy sheets (fig. 4). Lead mesh was used as a test for its potential as an alternative to lead spheres.

Each of the three displacer stages has a Rulon-band seal (see fig. 3) which is epoxied to the lower section, and was machined to fit their respective bores in the cold finger. The seals also act as bearings guiding the reciprocating motion of the displacer.

The temperature of the coldest stage was monitored with a helium gas thermometer. The 1st and 2nd stage temperatures were monitored with copper-constantan thermocouples mounted on the flanges of the cold finger. An electric resistance heater was mounted to the third stage to measure the cold production.

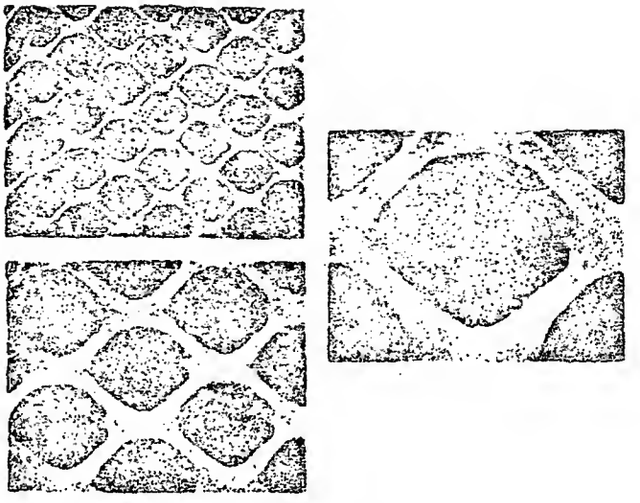

Figure 4. Magnified view of lead mesh

The refrigerator was first run with all contacting seals and a temperature of 9.4 K was reached. Table 1 summarizes the major dimensions and operating conditions of the refrigerator.

Table 1. Major refrigerator dimensions and operating conditions

	1st stage	2nd stage	3rd stage
Displacer diameters, mm	39.9	20.0	15.1
Regenerator:			
length, mm	39.4	29.4	28.5
mesh material	phosphor-bronze	phosphor-bronze	lead
mesh fill-factor	0.4	0.4	0.4
Piston diameter, mm	63.5		
Displacer stroke, mm	12		
Piston stroke, mm	32		
Displacer-piston phase angle	90		
Charge pressure, psia	89.6		
Speed, cps	640		
Piston swept volume c.c.	100.8		

3. Tests with clearance seal

After a temperature below 10 K was achieved with all contacting seals, the diameter of the third stage seal was reduced to provide a radial clearance seal. The seals/bearings on the second and third stage were responsible for guiding the displacer. The total indicated runout of the clearance seal was less than 0.0002". The refrigerator was re-run with a third-stage clearance seal of 0.0015" radial clearance. The test was then repeated with a 0.002" radial clearance seal.

4. Simplified model of gap regeneration

Working fluid leaking through the clearance seal flows past a long, narrow annular gap before reaching the expansion space (fig. 5). The leakage flow undergoes gap regeneration by exchanging heat with the two concentric walls surrounding the annulus. The loss in cold production due to clearance-seal leakage is a result of imperfect gap regeneration experienced by the leakage flow.

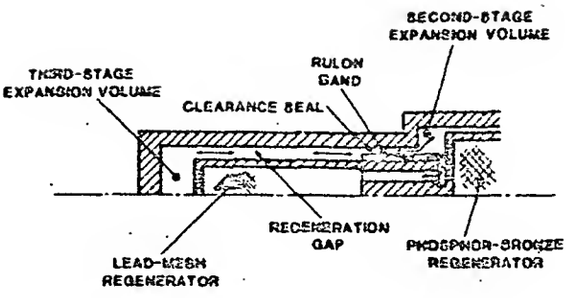

Figure 5. Schematic of leakage flow passing through the clearance seal and regeneration gap with dimension of the clearances exaggerated

A model was developed to estimate the regeneration loss of the leakage flow.

In order to treat the involved regeneration theory analytically, the following simplifications are made.

1. The temperature and pressure of the fluid in the regeneration gap vary spacially with axial position, z, only.
2. The time-averaged wall temperature varies linearly with z.
3. The thermal properties of both fluid and wall are constant.
4. The regeneration losses are the sum of the losses from two independent cases. In case 1, the regenerator has finite heat transfer rate but infinite wall heat capacity. In case 2, the regenerator has finite wall heat capacity but infinite heat transfer rate, and the fluid pressure fluctuates with time.

Case 1. Finite heat transfer

The leakage with an average mass flow rate of $\dot{m}_o$, flows through an annular regeneration gap with average diameter D and gap width s. If heat transfers between the fluid and wall through a coefficient h, the energy equation is:

$$\dot{m}_o c_p \frac{d T_g}{d z} = 2\pi D h (T_g - T_w), \tag{1}$$

where T_g = fluid temperature

T_w = wall temperature

c_p = specific heat of fluid

The heat transfer coefficient for flow through an annulus with equal linear temperatures on both walls is given by [3]

$$h = 8.23 \frac{k}{2s}, \quad \text{where } k = \text{thermal conductivity of fluid.}$$

With a linear wall temperature, eq. (1) can be integrated over the entire seal length L to yield

$$T_g(L) = T_c + \frac{T_h - T_c}{\Lambda} (1 - e^{\Lambda}) , \tag{2}$$

where T_h = temperature at the warm end of the regeneration gap,

T_c = temperature at the cold end of the regeneration gap,

and $$\Lambda = \frac{2\pi dLh}{\dot{m}_o c_p}$$

For laminar flow in the gap, the average mass flow rate in the gap can be expressed as

$$\dot{m}_o = \frac{\pi \rho D d^3 \Delta P}{12 \sqrt{2}\, \mu \ell} , \tag{3}$$

where ρ = fluid density,
μ = fluid viscosity,
d = clearance seal width,
ℓ = clearance seal length,

and

ΔP = pressure drop along the entire seal length.

The regeneration loss due to finite heat transfer, q_h is then given by

$$q_h = \dot{m}_o c_p (T_g(L) - T_c) ,$$

or using eq. (2),

$$q_h = \dot{m}_o c_p \frac{T_h - T_c}{\Lambda} (1 - e^{-\Lambda}) . \tag{4}$$

Case 2. Finite heat capacity and fluid pressure fluctuation

The wall heat capacity available for regeneration is limited by the thermal penetration depth, δ, of the wall material. Since heat transfer in or out of the wall over half of the cycle, δ is given as

$$\delta = \left(\frac{\alpha_w}{\omega}\right)^{1/2} ,$$

where α_w = thermal diffusivity of the wall

ω = angular frequency of the refrigeration cycle

Thus the wall heat capacity per unit length available for regeneration is $2\rho_w c_w \pi D\delta$, where ρ_w and c_w are density and specific heat of the wall material respectively.

Since the effects of finite heat capacity and fluid pressure fluctuation are time-varying, the transient energy equation must be used to analyze the effects. Applying the energy equation on a volume of fluid contained in a length of dz of the regeneration gap, one has [4]

$$-2\rho_w c_w \frac{\delta}{s} \frac{\partial T_w}{\partial t} = \rho c_p \frac{DT_g}{Dt} - \frac{DP}{Dt} , \tag{5}$$

where P is fluid pressure. If flow resistance is neglected and the assumption of infinite heat transfer (i.e., $T_w = T_g$) is used, eq. (5) can be written as

$$\frac{\partial T_g}{\partial t} = \frac{1}{c_m} \frac{\partial P}{\partial t} - \frac{\dot{m}}{\pi D s} \frac{C_p}{C} \frac{\partial T_g}{\partial z} , \tag{6}$$

where $c_m = \rho c_p + 2\rho_w c_w \frac{\delta}{s}$.

The time-varying pressure and mass flow rate can be expressed as

$$P = P_o - \hat{P} \cos \omega t \tag{7}$$

$$\dot{m} = \hat{m} \cos (\omega t - \theta) \tag{8}$$

$$\hat{m} = \sqrt{2}\, \dot{m}_o .$$

The fluctuation of pressure and mass flow in the regeneration gap are modeled as being in phase with the fluctuation in the main working volume.

Using eqs. (7) and (8), one can integrate eq. (6) to obtain

$$T_g = \frac{P}{c_m} - \frac{\hat{m}}{\pi D s \omega} \frac{c_p}{c_m} \frac{\partial T_g}{\partial z} \sin (\omega t - \theta) . \tag{9}$$

The regenerator loss due to finite heat capacity and pressure fluctuation, q_c, is given by the rate of flow of enthalpy, which is

$$q_c = \frac{\omega}{2\pi} \oint \dot{m} c_p T_g dt$$

$$= \frac{\omega}{2\pi} \frac{c_p}{c_m} \oint \dot{m} P dt ,$$

or

$$q_c = \frac{\hat{P}}{2} \frac{c_p}{c_m} \hat{m} \cos \theta . \tag{10}$$

The total loss due to clearance seal leakage is given by the sum of q_h and q_c.

5. Results and Discussion

Cold production of the triple-expansion refrigerator at temperatures ranging from 10 K to 20 K were measured. In figure 6, the top curve shows the performance of the refrigerator with line-to-line contacting seal, and the lower two curves represent the 0.0015" and 0.002" clearance seals. The differences between the top curve and the lower two are the losses in cold production due to the leakage of the clearance seals. These measured losses are plotted in figure 7 together with the losses predicted by eqs. (4) and (10).

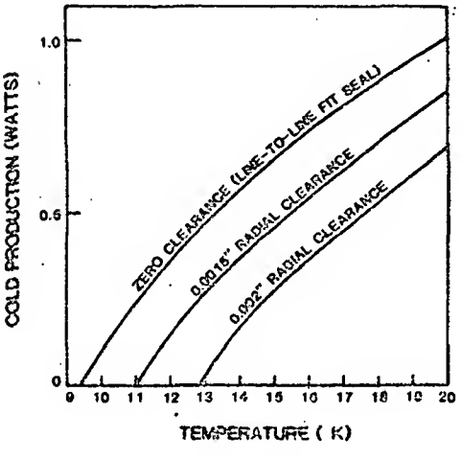

Figure 6. Cold production at the coldest stage

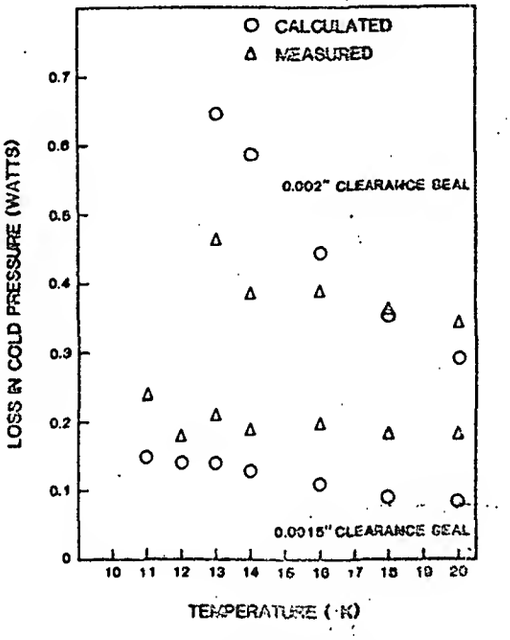

Figure 7. Loss in cold production due to clearance seal leakage

The discrepancy between the measured and calculated results is most likely due to the simplification made in the theoretical model for gap regeneration. Furthermore, friction heating by the contacting seal and slight eccentricity of the annular clearance seals were not accounted for in the model. But the comparisons show that eqs. (4) and (10) give good first order estimation of the loss due to the use of clearance seals in Stirling-cycle refrigerators.

This experiment shows that the clearance seal losses produce a warm-up of 1.6 K and 3.5 K with clearances of 0.0015" and 0.002", respectively. This is an acceptable penalty in the design of a refrigerator with long-life as the leading priority. Furthermore, the loss due to clearance seals can be significantly reduced by using seals with smaller clearances. At the present, refrigerator with clearance of 0.001" is in operation [1], and the design of refrigerator with clearances of 0.00075" is in progress [5].

6. Conclusions

Measurements from a triple-expansion Stirling refrigerator show that the loss caused by clearance seals is low and is an acceptable penalty in the design of a long-life cryogenic refrigerator. The losses due to clearance-seal leakage can be modeled as imperfect gap regeneration. A simple gap regeneration model gives good first order estimation of these losses.

This study is partially funded by the Satellite Systems Division, Rockwell International.

7. References

[1] Stolfi, F., Goldowsky, M., Keung, C., Knox, L., Lindale, E., Maresca, R., Ricciardelli, J., and Shapiro, P., Design and Fabrication of a Long-Life Stirling Cycle Cooler for Space Application, Philips Laboratories, Briarcliff Manor, N.Y., NASA Contract NAS5-25172, March 1983.

[2] Daniels, A. and duPré, F. K., Triple Expansion Stirling Cycle Refrigerator, Advances In Cryogenic Engineering, Vol. 16, pp. 178-184 (1971).

[3] Kays, W. M. and Crawford, M. T., Convective Heat and Mass Transfer, pp. 100 (McGraw-Hill Book Co., Inc, New York, N.Y., 1980).

[4] Schlichting, H., Boundary-Layer Theory, Seventh Edition, pp. 265-268, McGraw-Hill Book Co., Inc., New York, N.Y., 1979.

[5] Knox, L., Patt, P., Maresca, R., Design of a Flight Qualified Long-Life Cryocooler, presented at the 3rd Cryocooler conference on Refrigeration for Cryogenic Sensors and Electronic Systems, NBS, Boulder, Colorado, September 17-18, 1984.

D13

AN EXPERIMENTAL RECIPROCATING EXPANDER FOR CRYOCOOLER APPLICATION

Moses Minta and Joseph L. Smith, Jr.

Cryogenic Engineering Laboratory
Massachusetts Institute of Technology
Cambridge, MA 02139

An experimental reciprocating expander has been designed with features appropriate for cryocooler cycles. The expander has a displacer piston, simple valves, and a hydraulic/pneumatic stroking mechanism. The expander has a valve in head configuration with the valves extending out the bottom of the vacuum enclosure while the piston extends out the top. The expander has been tested using a CTI 1400 liquefier to supply gas at about 13 atm in the temperature range 4.2 to 12 K. Expander efficiency has been measured in the range 84 to 93% while operating the apparatus as a supercritical wet expander and in the range 91 to 93% as a single phase expander. The apparatus can also be modified to operate as a compressor for saturated helium vapor.

Key words: Cryogenic expander; two-phase expander; experimental expander; reciprocating expander; expander valve actuator; expander efficiency.

1. Introduction

Small cryogenic refrigerators have been extensively and successfully used to meet the low power refrigeration requirements of cryopumps, cryogenic sensors and electronic systems at temperatures above 20 K in the past decade. Most of these cryocoolers have been based on the Gifford-McMahon, Modified Solvay, Stirling, or Vuilleumier cycle. The modification required to meet low power refrigeration needs below 6 K result in considerable increase in cost, power and complexity. This makes cryocoolers based on work-extraction devices attractive, particularly because of increased efficiency.

Large capacity helium liquefiers invariably use the Collins two-expander cycle. These units use reciprocating expanders or turbo-expanders which appear unattractive for scaling down to low capacity helium liquefaction. In the case of turbo-expanders, this is because of an efficiency penalty since the losses scale down disproportionately with geometric size. By contrast, the principal losses associated with the reciprocating machine are heat transfer losses which may be minimized by proper design. These losses may be grouped, generally, into those affecting the power and those directly manifesting themselves as heat leaks to the working fluid.

The power losses are due to valve flow, leakage, mechanical friction, blow down, blow in, and cyclic heat transfer. The cyclic heat transfer loss is the result of periodic heating and cooling of the working gas by the cylinder walls. The incoming gas is warmer than the cylinder walls and is therefore cooled while the cold gas after the expansion process is warmed by the cylinder walls. The net effect is that the expander processes more gas without a corresponding increase in expander work per stroke. The heat input losses consist of static heat leak, shuttle heat transfer and cylinder-piston gap pumping loss.

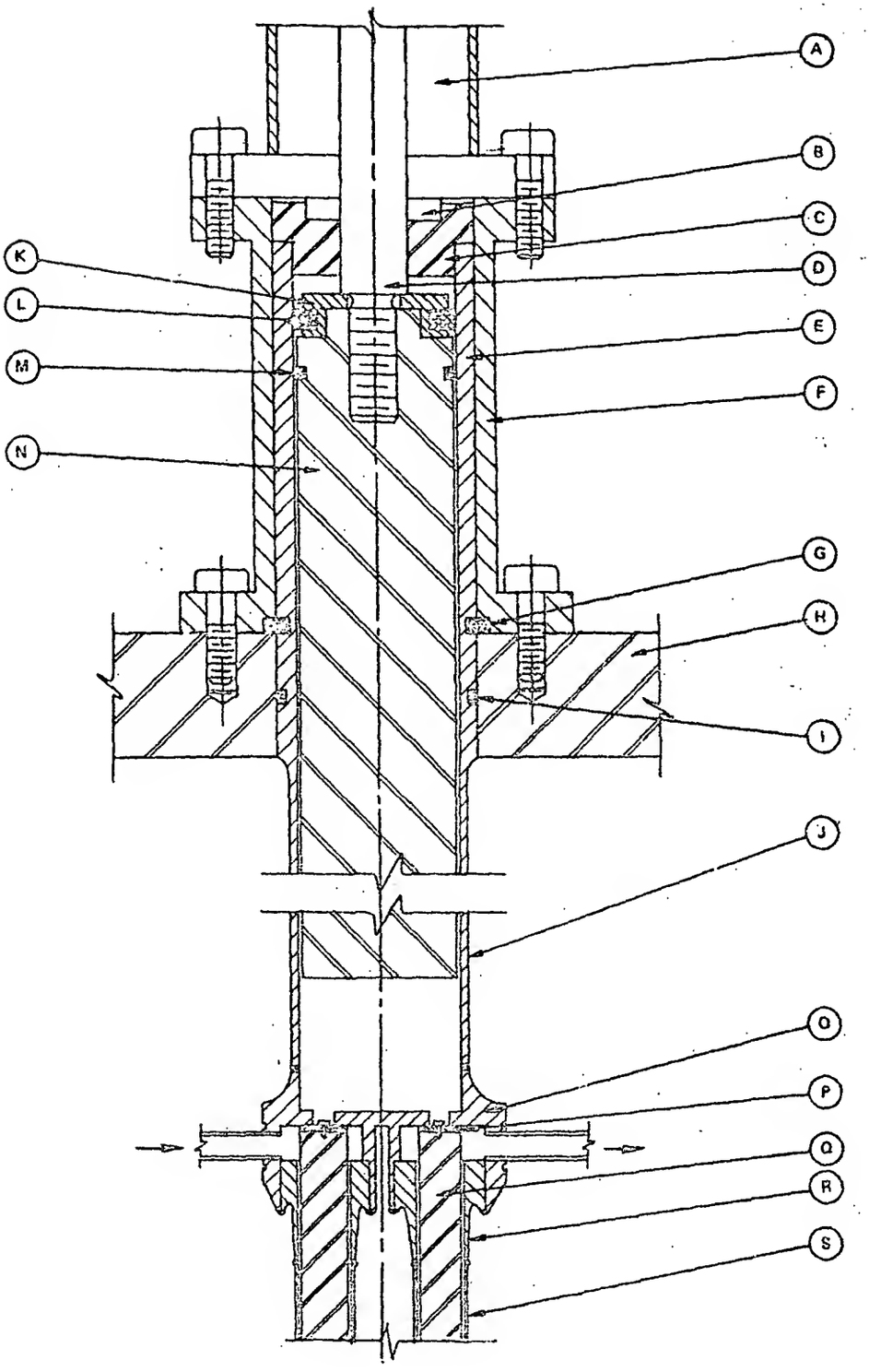

Figure 1. Cross section of expansion engine

Recent advances, especially in heat transfer analysis and experimentation have enhanced our understanding of the losses associated with the expander, and analytical models of varying sophistication and adequacy are now available for the losses[1-3]. This has made it possible to design an efficient reciprocating expander. However, noise vibration and size considerations of the work-absorbing assembly associated with the conventional reciprocating expanders still limit the practicality of scaling down these units. This paper describes an experimental reciprocating expander[4] which has been designed for high efficiency and uses a hydraulic-pneumatic drive mechanism and a pneumatic valve actuator in place of the flywheel, brake motor, mechanical cam-actuator assembly used in conventional large capacity liquefiers. The device can therefore be scaled down for cryocooler applications.

2. Description of expander

The reciprocating expansion engine, Fig. 1, consists of a long displacer closely fitted inside a long cylinder which hangs from a base plate, which is the top plate of a vacuum chamber. Above the base plate is an adjustable hydraulic-pneumatic system for piston motion and valve control. The valves for the engine extend down from the cylinder head. Surge chambers are located at the inlet and exhaust of the expansion engine to convert the pulsatile flow to a relatively smooth and continuous flow. Detailed description of these components follow.

The cylinder is made of 304 stainless steel because of its high strength to thermal conductivity ratio, low specific heat capacity and lack of brittleness at low temperatures. The thin wall of the cylinder coupled with low thermal conductivity of the material minimizes the conduction loss. Stiffening rings spaced 1.5 in apart around the outside diameter keep the tubing round. The thin wall tubing is TIG welded to the valve block (cylinder head containing the valve ports) at one end and a thick wall tube at the warm end used for mounting the engine. A solid phenolic micarta rod is used for the displacer because of its good wear characteristics. Also the thermal contraction characteristics closely match those of the stainless steel. The diametral clearance between the piston and cylinder is 0.006 in and is chosen by consideration of the shuttle heat transfer loss, the possibility of seizure due to small solid impurities and the possibility of displacer-cylinder contact.

The engine uses a single buna O-ring seal M at the warm end of the displacer-cylinder assembly. An oily felt washer L provides continuous lubrication for the O-ring. Thus there is minimal wear which reduces the possibility of wear material contamination. Also the small frictional heat generated is dumped into the atmosphere and does not detract from the cooling power of the engine.

Since the radial clearance on the 33-in-long displacer N is 0.003 in, only a small misalignment will cause the displacer-cylinder assembly to bind. The vertical alignment of the engine avoids gravity side loads and associated rubbing. The displacer is rigidly threaded to the piston rod D of a tandem cylinder assembly A. The tandem cylinder has four rod seals and two piston seals. Therefore the integral unit consisting of the tandem piston rod and the engine displacer ride on a total of seven supports of close tolerances. By proper initial positioning, the unit can be maintained reasonably well aligned in the vertical. The axes of the engine cylinder and the tandem cylinder are aligned by piece C, which fits inside the engine cylinder E and outside the bushing B at the end of the tandem cylinder. The cylinder is rigidly supported at the warm end on top plate H and extends into the vacuum chamber. The warm end of the cylinder E is attached to the plate by a split ring, groove and clamp flange, G and F.

Since throttling in the valves degrades the performance, the valve ports are located in the cylinder head to allow for reasonably large ports with minimum throttling. This port location also helps to reduce the clearance volume. The ports are 1/4-in holes drilled through the valve block/cylinder head O which is TIG welded to the cylinder J. Tubular valve sheaths S of 304 stainless steel are also welded to the valve block and extend from the bottom of the engine. These tubular sheaths enclose the valve pull-rods Q. The valve face, P, is a teflon disk mounted on the cold end of the phenolic micarta pull-rod with a screw and locked in place with a belleville washer. The valve is held closed by the spring in the miniature air cylinder which actuates the valve. A buna O-ring serves as the warm end seal on the valve rod which fits closely in the sheath. Because of the rather short travel of the pull-rods, no lubricant reservoir is provided for the O-ring. The pull rod is adequately guided by the sheath since the clearance in the sheath is only 0.003 in.

3. Hydraulic-pneumatic piston-motion control system

The overall layout for the control system is shown in Fig. 2. Air limit switches send position signals to the air controller. The controller sends direction and speed signals to the control valves to control piston direction and speed. The hydraulic controller absorbs the expander work, and sets three different speeds during the exhaust stroke, the intake stroke and the expansion stroke. The expander work is dissipated in flow control valves in the hydraulic circuit.

The principal components of the hydraulic controller are three adjustable flow control valves G1, G2, G3 and a three-way hydraulic valve H (Fig. 2). The three-way valve is a two-position, single-air-piloted, spring-return valve. The oil flow through this valve is through valve G3 when there is air pressure at the pilot, or through line G4 when there is no air pressure. The adjustable flow control valve is a throttle and check valve combination which allows throttled flow in one direction and full flow in the other. Valves G2 and G3 restrict flow during the power stroke, while valve G1 restricts flow during the exhaust stroke. Therefore the setting on valve G1 determines the engine speed during the exhaust stroke. Valve G3 is by-passed during this stroke. During the intake stroke, air pressure at the three-way valve H switches the oil flow to valve G3 which meters the flow together with valve G2. The valve settings on these two valves therefore determine the piston speed during the intake process. At cut off, air pressure is released on the three-way valve and the spring returns the oil flow to line G4. Valve G2 is now by-passed. There is full flow in valve G1 and metered flow in valve G2 which sets the piston speed during the expansion process. A bleed line L is provided for the hydraulic circuit. Also an air-pressurized oil reservoir is provided to maintain the oil under pressure and eliminate air leaks into the hydraulic circuit. With air in the oil the piston velocity cannot be controlled.

The heart of the air limit switch system is a miniature double-plunger two-position fully ported four-way spool valve F, Fig. 2. The valve is supported by threaded rods attached to the tandem-cylinder assembly. A yoke, BB, F1, and F2 is attached to the free end of the piston rod. At maximum volume, surface F1 actuates the plunger and at minimum volume surface F2 actuates the plunger of the spool valve. The stroke of the machine is adjusted by adjusting the vertical position of the four-way valve and the distance between F1 and F2. Threaded rods and nuts facilitate these adjustments.

The cut-off switch E sends a position signal to the pneumatic control at the end of the intake process. Switch E is a heavy duty miniature air limit switch. It is a two-position, plunger-actuated normally-closed valve. A cam, E1, attached to the piston rod actuates the cut-off switch. The output signal from switch E1 is used to actuate the expander inlet valve and the three-way hydraulic valve in the hydraulic controller. The cut-off switch is attached to the tandem cylinder with threaded rods for position adjustment. The expander cut-off point is adjusted by changing the position of this switch.

The two principal components of the pneumatic controller are a directional valve C and a NOT element B, which is described in the next paragraph. The directional valve is a heavy-duty, two-position, double-air-piloted, fully-ported, four-way spool valve. The pilot signals to operate the valve are supplied by the limit switches. The four way directional valve switches pressure and exhaust to the double acting pneumatic cylinder, thus providing pneumatic power for both the up (expansion) and down (exhaust) strokes. Thus the pneumatic driver can drive the piston even when no helium is being processed by the expander. This feature allows a later adaptation of the expander as a compressor.

The purpose of the NOT element is to provide the signals to open the engine inlet valve only at the end of the exhaust stroke, after the exhaust valve has been closed and to close the inlet valve at the cut-off point of the power stroke. The two input signals to this element are a signal from the cut-off switch to input port 1 and another signal from the end-of-stroke limit switch F to input port 2. The output of the NOT element is pressure at port 3 if there is pressure at input 1 and if there is no pressure at input 2. During the intake stroke the switch E is depressed sending pressure to port 1 of the not element B. There is no pressure at port 2 of B so pressure at 1 passes to 3. This pressure holds the inlet valve open and switches valve H causing hydraulic valve G3 to be active. At cut off, E switches which exhausts the pressure at 1. With no pressure at 1, the NOT element switches which exhausts the pressure at 3, closes the inlet valve, and allows valve H to spring return. At the end of the expansion stroke, valve F switches sending no pressure to E and pressure to port 2 which also opens the the discharge valve. Switch E has no pressure and no influence as it is depressed during the discharge stroke. At the end of the discharge stroke valve, F switches pressure through E to port 1. Only after the pressure in the discharge valve actuator has dropped, does the NOT element B see no pressure at 2 and switch pressure from 1 to 3 which the opens the inlet valve.

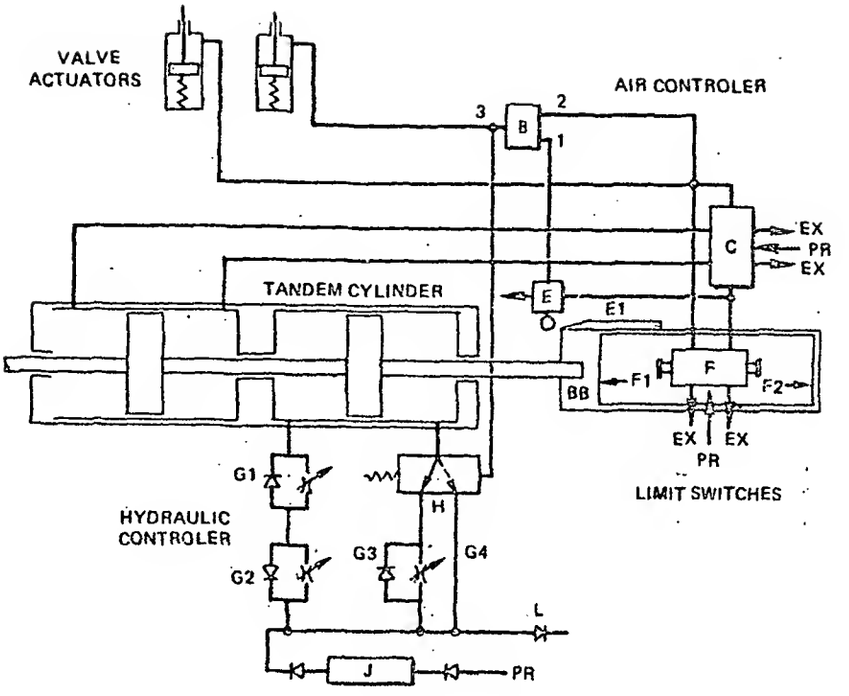

Figure 2. Hydraulic-pneumatic control system

4. Debugging the pneumatic circuit

The hydraulic and pneumatic system was assembled from standard catalogue item components. Since these were not optimum components and their internal design and port sizes were not readily available, an experimental rather than an analytical approach was used to tune and adjust the system. The pneumatic circuit was instrumented with several pressure transducers. The engine was instrumented for cylinder pressure and piston position. Data from these instruments were observed and recorded with a digital oscilloscope and subsequently transferred to a VAX computer for analysis. This data was sufficient to tune the system for satisfactory operation. Typical curves showing the phase relationships are shown in Fig. 3.

5. Time sequence in the expander

Fig. 3 shows piston position, inlet valve actuator pressure, exhaust actuator pressure, and expander cylinder pressure on the same time base for a typical cycle. Starting at TDC (minimum volume) with the inlet pressurized (open) and the exhaust closed (depressurized), the piston moves up at low velocity until the cutoff point (CO) is reached. The inlet valve closes and the hydraulic three-way valve switches to a low flow resistance (G4 of Fig. 2). The cylinder pressure falls rapidly and the piston velocity increases. When the piston reaches BDC (maximum volume) the exhaust pressurizes (opens) and the piston reverses direction. The piston moves rapidly to TDC (minimum volume). Subsequently the piston switches direction, the exhaust depressurizes (closes), and the three-way hydraulic valve switches to high flow resistance G3. The inlet then pressurizes (opens), to repeat the cycle. The cut off switch resets on the exhaust stroke, but has no action since it has no pressure supply.

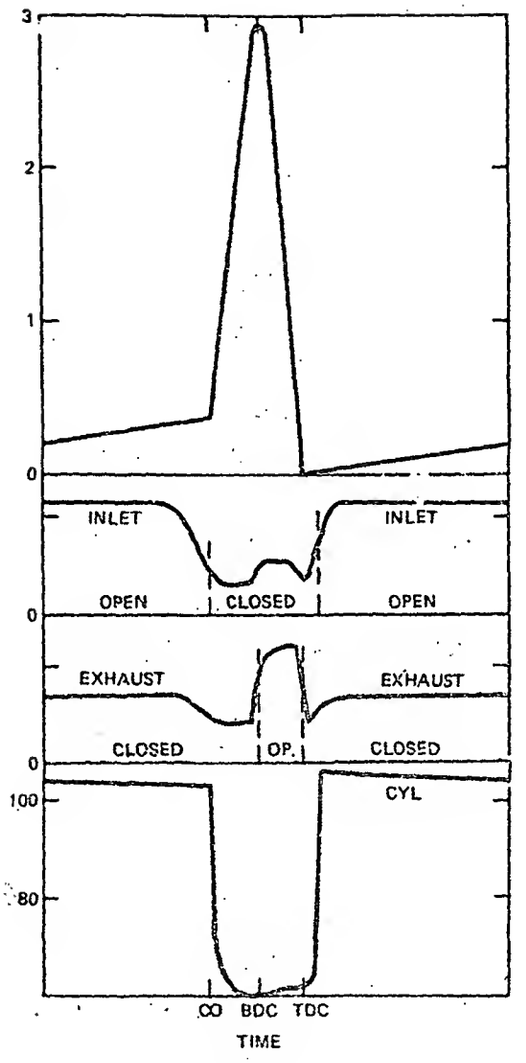

Figure 3. Expander cycle

Fig. 3 also shows that the times required to pressurize and depressurize the valve actuators are significant. The inlet valve actuator takes about 0.14 s to 0.16 s to pressurize up to full pressure (80 psig). However it takes about 0.06 to 0.085 s to reach the level high enough to switch the valve. On the other hand, depressurization takes about 0.20 to 0.24 s. Again the valve closes after about 0.16 s. Similarly, pressurization of the exhaust valve actuator takes between 0.10 and 0.12 s and depressurization about 0.14 s. The quicker response of the exhaust actuator results from its being connected directly to the limit switch whereas the inlet actuator is connected to the limit switch through a NOT element with a smaller port size than the air limit switch (Fig. 2). There is always a residual pressure at one of the actuators whenever there is pressure in the other. The residual pressure is about 6 psig for the inlet valve actuator and 12 psig at the exhaust valve actuator. There is no pressure in either actuator only during the expansion process (and also briefly at the end of the exhaust stroke before the inlet valve opens). There is also evidence of pressure signals propagating between components through the air pressure source because of the source impedance.

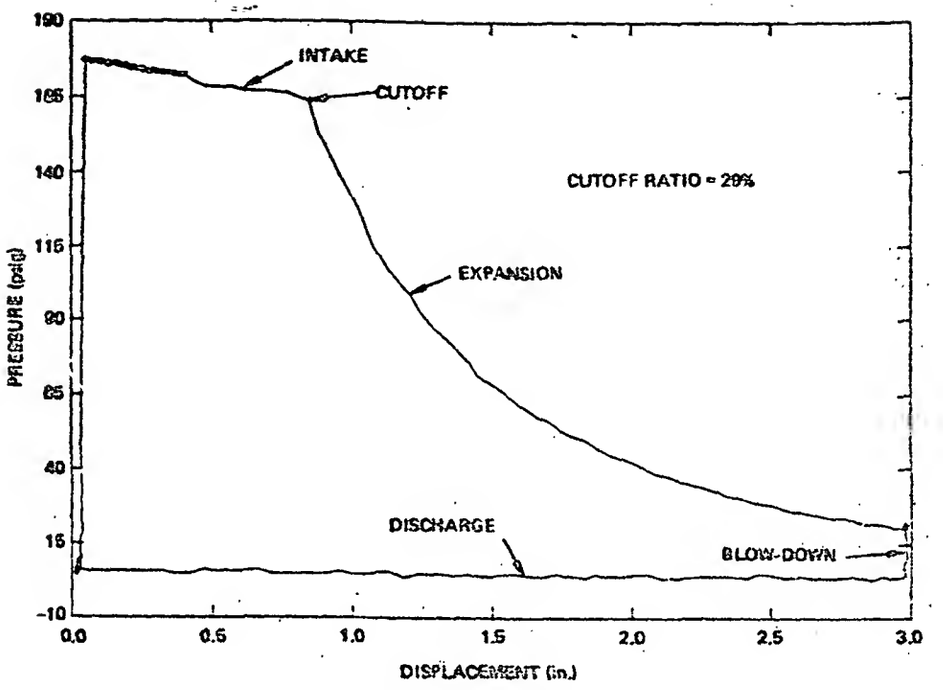

Figure 4. Pressure-displacement diagram for single-phase operation

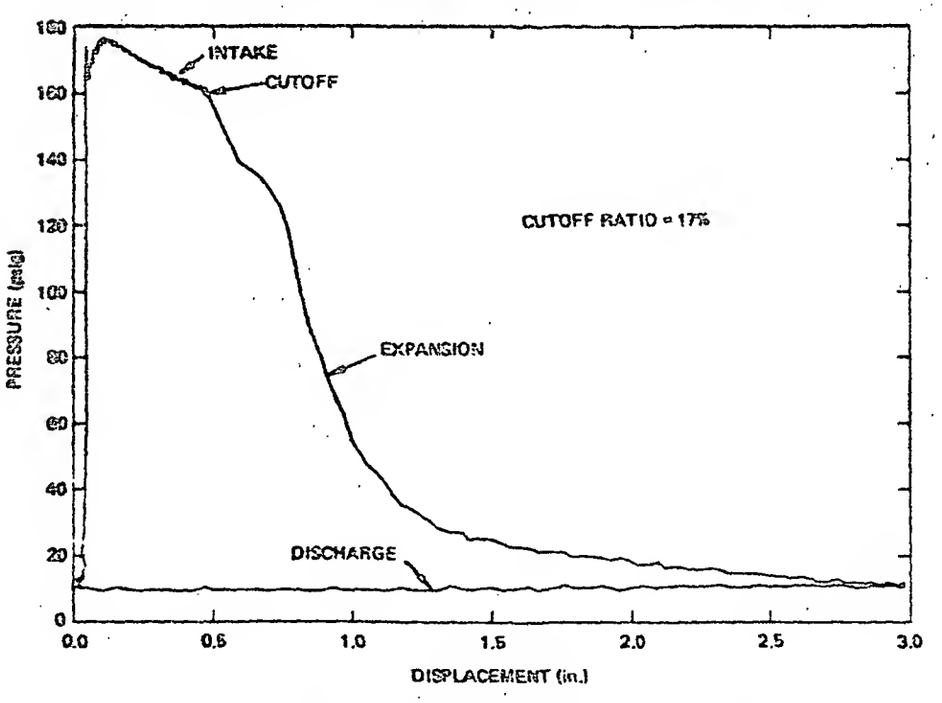

Figure 5. Pressure-displacement diagram for single-phase operation

6. Expander diagrams

Figures 4, 5, and 6 show typical pressure-displacement diagrams for the expander. The diagrams show a significant drop in pressure during the intake process. A surge chamber of approximately ten times the expander displacement was provided at the inlet and the piston speed during intake was kept minimal. The cause of the pressure drop in spite of these precautions is the high flow resistance in the J-T stage of the Model 1400 liquefier that supplied the inlet gas. A fairly constant inlet pressure was obtained in Fig. 4 for operation in the single phase region with a slow intake process. Table I summarizes time and speed distribution for a typical cycle.

Table 1. Typical time distribution for expander cycle

process	piston speed (in/s)	time (s)
intake	0.21	1.87
expansion	9.14	0.28
exhaust	7.76	0.38
dwell at TDC	-	0.10
dwell at BDC	-	0.04
	total	2.76

The cycle of Fig. 4 has a blow down loss, while, in contrast, the cycle in Fig. 5 shows complete expansion. It was possible to adjust the cut-off point to ensure negligible blow down loss at the expense of expander capacity. The two cycles just described in Figs. 4 and 5 were obtained for single phase operation of the expander. The cut-off ratio is about 20%, which is defined as cylinder volume at the closing of the inlet valve divided by the maximum cylinder volume at the end of the stroke. The diagram of Fig. 6 was obtained for a comparable cut-off ratio and for operation in a two-phase expander mode. The diagram indicates an overexpansion followed by a small recompression.

7. Evaluation of engine performance

The reciprocating expander was tested as a supercritical wet expander and as a single phase expander using a CTI model 1400 liquefier to supply gas at about 13 atm in the temperature range of 4.2 to 12 K. The efficiency of the wet expander is defined with reference to Fig. 7 as

$$\text{efficiency} = W_{act} / W_{rev} \qquad (1)$$

where

$$\text{actual work} = W_{act} = m(h_1 - h_3) + Q_{act}$$

$$\text{reversible work} = W_{rev} = m(h_1 - h_3) + Q_{rev}$$

$$\text{mass flow rate} = m$$

$$\text{actual refrigeration} = Q_{act}$$

$$\text{reversible heat input} = Q_{rev} = m\, T_{sat}(s_3 - s_1)$$

$$\text{inlet enthalpy} = h_1$$

$$\text{saturated vapor enthalpy} = h_3$$

The actual work is also given by the difference between the indicated work and the heat leak. This gives an alternative method for evaluating the efficiency. The measurements required to evaluate the performance are therefore: 1. The state (temperature and pressure) of the working fluid at the inlet and at the exhaust. 2. The actual refrigeration effect. 3. The indicated work from a P-V trace. 4. Heat leak by static conduction 5. Heat leak due to piston motion.

The experimental setup for obtaining these measurements is shown in Fig. 8. The states of the helium were measured in the inlet and in the heater tanks. The pressure was measured with a Bourdon pressure gage connected with capillary tubing. The temperature was measured using helium vapor pressure thermometers.

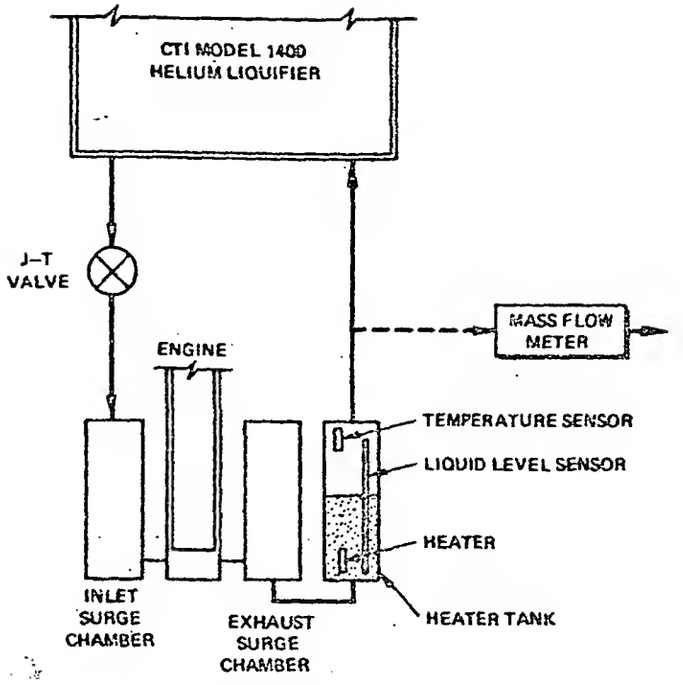

Figure 8. Expander test setup

Actual refrigeration capacity was measured as the power to the heating element. The heater power supplied was adjusted to be just sufficient to evaporate the liquid resulting from the expansion process so that the leaving stream was saturated vapor. The helium vapor pressure thermometer was provided to monitor that the gas was not overheated. It was also found necessary to use a liquid level gauge to maintain a steady liquid level in the heater tank.

The indicated Work was calculated from measurements of the pressure inside the expander working space and the piston position. The pressure was measured using a high-impedance piezoelectric miniature pressure transducer operating at expander temperature. The charge output of the sensing element, a quartz crystal, was fed to a signal conditioning module and converted into a proportional voltage signal. The transducer was threaded into a mounting adaptor which was connected to the cylinder through a short capillary tube.

The static heat leak to the expander was measured with the engine valves propped open. The expander and the peripheral apparatus were then cooled down to the operating temperature by operating the liquefier on the J-T valve. The two-phase flow from the J-T valve was gradually reduced until a small temperature rise was detected across the expander. The temperatures were recorded from vapor pressure thermometers. To measure the mass flow rate, the cold return gas from the engine was warmed up external to the liquefier and then passed through a calibrated mass flow transducer.

Piston motion heat transfer loss was measured with the setup shown schematically in Fig. 8. The engine was first cooled down to the operating temperature. Both valves were propped open and the refrigeration capacity of the liquefier operating with the J-T valve was determined by measurement of heater power required to achieve saturated vapor at the heater tank discharge. With the valves still propped open, the piston was shuttled by means of the piston motion control system. Because of the heat loss through this piston motion, the heater supply power to boil away the liquid (indicating the refrigeration capacity) was reduced. The difference between the two measured capacities gave the loss due to the piston motion.

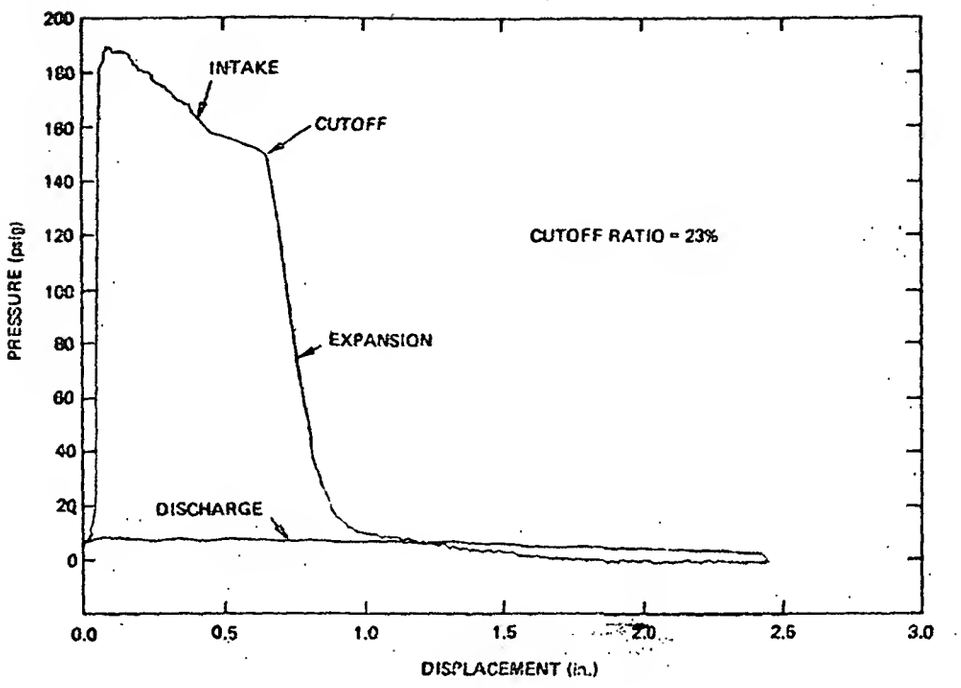

Figure 6. Pressure-displacement diagram for two-phase operation

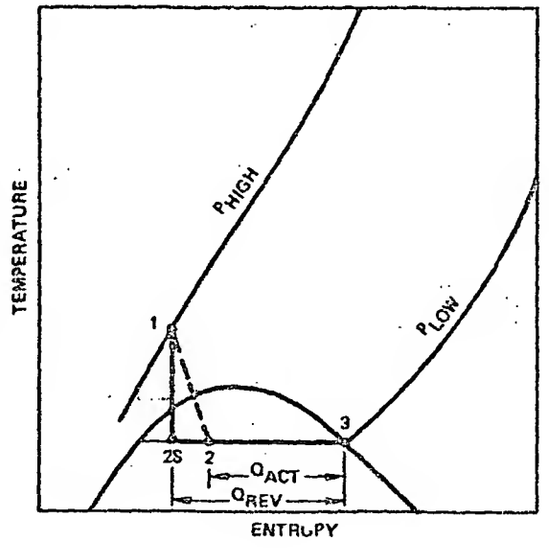

Figure 7. T-S diagram for two-phase expander

8. Results

Typical state point measurements are summarized in Table II. For the data of the Table, the single phase expander efficiency is 93 percent. For other tests the single phase expander efficiency ranged between 91 and and 93 percent.

Table 2. Expander performance data

	single phase operation	two phase operation
Inlet pressure (atm)	13.21	13.24
Inlet temperature (K)	11.51	6.55
exhaust pressure (atm)	1.2	1.2
exhaust temperature (K)	4.72	4.42

The performance of the expander operating in the two-phase region was evaluated. Typical data are:

Refrigeration effect = Q_{act} = 33.4 W

Mass flow rate = m = 2.18 g/s
(from displacement and inlet state)

Reversible work = W_{rev} = 21.8 W

Actual work = W_{act} = 20.4 W

Expander efficiency = 94%

The wet expander efficiency was also calculated from the indicated work and the measured heat leak losses. Typical data are:

Indicated work = W_{ind} = 21.4 W

Piston motion loss = 1.3 W

Static heat conduction loss = 1.6 W

Actual work = W_{act} = 18.5 W

Expander efficiency = 84.5%

The two methods always gave values which differed by less than 10 percent. A major source of inaccuracy in the result is calculating the mass flow rate from the expander inlet temperature

9. Conclusion

The hydraulic-pneumatic mechanism for piston motion and valve control enabled fairly good control over the cycle events in the expansion engine. The high efficiencies measured demonstrate the potential for scaling down reciprocating expanders for cryocooler applications.

The expander was run only long enough to obtain performance data. No endurance data was taken because the system was assembled from inexpensive catalogue items which were not designed for long life. Most of the experimental difficulties were the result of the compromises required to use standard items for the hydraulic-pneumatic control system.

The research plan is to modify the apparatus for testing as a vapor compressor operating at 4.2 K. This test will require modification of the connections to the helium liquefier and a modification of the valve control sequence. These modifications are rather simple since the apparatus was designed for the compressor tests. If the compressor tests are as successful as the expander tests, the plan is to demonstrate the full potential of the saturated vapor helium liquefaction cycle. This will require the design an expander and compressor module to match the model 1400 liquefier, and the replacement of the J-T heat exchanger in the liquefier.

10. References

[1] Rios, P. A., An approximate Solution to the Shuttle Heat Transfer Losses in a Reciprocating Machine, Journal of Engineering for Power, (April 1971).

[2] Radebaugh, R. and Zimmerman, J. E., Shuttle Heat Transfer in Plastic Displacers at Low Speeds, NBS Special Publication 508.

[3] Lee, K., Smith, J. L. Jr., and Faulkner, H. B., Performance Loss due to Transient Heat Transfer in the Cylinders of Stirling Engines, 15th Intersociety Energy Conversion Engineering Conference Proceedings, Vol 2, (1980).

[4] Hinte, H., Analytical and Experimental Studies of a Helium Liquefaction Cycle, ScD Thesis, Department of Mechanical Engineering, MIT, (Feb. 1984).

D14

EXPERIMENTS WITH A FULLY INSTRUMENTED SPLIT STIRLING CRYOCOOLER

Alain FAURE, Serge REALE, Philippe BERNHEIN

L'Air Liquide
Advanced Technology Division
Sassenage 38360 FRANCE

A development program is being undertaken by L'Air Liquide in order to establish a practical model that can be used to accurately size and optimise split stirling cryocoolers.

For any given application the performance of this type of refrigerator must be carefully optimised and,in addition,the specifications for one application may very greatly from those needed for another (eg. operating temperature, cold power, cold finger volume, size and dead volume in the interconnecting line etc...). The final optimised design for any particular application requires time consuming and expensive testing as no system exists for precisely calculating the design from the operating parameters.

It was necessary to develop a practical model that could be used to extrapolate existing designs to meet different specifications. However in order to do this detailed knowledge of the dynamic operating parameters of this type of cryocooler was required.

The first stage of the program has been to fully instrument a refrigerator so that various dynamic parameters could be measured.

The second stage of the program will involve the application of these measurements to the design and optimisation of a range of coolers.

Key words : cryogenic refrigerator, cryocoolers split stirling coolers, refrigeration cycle calculation model, displacer, regenerator, pneumatic displacer drive.

1 - Introduction

L'Air Liquide has been developing and producing miniature cryocoolers for the last ten years. Most of this work has been aimed at products mainly intended for military applications.

In addition to the range of open cycle coolers and flash coolers (ambient to 80 K in about one second), there is an increasing demand for coolers which can operate virtually continuously, and it was to meet this demand that L'Air Liquide undertook the development of split stirling cryocoolers.

As s result of this work an optimised split stirling cryocooler has beon designed and built . This machine is shown figure.1.

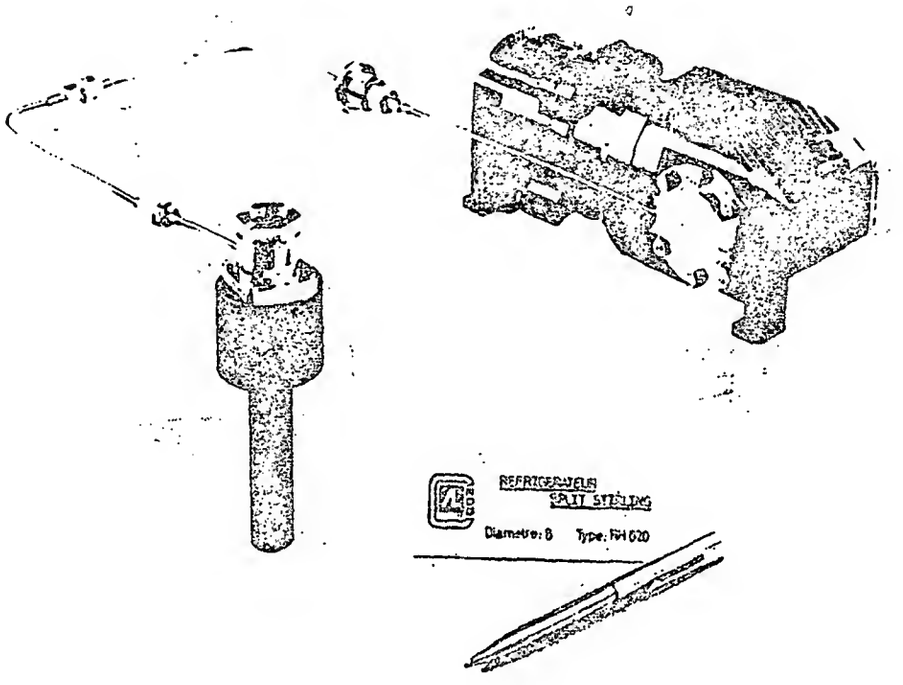

A major development progrem was necessary in order to optimise :
- the reliability of the cooler and
- the efficiency of the refrigeration cycle.

In order to improve relisbility, considerable effort has been devoted to the development and selection of technologies to minimise
- leake
- wear due to friction
- pollution caused by the compressor lubricents.

The estimeted without maintenance operating time, has been progressively increased from 500 h to 2000 h (ectual test results range from 3000 h to 6000 h).

In parallel, the efficiency of the refrigeration cycle hae been optimised for given and fixed values of various system perametere. These parameters include :
- thermal maee to be cooled,
- physical size of the dewer,
- thermal loeses in the dewer and
- distance between the dewar and the compressor

Some of the resulting operating characteristics are shown figure 2.

It is evident that for other applications these parameters, and to some extent the specifications (environment temperatures, cooldown time...), may vary significantly. Considerable effort would be required to extrapolate and optimise the existing design for other applications. Consequently a new development program was undertaken, concentrating on the development of a design model which would permit a range of cryocoolers to be optimised to meet specific requirements.

Figure 2. L'AL RH 820 split stirling cryocooler caracteristics

Nominal data	
base temperature	76 K (-197°C)
operating temperature range	- 40 °C + 70°C
cooling capacity at 76 K	150 - 1000 mW at 20 °C 150 - 800 mW at 70 °C
Cooldown time	4 min
power supply	20 - 30 V dc
power absorbed	60 W at maximum cooling capacity 25 W with a 200 mW heat load.
system relisbility	2000 operational hours (without any maintenance or gas purging)

2 - Initial design criteria

2.1. Method selection

Various starting points were considered, as there already exist different theoritical and practical operating models for the Split Stirling cycle. Such models vary from the extremely simple where, for instance the cycle is assumed to be isothermal, to the vastly complex, where each part of the cycle is modeled in detail.

The first type of model is not sufficiently accurate to optimise a practical machine and the second requiree the use of complex calculations and calculating methods, access to which is not always easily available.

Moreover, in order to verify any of the existing models it is necessary to compare the peformance they forecast with the performance and results obtained from real machine, specifically in the case of the split stirling cycle, where the phase shift between pressure and displacement of the piston, and consequently the performance, depend greatly on technological problems (friction, leaks etc...).The corresponding parameters can only be determined by experiment.

In order to do this one must have a system which can be used to measure all the relevant cycle parameters during the operation. Two experimental sproaches can be considered

- either build specific test facilities and measure the different parameters (pressure drop, leaks, friction loads, efficiency) under static conditions.
- or equip a real machine with different instruments and use it to measure the same or equivalent parameters under actual working conditions i.e. under variable cyclic pressure, temperature, volume etc...

The first method is the simplest way to handle the measurement problems.

However, it requires the construction of several specific test assemblies and the extrapolation of experimental results to actual cryocooler performance needs elaborate calculation. It will also include approximations resulting from discrepancies between test conditions and operating conditions. This method seems well adapted to the development of a rather multi-purpose model for the prediction of performance for a wide range of machines.

The second method, i.e. measurement of internal parameters on an operating machine, presents technological difficulties due to the small size of the cryocooler subassemblies and to the high rate of change of the parameters concerned. Provided the associated problems can be solved, this method enables the definition of a rather simpler model which is well adapted to the sizing of similar machines.

In view of our specific requirements, this second method has been selected. Our efforts were concentrated on the selection and development of the measurement methods and the measuring equipment.

2.2. Operating procedure

Generely speeking the starting point for cryocooler sizing is the power requirement at the end of the cold finger. This nett cooling power results from the difference between.

- the cold power generated during each cycle by the gas expansion or $\int PdV$ where P is the pressure at the cold tip and dV the variation of the cold volume and
- the thermal losses (heat conduction, shuttle losses...).

PV diagram recording and simultaneous measurement of the nett cooling power enable approximation of the total losses and the verification of the corresponding values calculated from the model.

In the same way, instantaneous measurements of pressure, temperature and volume at both, cold and warm ends of the cold finger can be used to calculate regenerator efficiency, pressure drop, etc...and to establish the correlation between the thermodynamic gas cycles at both ends of the finger.

Identical measurements in the compressor cylinder(s), the compressor crank case and the pneumatic spring volume of the cold finger give information which can be used to determine the total pneumatic power absorbed by the gas and the different losses due to

- the gas leak from the compressor cylinder to the crankcase
- the gas leak in the pneumatic spring
- the pressure drop in the connecting line

A power balance in the compressor (friction losses, motor efficiency, power supply and electronic efficiency) gives the required electrical power.

In parallel the force balance in the pneumatic spring allows a comparison between the forecast and actual displacement of the piston to be made thus determining the sizing of pneumatic drive .

With this step by step method, based on the previous experimental optimisation of a particular cryocooler for specific operating conditions, cryocoolers can be designed for differents conditions corresponding to other specifications.

However, in order to do thie the following parameters must be meaeured and recorded :

- the pressure end the temperetura at both cold end werm ends of the cold finger
- the pressure in the compreseor cylinder(s), the pneumetic spring end the compreesor crankceee.
- the poeition of the regeneretor-displacer piston end of the compressor piston(e)
- the gas flow in the connecting line

Thie edds up to a totsl of 10 operating perameters.

3 - Experimentel errengement :

3.1 - Test bed :

A RH 800 cryocooler hes been used, which is the first development version of the present standerd RH 820 unit. The RH 800 has the following differences in comparison with the present machine

- single cylinder compressor (The R H 820 is a flat twin compressor to reduce vibration)
- No temperature control,(the RH 820 model is equipped with a cold end temperature controller to monitor rotationsl speed end thus cold power with respect to actuel dewar heat losses when operating over the required - - 40°C to 70°C temperature renge).

The rotationsl speed can be adjusted from 800 to 1500 RPM. Apart from rotationsl speed other operating parameters can be adjusted :

- the mean pressure (from 9 to 25 bar)
- the connecting rod diameter of the pneumatic displacer spring
- the cold end temperature

A heater in the test Dewar allowed the temperature to be set at the desired level.

3.2. Operating method :

The refrigerator was equipped with the measuring instruments mentioned above which had to be adapted to cope with the small size end to speciel operating requirements, such as

- no increase of dead volume (pressure)
- no increase in heat loss (temperature)
- no perturbation of dynemic balence (displacement)
- high frequency response (cycle can last 50 ms and less)
- small dimensions

3.2.1. Pressure measuremcnt :

The pressure sensor must meet the following requirements :

- minute eize (sensor diameter 1,5 mm)
- no dead volume (less than a few mm3)
- frequency response 10 kHz
- high offset : small pressure variations at a high mean pressure (in crank case end pneumatic spring)
- low temperature operation (down to 50 K at cold end)

The two last requiremente become increasingly difficult when the first ones are met (problems of the differential pressure, eensor output verietions due to large tempereture differences).

3.2.2. Temperature measurement :

Whilst wall temperature measurements at the warm end present no specific problems this is not the case for the gas temperature measurements, specifically in the cold expension volume. Thermal inertia requirements leads to the choice of resistance wire of 1 to 5 μm.

The compromise between power input and temperature resolution at cold end has been difficult to reach.

3.2.3. Displacement measurement

The small volume available, both on the cold finger and on the compressor, as well as the problem of not disturbing the equilibrium of the system, have limited the choice to optical and Eddy current sensors. Availibity problems with these measuring sensors have delayed the optical measurements.

The Eddy current sensors have been installed perpendicular to the axis of the piston movements and measure the displacement/distance by means of an inclined groove in the piston, which is machined betwsen the piston rings.

3.2.4. Flow measurement :

Though difficult, a hot wire flow meter was installed in a 1 mm diameter tube, allowing the flow measurements to be made.

3.2.5. Data recording

The rapidly changing parameters required the use of a high performance, real time data logger to achieve high resolution (better than 1 %) at a rate of more than 100 samples per cycle for 10 measurements, some of which are low level.

3.2.6. Power measurement

A calorimetric bench was developped to measure the power balance in the compresor module. The compressor module was immersed in a boiling Freon bath . The freon vapor from the bath was condensed and weighed in order to measure the heat input to the bath.

Comparison with electrical input and PV measurements in the compressor cylinder gives an estimate of

- motor inefficiency (joule losses, eddy current losses)
- friction losses
- non isentropic compression

4. - First experimental results

A considereble amount of development work was required due to problems encountered with these type of measurement.

Solutions have been found and several hundred sets of parameters have been tested, each set consisting of :

- mean pressure
- compressor motor revolution speed
- connecting rod diameter for displacer
- regenerator diameter in the displacer
- cold end temperature

Some exemples of the recorded data are shown in figure 3.

The diagrams 3a and 3b represent an optimal situation. The PV diagram is virtually rectangular. The displacer moves exactly at the maximum and minimum pressures.

The diagrams 3c and 3d represent a non-optimised situation

A shape coefficient has been defined in order to measure the level of optimization .

The variations of the shape coefficient as a function of the parameters listed above and the influence of the connecting rod diameter of the displacer in connection with the other perametars are shown in figure 4.

This figure emphesizes the importance of pneumetic driva sizing in order to have the proper phase shift and thus the maximum cold power.

In addition it illustrates the difficulty in optimising a cryocooler for a wide operating range. A cryocoler can be optimised for the highest frequency and the maximum pressure and hence have the proper phasing at maximum cold power output resulting in the shortest cool down time and, non-optimized performance under nominal conditions or vice versa.

For instance a cool down time of less than 2 minutes has been obtained with a particular design, at the cost of lower specific performance under steady state conditions.

5 - Conclusion

The first steps in experimental modelisation of the split stirling cycle have been made. Having solved the delicate measurement problems a large amount of experimental data has become available and now awaits processing. The experiments described above give a better insight into the cycle and a better understanding of the various parameters involved with the dimensioning of cryoloolers.

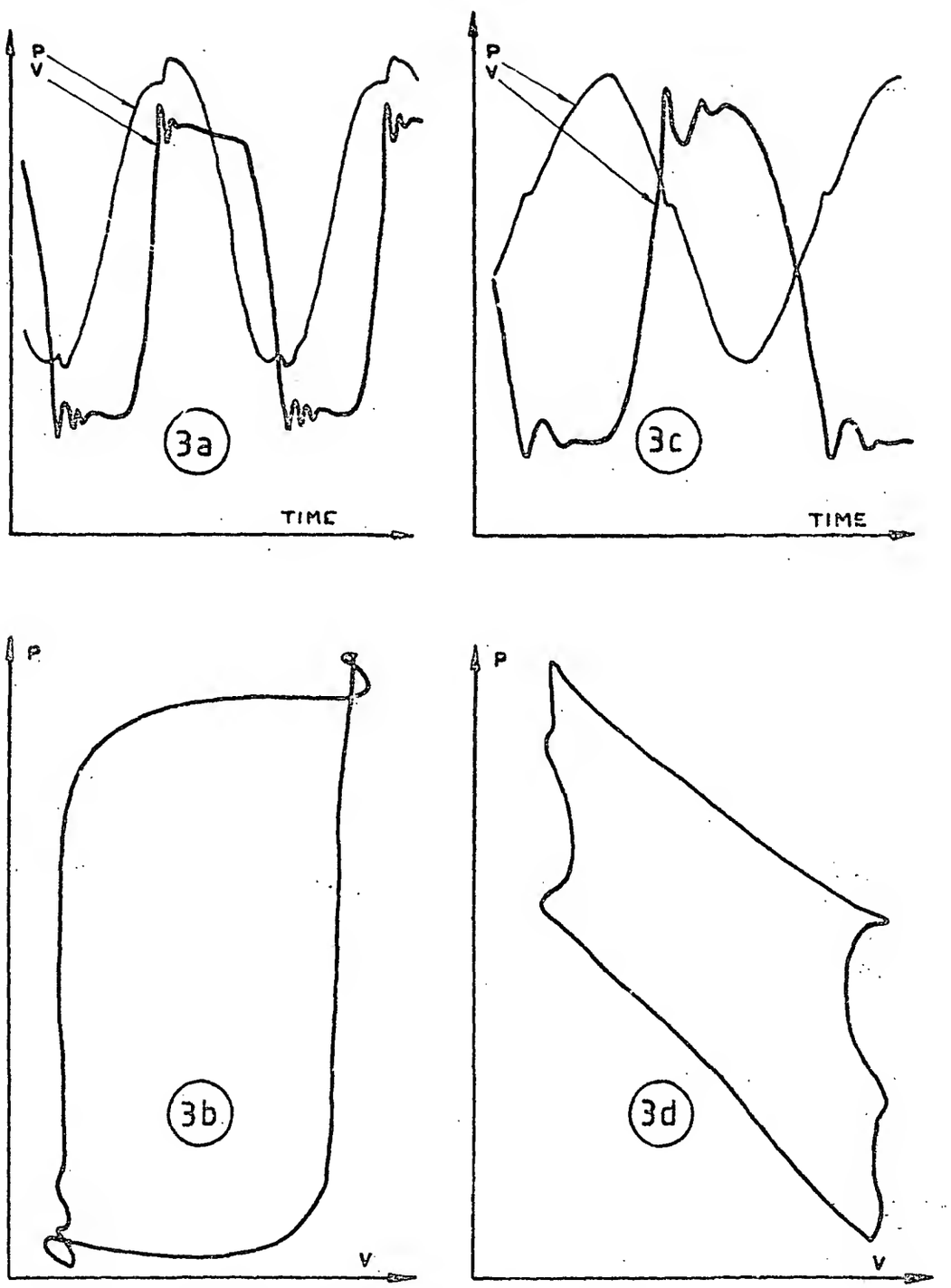

FIG.3 PV DIAGRAM AT THE COLD END

3a.3b OPTIMISED CONFIGURATION
3c.3d NON OPTIMISED CONFIGURATION

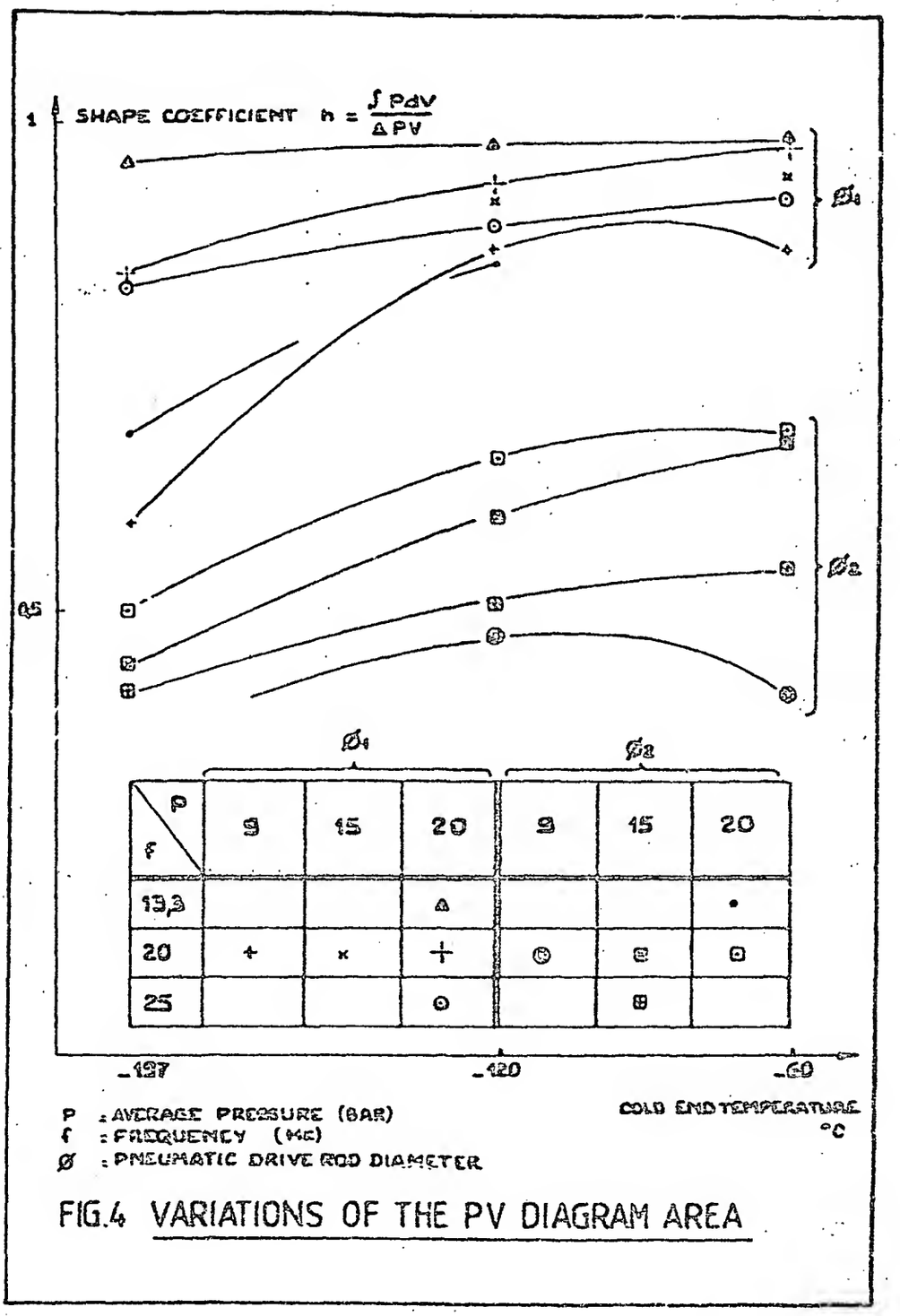

P / f	Ø1 9	Ø1 15	Ø1 20	Ø2 9	Ø2 15	Ø2 20
13,3			△			•
20	+	×	┼	⊛	⊜	⊙
25			⊙		⊞	

FIG.4 VARIATIONS OF THE PV DIAGRAM AREA

D15

LOW FREQUENCY SPLIT CYCLE CRYOCOOLER

S. X. Bian, Y. D. Zhang, W. W. Wan, L. Wang, and Q. C. Hu

Department of Power Machinery Engineering
Xian Jiaotong University
Xian, China

A split cycle Stirling cryocooler with two different drive motors and operating at a low drive frequency can have high thermodynamic efficiency. The temperature of the cold end of the cryocooler varies with drive frequency, voltage of the input electrical power and initial charge pressure values. The cryocooler operating at 8 Hz can provide 7 watts of refrigeration at 77 K for 230 watts of electrical input power.

Key Words: High efficiency; low power; Stirling cryocooler.

1. Introduction

Cryocoolers for infrared detectors must have high efficiency, small size and weight, low vibrational levels, high reliability, rapid cool-down and simple operation. If they are to be used in satellites, long unattended lifetime is also of great importance [1]. These requirements, generally speaking, can be satisfied by the Stirling cycle, and improvements in the operation of Stirling coolers have been reported in recent years [2]. In the case of direct crankshaft drive, it is not always possible to obtain ideal dynamic balance and the resulting vibrations may effect the performance of the infrared elements. For this reason, the split cycle was developed. However, the net refrigeration of the split cycle, either driven pneumatically or by a linear motor, is small. In order to get more refrigeration without sacrificing efficiency, we have tested a low frequency split cycle cryocooler which give 7 watts of refrigeration at 77 K for an input power of 230 watts.

2. Description

The prototype cryocooler consisted of two parts, a compressor unit and a displacer unit, which are connected by a small diameter tube 30 cm long. Figure 1 shows a sketch of the cryocooler. The compressor unit is a modified Stirling refrigerator driven by a small DC motor so that its speed can be easily controlled. The displacer unit is driven by a separate DC linear motor. The cold displacer is made of stainless steel. The case of the displacer is made of epoxy glass fibre in which a stainless steel net matrix is embedded. The phase angle between the compressor piston and the displacer is controlled by an electronic system. The consumption of power for the DC linear motor is less than 10 watts. Using two DC motors with respective voltage, control devices and the electronic system, it is possible to conveniently and individually control and adjust the speed of the compressor, the stroke of the displacer and the phase angle between the compressor piston and the displacer.

3. Results

It is well known that the performance of the cryocooler is dependent on the charge pressure, the speed of the motor, displacer stroke and compressor stroke, when the diameters of the compressor and displacer are given. Because the compressor and displacer are separated and driven by different DC motors, the speed of the compressor and the displacer stroke can be individually adjusted and controlled [3]. Hence there is an extra parameter - input voltage - added to the performance of the cryocooler [4].

3.1 Influence of Input Voltage to Linear Motor

During operation when the input voltage to the linear motor is varied, the stroke of the displacer is changed, and the performance of the cryocooler is varied. Figure 2 shows the variation in the performance of the cryocooler. As the input voltage increases, the stroke of the displacer increases rapidly. For input voltages greater than 18 V, the stroke is almost constant (curve Z). The temperature of the cold end is almost constant until the input voltage is over 27 V, when the temperature of the cold end slightly increases (curve $T_c - V_d$). The curve N_d shows variation of input power of the linear motor with V_d.

3.2 Influence of the Speed of the Cryocooler

It is well known that the performance of the cryocooler is dependent on speed for a constant charge pressure. Figure 3 shows the variation of the temperature of the cold end and of the stroke of the displacer with the speed of the cryocooler. The T_{min} of the cold end is obtained at a speed of 480 RPM. The stroke of the displacer also varies with speed. The curve illustrates that if the operation of the cryocooler deviates from optimum, the losses increase rapidly.

3.3 Influence of Charge Pressure

The cryocooler was operated with charge pressures ranging from 3.92 bar to 7.84 bar. Figure 4 shows that the temperature of the cold end varied with charge pressure which can be explained by the change in the stroke of the displacer as the charge pressure is varied.

3.4 Exergy Efficiency

This cryocooler has been tested at about 8 Hz. With the input voltage to the linear motor of 18 V and charge pressure is 7.84 bar, the minimum temperature of cold end is about 34 K. The cooling time from ambient temperature to T_{min} is about 20 minutes. The exergy efficiency of the cryocooler η_e is computed as follows [5]:

$$\eta_e = \frac{Q_c}{N_{tot}} \left(\frac{T_a}{T_c} - 1 \right), \tag{1}$$

where Q_c - - net refrigeration (W), T_a - - ambient temperature (K),
N_{tot} - - total consumed power (W), and T_c - - temperature of cold end (K).

It is rather satisfactory that a small cryocooler showed an exergy efficiency of 8.8%. Table 1 shows the exergy efficiency of different Stirling cycle cryocoolers.

Table 1. Exergy Efficiency of Different Stirling Cryocooler

Type	Refrigeration (Watt)	Consumed Power (Watt)	Exergy Efficiency (%)
Rhombic driven	0.3 (64 K - 70 K) 1.5 (135 K - 150 K)	30	3.68 - 3.26% 6.11 - 5.0%
Pneumatically driven	0.87 (73 K)	48	5.6%
Entirely electromagnetically driven[6]	0.5 (80 K)	30	4.6%
Prototype	7 (77 K)	230	8.8%

4. Conclusions

The prototype cryocooler showed that a single stage Stirling cooler with a two drive system and phase angle control can be operated with satisfactory results. It is possible to develop this drive system for larger systems and to minimize size and height.

5. Acknowledgment

The authors would like to thank Professor Z. Y. Zhang for his encouragement and advice.

6. References

[1] Leffel, C. S., and Wingate, C. A., "The stirling cycle cooler: approaching one year of maintenance-free life", Advances in Cryogenic Engineering, Vol. 23, 1977, p. 411.

[2] Horn, S. B., Lumpkin, M. E., and Walters, B. T., "Pneumatically driven split-cycle cryogenic refrigerator", Advances in Cryogenic Engineering, Vol. 19, 1973, p. 216.

[3] Polman, J., de Jonge, A. K., and Castelijns, A., "Free piston electrodynamic gas compressor", Proceeding of the 1980 Purdue Compressor Technology Conference", pp. 241-245.

[4] Pollak, Eytan, Soedel, W., Friedlaender, F. J., and Cohen, R. "Mathematical model of an electrodynamic oscillating refrigeration compressor", Proceedings of the 1980 Purdue Compressor Technology Conference", pp. 246-259.

[5] Bian, S. X., Gao, Y. Y., and Wan, W. W., "Small Cryocoolers", Book, written in Chinese, Machine-building Industry Press, Beijing, 1983, pp. 39-40.

[6] Davey, G., The Oxford University Miniature Cryogenic Refrigerator, University of Oxford, UK, 1983.

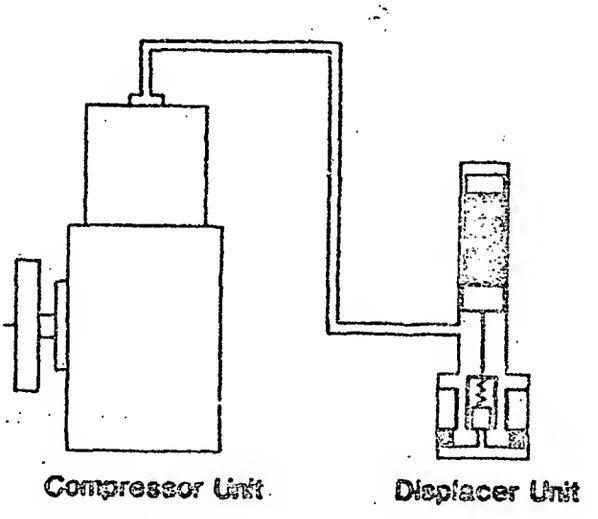

Figure 1. Sketch of the cryocooler.

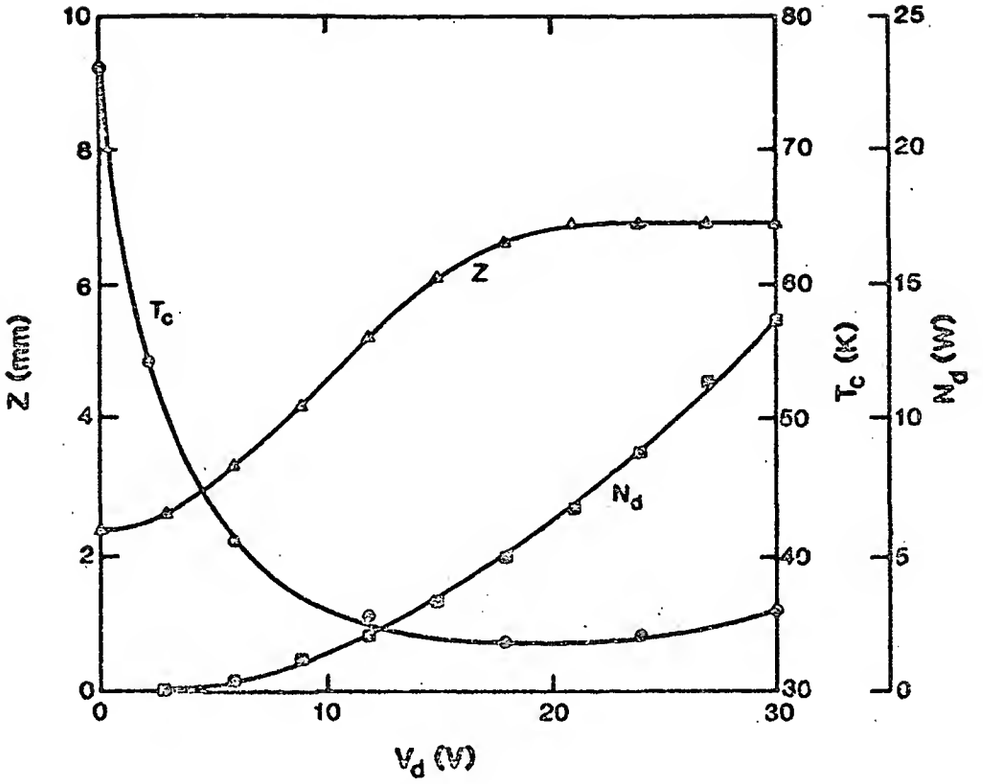

Figure 2. The performance of the crycooler as a function of voltage of linear motor (n = 420 rpm, p_{av} = 8 kg/cm^2).

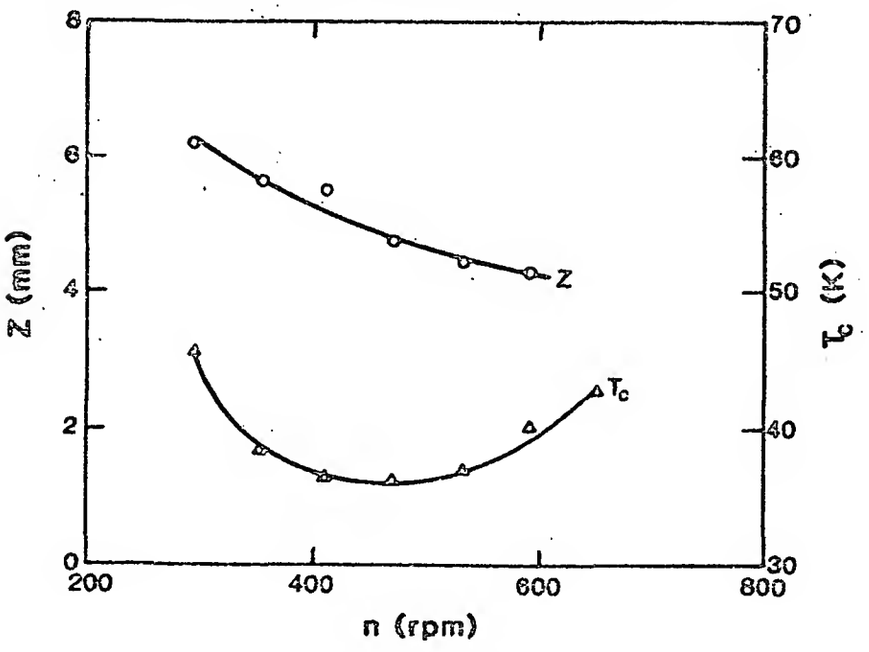

Figure 3. Temperature of the cold end T_c and stroke of the displacer Z as function of speed, (p_{av}= 8 kg/cm^2, V_d = 12 V).

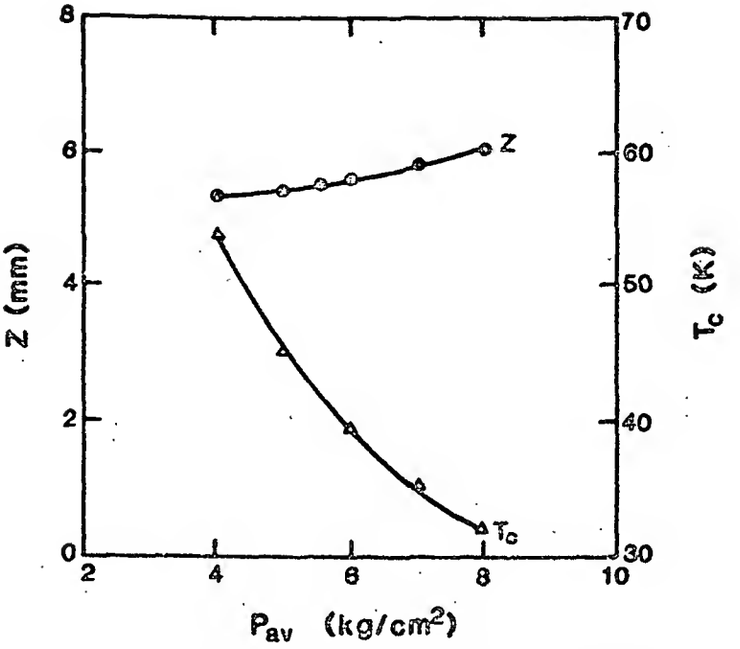

Figure 4. Temperature of the cold end T_c and stroke of the displacer Z as function of charge pressure p_{av} (n = 540 rpm, V_d = 27 V).

D16

PASSIVE MOTION CONTROL OF PNEUMATICALLY DRIVEN DISPLACERS IN CRYOGENIC COOLERS

N. Pundak; Ricor Ltd., En-Harod Ihud, Israel

and

S. Shtrikman, The Samuel Sebba Professor of Applied Physics
Department of Electronics
Weizmann Institute of Science
Rehovot, Israel

The split cryogenic cooler with a remote cold finger offers many advantages for use in cooling of infra-red systems. A pneumatic drive for the displacer in such coolers has since been adopted in many cryocooler designs. This concept can be significantly improved by causing the displacer to move sinusoidally rather than in an essentially square wave, as in most of the present models. The way this motion has been achieved passively is described in detail and its advantages outlined. Data of minicoolers using the above mentioned concept is presented.

Key Words: Cryocooler; displacer; eddy current; magnetic damper; phase delay; split Stirling; Stirling cycle.

1. Introduction

One of the major advantages of the Stirling type cooler is its simplicity - being a valveless system. The gross cooling power Q_c of thermodynamic cycles in general and the Stirling cycle in particular, can be expressed by the equation:

$$Q_c = \oint_T PdV < 0 \ . \qquad (1)$$

Note that negative Q_c means cooling. In steady state, both P and V are the periodical pressure and volume in the expansion chamber at a constant chamber temperature T. To a first approximation, both P and V very sinusoidally with time, and as shown directly from eq. (1), the volume change has to lag behind the pressure change to get cooling. For a given stroke and pressure pulse, the maximum gross cooling is obtained for a 90^0 phase delay of volume with respect to pressure. The optimal selection and the control of the phase angle between the pressure change and the expansion volume change has a great importance in determining the potential cooling power.

In the integral Stirling cooler the phase angle is maintained and kept constant by a crank mechanism. The Split Stirling version which gives significant advantage in some applications, for example to the electro-optic system designer, forces the designer to look for alternative solutions for the expansion volume cyclic change, and for the creation of the desired phase angle. A few mechanisms were developed and presented during the last decade; most of them are based on pneumatic drive of the expansion volume cyclic change and on a dry friction, viscous flow or electrical timing as a phase angle control mechanisms [1, 2, 3].

The major problem of the Split-type Stirling coolers is their relatively poor reliability. The primary factor affecting the reliability of this type of coolers is the dynamic seal wear in the compressor piston seal and the displacer seal of the expander unit. This statement is specially true in the case where the expander dynamic seal friction controls the motion of the displacer. Additional factors affecting reliability are solid or gaseous contaminants accumulated in the regenerator or around the displacer assembly, affecting its motion and degrading its efficiency. The "conventional" problems, such as external leaks, motor and bearing failure, can be considered a secondary mode of failure and are not part of this discussion.

2. Design Considerations

The basic approach of our new design concept is the elimination of the seal wear and contaminants modes of failure. The expander is based on a pneumatic drive. In order to allow high temperature vacuum baking, it is constructed of metal and of 3 Viton static O-rings only. The metal displacer has a screen type regenerator. The displacer and driving piston clearance type seals are constructed of metal (PH 5 - 15 Stainless Steel) and are located on the same plunger as shown in fig. 1. The all metal clearance type seals are characterized by their negligible wear rate and by their very low friction force.

The displacer motion phase delay control is governed by an independent passive mechanism located in the expander drive compartment. This mechanism consists of magnetic damper and helical suspension springs. By proper design of the damper mechanism, a near sinusoidal displacer motion - utilizing practically the full stroke available - with a prescribed phase delay relative to the pressure wave, can be achieved.

Assuming a sinusoidal pressure wave, the displacer driving force can be expressed by:

$$F_{drive} = A \Delta P \cos \omega t, \tag{2}$$

where A is the driving piston cross section area, ΔP = the difference between the maximum pressure and the mean pressure (equivalent to the pneumatic volume pressure) and ω is the angular frequency of the displacer. If the desired displacer motion is sinusoidal with, for example, a 90^0 phase delay to the pressure wave, it can be expressed by the following quotation:

$$X = Xo \sin \omega t, \tag{3}$$

where Xo symbolizes half the maximum stroke possible. The sum of the forces affecting the displacer motion (neglecting the low value of the dry friction created by the clearance type seal) can be expressed by the following differential equation:

$$F_{drive} + M\ddot{X} + C\dot{X} + KX = 0 , \tag{4a}$$

$$A\Delta P \cos \omega t + M\omega^2 Xo \sin \omega t + CXo\omega \cos \omega t + KX \sin \omega t = 0 , \tag{4b}$$

where C is the damping coefficient, M is the sum of all the expander moving masses and K is the spring coefficient. As is shown clearly in these equations, the necessary conditions for balance are:

$$A\Delta P = CXo\omega , \tag{5}$$

$$M \omega^2 = K. \tag{6}$$

Equation 5 shows that the peak damping force must be equal to the peak driving force and eq. (6) shows that the inertial forces must be balanced by the proper selection of the springs. In addition, the springs determine the average position of the displacer stroke, which is important in order to obtain symmetrical displacer motion around midstroke. It is important to emphasize that the damping forces used in these equations are the sum of the drag created by the viscous flow in the regenerator and the force created by the additional damper. The generator viscous flow drag is a parasitic by-produce of the regenerator operation. The use of this drag as a sole damping mechanism to control the proper phase angle (as applied in one of the alternative designs) (2), enforces a compromise in the regenerator design between the thermodynamic and the viscous drag requirements.

The magnetic damper, as used in our design, is shown in fig. 2. This device is basically a miniature eddy current generator in which an inverted cup-shaped copper body is reciprocated in radial magnetic field - created by rare earth permanent magnet rings. The copper cup shape is

bolted to the end of the displacer driving piston and therefore, both move simultaneously. The eddy currents generated by the copper cup moving in the magnetic field create a mechanical drag force proportional to the displacer linear velocity. Proper selection of the magnetic damper design parameters, taking into consideration the regenerator viscous flow drag, will result in smooth full stroke sinusoidal displacer motion and in the desired phase angle. The amount of damping forces related to the linear velocity and to the operational frequency, can affect the displacer stroke as shown in fig. 3. The damper design point must be selected to balance the driving force with the expander at its cold, steady state, condition.

By using the dry friction phase delay mechanism, almost rectangular in shape, indicator diagrams can be achieved. This results in maximum cooling power achievable in the given pressure and volume change made. The sinusoidal displacer motion, however, results in elliptical shape diagrams with an area about 20% smaller. This reduction is compensated by the lower dynamic thermal losses which depend on the working gas mass flow rate. These rates are much higher in the square type diagram than in the smooth elliptical shape diagram. The smooth non-contacting sinusoidal displacer motion is a very desirable characteristic from the acoustical and mechanical noise level point of view.

3. Conclusion

1/4 W Split Stirling coolers based on the eddy current damper and clearance seal design concepts are in production by RICOR LTD. in Israel since 1982. Several hundreds of coolers have been delivered and are accumulating laboratory and field experience. A 1/4 W Split Stirling cooler of this concept is shown in fig. 4. Several reliability demonstration tests of the expander units were performed as part of qualification programs and a proven MTBF higher than 1500 hours was demonstrated. Actually, the expander reliability is limited by contamination originated in the compressor, and accumulating on the cold surfaces inside the regenerator, around the displacer tube and in the clearance seals. The combination of our next generation contamination-free compressors and the present magnetic damper/clearance seal type expanders, will result in reliability greater than 2500 hours.

4. References

[1] Horn, S. B., Lumpkin, M. E., and Walters, B. T., "Pneumatically Driven Split Cycle Cryogenic Refrigeration", Advances in Engineering, 19. P216, 1973.

[2] De Junge, A. K., "Small Free Piston Stirling Refrigerator", 14th Intersociety Energy Conversation Engineering Conference, Paper 799245, P113, (1979).

[3] Ackerman, K. A., Bhate, S. K., Bryne, D. V., "Split Stirling Cycle Displacer Linear Electric Drive", Refrigeration for Cryogenic Sensors - NASA conference publication 2287, P231 (1983).

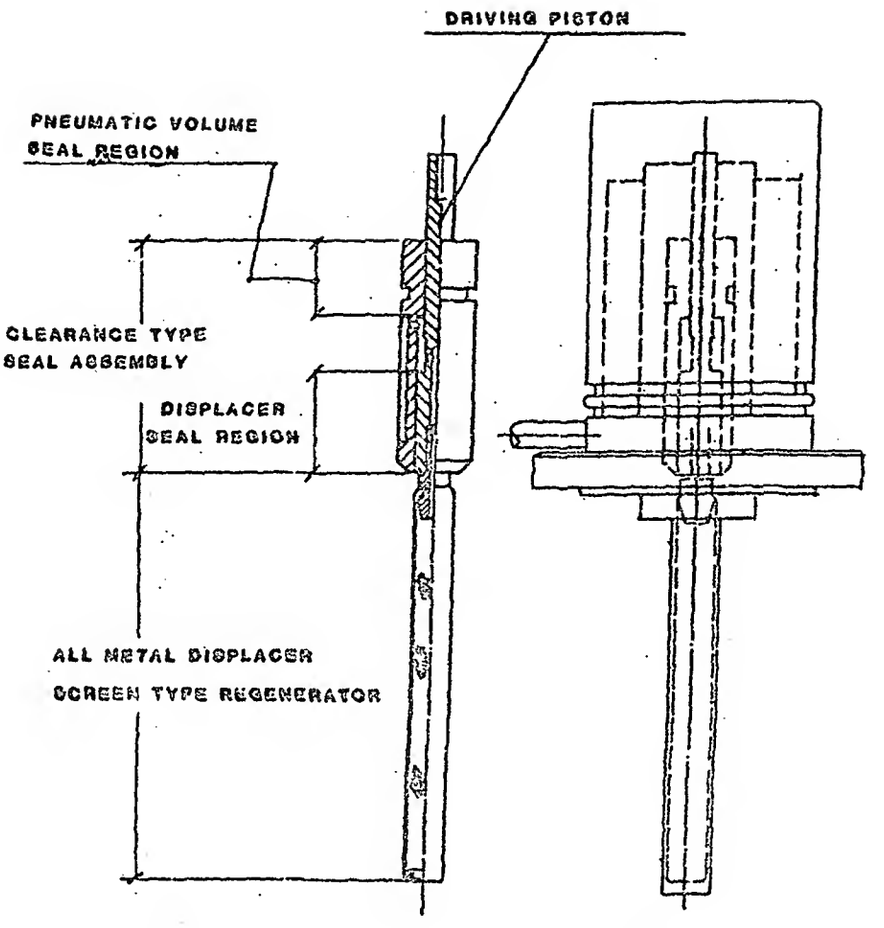

Figure 1. Expander clearance type dynamic seals.

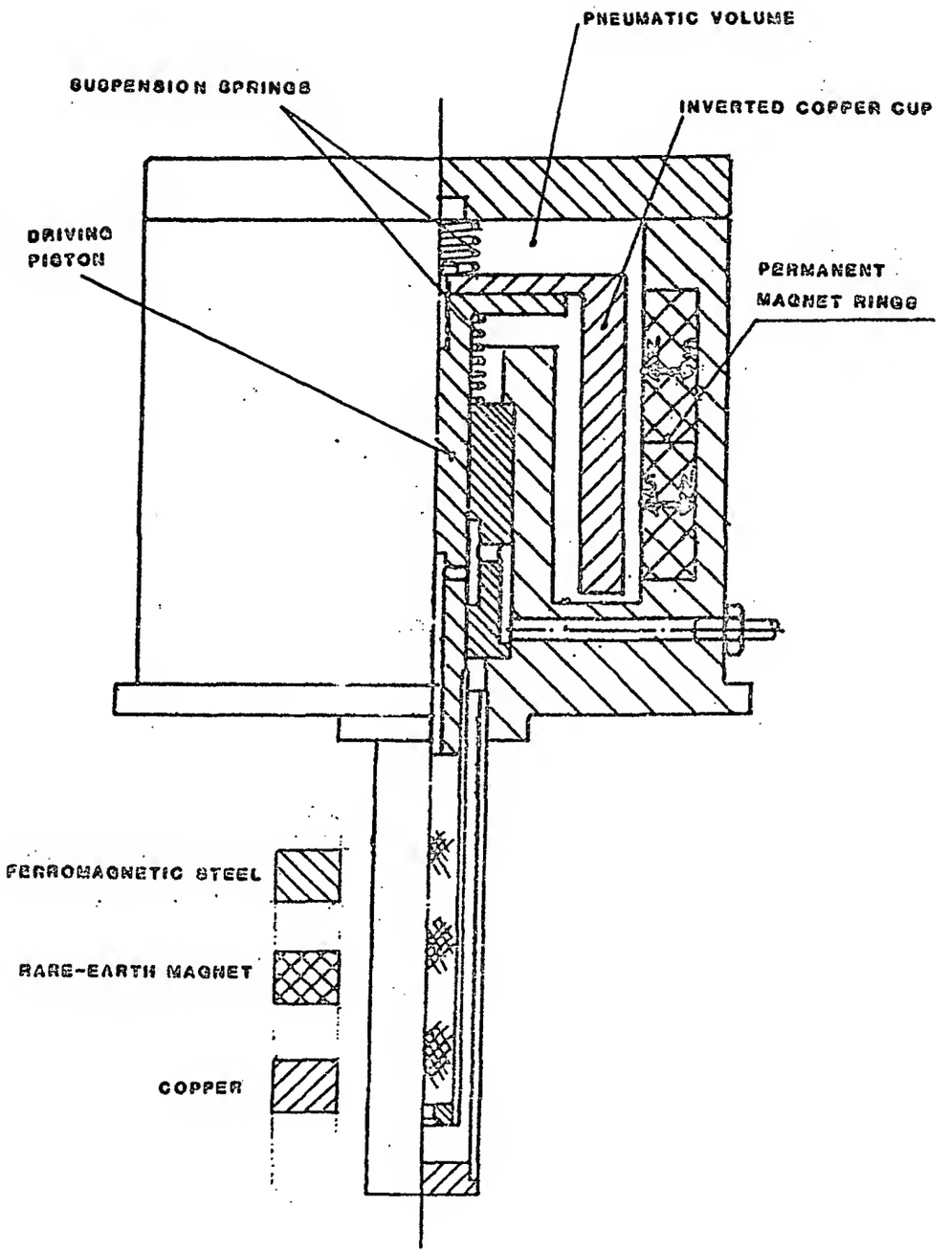

Figure 2. Magnetic damper - Conceptional scheme.

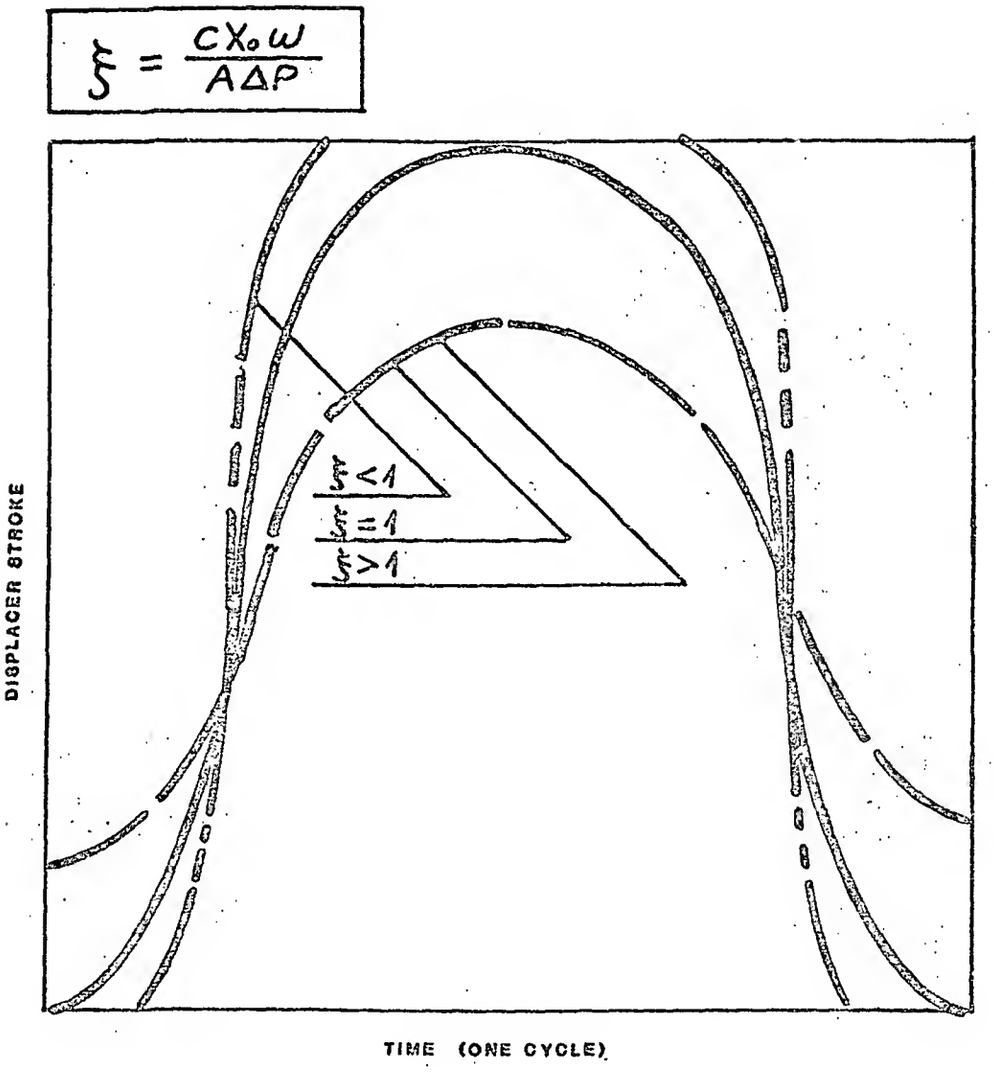

Figure 3. Displacer motion at different damping levels at constant frequency.

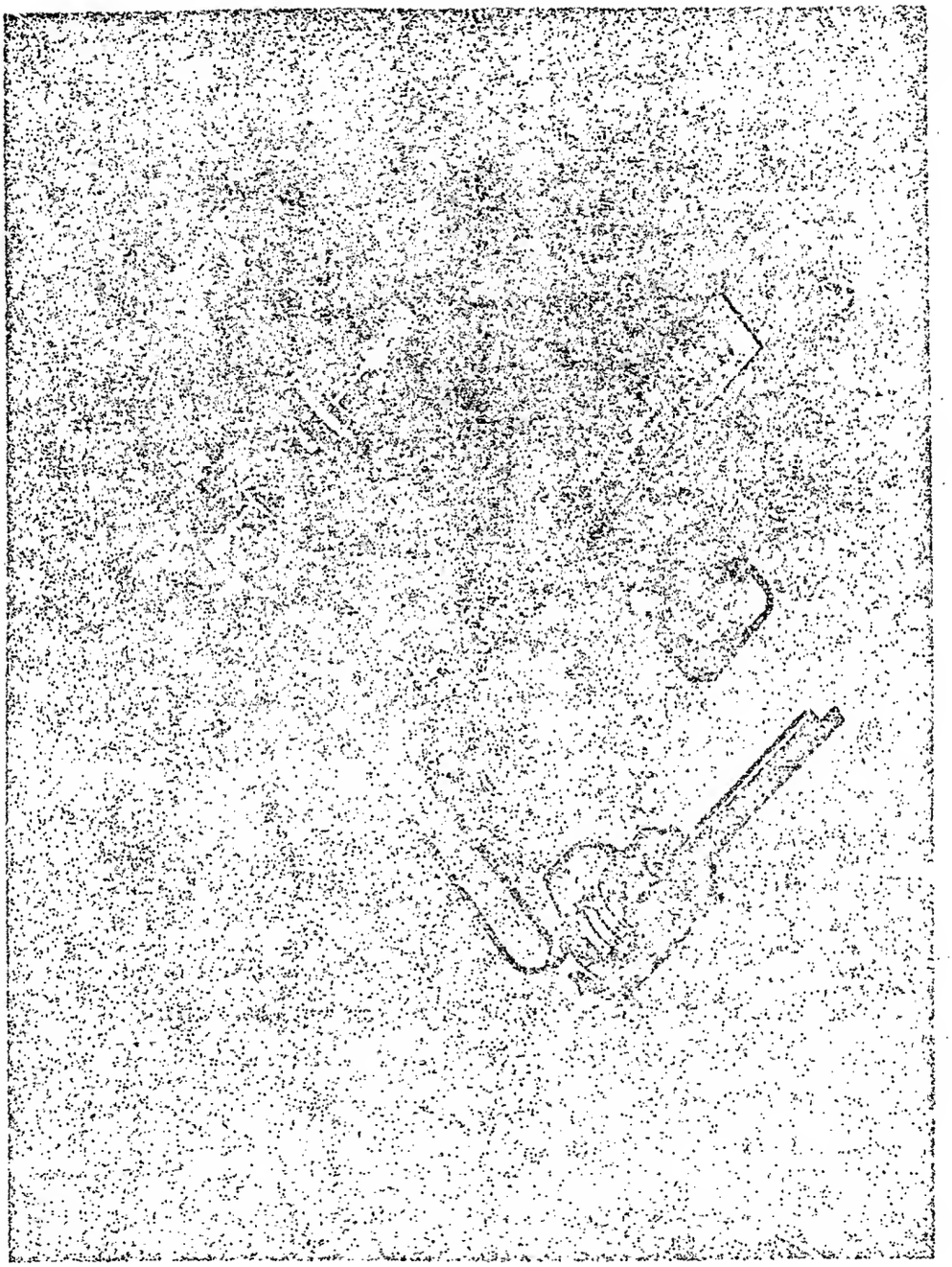

Figure 4. Ricor Mode K413H 1/4 split Stirling cooler - general view.

A NONPROPRIETARY, NONSECRET PROGRAM FOR CALCULATING STIRLING CRYOCOOLERS

William R. Martini

Martini Engineering
2303 Harris
Richland, WA 99352, USA
(509) 375-0115

Using entirely nonproprietary and nonsecret sources of information, a design program for an integrated Stirling cycle cryocooler has been written on an IBM-PC computer. The program is easy to use and shows the trends and itemizes the losses. The calculated results have been compared with some measured performance values. In its present form the program predicts somewhat optimistic performance. The program needs to be calibrated more with experimental measurements. As has been done before, adding a multiplier to the friction factor can bring the calculated results in line with the limited test results so far available. The program is offered as a good framework on which to build a truly useful design program for all types of cryocoolers.

Key words: Analysis; computer program; cryocooler; integral cooler; second order; Stirling cycle.

1. Introduction

When I received a request from a client to produce a cryocooler design program for the IBM-PC, which both they and I had available, I assumed that such a program would be readily available from a government agency with an interest in this technology. It would simply be a matter of adapting it to the client's computer. We found, however, that access to all these programs is restricted, usually, to U. S. companies who already have a contract with a government agency to make cryocoolers. It is perfectly legitimate to have such restrictions. However, there needs also to be available a program that can be used in schools and by companies who do not have an official need to know.

Since I had written two design manuals for Stirling engines, and since many of the equations that were used in these manuals came from earlier publications showing how to design cryocoolers, I have undertaken the process of producing a cryocooler design program analogous to my numerous Stirling engine design programs.

The previous literature will be cited. The method of analysis will be explained in general. The specific arrangement of a Stirling cycle cryocooler for which the program was written is given. A full list of input values is presented with typical input values. A sample of the full calculated output is given and explained. Limited test results are compared with calculated performance and discussed. Application areas for this type of design program are suggested. Finally, conclusions are drawn about the utility of this type of design program.

2. Literature Review

A full literature review on cryocooler anslysis is not attempted. Only those antecedent publications that hsve a bearing on the computer program described in this paper will be given. In 1968 the author lead a group of engineers at the Donald W. Douglas Laboratories, in Richlsnd WA .In developing a Stirling engine for an artificial heart. We developed our own design mstnod. Gradually we became awsre of other methods of analysis. We had simple methods and very complicated and time consuming methods. Later the author now at the Joint Center for Graduate Study, University of Washington and sponsored by NASA-Lewis, wrote two design msnuals for Stirling engines [1,2]. Also a long IECEC paper outlined in detail this design method [3]. As a result of these publications this method of design has been used widely among those who had no access to proprietary information.

There were a number of prior publications which were discovered in a literature search which had an important bearing in selecting the equations that were recommended in the design

program which was presented. Crouthamel and Shelpuk [4] gave all the design equations for a VM cycle cooler. Zimmerman and Longsworth [5] contributed to our understanding of shuttle heat loss as did Rios [6]. Leo [7] supplied the equation for appendix loss. Corring [8] supplied the equation for matrix conduction. Note that many of these publications are in the cryocooler literature.

Since the design manuals have been written the author has continued to evaluate and perfect the isothermal analysis. A 1980 IECEC paper showed that up to that time the isothermal analysis was as good as any other available [9]. A further extension of this isothermal program for large machines was done in which the effect of adiabatic hot and cold gas spaces was included for both heat engines and heat pumps. This effect is particularly serious for engines or heat pumps that operate over a small temperature ratio. The 1983 IECEC paper showed that the improved isothermal analysis agreed with some engine test data over almost the full operating range for both power output and efficiency to within plus or minus 10 percent with absolutely no adjustments [10]. Finally the isothermal analysis has been extended to predict the operation of free-piston machines and search for an optimum design [11].

3. Method of Analysis

In the literature of Stirling engine design, methods are classified as first, second, and third order. First order methods use variations of the Beale equation [12] to predict what the power can be, given the displacement, speed, pressure and temperatures. This method has been extended to large cryogenic refrigerators by Walker [13]. It does not apply to miniature cryocoolers. The method suggested in this paper is second order. It will be defined in more detail later. Second order methods are the simplest methods that take into account all the dimensions that influence performance. Third order methods use nodal analysis to simulate the physical process very closely. They are expensive to run because they use a large amount of time on the very largest and fastest computers. They are useful for special studies, but are not practical to be used in search routines to find the best design.

The basic assumption of the isothermal, second order analysis is that at each point in the cycle the pressure throughout the working gas volume is the same for each instant in time. In reality there are pressure differences between the different parts of the working gas due to flow friction. In a well designed machine these differences are small in comparision to the pressure changes due to expansion and compression. Neglecting the pressure differences at this stage greatly simplifies and speeds the calculation with little loss in accuracy.

It is also assumed that an effective gas temperature can be identified for each part of the working gas volume which holds for the full cycle. This assumption is easy to defend in the regenerator where gas is in close thermal contact with the solid. It is not true and requires corrections [10] for the hot and cold spaces of large machines. Careful measurements of the pressure and total gas volume during one cycle in a Stirling engine for artificial heart power showed that on this scale the isothermal assumption was better than the adiabatic assumption. The artificial heart engine is on the same order of size as the miniature cryocoolers.

Using the two above assumptions, it is a simple matter to calculate the pressure during the cycle usually using the perfect gas law. If the pressure of the working gas is plotted against the volume of gas in the cold space, a closed curve is produced. The area inside this curve is equal to the heat absorbed by the working gas in one cycle. When multiplied by the frequency we call this the thermodynamic heat input. If the pressure of the working gas is plotted against the total working gas volume, a closed curve is also produced. The area inside this curve is equal to the work required to be applied in a perfect machine during one cycle. When multiplied by the frequency, we call this the thermodynamic power input.

These basic thermodynamic values must be modified by the many losses that occur in a real cryocooler. To the basic thermodynamic power must be added the flow losses of the working gas, chiefly in the regenerator matrix. Also the seal friction, the mechanical friction, and the electric motor losses must be added to obtain an estimate of the power required.

From the basic thermodynamic cooling effect must be deducted all the thermal conduction and radiation heat losses. Also the flow losses in the cold part are converted to heat which must also be deducted. The matrix heat transfer is not perfect. Therefore, the gas returning back to the cold space is at a higher temperature than when it left and must be recooled. Finally, there is a loss involving the gap between the displacer and the cold finger cylinder. Heat is transferred by this shuttle loss only when the displacer oscillates.

Each one of these losses mentioned above is calculated by an equation. In the second order method there is assumed to be no interaction between the various loss mechanisms. In a miniature cryocooler accurate estimation of these loss mechanisms is especially important. We find that in most cases the mechanical and electrical losses are more important than the gas flow losses and the thermodynamic power in determining the electric power requirement. On the cooling side, we find that the thermal

losses consume most of the thermodynamic cooling effect. Therefore the net cooling effect is subject to relatively large errors because it is the small difference between large numbers.

In a miniature cryocooler there is so much heat transfer area for so little volume that one would be tempted to assume that the heat transfer is nearly perfect. If tests show that this is so, calculation of the performance would be speeded and simplified. We did not make this assumption. We calculated a heat transfer coefficient for the hot space and the cold space and also decided on a heat transfer area. By trial and error we found an effective cold gas temperature lower than the specified cold metal temperature such that the heat that can be transferred based upon the calculated area and heat transfer coefficient is equal to the heat that needs to be transferred. At the same time by trial and error we found an effective warm space temperature that is higher than the specified warm metal temperature such that the heat that can be removed from the warm space is equal to the heat that must be removed. When the fractional error in the heat balance at both ends is less than the convergence criteria for two trials in a row, the calculation ends and the results are printed out.

4. Cooler Geometry

Although this program can be adapted to any type of Stirling cryocooler, it is particularly set up for an integral cryocooler shown schematically in figure 1. An hermetically sealed electric motor operates two cranks. One crank operates the displacer in the normal manner. The other crank operates the displacer piston in the inverted manner. The cold finger containing the displacer is in the same plane as the compressor piston. The two cranks are offset 90 degrees to provide the proper phase relationship. The program takes into account the slightly non-sinusoidal nature of the piston and displacer motion due to the crank geometry.

Figure 1. Schematic of Cooler Geometry

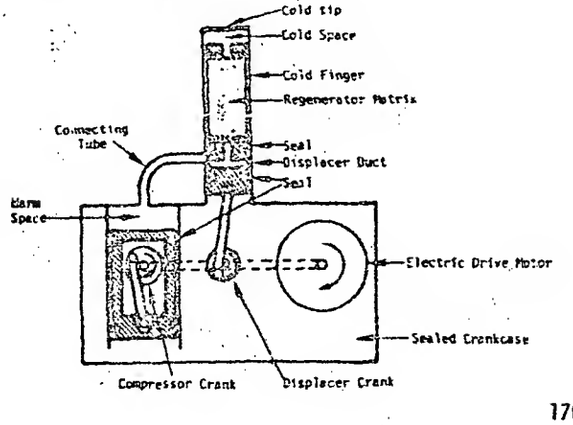

5. Input Values

The program stores all the input data on a disk file. The user has the option of starting with the set of input data which was used last which is on this disk file, or using base case input data which is written into the program. The operator makes this decision to start the program. Then the main menu is displayed on the screen (table 1). The operator can start calculating the next case by keying in a 1 or look at one of seven submenus by keying in 2 thru 8.

Table 1. Main menu for input.

[illegible]

1 — Start calculation next case.
2 — Program control parameters.
3 — Engine operating conditions.
4 — Pistons and connecting rods and crank case.
5 — Gas flow passages.
6 — Regenerator properties.
7 — Cold flow passages.
8 — Heat cond., seals and motor.
Your choice is — (Key number and enter) —5

Program control parameters. Table 2 shows the menu for all the program control parameters. On the left hand side is the menu number. In the middle is the definition. On the right hand side is the current value. Note that at the bottom of the table a menu number is called for. The operator puts in an integer between 1 and 8 (No decimal point.). If a real number with a decimal point, or an integer outside of the specified range is entered the program displays the appropriate error message and asks for the menu number again. If 1 is entered the program displays the master menu again.

Table 2. Submenu for Program Control Parameters

Program control parameters:
1 — Return to main menu.
2 — Convergence criteria. _____ .0010
3 — Case number defined by operator. _____ 31
4 — Graphic option — Basic lines. _____ 1
5 — Printing option — Basic lines. _____ 0
6 — Number of time steps per cycle. _____ 24
7 — Pressure drop option _____ 1
0 = Calculate from pressure drop correlation.
1 = Calculate from pressure drop test.
8 — Reheat loss option _____ 0
0 = Calculate from heat transfer correlation.
1 = Calculate from pressure drop test using Reynolds analogy.
9 — Multiplier for friction factor _____ 1.00
Menu number? 1

If 2 is entered, the program then asks that a real number be entered with a decimal point. This convergence criteria is compared

with the fractional change from one trial to the next of the thermodynamic power input and the thermodynamic heat input. This criteria must be a small positive real number. The program checks to see if the number input is between 0.0 and 0.1. If it is, the convergence criteria is changed to the new value, and the menu is displayed again with the new value in place. If the number that is input is not within the specified range, an error message is displayed, and the menu is redisplayed without change.

If 3 is entered, the program asks for an integer. If this case number is negative, the program rejects it and asks for another. Otherwise the case number can be set to any number desired. The case number is automatically indexed without operator attention.

If 4 is entered, the graphic option can be changed. Some IBM-PC's have the ability to draw graphs on the screen. Others do not. The program can be used either way. If the computer does not have the ability to do graphics and the graphics option is set at 1, the computer will probably hang up. The program will have to be restarted.

If 5 is entered, the printing option can be changed. Since some computers are equipped with printers and others are not, the program can be used either way. If a printer is called for but is not connected, the program will stop.

If 6 is entered, the number of time steps per cycle can be changed. More time steps leads to higher accuracy at the expence of speed of computation. Twenty-four has been found to be a good compromise. A formula has been developed to compensate for a small number of time steps [1]. However, is has not been used in this particular program.

If 7 is entered, the option on the way flow losses are calculated can be changed. For the 0 option, the flow loss is determined based upon a correlation by Kays and London as simplified by Martini [2]. For the 1 option, the flow resistance test used to qualify the displacer for use is employed instead. Other options can be added as needed.

If 8 is entered, the option on the way the heat transfer coefficient for the regenerator is calculated can be changed. For the 0 option, a simplified Kays and London correlation is used [2]. For the 1 option, the heat transfer coefficient is derived from the flow friction test using Reynolds analogy. Other options can be added as needed.

If 9 is entered, a multiplier on the friction factor can be changed. If the Kays and London correlation is used, this factor is multiplied by the calculated friction factor to give the friction factor used to calculate flow loss. If the pressure drop test data is used, the computed pressure drop is multiplied by this factor.

Engine operating conditions. Table 3 shows the menu for the engine operating conditions. The menu is shown twice to illustrate how it is changed. The inputs are self explanatory. The program adjusts the working gas inventory for the first 4 cycles to make the time averaged working gas pressure equal to the input value. After that leakage continues to operate between and crank case and the working gas. An effort has been made to ask for the input values in customary units. They are then converted to a consistent set of units in the program.

Table 3. Submenu for Engine Operating Conditions

```
Engine operating conditions:
1 — Return to main menu.
2 — Average working gas pressure, psia _____ 650.00
3 — Motor speed, rpm _____ 1200.00
4 — Metal temperature in cold space, K _____ 70.00
5 — Metal temperature in warm space, F _____ 80.00

Menu number? 4
Value? (with decimal point)80.
Engine operating conditions:
1 — Return to main menu.
2 — Average working gas pressure, psia _____ 650.00
3 — Motor speed, rpm _____ 1200.00
4 — Metal temperature in cold space, K _____ 80.00
5 — Metal temperature in warm space, F _____ 80.00

Menu number?
```

Pistons -- connecting rods -- crankcase Table 4 shows the menu which allows values connected with the mechanical motion to be changed. The same organization is used as with previous tables. There is enough space to clearly define each input value and give the units. At present the volume of the crank case space is not known very well and is not used in the calculation. Strictly, however, it should be used in leakage calculations and in kinetic simulations of the cooler.

Table 4. Submenu to change inputs related to pistons, connecting rods and crankcase

```
Pistons and connecting rods and crank case.
1 — Return to main menu.
2 — Crank angle, degrees _____ 90.00
3 — Diameter of compressor piston, inch _____ .5620
4 — Seal diameter at displacer, inch _____ .1875
5 — Radius of compressor piston crank, inch _____ .0620
6 — Radius of displacer drive crank, inch _____ .0650
7 — Length of compressor piston conn. rod, inch _____ .6100
8 — Length of displacer drive conn. rod, inch _____ 1.2100
9 — Volume of crank case space, cu. inches _____ 2.0000

Menu number? 1
```

Warm flow passages Table 5 shows the submenu which allows values connected with the warm flow passages to be changed. Most of the entries are self explanatory by reference to figure 1. The warm displacer duct is the hole thru the seal and bearing part of the displacer to allow gas to pass from the connecting tube to the warm end of the regenerator matrix. The number of velocity heads are used to account for the flow resistances of entrances, exits and bends in the gas flow passages. Standard handbook values were used [13]. The dead volume is an estimate of the dead volume in the warm space in addition to that in the piston end clearance, connecting tube, and the warm displacer duct.

Table 5. Submenu for Warm Flow Passage Values

```
Warm flow passages:
1 — Return to main menu.
2 — Diameter of connecting tube, inch ____________ .1875
3 — Diameter of warm displacer duct, inch ________ .6875
4 — Effective compressor piston clearance, inch ____ .0035
5 — Length of connecting tube, inch ______________ 2.2500
6 — Length of warm displacer duct, inch __________ .4000
7 — Number of velocity heads in connecting tube ____ 2.25
8 — Number of velocity heads in displacer duct _____ 2.25
9 — Dead volume at warm end of displacer, cu. inch _ .003359
Menu number? 1
```

Regenerator properties Table 6 shows the submenu which allows values connected with the regenerator to be changed. The length of the regenerator matrix includes space for the two coarse screens on each end. The porosity of the matrix is computed from the total volume of the fine matrix, the weight of the fine screens, and the density of stainless steel (7.817 g/cc)

Table 6. Submenu for Regenerator Properties

```
Regenerator properties:
1 — Return to main menu.
2 — Inside diameter of displacer cylinder, inch ____ .1875
3 — Diameter of regenerator matrix, inch __________ .1250
4 — Wire diameter in regenerator matrix, inch _____ .0030
5 — Square mesh of screens in reg. matrix, wires/in.  500.00
6 — Number of fine screens in reg. matrix _________ 350
7 — Length of regenerator matrix, inch ____________ 2.2500
8 — Weight of fine regenerator screens, grams _____ 1.3180
9 — Number of coarse end screens in matrix _______ 4
10 - Thickness of each coarse end screen, inch _____ .0160
11 - Test flow rate of H2 thru displ., std cc/min. __ 710.00
12 - Pressure drop at test flow rate, psi _________ 15.00
Menu number? 1
```

Cold flow passages Table 7 shows the submenu which allows values connected with the cold flow passages to be changed. In this case there is a single orifice which squirts gas into the cold space. The correlation by Hauser [16] was used to calculate the heat transfer coefficient in the cold space.

Table 7. Submenu for Cold Flow Passages

```
Cold flow passages:
1 — Return to main menu.
2 — Diameter of cold orifice, inch _____________ .0700
3 — Effective displacer clearance at cold end, inch__ .0035
4 — Length of cold orifice, inch _______________ .0400
5 — Number of velocity heads in cold orifice _____ 1.50
Menu number? 1
```

Heat conduction, seal, and motor properties Table 8 shows the submenu which allows values connected with heat conduction, seal, and motor properties to be changed. All the input values in this list, except for the inch dimensions are difficult to determine. The emmissivities can vary over a wide range depending upon the exact properties of the surfaces. However the heat loss thru the vacuum insulation is small in any case, so these errors are unimportant. The efficiency of the drive motor and the seal and mechanical friction are very important. They must be measured by separate tests. In this case the efficiency of the motor was estimated from the motor specifications. The seal and mechanical friction was determined by adjusting it so that the electric power demand at the very beginning of a cool down test was about right. The speed of the motor during this test was not recorded and had to be estimated. In reality the seal and mechanical friction should depend upon engine speed and working gas pressure. More realistic friction can be added when the information is available.

Table 8. Submenu for Heat Conduction, Seal and Motor Values.

```
Heat conduction, seal, and motor values:
1 — Return to main menu.
2 — Diameter of vacuum insulation chamber, inch ____ .84
3 — Efficiency of drive motor, % _________________ 80.00
4 — Emissivity of cold finger ____________________ .0400
5 — Emissivity of vacuum insulation chamber _______ .0300
6 — Combined seal tension, cu.inch/sec/psi _______ .0004
7 — Seal and mechanical friction, watts _________ 7.0000
8 — Thickness of cold finger wall, inch _________ .0200
9 — Gap between cold finger wall and displacer, inch .0020
Menu number? 1
```

6. Calculated Outputs

During solution two outputs are possible. If the graphic option is on, a display is shown on the screen like that shown in figure 2. This display is very useful to show at a glance whether the solution is converging and where some of the problems in design are. The ellipses at the right show the gas pressure plotted against the total volume. The first cycle is on

top. The other 6 cycle are below as the gas pressure is adjusted. The ellipses at the left are the cold gas volume plotted against the working gas pressure. The sine curve at the top is the displacer motion for one cycle. The sine curve at the bottom is the compressor motion for one cycle. The nearly horizontal line at the top left records the trials of the effective warm space temperature. Full vertical scale is 0-400 K. Note that most of the adjustment is made after the first cycle. The nearly horizontal line at the bottom left records the trials for the effective cold space temperature. Note that there was little change.

Figure 2. Graphical Display during Solution

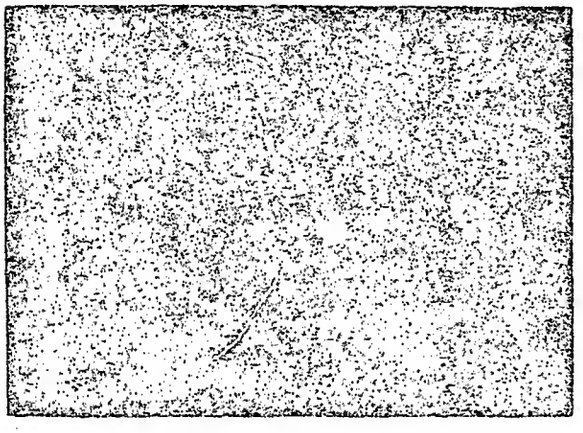

If the graphic option is off, Table 9 is displayed on the screen. The numbers in the first two columns are the numbers that are compared with the convergence criteria which is shown in the top line of Table 9. These fractional changes for cycle 6 and 7 were all under 0.001. Note that the work in and the heat out are now only changing in the fourth significant figure. The last column, the gas inventory, has unusual units. It is the gas inventory in gram moles multiplied by the universal gas constant, 8.314 J/(gmol*K).

Table 9. Progress to convergence table

Convergence criteria is [illegible] for Pcm 0 31

Cycle Numb.	Change Power In Frac.	Change Cool In Frac.	Work In Joules	Cooling In Joules	End Pressure MPa	Time Step Msec.	Gas Invent. J/K
1	[illegible]	[illegible]	[illegible]	[illegible]	[illegible]	[illegible]	[illegible]
2	[illegible]	[illegible]	[illegible]	[illegible]	[illegible]	[illegible]	[illegible]
3	[illegible]	[illegible]	[illegible]	[illegible]	[illegible]	[illegible]	[illegible]
4	[illegible]	[illegible]	[illegible]	[illegible]	[illegible]	[illegible]	[illegible]
5	[illegible]	[illegible]	[illegible]	[illegible]	[illegible]	[illegible]	[illegible]
6	[illegible]	[illegible]	[illegible]	[illegible]	[illegible]	[illegible]	[illegible]
7	[illegible]	[illegible]	[illegible]	[illegible]	[illegible]	[illegible]	[illegible]

Speed of Solution On the IBM-PC equipped with the 8087 coprocessor, and running Microsoft FORTRAN-77, the solution time for the above same case with 7 iterations is 6 seconds without graphics and 20 seconds with graphics. This does not include the time for printing out or displaying the solution. The display of the output to the screen takes 2.4 seconds additional. The printout takes much longer and depends upon the type of printer that is being used. With some type of spooler, printing can lag behind. Meanwhile the operator may investigate new possibilities using the information available at the monitor.

Calculated Performance At the end of the solution, the table of calculated performance is displayed on the monitor and is printed out as well, if the print option is on. Table 10 is the calculated performance for the input values given in Tables 2 to 8. The first thing to notice is that some losses are very important and some are negligible. However, it is dangerous to neglect the negligible losses in the design calculation. If you do your search for a better design will lead you into an area where these negligible losses are no longer negligible.

Table 10. Calculated Performance

Martini Eng. Analysis of Stirling Cycle Cryocooler
Integral Cooler, [illegible]

POWER REQUIREMENT, WATTS		COOLING EFFECT, WATTS	
Thermodynam. Power	4.5144	Ther. Dyn. Cooling Eff.	1.6127
Cld. Orfc. F.L.	[illegible]	Cld. Cyct. Fric. Heat	[illegible]
Reg. Flow Loss	1.2365	Regen. Fric. Heat	[illegible]
Disp. Displ. F.L.	[illegible]	Shuttle Heat Loss	[illegible]
Comp. Flow F.L.	[illegible]	Natural Loss	[illegible]
Mech. Friction	7.[illegible]	Radiation Loss	[illegible]
Elect. Mtr. Loss	9.[illegible]	Temp. Swing Loss	[illegible]
		Cld. Finger Wall Cnd.	[illegible]
Elect. Pwr. In	22.[illegible]	Disp. Wall Cond.	[illegible]
		Reg. Mtx. Cond.	[illegible]
Eff. Cld. Sp. Temp.	78.12[illegible]	Vac. Insul. Heat Loss	[illegible]
Eff. Wrm. Sp. Temp.	324.5[illegible]	NET COOLING EFFECT	[illegible]

On the power requirement side, note the mechanical friction and the electrical motor losses are the two big ones accounting together for 74.4 % of the power requirement. The flow loss thru the regenerator accounts for 5.5 % of the power requirement. All the other flow losses account for only 0.2 %, leaving 19.9 % for the necessary thermodynamic power. Obviously the place to start with improvements is to find some way to reduce the mechanical and electrical losses.

On the cooling effect side, it appears that only 26.2 % of the thermodynamic cooling effect survives the gauntlet of losses to become net cooling effect. In this analysis it is assumed that all the cold orifice flow loss and half the regenerator flow loss must be

deducted as heat loss from the thermodynamic cooling effect.

The shuttle heat loss and the appendix loss must be considered together, because as one increases the other decreases. Shuttle heat loss occurs by radial conduction across the gap between the cold finger cylinder and the displacer. Because of the longitudinal temperature gradient along the cold finger cylinder and along the displacer, when the displacer is at the warm end of its stroke it is colder than the cold finger cylinder all the way along, so it heats up. When the displacer is at the cold end of its stroke, it is warmer than the cold finger cylinder, so it cools down. Each cycle this process moves the heat that has been transferred one stroke length toward the cold end. This important heat loss can be minimized by using low conductivity cylinder walls such as plastic or glass or ceramic. The loss can be minimized by increasing the gap and increasing the length of the regenerator.

Appendix loss occurs as the gas is packed into and unpacked from the appendix gap between the displacer and the cold finger wall. This gap is closed off at the warm end with a sliding seal and is open at the cold end to the cold space. As the pressure increases cold gas is packed into this space. As the pressure decreases hot so cold gas flows back into the cold space. Increasing the thickness of the gap reduces shuttle loss but increases the appendix loss.

A number of equations have been published for shuttle heat loss and for appendix heat loss. As far as is known there has been no experimental confirmation published of any of these equations.

The reheat loss should, for a cryocooler, be called the recool loss. Both due to pressure changes and flow, a large amount of heat must be transferred each cycle in the regenerator. No matter how good the heat transfer, the gas always re-enters the cold space warmer than when it left. The reheat loss can be made small at the expense of making the flow heating or the heat conduction loss or both too large. A careful balancing of dimensions is needed.

The temperature swing loss is a correction to the reheat loss to compensate for the heat capacity of the regenerator being less than infinite. In this case it is negligible, but it can be important.

The last 4 losses are heat conduction or radiation losses that go on whether the displacer moves or not. By far the largest is the cold finger wall since this must be thick and metal to hold back the pressure and contain the helium. The displacer wall conduction is much less because this is made of plastic. The displacer matrix conduction is even smaller because the metal screens are divided and make contact only in a few spots. Vacuum insulation loss is negligible.

Record keeping The operator can continue to experiment with the computer program to see how different inputs affect the output. He can do this without waiting for the printer on line at all. However with a spooler of some sort, the printer can keep track of all the inputs and all the outputs for further study. It may be running many cases behind what the operator is considering. After the output of table 10, the full input values are printed out. These values are printed out in the same order as they are shown in tables 2 to 8.

7. Results and Discussion

Figure 3 shows how the computed performance without any adjustmentof the calculation proceedure with test results. The net cooling effect is plotted against the cold finger temperature. Note that if the flow resistance data is used for both the flow loss and the reheat that the net cooling is too optimistic by 0.2 to 0.3 watts. If the Kays and London correlations are used, the net cooling is optimistic by 0.12 watts. From the data that so far has been obtained, it appears that when the cryocooler motor speed was not measured that it was running at 1600 to 1700 rpm. Figure 3 shows that the calculated and measured performance shows the same trend.

For the flow rate that results in a 10 psi pressure drop thru the displacer, the Kays and London correlation calculated 18.4 psi. Also a number of investigators have found that the flow resistance calculated for steady flow must be multiplied by a factor to make the measurements and the predictions for engines agree more closely. At one time the author used a factor of 2.9 to make the calculated output agree with measurements for both helium and hydrogen [17]. Tew [18] used a factor of 4 for hydrogen and 3 for hellum to make his calculations agree with test results. A recent test reported by Taylor and Aghili [14] showed that oscillating flow in tubes increased the friction factor by a factor of about 3. Possibly finding the right multiplier between reversing flow and steady flow resistance and the right way to apply this multiplier could bring the experimental and test results into agreement.

Figure 4 shows the first attempt at adjusting the program to fit the current experimental data. When the flow resistance teat data are used, a mutiplier on the computed pressure drop of 3.3 to 3.6 is needed to bring the computed results in line with the measurements. The measurements are consistant in that they show a trend with very little scatter. The computed results derived from flow resistance test data do not show quite the same trend.

When the Kays and London flow correlation is used, the multiplier only has to be 1.25. Also the trends in the data and the adjusted calculation are the same. The correlation shows a transition from pressure drop proportional to flow rate to pressure drop proportional to the square the the flow rate in a smooth manner over a factor of about 10 in flow rate. Possibly the pressure drop is not directly proportional to the flow rate.

These exercises in adjustment have been successful in showing that adjustments can be made. However, when we have more information, particularly the motor speed, for each point, our conclusions may be quite different than they are now. However, the isothermal method has an important advantage in that it itemizes the losses and therefore gives guidance about where to make improvements.

8. Application Areas

Although the specific cryocooler design program described in this paper is for an integral Stirling cryocooler, The same programing concept can be applied to split Stirling and free-piston Stirling machines. A free-piston engine has been calculated using this type of analysis [11]. The speed for calculating each case is fast enough so that once the design method is calibrated, an optimization search can be programed to search for the best design automatically. A thorough optimization search is already programed [11].

9. Conclusions

Using only open sources of information, a cryocooler design program has been written which gives reasonable results. It requires inputs of cooler dimensions, measured flow losses, mechanical friction, and electric motor losses. Since the current error between calculated and measured performance is not large, and since the calculated performance shows the same trend as the measured performance, we expect that this computer program can be adjusted to model a real cryocooler quite exactly. The program needs to be adapted and customized for each user since there are so many ways to build a cryocooler. Also skill is needed in making the proper adjustments so that the program will be accurate over a wide range of design options. In itemizing the losses the program shows clearly where the greatest improvements in design can be made.

10. References

[1] Martini, W. R., Stirling engine design manual, DOE/NASA/3152-78/1 NASA CR-135382 (April 1978)

[2] Martini, W. R., Stirling engine design manual, second edition, DOE/NASA/3194-1 NASA CR-168088 (Jan. 1983)

[3] Martini, W. R., A simple method of calculating Stirling engines for engine design optimization, 1978 IECEC Record 1753-1752.

[4] Crouthamel, M. S., and Shelpuk, B., Regenerative gas cycle air conditioning using solar energy, Advanced Technology Laboratories ATL-CR-75-10 (Aug. 1975)

[5] Zimmerman, F. J., and Longsworth, R. C., Shuttle heat transfer, Advances in Cryogenic Engineering, Vol. 16, 342-351, Plenum Press (1971)

[6] Rios, P. A., An approximate solution to the shuttle heat-transfer losses in a reciprocating machine, Journal of Engineering for Power, 177-182, (April 1971)

[7] Leo, B., Designer's handbook for spaceborne two-stage Vuilleumier cryogenic refrigerators, Air Force Flight Dynamics Laboratory, Report No. AFFDL-TR-70-54, (June 1971)

[8] Corring, R. L., and Churchill, S. W., Thermal conductivity of hetrogeneous materials, Chemical Engineering Progress, 53-59 (July 1961)

[9] Martini, W. R., Validation of published Stirling engine design methods using engine characteristics from the literature, 1980 IECEC Record, 2245-2250

[10] Martini, W. R., A revised isothermal analysis program for Stirling engines, 1983 IECEC Record, 743-748

[11] Martini, W. R., Development of free-piston Stirling engine performance and optimization codes based on Martini simulation technique (May 1984) To be published by NASA-Lewis.

[12] Stirling Engine Newsletter, p. 5 (May 1982) Martini Engineering

[13] Walker, G., Design guidelines for large Stirling cryocoolers, University of Calgary, Mechanical Engineering Dept. (1982)

[14] Taylor, D. R., and Aghili, H., An investigation of oscillating flow in tubes, 1984 IECEC Record, 2033-2036 (Aug. 1984)

[15] Perry, J. H., (editor) Chemical engineers' handbook, Third Edition, McGraw-Hill 388 (1950)

[16] Hauser, S. G., Experimental messurements of transient heat transfer to gas inside a closed space, Masters thesis, University of Washington (1979)

[17] Martini, W. R., A simple, non-proprietary code for Stirling engine design, Presented at DOE Highway Vehicle Systems Contractors' Coordination Meeting, 16-20 Oct. 1978.

[18] Tew, R. C., Thieme, L. G., and Miao, D., Initial comparison of single cylinder Stirling engine computer model predictions with test results., DOE/NASA/1040-78/30 NASA TM-79044, Presented at International Congress and Exposition SAE, Detroit, MI Feb.26 - Mar. 4, 1979

Figure 3 Comparison of calculated cooling effect without adjustments with measurements.

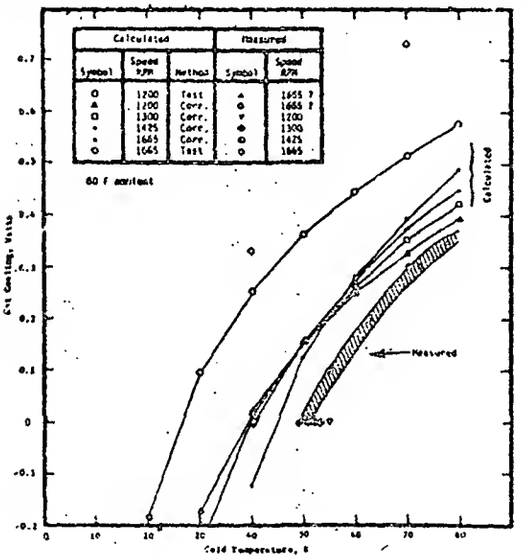

Figure 4. Comparison of calculated cooling effect with adjustments with measurements

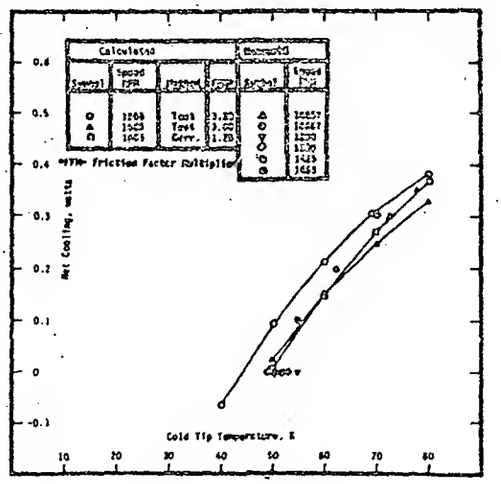

D18

A SIMPLE, FIRST STEP TO THE OPTIMIZATION OF REGENERATOR GEOMETRY*

Ray Radebaugh and Beverly Louie

Chemical Engineering Science Division
National Bureau of Standards
Boulder, Colorado 80303

This paper presents a simplified set of equations for calculating and optimizing regenerator geometries. A number of competing parameters must be accounted for in the design of a regenerator. To obtain high values of effectiveness, there is need for a large surface area for heat transfer and high heat capacity. The void volume should be small to maintain the pressure ratio in the entire system. Moreover, the pressure drop should be small compared to the absolute pressure. With the assumptions made here, the calculations can be done with a hand calculator.

The equations show that the optimum regenerator length, hydraulic radius, and porosity are independent of mass flow rate and the gas cross-sectional area is proportional to the mass flow rate. It is shown that using gas gaps between parallel plates produces a significantly better regenerator than is possible with packed spheres or screens, particularly at temperatures below approximately 50 K. The improvement is due to enhanced heat transfer and the flexibility in using a lower porosity in the gap configuration.

Key Words: Cryocoolers, cryogenics, gaps, geometry, heat exchangers, optimization, packed spheres, regenerators.

1. Introduction

The regenerator is often one of the major loss sources in regenerative-cycle refrigerators. It contributes loss terms due to its limited heat transfer units, limited matrix specific heat, pressure drop, dead volume, and axial thermal conduction. An optimum design of these regenerators would significantly improve the performance of the overall refrigerator.

The calculation of regenerator performance with various assumptions has been discussed extensively in the literature. First order calculations assume the void volume in the regenerator is zero. Such calculations were first done by Lambertson [1] and Hausen [2] with graphs and tables presented in the books by Kays and London [3] and Schmidt and Willmott [4]. Second order calculations take into account the regenerator void volume but neglect any pressure oscillation in the void volume gas. These calculations have been done by Heggs and Carpenter [5], by Daney and Radebaugh [6], and by others cited in these two works. A third order calculation considers void volume in the regenerator and a pressure oscillation as seen by regenerators in regenerative-cycle refrigerators. Gary, et al. [7] discuss such a third order calculation where very few assumptions are made.

*Work partially funded by the David Taylor Naval Ship R&D Center and the Office of Naval Research.

All of the cited calculations require the regenerator geometry as the input parameter and compute the regenerator effectiveness. The problem facing the designer is how to determine the optimum geometry without resorting to trial and error through such performance calculations. Such an approach can be very costly and time consuming, especially for third order calculations where considerable computer time is required for each case. In this paper we discuss a simple technique for determining the optimum geometry associated with a desired value of regenerator effectiveness. The technique reverses the "normal" first order calculations and computes the various geometrical parameters that give the minimum regenerator void volume. If the void volume is not negligible a second iteration should be done with reversed second or third order calculations.

2. Basis for optimization

In any optimization scheme it is important to determine the proper parameter to be optimized. Most often the input power is minimized for a refrigerator with a specified net refrigeration power. (In some applications, such as cooling SQUID's, the net refrigeration power is zero and the gross refrigeration is used entirely for loss terms. Nevertheless, the input power is still the quantity to be minimized in SQUID cryocoolers.) It would appear that a general system requirement would preclude a simple optimization of a single component like a regenerator, especially when the regenerator may consist of several stages. Any exact analysis must consider the entire system as a coupled system and various loss terms will necessarily be dependent on each other. However, Smith and coworkers [8-11] have found that a decoupled approach to the loss terms has resulted in relatively good approximations to the overall system performance. In the decoupled approximation the gross refrigeration power, $\dot{Q}_r$, is absorbed by several independent terms:

$$\dot{Q}_r = \dot{Q}_{net} + \dot{Q}_{rad} + \dot{Q}_c + \dot{Q}_{reg} + \dot{Q}_s + \dot{Q}_h + \ldots, \qquad (1)$$

where $\dot{Q}_{net}$ is the net refrigeration power, $\dot{Q}_{rad}$ is the radiation loss, $\dot{Q}_c$ is the conduction loss, $\dot{Q}_{reg}$ is the loss due to regenerator ineffectiveness, $\dot{Q}_s$ is the shuttle heat loss due to the oscillating displacer, and $\dot{Q}_h$ is the loss caused by an excess enthalpy flow through the regenerator during the hot blow for certain conditions with a non-ideal gas. Another possible term would be one due to the pressure drop, ΔP, in the system. That term would be used whenever $\dot{Q}_r$ is calculated from the pressure amplitude at the compressor. If $\dot{Q}_r$ is calculated from the pressure amplitude at the expansion space, then no such term would be used, but the pressure drop would indicate the required pressure amplitude at the compressor.

In the decoupled approximation of eq.(1) the entire system is optimized by minimizing $\dot{Q}_r$ for a fixed value of $\dot{Q}_{net}$. For an ideal gas $\dot{Q}_h = 0$. For the second and third stages $\dot{Q}_{rad}$ is often negligible. The other terms, $\dot{Q}_c$, $\dot{Q}_{reg}$, and $\dot{Q}_s$, are then usually of comparable values when a minimum $\dot{Q}_r$ is found. Likewise, the percentage loss due to a pressure drop, $\Delta P/P$, will be comparable to the percentage loss of these other three terms. The simplest approximation for $\dot{Q}_r$ assumes an isothermal expansion. If an adiabatic expansion is considered, $\dot{Q}_r$ is reduced by approximately a factor of two [12].

In dimensionless form eq.(1) is given as

$$\dot{Q}_{net}/\dot{Q}_r + \dot{Q}_{rad}/\dot{Q}_r + \dot{Q}_c/\dot{Q}_r + \dot{Q}_{reg}/\dot{Q}_r + \dot{Q}_s/\dot{Q}_r + \dot{Q}_h/\dot{Q}_r + \ldots = 1 \qquad (2)$$

For any particular refrigerator an experienced designer can then make reasonable estimates of such terms as $\dot{Q}_c/\dot{Q}_r$ and $\dot{Q}_{reg}/\dot{Q}_r$ and $\Delta P/P$. For example, with an ideal gas in a cryocooler where $\dot{Q}_{net}/\dot{Q}_r$ is to be small, the aforementioned terms may be approximately 0.1-0.2. Good estimates of these terms are the first and most important step in the optimization of a regenerator. The performance of the overall system is also affected by the void volume of the regenerator, V_{rg}. A normalized void volume would be V_{rg}/V_e, where V_e is the expansion space volume. The four terms $\dot{Q}_{reg}/\dot{Q}_r$, $\dot{Q}_c/\dot{Q}_r$, $\Delta P/P$, and V_{rg}/V_e are interrelated; a decrease of one must cause an increase of another.

The basis for the optimization procedure described herein is to use $\dot{Q}_{reg}/\dot{Q}_r$, $\dot{Q}_c/\dot{Q}_r$, and $\Delta P/P$ as known input parameters and then find the geometry which gives a minimum V_{rg}/V_e. At an early, intermediate point, the regenerator ineffectiveness assoicated with $\dot{Q}_{reg}/\dot{Q}_r$ is calculated. If $V_{rg}/V_e \ll 1$, then the input parameters could be decreased to the point where V_{rg}/V_e becomes significant. If $V_{rg}/V_e \gg 1$, then the three input parameters must be increased. If the values are as large as they can be, the process probably is not feasible with the conditions chosen, unless an abnormally large compressor is used. The optimization done here is not fully rigorous since estimates are used for the input parameters and the effects of $\Delta P/P$ and V_{rg}/V_e on the system are not fully quantified.

The geometry of a regenerator can be divided into two components: (a) the configuration of the packing, such as packed spheres, plates, tubes, etc. and (b) the macroscopic geometry, such as cross-sectional area, porosity, length, and hydraulic radius. The optimization procedure discussed here treats both components. The best configuration is the one which has the highest heat transfer rate for a fixed pressure drop. However, any configuration may be chosen and the optimization procedure then gives the best geometrical parameters. Pressure drop and heat transfer correlations often incorporate the friction factor, f, and the Stanton number

$$N_{st} = h/(\dot{m}/A_g)c_p, \qquad (3)$$

where h is the heat transfer coefficient, $\dot{m}$ is the mass flow rate, A_g is the gas cross-sectional area, and c_p is the specific heat of the gas at constant pressure.

Figure 1 shows a plot of $N_{st}N_{pr}^{2/3}$ and f as a function of the Reynolds number, N_r, for one particular configuration, an infinitely long and wide gap. The two curves of $N_{st}N_{pr}^{2/3}$ are for the case of constant heat flow and for constant temperature. Kays and London [3] provide the correlations for gaps and several other configurations. The Prandtl number N_{pr} is included to make the correlations valid for a wide range of fluids. For helium gas $N_{pr} = 0.666$ under ideal conditions. Note that both $N_{st}N_{pr}^{2/3}$ and f have nearly the same dependence on N_r. For regenerators the curve of interest is that of constant heat flow. The practical difficulty in

achieving a uniform hydraulic radius, however, suggests the lower, constant temperature curve may be more realistic.

We define the ratio:

$$\alpha = N_{st} N_{pr}^{2/3} / f \qquad (4)$$

A high value of α is desired since it gives a high heat transfer for a given pressure drop. (A more quantitative argument is given later.) Figure 2 shows α as a function of the Reynolds number for several packing configurations and for a constant temperature heat transfer. The data are from Kays and London [3]. The two important points to note from these curves are (a) they are nearly independent of Reynolds number, and (b) a gap configuration has the highest α - significantly higher than that of a packed bed of spheres. Because α is nearly independent of Reynolds number, it becomes a useful parameter to use in calculations since there is no need to specify the flow rate.

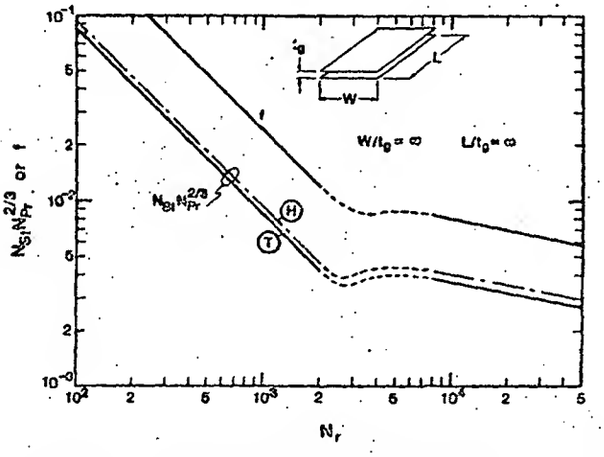

Figure 1. Heat transfer and friction factor curves as a function of Reynolds number for gas flow in a gap.

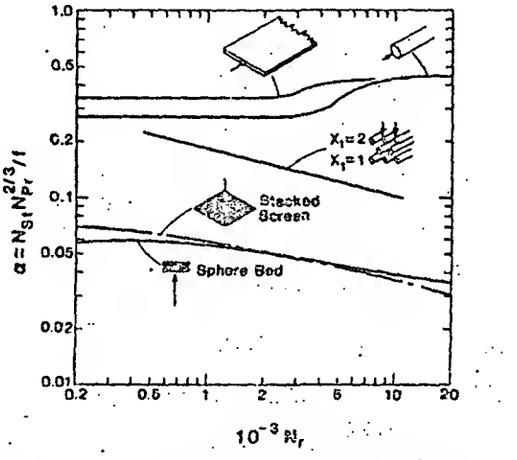

Figure 2. Ratio of Heat transfer and friction factor curves as a function of Reynolds number for several configurations.

3. Optimization procedure

The equations which are developed in the following sections describe the procedure to calculate the actual dimensions of an optimum regenerator geometry. The development begins by relating Q_c/Q_r to a regenerator ineffectiveness. By using published performance curves for regenerators, a set of values for the number of heat transfer units per half cycle, N_{tu}, and the ratio of matrix heat capacity to the heat capacity of the fluid that passes through the regenerator, C_r/C_f, can be found that yields the correct ineffectiveness. Because an infinite set of values will yield the same ineffectiveness, the goal is to find the set of N_{tu} and C_r/C_f values that gives the minimum V_{rg}/V_e. Expressions for the geometrical parameters of cross-sectional area, length, porosity, and hydraulic radius are developed in terms of the optimized N_{tu} and C_r/C_f and the input parameters Q_c/Q_r and $\Delta P/P$. The configurational parameter α is used in the equations to make them valid for all N_r and to show how a maximum α produces a minimum V_{rg}/V_e.

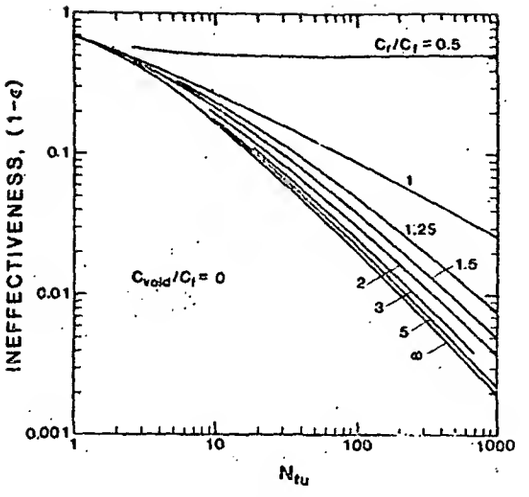

Figure 3. Calculated regenerator ineffectiveness for zero void volume.

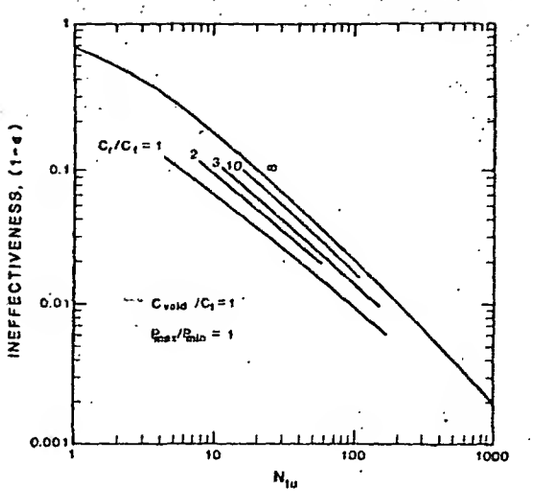

Figure 4. Calculated regenerator ineffectiveness for a finite void volume but with no pressure wave.

3.1 Performance curves

The effectiveness, ε, of a regenerator is defined as the ratio of heat actually transferred to the maximum possible heat transfer. The first optimization step utilizes the performance curves as shown in figures 3 and 4. Figure 3 shows the ineffectiveness, $1 - \varepsilon$, as a function of N_{tu} and C_r/C_f. The plot assumes zero void volume, zero thermal conductivity in the axial direction, infinite thermal conductivity in the radial direction, gas and matrix thermal properties independent of temperature, constant inlet temperatures, constant flow rate, and constant heat transfer coefficient. The curves in figure 3 are plotted from data in Kays and London [3] modified by the appropriate change for our definition of N_{tu}. Figure 4 is for the case of a finite void volume without a pressure wave [5,6]. All other assumptions are the same as for figure 3. Other curves could be generated using fewer assumptions. Since the thermal conductivity in the axial direction is taken into account separately via a decoupled loss term, it should always be neglected in the performance curves.

For a predetermined value of $\dot{Q}_{reg}/\dot{Q}_r$ a value of $1 - \varepsilon$ can be calculated for a regenerator operating between some upper temperature T_U and a lower temperature T_L. By definition

$$1 - \varepsilon = \dot{Q}_{reg}/\dot{m}(H_U - H_L), \tag{5}$$

where H is the enthalpy per unit mass. Since refrigeration in a regenerative-cycle cryocooler occurs only during one half-cycle, the refrigeration rate is given as

$$\dot{Q}_r = \dot{m}q_r/2, \tag{6}$$

where q_r is the heat absorbed per unit mass during the expansion process. Combining eqs. (5) and (6) gives

$$1 - \varepsilon = (\dot{Q}_{reg}/\dot{Q}_r)q_r/2(H_U - H_L). \tag{7}$$

As shown in figure 3, a given ineffectiveness is satisfied by a wide range of N_{tu} and C_r/C_f values. The optimum combination will become evident later, but we proceed with the optimization procedure assuming that the best N_{tu} and C_r/C_f have already been determined.

3.2 Gas cross-sectional area, A_g

A high N_{tu} in a heat exchanger is achieved by using a high surface area, but the high surface area will also lead to a large pressure drop unless the cross-sectional area is sufficiently large. The pressure drop in the core of the regenerator is given by

$$\Delta P = f(\dot{m}/A_g)^2 \, L/2\rho r_h, \tag{8}$$

where f is the friction factor, L is the regenerator length, ρ is the gas density, and r_h is the hydraulic radius. Equation (8) does not consider the entrance and exit pressure changes associated with acceleration and deceleration, but these terms are generally negligible in a well designed regenerator. By using the term α from eq. (4) the pressure drop in eq. (8) can be related to the heat transfer by

$$\Delta P = N_{st}N_{pr}^{2/3}(\dot{m}/A_g)^2 \, L/2\alpha\rho r_h. \tag{9}$$

By using the definition for N_{st} in eq. (3) and the following definitions

$$N_{tu} = hA/\dot{m}c_p \tag{10}$$

$$r_h = LA_g/A, \tag{11}$$

where A is the total heat transfer area, we can express N_{tu} in terms of N_{st} as

$$N_{tu} = N_{st}L/r_h. \tag{12}$$

Rearranging eq. (12) and substituting into eq. (9) for N_{st} allows us to write for the gas cross-sectional area

$$A_g/\dot{m} = [N_{tu}N_{pr}^{2/3}/2\alpha\rho\Delta P]^{\frac{1}{2}}. \tag{13}$$

Equation (13) is one of the most important equations in the design of a heat exchanger, whether it is regenerative or recuperative. It gives the gas cross-sectional area needed to achieve a given N_{tu} for a fixed value of ΔP across the exchanger. Equation (13) also shows that A_g should be linearly proportional to $\dot{m}$ and that a large α means a small A_g. The term α is nearly constant for a given heat exchanger packing and is taken from figure 2. An average value of ρ must be used when large temperature differences occur from one end to the other. In dealing with a mass flow rate that is not constant, e.g. sinusoidal flow, the average $\dot{m}$ should be used to determine A_g. Likewise the ΔP then corresponds to the average $\dot{m}$ and not the peak.

3.3 Regenerator length, L

Equation (13) shows that V_{rg} could be made as small as desired by using a short regenerator. However conduction in the regenerator would then become large. We now calculate the length assoicated with the given value of $\dot{Q}_c/\dot{Q}_r$. By definition

$$\dot{Q}_c = (A_m/L) \int_{T_L}^{T_U} k dT, \tag{14}$$

where A_m is the regenerator solid or matrix cross-sectional area and k is its thermal conductivity. The term A_m is related to A_g through the porosity n_g by

$$n_g = A_g/(A_m + A_g). \tag{15}$$

Equations (15) and (6) are substituted into eq. (14) to yield

$$L = \frac{2(A_g/\dot{m})(1 - n_g) \int k dT}{n_g c_r (\dot{Q}_c/\dot{Q}_r)}. \tag{16}$$

For some packing configurations n_g is fixed, such as packed spheres or stacked screens. In those cases, L can then be calculated from the known input parameter $\dot{Q}_c/\dot{Q}_r$. For other configurations, such as gaps, the porosity is entirely flexible and L cannot be calculated until the porosity is first calculated. Note that eq. (16) also applies to either recuperative or regenerative heat exchangers, since the C_r/C_f term has not been used.

3.4 Porosity, n_g

In configurations where the porosity is flexible, additional matrix heat capacity can be obtained by adding more matrix material and still keeping A_g constant. However, at some point conduction effects become important. The regenerator matrix heat capacity is given by

$$C_r = V_m \rho_m c_m, \tag{17}$$

where ρ_m is the matrix density, c_m is the matrix specific heat, and V_m is the matrix volume

$$V_m = A_m L. \tag{18}$$

Equation (15) is used to express V_m in terms of A_g by

$$V_m = A_g L(1 - n_g)/n_g. \tag{19}$$

Substitution of eq. (19) into eq. (17) gives

$$C_r = \rho_m c_m A_g L(1 - n_g)/n_g. \tag{20}$$

The heat capacity of the fluid that passes through the regenerator is

$$C_f = \dot{m} c_p \tau/2 = \dot{m} c_p/2\nu, \tag{21}$$

where τ is the period of one cycle and ν is the frequency of operation for the regenerative cryocooler. The use of eq. (21) now restricts subsequent results to regenerative heat exchangers. When eq. (20) is divided by eq. (21) and rearranged the result is

$$n_g/(1 - n_g) = 2\nu(\rho_m c_m)(A_g/\dot{m})L/c_p(C_r/C_f). \tag{22}$$

For simplicity in subsequent calculations we define X as

$$X = n_g/(1-n_g) \tag{23}$$

or

$$n_g = X/(1 + X) \tag{24}$$

The length in eq. (16) is substituted into eq. (22) to yield

$$X = 2(A_g/\dot{m}) \left[\frac{\nu(\rho_m c_m)\int k dT}{c_p q_r (C_r/C_f)(\dot{Q}_c/\dot{Q}_r)}\right]^{\frac{1}{2}} \tag{25}$$

In calculating n_g the ratio C_r/C_f is assumed to be known from the performance curves in figure 3, although any combination of N_{tu} and C_r/C_f can be used. The optimum combination is yet to be determined. Equations (24) and (25) show that the porosity is independent of the refrigerator capacity since $(A_g/\dot{m})$ and the other terms are independent of mass flow rate. Likewise the length in eq. (16) is independent of mass flow rate or refrigerator capacity. Also, the porosity equation applies to the case of variable porosity. The proper technique for dealing with a fixed porosity is discussed in section 5.

3.5 Regenerator gas volume, V_{rg}

With A_g and L already determined, V_{rg} is easily calculated. However the ratio V_{rg}/V_e needs to be calculated to determine what effect V_{rg} will have on the system. The volume of gas in the regenerator void space can be given by

$$V_{rg} = XV_m \tag{26}$$

The matrix volume can be expressed as

$$V_m = C_r/\rho_m c_m, \tag{27}$$

which means eq. (26) becomes

$$V_{rg} = XC_r/\rho_m c_m. \tag{28}$$

The expansion space volume is given by

$$V_e = C_f/\rho_e c_p, \tag{29}$$

where ρ_e is the density of gas in the expansion space. The term ρ_e should be evaluated at the temperature and pressure of the expansion space at the time of flow reversal. For a first approximation the lower temperature T_L and the average pressure are used. From eqs. (28) and (29) the volume ratio becomes

$$V_{rg}/V_e = X(C_r/C_f)\rho_e c_p/(\rho_m c_m) \tag{30}$$

This simple expression for V_{rg}/V_e is useful when X has already been calculated. However, since the optimum N_{tu} and C_r/C_f have not been selected, we now develop an expression, for V_{rg}/V_e in terms of N_{tu} and C_r/C_f. We substitute eq. (25) for X into eq. (30), and at the same time eq. (13) is used for $A_g/\dot{m}$ in the expression for X. The resultant volume ratio becomes

$$V_{rg}/V_e = p_e \left[\frac{2N_{tu}(C_r/C_f)N_{pr}^{2/3}\nu c_p \int k dT}{\alpha \rho \Delta P q_r (\dot{Q}_c/\dot{Q}_r)(p_m c_m)} \right]^{\frac{1}{2}} \tag{31}$$

It now becomes clear how V_{rg}/V_e depends on the various input and material parameters and the packing configuration. The volume ratio is minimized when the configurational parameter α is largest. Figure 2 shows that gaps offer the largest α for the configurations compared. The authors are unaware of other configurations with a higher α. Of course, the equations derived here are valid if one chooses to use a configuration with a smaller α. In regard to matrix material parameters, the ratio $[\int k dT/(\rho_m c_m)]^{\frac{1}{2}}$ should be minimized. The input parameters $\Delta P/P$ and $\dot{Q}_c/\dot{Q}_r$ should be made large to reduce V_{rg}/V_e but they cannot be made larger than about 0.1-0.2.

A minimum value for V_{rg}/V_e is obtained when the product $N_{tu}(C_r/C_f)$ is a minimum. Figure 5 shows curves of $N_{tu}(C_r/C_f)$ vs. (C_r/C_f) for various values of ineffectiveness. We see from figure 5 that $C_r/C_f = 1.8$ gives a minimum in $N_{tu}(C_r/C_f)$ for all values of $1 - \varepsilon$ shown. The curves of figure 5 are subject to some uncertainty since they were derived from the graph in figure 3 rather than using numerical calculations. Fortunately the minimum in $N_{tu}(C_r/C_f)$ is fairly broad so some uncertainty can be tolerated. The calculation of $(A_g/\dot{m})$, L, n_g, and V_{rg}/V_e is now done using the optimum N_{tu} and C_r/C_f combination from figure 5.

For an ideal gas and isothermal expansion we have

$$\rho = P/RT \tag{32}$$

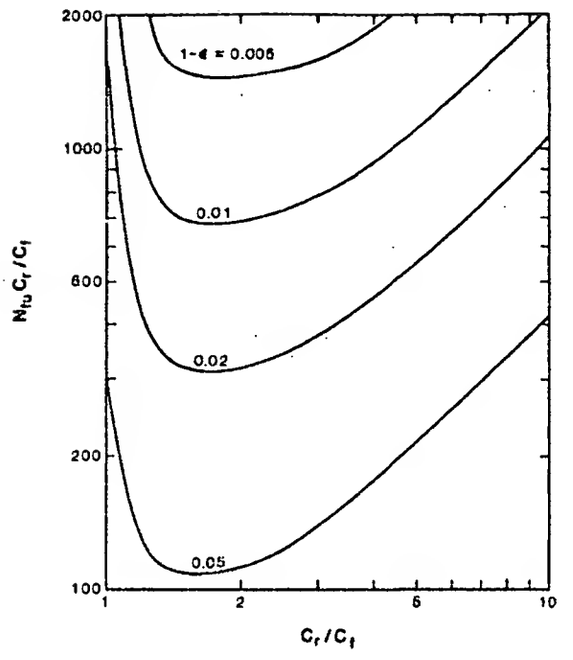

Figure 5. The $N_{tu}(C_r/C_r)$ product for several values of regenerator ineffectiveness from the case of zero void volume.

$$\rho_e = P/RT_e \quad . \tag{33}$$

$$q_r = RT_e \ell n(P_h/P_\ell), \tag{34}$$

where R is the gas constant, P is the average pressure, P_h is the high pressure, P_ℓ is the low pressure, and T_e is the expansion space temperature. (Usually $T_e = T_L$). Then eq. (31) becomes

$$V_{rg}/V_e = \frac{1}{RT_e}\left[\frac{2N_{tu}(C_r/C_f)N_{pr}^{2/3}c_p T\nu\int k dT}{T_e\alpha(\rho_m c_m)(\dot{Q}_c/\dot{Q}_r)(\Delta P/P)\ln(P_h/P_\ell)}\right]^{\frac{1}{2}} \tag{35}$$

for an ideal gas and isothermal expansion.

Equation (35) shows that the volume ratio is independent of pressure and will increase as the temperature T_e is lowered. For the optimum $(C_r/C_f) = 1.8$, the ineffectiveness is approximately

$$1 - \varepsilon = 2.1N_{tu}^{-0.9}, \tag{36}$$

for $N_{tu} > 50$. The term N_{tu} is then proportional to $(1 - \varepsilon)^{-1.1}$ and using eq. (7) for $(1 - \varepsilon)$ shows N_{tu} is proportional to $(\dot{Q}_{reg}/\dot{Q}_r)^{-1.1}$. The denominator inside the brackets of eqs. (31) and (35) subsequently contains the three input parameters in the form of $(\dot{Q}_{reg}/\dot{Q}_r)^{1.1}(\dot{Q}_c/\dot{Q}_r)(\Delta P/P)$. Such an expression would suggest that $(\dot{Q}_{reg}/\dot{Q}_r)$ should be larger than the other terms for minimizing V_{rg}/V_e.

There may be instances where the total regenerator volume is to be minimized. This possibility may occur when there are external packaging constraints or in cases where no pressure wave exists. For instance, regenerators used in magnetic refrigerators operate at constant pressure. Here, the void volume is often of little concern. Of more importance is the total regenerator volume, since it may need to fit inside a magnetic field region. The total regenerator volume, V_{rt}, can be expressed in reduced units by

$$V_{rt}/V_e = V_{rg}/V_e n_g. \tag{37}$$

The use of eqs. (24), (25), and (30) leads to

$$V_{rt}/V_e = \frac{\rho_e (C_r/C_f) c_p}{(\rho_m c_m)} + \rho_e \left[\frac{2N_{tu}(C_r/C_f)N_{pr}^{2/3} \nu c_p \int k dT}{\alpha \rho \Delta P q_r (\dot{Q}_c/\dot{Q}_r)(\rho_m c_m)} \right]^{\frac{1}{2}}. \tag{38}$$

The first term on the right hand side of eq. (38) is the reduced matrix volume and the second term is V_{rg}/V_e of eq. (31). It is now apparent that the minimum in V_{rt}/V_e occurs at a smaller value of (C_r/C_f) than the 1.8 used for V_{rg}/V_e, and the N_{tu} will be higher than for that case.

3.6 Hydraulic radius

Here we derive the hydraulic radius and other characteristic dimensions of the regenerator packing that must be used to give the desired N_{tu} in a regenerator with a length and cross-sectional area as previously calculated. When both sides of eq. (12) are multiplied by $N_{pr}^{2/3}$ and rearranged, the result is

$$N_{st}N_{pr}^{2/3} = N_{tu}N_{pr}^{2/3} r_h/L. \tag{39}$$

The Reynolds number is defined as

$$N_r = 4r_h/\mu(A_g/\dot{m}), \tag{40}$$

where μ is the gas viscosity.

For every geometry of interest there is some function g where

$$N_{st}N_{pr}^{2/3} = g(N_r). \tag{41}$$

Equations (39-41) represent three equations in the three unknowns, r_h, N_r, and $N_{st}N_{pr}^{2/3}$ that must be solved numerically in the general case. When g is in graphical form, the solution is easily found by trial and error. For a chosen value of r_h, eq. (39) is used to find $N_{st}N_{pr}^{2/3}$. The same value of r_h gives N_r from eq. (40) which in turn gives a value of $N_{st}N_{pr}^{2/3}$ from the graph of eq. (41). If the two values of $N_{st}N_{pr}^{2/3}$ do not agree, another value of r_h is chosen until the two $N_{st}N_{pr}^{2/3}$ values agree.

For laminar flow, eq. (41) is

$$N_{st}N_{pr}^{2/3} = a/N_r, \tag{42}$$

where a is a constant depending on geometry. For infinitely wide and long gaps with constant temperature heat transfer, a = 8.5. For infinitely long tubes, a = 4.2. Equations (39), (40), and (41) are solved then by

$$r_h = \left[\frac{aL\mu(A_g/\dot{m})}{4N_{tu}N_{pr}^{2/3}}\right]^{1/2} \tag{43}$$

In the high-performance heat exchangers discussed here, the flow is usually laminar. The value of α in figure 2 can be refined with N_r if necessary. Since α is only a weak function of N_r, further iterations may not be necessary.

The characteristic dimension of a heat exchanger may be expressed in terms of the hydraulic radius. They are given for various geometries as follows:

$$t_g = 2r_h \quad \text{gap thickness} \tag{44}$$

$$d = 4r_h \quad \text{tube diameter} \tag{45}$$

$$d = 6r_h/X \quad \text{sphere diameter} \tag{46}$$

$$d = 4r_h/X \quad \text{wire diameter.} \tag{47}$$

For a gap configuration the thickness of the plates that comprise the matrix is

$$t_m = t_g/X. \tag{48}$$

For all of the preceding calculations to be valid, the thermal penetration depth λ must be large enough to penetrate throughout the matrix. For a semi-infinite plate the thermal penetration depth for sinusoidal heat flow is

$$\lambda = [k/(\rho_m c_m)\pi\nu]^{\frac{1}{2}}. \tag{49}$$

For a set of stacked plates with gas on both sides we require

$$t_m < 2\lambda. \tag{50}$$

3.7 Equation summary

As an aid to computations for regenerators, the significant steps and equations are summarized in the order necessary for a regenerator with flexible porosity.

1. Determine largest input parameters $\dot{Q}_{reg}/\dot{Q}_r$, $\dot{Q}_c/\dot{Q}_r$, $\Delta P/P$ the overall system can tolerate.
2. Evaluate system and material parameters ν, T_U, T_L, R, P, q_r, ρ, ρ_e, c_p, N_{pr}, μ, $(\rho_m c_m)$, and $\int k dT$.
3. Ineffectiveness: $1 - \varepsilon = (\dot{Q}_{reg}/\dot{Q}_r)q_r/2(H_U - H_L)$.
4. From figure 3 or 5 determine: N_{tu} at $C_r/C_f = 1.8$.
5. Determine packing parameters α from figure 2 and laminar coefficient a in eq. (42).
6. Gas cross-sectional area: $A_g/\dot{m} = [N_{tu}N_{pr}^{2/3}/2\alpha\rho\Delta P]^{\frac{1}{2}}$.
7. Porosity: $n_g = X/(1 + X)$,

$$X = 2(A_g/\dot{m}) \left[\frac{\nu(\rho_m c_m)\int k dT}{c_p q_r (C_r/C_f)(\dot{Q}_c \dot{Q}_r)}\right]^{\frac{1}{2}}.$$

(in original parameters) $$X = 2\left[\frac{N_{tu}N_{pr}^{2/3}\nu(\rho_m c_m)\int k dT}{2\alpha\rho\Delta P c_p q_r (C_r/C_f)(\dot{Q}_c/\dot{Q}_r)}\right]^{\frac{1}{2}} \quad (51)$$

8. Regenerator gas volume: $V_{rg}/V_e = X(C_r/C_f)c_p\rho_e/(\rho_m c_m)$.

(in original parameters) $$V_{rg}/V_e = \rho_e\left[\frac{2N_{tu}(C_r/C_f)N_{pr}^{2/3}\nu c_p\int k dT}{\alpha\rho\Delta P q_r(\dot{Q}_c/\dot{Q}_r)(\rho_m/c_m)}\right]^{\frac{1}{2}}$$

9. Regenerator length: $L = 2(A_g/\dot{m})\int k dT/X q_r(\dot{Q}_c/\dot{Q}_r)$.

(in original parameters) $$L = \left[\frac{c_p(C_r/C_f)\int k dT}{\nu(\rho_m c_m)q_r(\dot{Q}_c/\dot{Q}_r)}\right]^{\frac{1}{2}} \quad (52)$$

10. Hydraulic radius: $r_h = \left[\frac{aL\mu(A_g/\dot{m})}{4N_{tu}N_{pr}^{2/3}}\right]^{\frac{1}{2}}$, <u>laminar flow</u>.

(in original parameters) $$r_h = (a\mu)^{\frac{1}{2}}\left[\frac{c_p(C_r/C_f)\int k dT}{2\alpha\rho\Delta P N_{tu}N_{pr}^{2/3}\nu(\rho_m c_m)q_r(\dot{Q}_c/\dot{Q}_r)}\right]^{\frac{1}{3}} \quad (53)$$

11. Reynolds number: $N_r = 4r_h/\mu(A_g/\dot{m})$
Recalculate r_h if flow not laminar.

12. Reevaluate α. If necessary, repeat from step 6.

13. For gaps: $t_g = 2r_h$, $t_m = t_g/X$

14. Thermal penetration depth in plates: $\lambda = [k/(\rho_m c_m)\pi\nu]^{\frac{1}{2}}$, <u>sinusoidal flow</u>.

15. Check to see if: $t_m < 2\lambda$.
If not, increase ν to decrease t_m.

16. Error check: (a) $\Delta P = fL/2\rho r_h(A_g/\dot{m})^2$,
with f from figure 1 or similar curve.
Calculated value should equal input value.

(b) $V_{rg}/V_e = 2(A_g/\dot{m})L\nu\rho_e$,
should be same as from step 8.

4. Example solutions

The solution to the design equations can best be illustrated through some examples. In the design of a cryocooler for a SQUID, nonmagnetic and nonmetallic parts need to be used in the cold parts to prevent magnetic noise. The regenerator material chosen for this illustration is G-10 fiberglass epoxy. Even though its volumetric heat capacity is small compared with lead and other regenerator materials, its very low thermal conductivity gives it a desirably small value of $k/\rho_m c_m$, the important material parameter which appears in eq. (31). In fact G-10 may have a lower $k/\rho_m c_m$ than Pb-5% Sb although k for the latter has not been measured.

The parameters chosen for the example solution are given in table 1.

Table 1. Input parameters for example solutions

$1 - \varepsilon = 0.01$ $(\dot{Q}_{reg}/\dot{Q}_r = 0.22)$	$T_U = 4T_L$
$\dot{Q}_c/\dot{Q}_r = 0.1$	$\alpha = 0.35$ (gap)
$\Delta P/P = 0.05$	regenerator material: G-10
$P = 0.5$ MPa	fluid: ideal helium gas
$P_h/P_\ell = 2.0$	isothermal expansion

The temperature T_L is allowed to vary from 4 K to 100 K to evaluate the temperature dependence of the optimum geometry. The upper temperature T_U of the regenerator is assumed to be $4T_L$, which is typical for cryocoolers. Such a dependence of T_U on T_L means that eq. (7) may be written as

$$1 - \varepsilon = (\dot{Q}_{reg}/\dot{Q}_r)q_r/6c_pT_L \tag{54}$$

for the case of an ideal gas. Also, for an ideal gas q_r from eq. (34) can be substituted into eq. (54), and for the normal case of $T_e = T_L$, we obtain

$$1 - \varepsilon = (\dot{Q}_{reg}/\dot{Q}_r)R\ell n(P_h/P_\ell)/6c_p \tag{55}$$

For the input parameters in table 1, $(\dot{Q}_{reg}/\dot{Q}_r) = 0.22$ from eq. (55).

The material parameters needed in the calculations are $(\rho_m c_m)$ and $\int k dT$. Figure 6 shows $(\rho_m c_m)$ for G-10 fiberglass-epoxy, Pb [13], and GdRh [14]. The alloy Pb + 5% Sb is commonly used as a regenerator material and GdRh is a potential regenerator material because of its high specific heat $(\rho_m c_m)$ at low temperatures. The thermal conductivity of G-10 is the average of the parallel and perpendicular heat flow directions from the work of Kasen, et al. [15]. Table 2 gives representative values of $(\rho_m c_m)$, k, and $\int k dT$ used in our calculations.

For the ideal helium gas we use $c_p = 5.19$ J/g·K, $R = 2.077$ J/g·K, $N_{pr} = 0.666$. The viscosity values from McCarty [16] are nearly independent of pressure over the range we have considered and are approximated by $\mu = 5.0 \times 10^{-6} + 4.6 \times 10^{-6}T^{0.65}$ g/cm.s over the range of 10-300 K.

Figure 7 shows $(A_g/\dot{m})$ and the length of the regenerator as a function of T_L for three different frequencies. The term $(A_g/\dot{m})$ is independent of frequency. The porosity, n_g, and the volume ratio, V_{rg}/V_e, are shown in figure 8.

Note that the optimum porosity is on the order of 0.01 for $T_L = 5$K. Such a low porosity allows a large volume of regenerator material to be used to obtain a reasonably high total heat capacity. The volume ratio V_{rg}/V_e is insignificant at higher temperatures and remains smaller

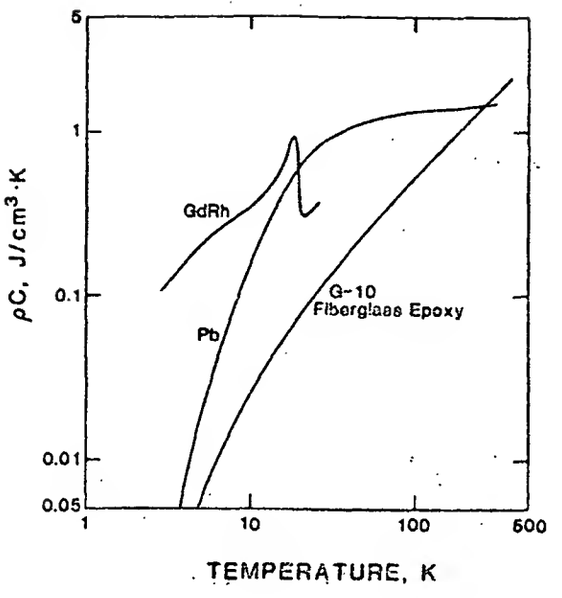

Figure 6. The volumetric heat capacity of candidate regenerator materials.

Table 2. Thermal properties of G-10 fiberglass epoxy

T (K)	$\rho_m c_m$ (J/cm³·K)	k (W/cm·K)	$\int_0^T k dT$ (W/cm)
5	0.0058	0.815×10^{-3}	2.00×10^{-3}
10	0.0255	1.24×10^{-3}	7.23×10^{-3}
20	0.078	1.73×10^{-3}	22.3×10^{-3}
50	0.245	2.66×10^{-3}	89.1×10^{-3}
100	0.520	3.76×10^{-3}	$251. \times 10^{-3}$
200	1.10	5.53×10^{-3}	$718. \times 10^{-3}$
300	1.64	7.17×10^{-3}	$1355. \times 10^{-3}$

than 1.0 even at T_L = 5K. For the case of ν = 1 Hz the volume ratio is small enough that the assumption of zero void volume in the performance curve of figure 3 may hold. For higher frequencies, a more realistic performance curve probably should be used for the lowest temperatures. The small values of V_{rg}/V_e also imply that the entire process for refrigeration at 4-5 K is feasible with an ideal gas. (Calculations for a real gas are easily done but are not shown here.)

Figure 9 shows the gap and matrix thicknesses as a function of T_L. Shown for comparison with the matrix thickness, t_m, is the thermal penetration depth, 2λ. For all cases except at 1 Hz and the lowest temperature $t_m << 2\lambda$. When $t_m \cong 2\lambda$, there will be a slight degredation in regenerator performance because the term C_r will be reduced. The gap thickness has a slight dependence on temperature and is in the range of 10^{-3} cm. An extremely small t_g could present some practical problems in the construction of the regenerator. The Reynolds number also is very small - in the range of 10-200 - with higher values occurring at lower temperatures and lower frequencies.

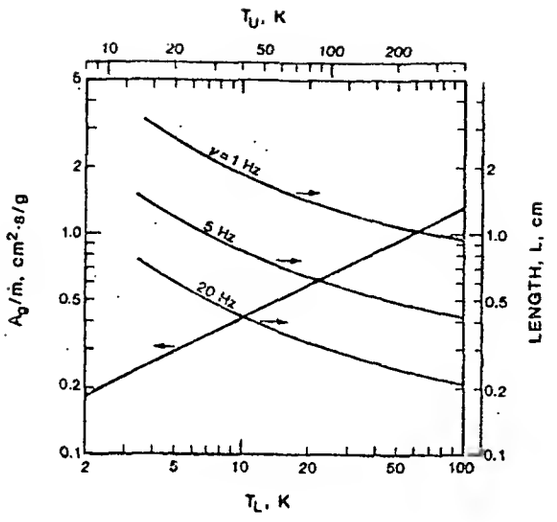

Figure 7. The calculated gas cross-sectional area per unit mass flow, and the regenerator length for the conditions in table 1.

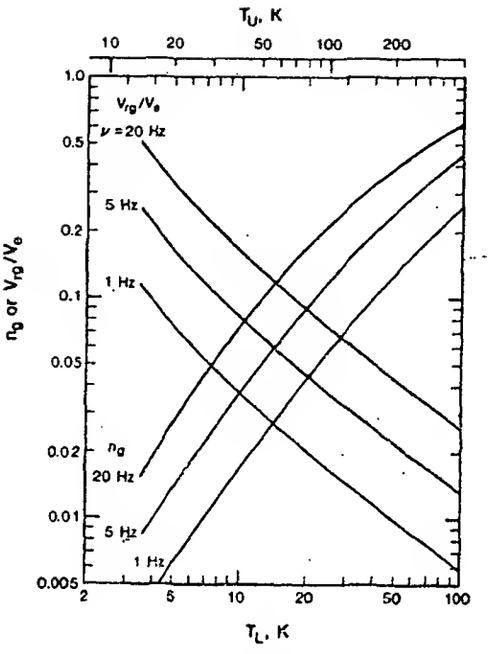

Figure 8. The calculated porosity and the reduced regenerator gas volume for the conditions in table 1.

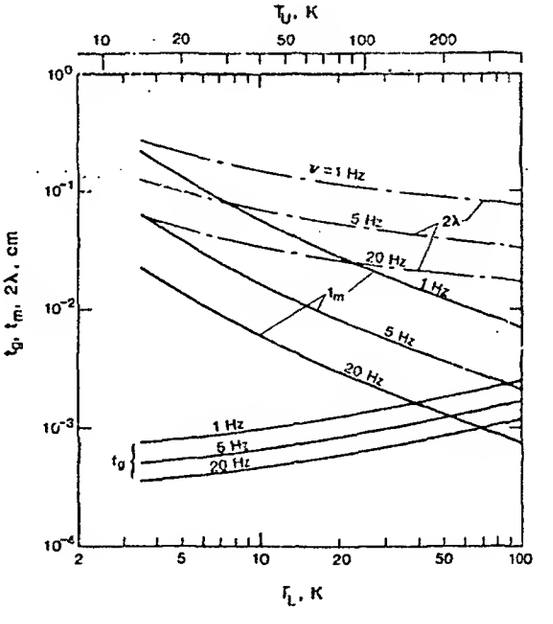

Figure 9. The calculated gap thickness, matrix thickness and thermal penetration depth in the regenerator with conditions in table 1.

5. Comparison of gap and packed sphere configurations

Packed spheres are commonly used for regenerator packings since such regenerators are simple to make. However α is significantly lower for packed spheres than for gaps. Also, the porosity of packed spheres is fixed at about 0.38, which is much higher than optimum for temperatures below about 50 K according to figure 8. In this section we show how much inferior a packed sphere bed is in comparison with the gap configuration. Of course, the packed sphere bed still has the advantage of simplicity. For a fixed n_g, eq. (51) is solved for the ratio $N_{tu}/(C_r/C_f)$. The optimum values for N_{tu} and C_r/C_f are found by simultaneous solution with the $N_{tu}(C_r/C_f)$ curves of figure 5. This approach maintains $(\dot{Q}_c/\dot{Q}_r)$ at the fixed input of value. Included in the assumptions is that $\int k dT$ for spheres is the same as for the bulk material. After N_{tu} and C_r/C_f are determined, the parameters $A_g/\dot{m}$, L, V_{rg}/V_c, and r_h are calculated from the appropriate equations.

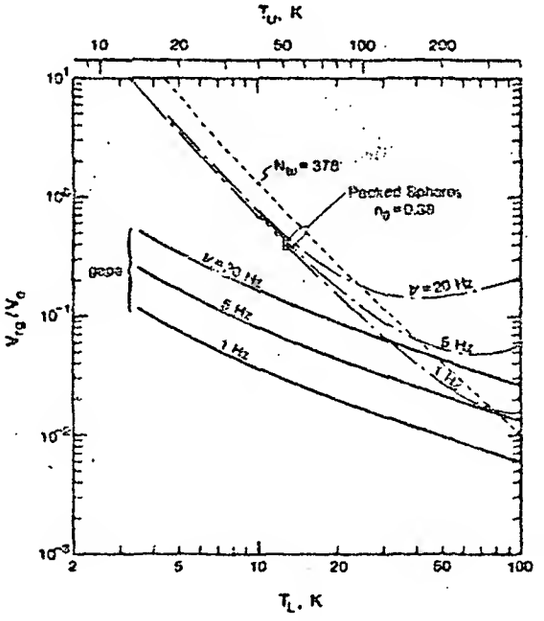

Figure 10. The reduced regenerator gas volume for gaps and for packed spheres. See test for details of packed-sphere curves.

Figure 10 shows V_{rg}/V_e for both packed spheres of G-10 and gaps between plates of G-10. At higher temperatures the difference between the two sets of curves is mainly due to the higher α for gaps. At lower temperatures the much smaller V_{rg}/V_e for gaps is due to both the higher α and the lower porosity. Also shown in figure 10 for packed spheres is the curve labeled $N_{tu} = 378$, which is the value used for the gaps. At higher temperatures this curve gives a lower V_{rg}/V_e because $\dot{Q}_c/\dot{Q}_r$ is greater than 0.1. At lower temperatures the reverse is true, and $\dot{Q}_c/\dot{Q}_r$ is less than 0.1. Wherever the packed-sphere curves are below the $N_{tu} = 378$ curve, the N_{tu} is greater than 378. In fact, for temperatures less than 15 K the N_{tu} is rapidly approaching numbers as high as 10^5, a practical impossibility. Even an N_{tu} of 378 may be difficult to achieve in practice without extreme care in making all flow channels the same size. If a smaller $\int k dT$ is used in the calculations of the packed powder, an even higher N_{tu} is needed for the optimum condition. However, the reduction in V_{rg}/V_e is insignificant at temperatures below about 15 K. The $N_{tu} = 378$ curve should be considered a lower practical limit for the V_{rg}/V_e of the packed spheres.

6. Conclusions

A simple scheme for optimizing regenerators in cryocoolers has been developed which uses the system loss terms, $\dot{Q}_{reg}/\dot{Q}_r$, $\dot{Q}_c/\dot{Q}_r$, and $\Delta P/P$ as input parameters. Any set of regenerator performance curves can be used, although the examples discussed here use the simplest one of zero void volume. A set of equations were developed to determine the regenerator geometry that yields the minimum void volume. In comparison with other packing configurations It is shown that gaps between parallel plates is the best, producing regenerator dead volumes one to two orders of magnitude smaller for temperatures in the range of 5-10 K. It is shown that G-10 fiberglass-epoxy is a favorable material for a multiple gap regenerator because of its relatively low $k/\rho_m c_m$ ratio.

The authors are grateful to David Daney and James Zimmerman, both of NBS, for some valuable discussions. Debra Schlender is acknowledged for careful preparation of the manuscript.

7. References

[1] Lambertson, T. J., Performance factors of a periodic-flow heat exchanger, Trans. ASME 80, 586-592 (1958).

[2] Hausen, H., in Wärmeübertragung im Gegenstrom, Gleichstrom und Kreuzstrom (Springer-Verlag, Berlin, 1950).

[3] Kays, W. M., and London, A. L., in Compact Heat Exchangers, 2nd ed. (McGraw-Hill Book Co., New York, 1964).

[4] Schmidt, F. W., and Willmott, A. J., in Thermal Energy Storage and Regeneration, 114 (McGraw-Hill Book Co., New York, 1981).

[5] Heggs, P. J. and Carpenter, K. J., The effect of fluid hold-up on the effectiveness of contraflow regenerators, Trans. Instn. Chem. Engrs. 54, 232-238 (1976).

[6] Daney, D. E., and Radebaugh, R., Non-ideal regenerator performance - the effect of void volume fluid heat capacity, Cryogenics 24, 499-501, (1984).

[7] Gary, J. M., Radebaugh, R., and Daney, D. E., A numerical model for a regenerator, Proc. 3rd Cryocooler Conf. (this publication, 1985).

[8] Qvale, E. G., and Smith, J. L., Jr., Trans. ASME, J. Eng. for Power, 91A, 109 (1969).

[9] Rios, P. A., Smith, J. L., Jr., Qvale, E. G., An analysis of the Stirling-cycle refrigerator, in Advances in Cryogenic Engineering, Vol. 14, 332-342 (Plenum Press, New York, 1969).

[10] Rios, P. A., and Smith, J. L., Jr., An analytical and experimental evaluation of the pressure-drop losses in the Stirling cycle, ASME paper no. 69-WA/Ener-8, ASME, New York (1969).

[11] Harris, W. S., Rios, P. A., and Smith, J. L., Jr., The design of thermal regenerators for Stirling-type refrigerators, in Advances in Cryogenic Engineering, Vol. 16, 312-322 (Plenum Press, New York, 1971).

[12] Walker, G., in Cryocoolers, part 1: Fundamentals, 126-127 (Plenum Press, New York, 1983).

[13] Johnson, V. J., A compendium of the properties of materials at low temperatures (phase I), part II. Properties of Solids, Wright Air Development Division Technical Report 60-56 (1960).

[14] Buschow, K. H. J., Olijhoek, J. F., and Miedema, A. R., Extremely large heat capacities between 4 and 10 K, Cryogenics 15, 261-264 (1975).

[15] Kasen, M. B., MacDonald, G. R., Beekman, D. H., Jr., and Schramm, R. E., Mechanical, electrical, and thermal characterization of G-10CR and G-11CR glasscloth/epoxy laminates between room temperature and 4K, in Advances in Cryogenic Engineering, Vol. 26, 235-244 (Plenum Press, New York, 1980).

[16] McCarty, R. D., Thermophysical properties of helium-4 from 2 to 1500 K with pressures to 1000 atmospheres, NBS Technical Note 631 (1972).

8. Nomenclature

English letter symbols		SI units
A	regenerator total heat transfer area	m^2
A_g	gas cross-sectional area	m^2
A_m	matrix cross-sectional area	m^2
a	geometrical constant for laminar flow	
C_f	heat capacity of fluid passed through regenerator	J/K
C_r	heat capacity of regenerator matrix	J/K
C_{void}	heat capacity of gas in regenerator void volume	J/K
c_m	specific heat of matrix	J/kg·K
c_p	specific heat at constant pressure of gas	J/kg·K
d	tube, sphere, or wire diameter	m
f	friction factor	
H_U, H_L	specific enthalpies at T_U and T_L	J/kg
h	heat transfer coefficient	$W/m^2 \cdot K$
k	thermal conductivity of matrix	W/m·K
L	length of regenerator	m
$\dot{m}$	mass flow rate of gas through regenerator	kg/s

N_{pr}	Prandtl number, a fluid properties modulus	
N_r	Reynolds number, a flow modulus	
N_{st}	Stanton number, a heat transfer modulus	
N_{tu}	Number of heat transfer units per half cycle	
n_g	porosity of regenerator = $A_g/(A_g + A_m)$	
P	average pressure	Pa
P_h, P_ℓ	high and low pressures	Pa
ΔP	pressure drop in regenerator	Pa
$\dot{Q}_c$	conduction heat loss	W
$\dot{Q}_h$	enthalpy deficit loss	W
$\dot{Q}_{net}$	net refrigeration power	W
$\dot{Q}_r$	gross refrigeration power	W
$\dot{Q}_{rad}$	radiation heat loss	W
$\dot{Q}_{reg}$	regenerator loss	W
$\dot{Q}_s$	shuttle heat loss	W
q_r	heat absorbed per unit mass during expansion	J/kg
R	gas constant	J/kg·K
r_h	hydraulic radius (LA_g/A)	m
T_e	expansion space temperature	K
T_U, T_L	upper and lower temperatures of regenerator	K
t_g	gap thickness	m
t_m	thickness of plates in gap regenerator	m
V_e	maximum expansion space volume	m^3
V_m	matrix volume	m^3
V_{rg}	regenerator void volume	m^3
V_{rt}	regenerator total volume	m^3
X	porosity parameter $[n_g/(1-n_g)]$	

Greek letter symbols

α	ratio of heat transfer and friction terms ($N_{st}N_{pr}^{2/3}/f$)	
ε	regenerator effectiveness	
$1-\varepsilon$	regenerator ineffectiveness	
λ	thermal penetration depth in matrix	m
μ	gas viscosity	kg/m·s
ν	cycle frequency	Hz
ρ	gas density in regenerator	kg/m^3
ρ_e	gas density in expansion space	kg/m^3
ρ_m	matrix density	kg/m^3
τ	period of one cycle	s

D19

A COMPUTATIONAL MODEL FOR A REGENERATOR

John Gary
Scientific Computing Division

David E. Daney
Ray Radebaugh

Chemical Engineering Science Division
National Bureau of Standards
Boulder, Colorado 80303

This paper concerns a numerical model of a regenerator running at very low temperatures. The model consists of the usual three equations for a compressible fluid with an additional equation for a "matrix temperature." The main difficulty with the model is the very low Mach number (approximately 1.E-3). The divergence of the velocity is not small, the pressure divergence is small, and the pressure fluctuation in time is not small. An asymptotic expansion based on the "bounded derivative" method of Kreiss is used to give a "reduced" model which eliminates acoustic waves. The velocity is then determined by a two-point boundary value problem which does not contain a time derivative. The solution obtained from the reduced system is compared with the numerical solution of the original system.

Key words: bounded derivative; compressible flow; cryocoolers; heat transfer; implicit scheme; numerical model; regenerator; stiff equations.

1. The differential equations

The oscillating flow takes place in a cylinder filled with small metal spheres [1]. The compressible flow equations are used to describe the flow around the spheres. A "resistance" term involving the resistance factor F is used to account for the porous media effects. The "matrix" of spheres has a heat capacity and heat can be transferred between the matrix and the gas. This conductance is determined by the coefficient h. The temperature of the matrix is given by T_m. The variables are listed in the appendix. The partial differential equations for these variables are the following.

$$\frac{\partial p}{\partial t} = -u\frac{\partial p}{\partial x} - \rho c^2 \frac{\partial u}{\partial x} + \frac{4G_r h}{D_h}(T_m - T) + \frac{2G_r F}{D_h}\rho|u|^3 \qquad (1)$$

$$\frac{\partial T}{\partial t} = -u\frac{\partial T}{\partial x} - G_r T \frac{\partial u}{\partial x} + \frac{4h}{C_v D_h}\frac{1}{\rho}(T_m - T) + \frac{2F}{C_v D_h}|u|^3 \qquad (2)$$

$$\frac{\partial u}{\partial t} = -u\frac{\partial u}{\partial x} - \frac{1}{\rho}\frac{\partial P}{\partial x} - \frac{2F}{D_h}u|u| \tag{3}$$

$$\frac{\partial T_m}{\partial t} = -\frac{4h\phi}{(1-\phi)\rho_m C_m D_h}(T_m - T) + \frac{\sigma}{\rho_m C_m}\frac{\partial^2 T_m}{\partial x^2} \tag{4}$$

The domain is $0 \leq x \leq L$. We will discuss the boundary and initial conditions in the next section. Their determination is crucial to the success of the numerical approximation.

To set up the numerical approximation we need to write these equations in dimensionless form. For this purpose we assume an ideal gas described by the following relations.

$$\rho = \frac{P}{R_c T} \qquad \rho c^2 = \frac{P}{\gamma} \qquad R_c = 2.03\ E{+}3\ J/kg{\cdot}K \qquad \gamma = 0.6$$

The scaling factors for the basic variables are the constants $(\bar{p}, \bar{u}, \bar{T})$. The time is scaled by the period (t) of the imposed oscillation in the mass flow. This is the same as the period of the piston oscillation. The x coordinate is scaled by the length L. We use $(\hat{p}, \hat{u}, \hat{T}, \hat{T}_m)$ for the scaled variables $(p/\bar{p}, u/\bar{u}, T/\Delta T, T_m/\Delta T)$.

$$\frac{\partial \hat{p}}{\partial t} = -\tau_1 \hat{u}\frac{\partial \hat{p}}{\partial x} - \frac{\tau 1}{\gamma}\hat{p}\frac{\partial \hat{u}}{\partial x} + \alpha_1 h\left(\hat{T}_m - \hat{T}\right) + \frac{\beta_1 \hat{p}\hat{F}}{\hat{T}}|\hat{u}|^3 \tag{5}$$

$$\frac{\partial \hat{T}}{\partial t} = -\tau_2 \hat{u}\frac{\partial \hat{T}}{\partial x} - G_r \tau_2 \hat{T}\frac{\partial \hat{u}}{\partial x} + \alpha_2 \frac{h}{\hat{p}}\left(\hat{T}_m - \hat{T}\right) + \beta_2 \hat{F}|\hat{u}|^3 \tag{6}$$

$$\frac{\partial \hat{u}}{\partial t} = -\tau_2 \hat{u}\frac{\partial \hat{u}}{\partial x} - \frac{1}{\epsilon}\frac{\hat{T}}{\rho}\frac{\partial \hat{p}}{\partial x} + \frac{1}{\epsilon}\frac{\beta_1}{G_r \tau_1}|u|u \tag{7}$$

$$\frac{\partial \hat{T}_m}{\partial t} = -\alpha_3 h\left(\hat{T}_m - \hat{T}\right) \tag{8}$$

Typical values of these dimensionless parameters are:

$\tau_1 = 0.92$	$\tau_2 = 14$	$\alpha_1 = 70$	$\alpha_2 = 709$
$\alpha_3 = 64$	$\beta_1 = 5.8E\text{-}4$	$\beta_2 = 8.7E\text{-}3$	$\varepsilon = 1.4E\text{-}5$

This is based on the values

$\bar{t} = 0.5$ s	$\bar{U} = 0.12$ m/s	$L = 0.057$ m	$R_c = 2.03E+3$ J/kg·K
$G_r = 0.65$	$C_v = 3.1E+3$ j/kg·K	$\bar{h} = 8.7E+3$ W/m^2·K	
$\bar{T} = 15$ K	$D_h = 1.2E\text{-}4$	$\bar{P} = 2$	

Clearly the term with the dominant coefficient is the one containing the factor ε^{-1}. The pressure must be very nearly constant in order to balance the terms in these equations. In order to avoid high velocity sound waves we must carefully set the initial and boundary conditions. The "bounded derivative" method of Kreiss is used to set the initial conditions. We chose the initial conditions so that the first two derivatives of the basic variables with respect to time are $O(1)$ rather than $O(\varepsilon^{-1})$. The work of Kreiss indicates that we can expect the time derivatives to remain bounded during the time integration of the partial differential equations. This implies that the fast sound waves do not appear, since their presence would require derivatives which are $O(\varepsilon^{-1})$.

2. The bounded derivative expansion

This method was developed by Kreiss [4]. Gustafsson has shown that, in certain cases, the results of Kreiss can be obtained by an asymptotic expansion [3]. Gustafsson has given a good expository treatment of the method [2]. If we assume an expansion of the basic variables in the form

$$\hat{p}(x,t) = \hat{p}_0(x,t) + \varepsilon \hat{p}_1(x,t) + \cdots$$

then we obtain a new system of equations for the functions (p_i, T_i, u_i, T_{mi}), $i = 0, 1, \ldots$ by equating like powers of ε in the usual way. Thus, we obtain from the velocity eq (7)

$$\frac{\partial \hat{p}_0}{\partial x} = 0.$$

The first term in the pressure expansion is therefore independent of x. Using this fact, eq (1) can be differentiated with respect to x to obtain an equation for the velocity (hereafter we drop the subscript "o" and the "^" modifier for the asymptotic expansion).

$$\frac{\partial}{\partial x}\left(\rho c^2 \frac{\partial u}{\partial x}\right) = \frac{\partial}{\partial x}\left[\frac{4hG_r}{D_h}(T_m - T) + \frac{2FG\rho|u|^3}{D_h}\right] \tag{9}$$

If the functions T and p are known and u is known at the boundary, then this equation can be solved for $u(x)$ in the interior. Equation (9) implies that the right side of the pressure eq (1) is independent of x. Therefore eq (1) can be regarded as an ordinary differential equation for $p(t)$.

Equation (2) can be regarded as a hyperbolic partial differential equation for $T(t,x)$ and eq (4) is an ordinary differential equation for $T_m(t,x)$. Note that these equations do not require any boundary conditions for the pressure p or the temperature T_m. If we regard the equation for the gas temperature as a hyperbolic equation, then we must specify T at an inflow boundary and leave it unspecified at an outflow boundary. We want to specify constant temperatures $T(t,o) = T_L$ and $T(t,L) = T_R$ at the boundary. However, when the flow reverses this would cause a discontinuity in the temperature at the boundary. Therefore we impose a fast exponential decay in time from the temperature at the time of reversal to the desired temperature T_L or T_R.

The velocity boundary values are chosen so that the mass flow is sinusoidal, that is

$$\rho(t,o)u(t,o) = C_o \sin(\omega t)$$

$$\rho(t,L)u(t,L) = C_L \sin(\omega t+\theta)$$

These conditions insure that mass is conserved over a cycle.

3. The numerical scheme for the asymptotic expansion

A finite difference mesh (t_n,x_i) is used where $t_n = n\Delta t$, and $x_i = iL/N$ for $0 \le i \le N$. The spatial derivatives are approximated by centered second order differences, for example

$$\frac{dT}{dX}(t_n,x_i) \cong \frac{T_{i+1}^n - T_{i-1}^n}{2\Delta x}$$

where T_i^n is the approximation for $T(t_n,x_i)$. An implicit type of predictor corrector is used which is similar to a Crank-Nicolson scheme. We will not write out the complete scheme for the full equations; instead we describe the scheme for the following simple equation

$$\frac{du}{dt} = u\frac{du}{dx}$$

Given the values at the nth time level, U_i^n, and an approximation $\hat{U}_i^o$ for U_i^{n+1}, then compute a corrected approximation $\hat{U}_i^1$ from

$$\frac{\hat{U}_i^1 - \hat{U}_i^n}{\Delta t} = \frac{\left(\hat{U}_i^o + U_i^n\right)}{2} \frac{\left(\hat{U}_{i+1}^1 + U_{i+1}^n - \hat{U}_{i-1}^1 - U_{i-1}^n\right)}{4\Delta x}$$

This is a tridiagonal linear system for the unknown vector $\hat{U}_i^1$. A correction is made for the variables p,T, and T_m in that order; then an updated value of the velocity is obtained by solving a finite difference version of eq (9) for U_i^n. If the heat transfer cofficient, h, is constant, then this is another tridiagonal linear system. If $h = h(u)$ depends on the velocity, then the resulting nonlinear equation is solved by a Newton iteration. The boundary conditions are described in the previous section. Generally, from two to five iterations (or corrections) were used. On the first iteration $\hat{U}_i^o = U_i^n$.

4. A fully implicit scheme for the original equations

We have a second computer code which is based on the original eqs (1) through (4) rather than the asymptotic expansion. Since $M_0^2 = \varepsilon$ is small we expect this sytem to be very stiff. Therefore, we expect that an implicit scheme is required. However, we use a CN (Crank-Nicolson) scheme rather than a BDF (backward-difference-formula). We choose the initial conditions to avoid the fast moving acoustic waves; therefore we do not need the BDF scheme to damp out the fast waves. We can choose arbitrary initial values for T(x,o); however p(x,o) is required to be constant and u(x,o) must satisfy (9). This is the bounded derivative principle of Kreiss. The initial conditions are chosen so that the first two time derivatives of the solution (p, T, u, T_m) at t = 0 are bounded independent of ε.

The finite difference scheme uses three-point centered approximations for the spatial derivatives except at outflow boundaries, where a one-sided first order approximation is used. A Crank-Nicolson approximation is used in time. The difference scheme for each of the four variables is thus similar to (1) for the asymptotic approximation. However, the four equations are now coupled. Therefore, each time step requires the solution of a linear block-tridiagonal system with 4x4 blocks. We do not use a Newton iteration to deal with the nonlinearity. Instead, we use an iteration and evaluate the coefficients of the derivative terms at the previous iteration.

The boundary approximation for the temperature T(x,t) is the same as for the asymptotic equations. The boundary conditions for u(x,t) are specified at all times using the same values as in eq (6). There is no boundary condition for the p equation; instead one-sided differences are used to approximate derivatives at the boundary. No boundary condition is needed for the T_m equation since this equation contains no spatial derivatives.

5. Computational results

In this section we give some results obtained from the two numerical methods described in the previous sections. Unless otherwise stated, the results were obtained using the bounded derivative (i.e. asymptotic expansion) model. Within SI, many units choices exist for most quantities! In all of these runs the heat transfer coefficient between the gas and matrix was given by the term

$$h(m) = 40 \exp(-1.6m) + 220(1-\exp(-1.6m))m$$

where

$$m = \rho|u|.$$

The exponential factor is included to avoid a discontinuous derivative of $h(|\rho u|)$ with respect to to u at u=0.

The formula used to bring the boundary temperature of the gas back to its constant inflow value when the velocity reverses is

$$T(t) = T_L + \left(T_{rev} - T_L\right)\exp\left(\left(t_{rev}-t\right)/\tau\right)$$

Here T_L is the constant inflow temperature (15 K at the left boundary and 10 K at the right boundary for most of our runs) and T_{rev} is the temperature of the gas at the time when the velocity reverses direction. The time of reversal is t_{rev} and τ is an input parameter, whose value was 0.05P where P is the period of the mass flow oscillation.

The mass flow at the boundary is given by

$$\rho u = C \sin(2\pi ft+\theta)$$

where f is the frequency and θ is the phase. At the left boundary $\theta=0$, at the right values in the range $-45^{\circ}\leq\theta\leq 0^{\circ}$ were used.

All runs assumed an ideal gas with equation of state

$$p = Rc\ \rho T.$$

The specific heat of the gas at constant volume was

$$C_v = 3120.\ \ J/kg\cdot K$$

The thermal conductivity of the matrix was 0.3 W/m·K and of the gas was 0.13 W/m·K. The regenerator length was 0.0572 m.

5.1 The temperature and pressure wave forms

The temperature as a function of time at the left and right boundaries is given in figures 1 and 2. In this case, which we refer to as case I, the inflow temperatures at these boundaries were 15 K and 10 K; the mass flow amplitude was 77.9 kg/m^2s; the starting pressure was 3.3 Mpa; the heat capacity of the matrix was 2.64E+5; the hydraulic diameter was 1.21E-4; and the frequency was 5 Hz. The time interval shown is $12\leq t\leq 13$, that is, the system has been run for 60 cycles before these curves are drawn. The matrix temperature is shown as a dashed line; the gas temperature is a solid line. In this case, the two temperatures were almost identical. The temperature at a point 4/5 of the distance across the regenerator ($x=0.8$) is shown in figure 3.

The temperature as a function of position x across the regenerator at certain times in the cycle is shown in figure 4. The pressure oscillation is shown in figure 5.

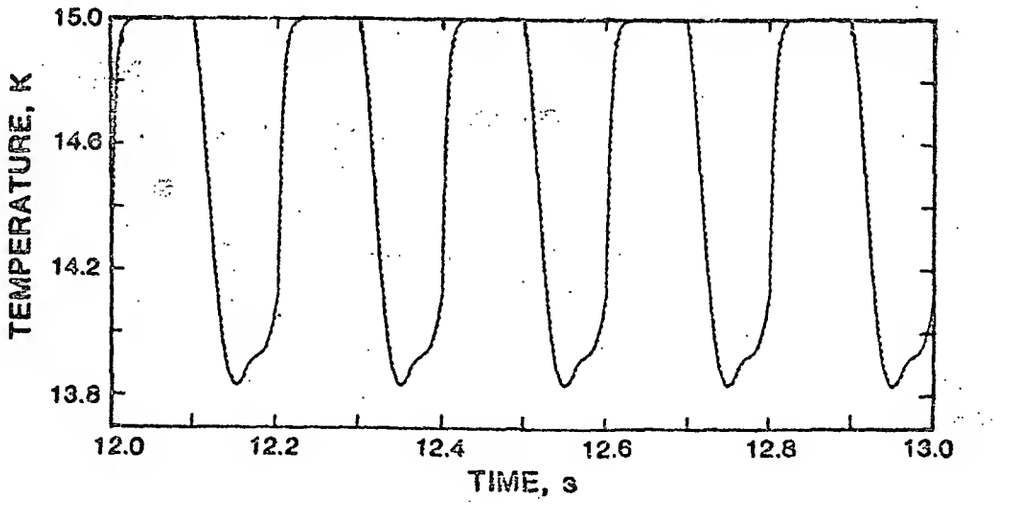

Figure 1. Temperature (K) vs. time (a) at x = 0 for case I.

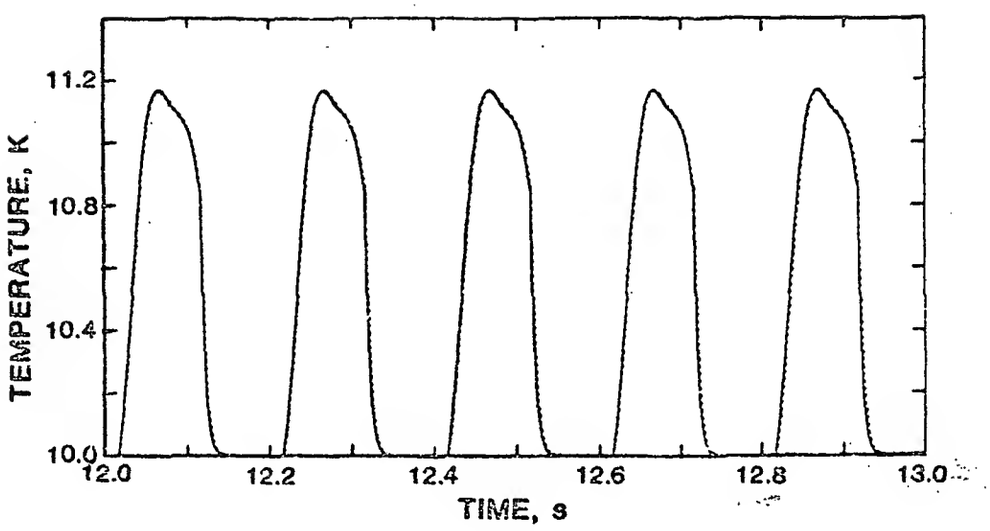

Figure 2. Temperature vs. time at x = 1.0 for case I.

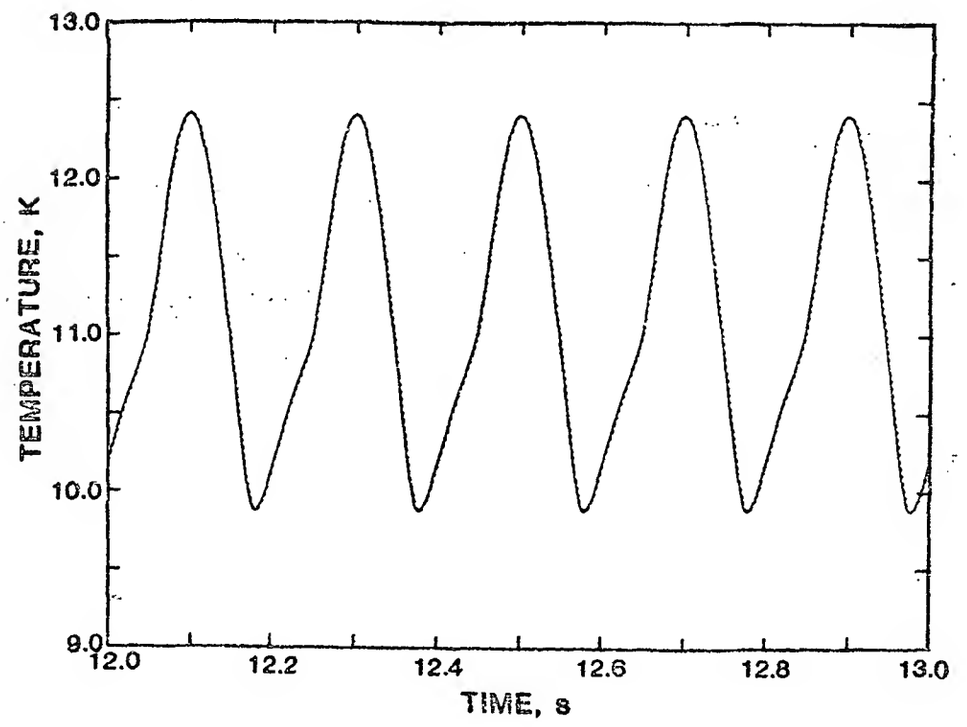

Figure 3. Temperature vs. time at x = 0.8 for case I.

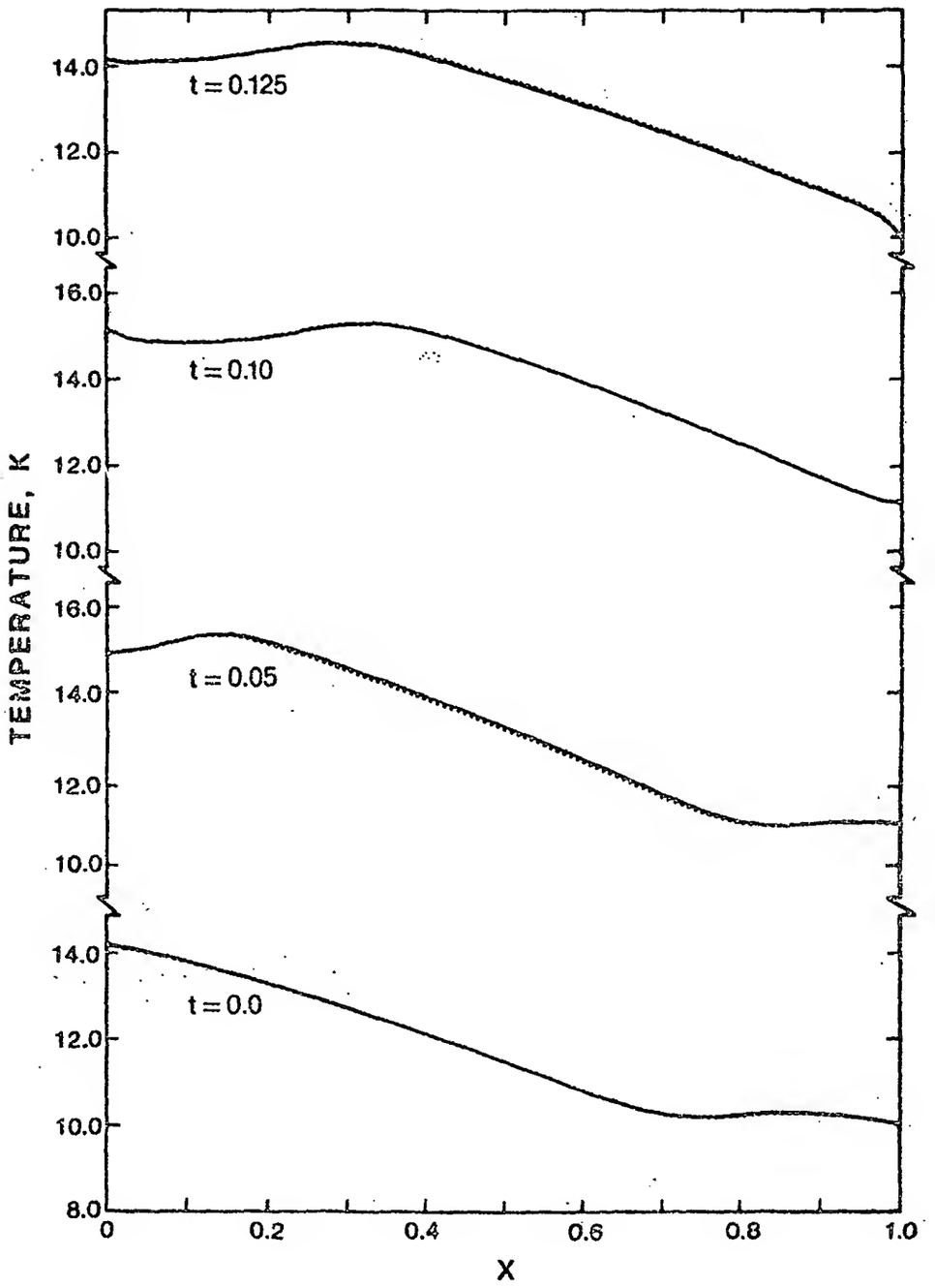

Figure 4. Temperature vs. x at the given t for case I.

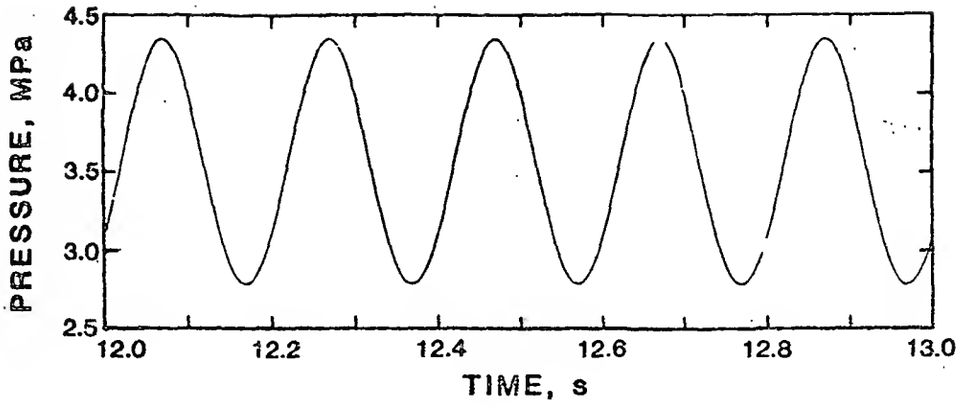

Figure 5. Pressure vs. time for case I.

5.2 The effect of the hydraulic diameter and matrix heat capacity

In figure 6 the temperature wave at the right boundary is shown. All parameters are the same as in case I above, except the hydraulic diameter has been increased by a factor of four. There is

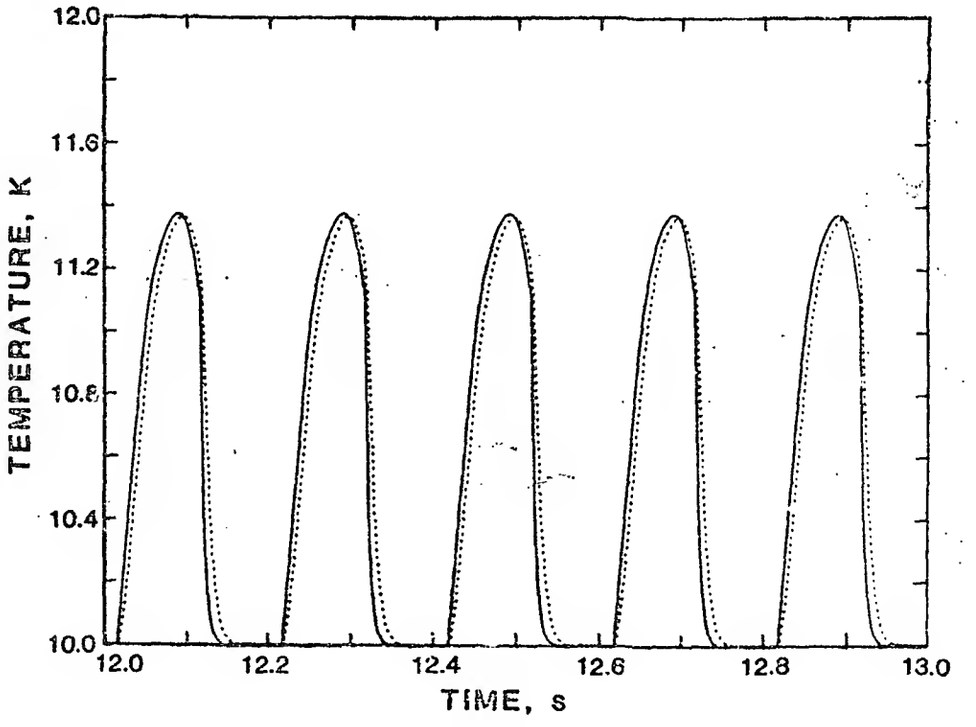

Figure 6. Temperature vs. time at x = 1.0 with D_h (hydraulic diameter) = 4.84E-4 m.

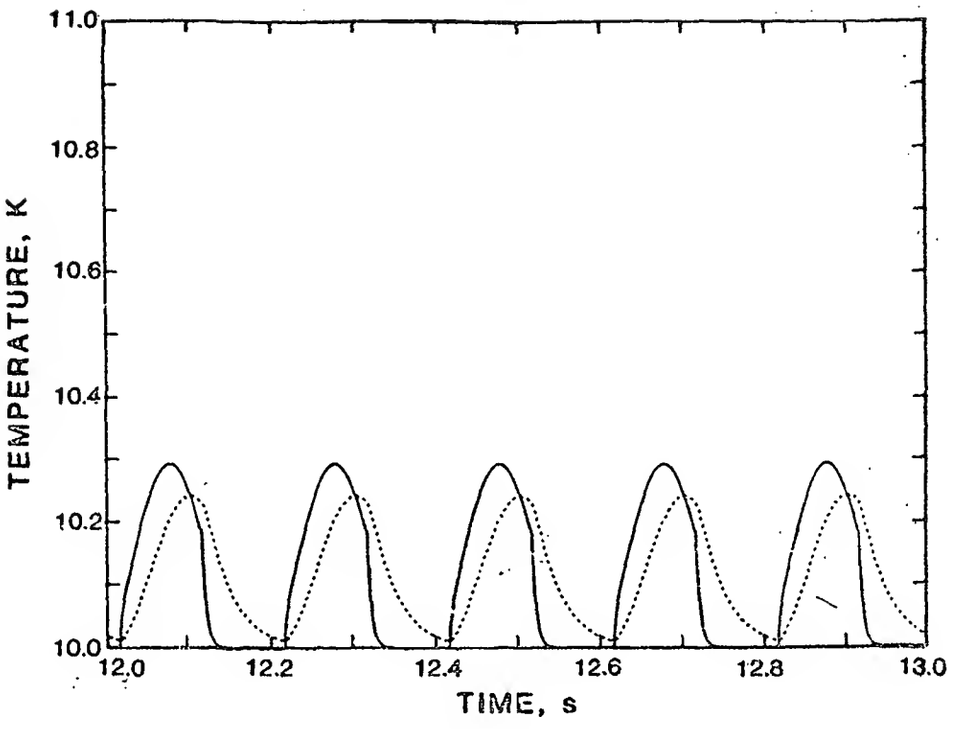

Figure 7. Temperature vs. time at x = 1.0 with $\rho_m C_m$ = 5.28E+6 J/kg·m^3.

now some separation of the matrix and gas temperature. A greater separation is seen in figure 7. Here the heat capacity of the matrix has been increased by a factor of 20 over case I.

Our definition of the ineffectiveness is given by the following integral which is taken over the outflow portion of the cycle,

$$\int \rho |u| (T(L,t)-T_L)dt \; / \; \int \rho |u| (T_o-T_L)dt.$$

Here T_o and T_L denote the fixed gas temperature and $T(L,t)$ denotes the gas temperature of outflow. The ineffectiveness as a function of hydraulic diameter, D_h, is shown in figure 8 for the conditions of case I. In figure 9 the variation with matrix heat capacity, $\rho_m C_m$, is shown.

In table 1, we compare our computed ineffectiveness with that obtained by Daney using a model which assumes no pressure variation. Our results are higher, which is probably explained by our non-zero pressure swing during the cycle. The table shows that ineffectiveness increases with the pressure swing.

5.3 The accuracy and consistency of the model

In table 2 the value of the ineffectiveness is shown as a function of the numerical resolution. These results are for case I where the frequency is 5 Hz. Note that with Δt = 0.001 s and Δx = 0.1 we have 10 mesh intervals across the regenerator and 200 time steps per cycle. The last run with Δt = 0.004 s did not yield valid results. The need for a small time step may be explained by the rapid change in the temperature at the boundary. When the flow changes from outflow to inflow the temperature is raised to the boundary value in about 0.01 seconds in this case. Therefore we might expect some trouble with the larger time step.

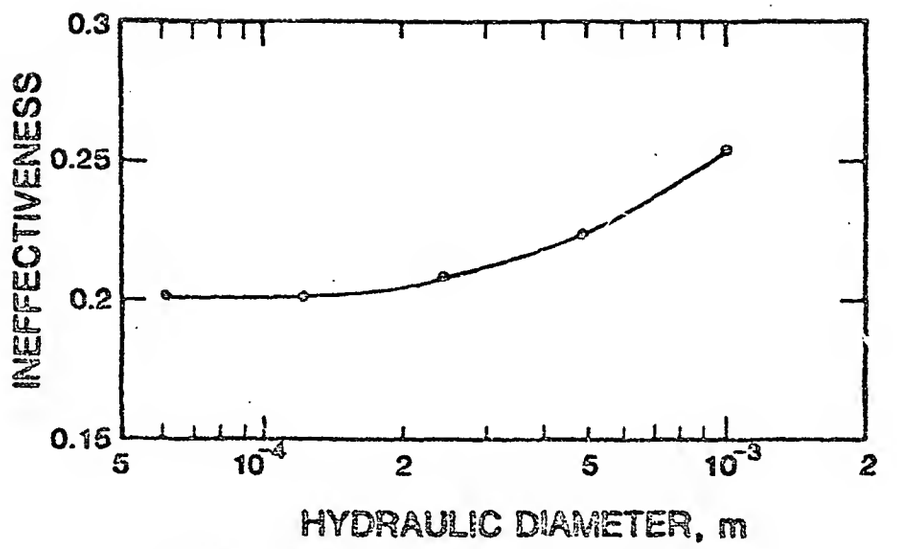

Figure 8. Ineffectiveness vs. hydraulic diameter.

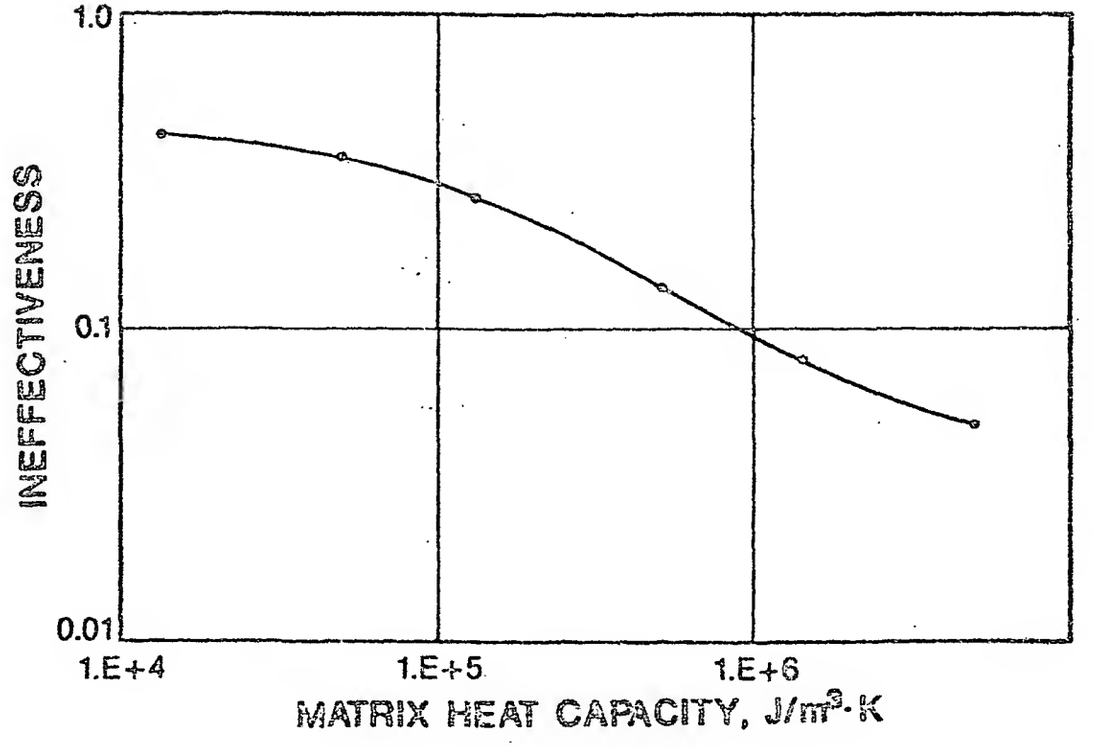

Figure 9. Ineffectiveness vs. matrix heat capacity.

Table 1. Comparison with Constant Pressure Model.

Model	Ineffectiveness	Temperature Swing K	Pressure Swing MPa
constant pressure (Daney)	0.015	—	
phase = 0.0	0.027	10.0 - 10.50	2.9 - 3.3
phase = -14°	0.079	10.0 - 10.62	2.8 - 3.8
phase = -29°	0.122	10.0 - 10.79	2.6 - 4.5

Table 2. Accuracy.

Resolution	Ineffectiveness
Δt = 0.001 s Δx = 0.1	0.207
Δt = 0.001 s Δx = 0.05	0.202
Δt = 0.0005 s Δx = 0.025	0.201
Δt = 0.004 s Δx = 0.05	0.23*

*Did not reach a steady state - mass loss 1% per cycle.

In table 3 we compare the results for case I obtained from the two models. The full equation solution shows a small oscillation in the velocity field which is not present in the solution using the reduced equations. The CPU time is on a CDC Cyber 750. The results for the two models seem to be in good agreement.

5.4 Achieving a quasi-steady state

The results described above were obtained by running the model for 66 cycles. At this point there is very little change of average or maximum values from one cycle to the next. For example, in case I the maximum gas temperature at the cold end is changing at a rate of 10^{-4} K per cycle. This is a very small change; however, this rate appears to be virtually constant over the last 10 or 20 cycles. Therefore, we don't know how close we are to a steady oscillation. At this rate 1000 cycles would be required to effect a 10 percent change in this maximum temperature. We need to find a method to accelerate convergence.

Table 3. Comparison of Reduced and Full Equations Models.

Model	Ineffectiveness	Temperature Swing K	Pressure Swing MPa	CPU Time/Cycle s
Reduced	0.202	10.0 - 11.2	2.7 - 4.3	6.8
Full	0.186	10.0 - 11.1	2.8 - 4.3	23

6. References

[1] Daney, D. and Radebaugh, R., Nonideal Regenerator Performance - the Effect of Void Volume Fluid Heat Capacity, Cryogenics 24, 499-501 (1984).

[2] Gustafsson, B., Numerical Solution of Hyperbolic Systems with Different Time Scales Using Asymptotic Expansions, Jour. Comp. Phys. 36, 209-235 (1980).

[3] Gustafsson B. Asymptotic Expansions for Hyperbolic Problems with Different Time-Scales, 17, 623-634 (1980).

[4] Kreiss, H., Problems with Different Time Scales for Partial Differential Equations, Comm. Pure. App. Math, XXXIII, 399-439 (1980).

Notation			SI Units
P	-	pressure	MPa
ρ	-	gas density	Kg/m^3
ρ_m	-	matrix density	kg/m^3
c	-	acoustic velocity	m/s
u	-	velocity	m/s
G_r	-	Grueneisen parameter	
h	-	heat transfer coefficient	$W/m^2 \cdot K$
D_h	-	hydraulic diameter	m
T	-	gas temperature	k
T_m	-	matrix temperature	k
F	-	friction factor	
C_v	-	gas heat capacity	$J/kg \cdot K$
c_m	-	matrix heat capacity	$J/kg \cdot K$
ϕ	-	porosity	
R_c	-	gas constant	$J/kg \cdot K$
γ	-	ratio of specific heats	
L	-	length of regenerator	m
$a(t)$	-	left endpoint (piston position)	m
$b(t)$	-	right endpoint	m

D21

CRITERIA FOR SCALING HEAT EXCHANGERS TO MINIATURE SIZE

Philipp B. Rudolf von Rohr and Joseph L. Smith, Jr.
Massachusetts Institute of Technology
Cryogenic Engineering Laboratory
Cambridge, MA 02139

ABSTRACT

The purpose of this work is to highlight the particular aspects of miniature heat exchangers performance and to determine an appropriate design approach. A thermodynamic analysis is performed to express the generated entropy as a function of material and geometric characteristics of the heat exchangers. This expression is then used to size miniature heat exchangers.

Key words: Miniature heat exchanger design; laminar flow heat exchanger optimization; second law analysis.

1. Introduction

In recent years a large number of applications have been developed for small superconducting devices being cooled around 4.2 K . Their viability will depend on the availability of closed cycle, efficient refrigerators. An extended survey [1] has shown that small scale refrigerators, for loads around 1 watt, are not commercially available.

Different approaches have been undertaken to build reliable and efficient closed-cycle refrigerators. In particular, Vuilleumier, Gifford-McMahon and Stirling cycles were investigated. These cycles are efficient at temperatures greater than 10 K. The main problems in these pressure-cycling refrigerators for liquid helium temperatures are rooted in the poor heat capacity of regenerators materials at low temperatures. Preliminary studies [2] show that for small loads Collins cycle refrigerators are advantageous.

As part of a program to develop an efficient, closed cycle Collins type refrigerator for 1 watt at 4.2 K, we investigate the performance of miniature helium plate heat exchangers (Fig. 1). Due to the mass flows involved, these heat exchangers operate in laminar flow conditions.

We will show that the axial conduction in the solid wall has a considerable impact on the performance of low temperature miniature heat exchangers.

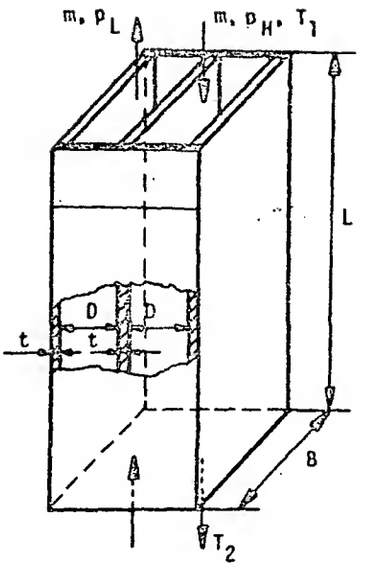

Figure 1: Plate heat exchanger

2. Thermodynamic analysis

The three major contributions to irreversibilities in heat exchangers are:

2.1. Entropy generation due to friction, S_p
2.2. Entropy generation due to temperature difference between the heat exchanger streams, S_T
2.3. Entropy generation due to heat conduction in the solid wall, S_c

Their sum will furnish the generated entropy for the isolated heat exchanger:

$$S = S_p + S_T + S_c \quad (1)$$

2.1. Entropy generation due to friction

Assuming that helium behaves as a perfect gas, we find that the entropy generation due to flow friction is given by:

$$S_p = mR[(\Delta p_L/p_L) + (\Delta p_H/p_H)] \quad (2)$$

where: m = mass flow
R = gas constant
p_L = low pressure
p_H = high pressure

Since the high pressure stream friction loss is negligible, S_p is given by:

$$S_p = mR(\Delta p_L/p_L) \quad (3)$$

where:

$\Delta p_L = [m^2/(\rho B^2 D^2)](f/2Re)(L/D)$

$f/4Re$ = friction factor [3]

Re = Reynolds number

ρ = density

B, D, L = geometric parameters (Fig. 1).

Substituting Δp_L into eq. (3), we find:

$$S_p = (m^2 R/p_L)(f/2Re)[L/(B^2 D^2)] . \qquad (4)$$

It may be immediately seen from eq. (4) that entropy generation by friction will increase with increasing heat exchanger length L and decreasing breadth B and wall-to-wall distance D.

2.2. Entropy generation due to finite temperature difference

The generated entropy due to finite temperature difference is:

$$S_T = m^2 c_p^2 [(2D/(k_f Nu) + t/k_w)][(T_1-T_2)/(T_1 T_2)](1/(BL)) , \qquad (5)$$

where: c_p = specific heat at constant pressure of the fluid

k_f = fluid thermal conductivity

k_w = wall thermal conductivity

Nu = Nusselt number.

The derivation of eq. (5) is summarized in the Appendix.

It may be seen from eq. (5) that the entropy generation will decrease with decreasing wall-to-wall distance D and wall thickness t and increasing plate breadth B and heat exchanger length L.

2.3. Entropy generation due to heat conduction in the solid wall

The temperature gradient in the heat exchanger walls is linear and the heat conductivity k_w and the crossectional area A_s are constant; then the entropy generation S_c associated with the heat transfer by conduction, Q_c is:

$$S_c = Q_c(T_1-T_2)/(T_1 T_2) , \qquad (6)$$

where:

$$Q_c = (T_1-T_2)k_w A_s/L . \qquad (7)$$

It may be seen from eqs. (6) and (7) that the entropy generation by axial wall conduction will increase with increasing crossectional area $A_s = 38t$ and decreasing heat exchanger length L.

2.4. Overall entropy generation

The generated entropy in a laminar counterflow heat exchanger, assuming helium behaves as perfect gas and with constant material properties, is derived from eqs. (1),(3),(4),(5) and (6):

$$S = m^3R[f/(2\rho_L Re_{p_L})][L/(B^2D^3)] +$$
$$m^2c_p{}^2[(2D/k_f Nu) + t/k_w)][(T_1-T_2)/(T_1T_2)][1/(BL)] + \quad (8)$$
$$k_w[(T_1-T_2)^2/(T_1T_2)](Bt/L) .$$

It will be useful, for the purposes of simplifying the expression of S and to recognize familiar dimensionless parameters, to obtain a dimensionless form for eq. (8). This is achieved by dividing eq. (8) by $[(k_f/\upsilon)m]$, that is constant at pressures below 20 atm [4]. Equation (8) then becomes:

$$\begin{aligned} S/[(k_f/\upsilon)m] = {} & [(k_w/k_f)(t/L)(1.5/Re)(T_1-T_2)^2/(T_1T_2))] + \\ & [((T_1-T_2)^2/(T_1T_2))(Pr^2Re/Nu)(D/L)] + \\ & [(k_f/k_w)(t/L)(RePr^2/2)((T_1-T_2)^2/(T_1T_2))] + \\ & [(R/c_p)(PrRe)(f\upsilon^2/(8p_L\rho_L))(L/D^3)] . \end{aligned} \quad (9)$$

This is the entropy S generated in a counterflow laminar heat exchanger, valid for ideal gases in the laminar flow range with Re larger than 100 [3].

3. Heat exchanger sizing

The geometrical parameters chosen are the wall thickness t, the breadth B, the wall-to-wall distance D and the heat exchanger length L. Material properties are defined by k_w.

Results will show that the entropy generation decreases with decreasing t and increasing L and B, with $k_w = k_w(B)$ and $D = D(L)$.

3.1 General methodology for miniature heat exchanger sizing

Equation (9) shows that the wall thickness t needs to be small for minimum entropy generation. Consequently its value will be determined by structural requirements.

The first derivative of S with respect to k_w is set to zero:

$$k_w = 0.32RePrk_f . \quad (10)$$

Equation (10) has a form that is similar to the optimized wall thermal conductivity for a concentric tube heat exchanger [5].
For B considerably larger than D, the Reynolds number may be expressed as:

$$Re = 2m/(B\upsilon) . \quad (11)$$

Substituting eq. (10) into eq. (9), we find:

$$\begin{aligned} S/[(k_f/\upsilon)m] = {} & 1.22Pr((T_1-T_2)^2/(T_1T_2))(t/L) + \\ & (Pr^2Re/Nu)(T_1-T_2)^2/(T_1T_2)(D/L) + \\ & (PrRe)(R/c_p)(f\upsilon^2/18p_L\rho_L))(L/D^3) . \end{aligned} \quad (12)$$

The minimum of the entropy generation with respect to the wall-to-wall distance D is then determined similarly:

$$D = [((R/c_p)(f\dot{\omega}^2/(2p_L\rho_L))(Nu/Pr))/((T_1-T_2)^2/(T_1T_2))]^{.25}[L]^{.5}. \quad (13)$$

Equation (13) is substituted into eq. (12); S is then expressed as a function of L and Re, where Re is defined by eq.(11):

$$S/[(k_f A_\omega)m] = c_1(t/L) + c_2 Re(L)^{-.5} , \quad (14)$$

where:

$$c_1 = 1.22Pr((T_1-T_2)^2/(T_1T_2))$$

$$c_2 = 1.05(Pr^{1.75}/Nu^{.75})((T_1-T_2)^2/(T_1T_2))^{.75}(R/c_p)^{.25}(f\dot{\omega}^2/(p_L\rho_L))^{.25}.$$

The function S is monotonic decreasing with increasing L and decreasing Re. The remaining parameters B and L may be evaluated by considering space limitation, heat leak to the surrounding and manufacturing costs.

3.2. Applications for helium heat exchangers

We take into consideration a laminar counterflow plate heat exchanger for a two-expander-saturated-vapor-pressure cycle refrigerator [6] with a cooling load of 1 watt at 4.2 K. With a reasonable expander efficiency, the mass flow in the balanced heat exchanger between 300 K and 60 K is 0.1 g/s, while the mass flow in the heat exchanger between 30 K and 14 K is 0.085 g/s.

The generated entropy as a function of the length L, using the Reynolds number as a parameter, is shown in Figures 2 and 3 for the two heat exchangers.

The heat exchangers breadth B is computed from eq. (10) for two Reynolds numbers :
Figure 2: for Re = 100, B = 0.171 m and for Re = 300, B = 0.057 m
Figure 3: for Re = 150, B = 0.294 m and for Re = 300, B = 0.147 m.

The optimized wall-to-wall distance D is computed from eq. (13):
Figure 2: for 0.1m< L < 1.0m 0.26mm < D < 0.82mm
Figure 3: for 0.1m< L < 1.0m 0.06mm < D < 0.19mm .

Figures 2 and 3 also show the entropy generation due to axial wall conduction. Its contribution to the total entropy generation is particularly significant for the cold miniature heat exchanger and, in general, for low Reynolds numbers.

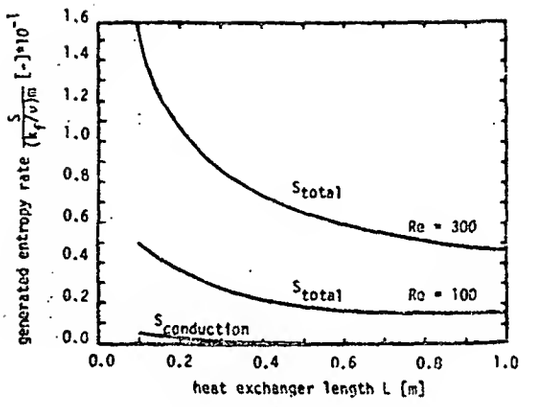

Figure 2: Entropy generation rate vs. length of heat exchanger for two Reynolds numbers
(T_1 = 300 K, T_2 = 60 K, p_L = 2 bar, p_H = 20 bar)
($\dot{m}$ = 0.1 g/s, t = 0.2 mm)

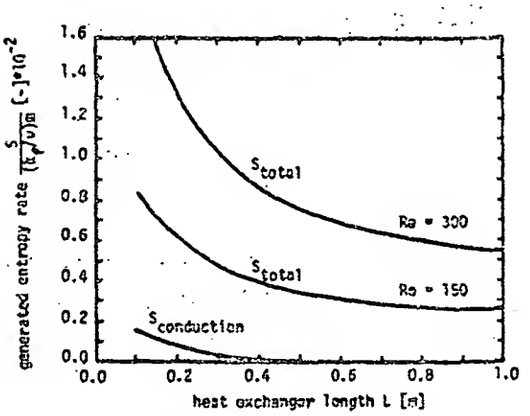

Figure 3: Entropy generation rate vs. length of heat exchanger parameter: Reynolds number Re
(T_1 = 30 K, T_2 = 14 K, p_L = 2 bar, p_H = 20 bar)
($\dot{m}$ = 0.085 g/s, t = 0.2 mm)

4. Conclusions

The thermodynamic analysis performed in this work consists of:
- expressing the entropy generation contributions due to the axial wall conduction, due to the pressure loss and due to the finite temperature difference as a function of four geometrical parameters and one material characteristic.
- minimizing the generated entropy and thereby reducing the set of independent parameters.

In miniature heat exchangers, axial conduction in the wall may become an important phenomenon.

It is shown that the miniature heat exchanger design may not be performed by simply scaling down standard heat exchangers because of the short heat exchanger length and the laminar flow.

Acknowledgments

Ph. B. Rudolf von Rohr was supported by the "Schweizerischer Nationalfonds".

Appendix

The temperature difference ΔT between the streams compared to the axial temperature difference (T_1-T_2) is assumed to be small, then the heat transfer rate through the heat exchanger surface A is:

$$Q = mc_p(T_1-T_2) = h\Delta TA \quad . \tag{A1}$$

Assuming the same convective heat transfer coefficients h_{co} for the high and low pressure streams, we find:

$$h_{co} = (Nuk_f)/D \quad . \tag{A2}$$

Thus the overall heat transfer coefficient h is:

$$1/h = 2/h_{co} + t/k_w \quad . \tag{A3}$$

Considering the fluid heat conductivity k_f independent of the pressure, eq. (A2) shows that the wall-to-wall distance D is equal for both channels.

The finite temperature difference is derived from eqs. (A2),(A3) and (A1):

$$\Delta T = (mc_p/A)(T_1-T_2)[(2D/(k_fNu)) + (t/k_w)] \quad . \tag{A4}$$

The entropy generation due to the finite temperature difference ΔT is:

$$S_T = mc_p\Delta T(T_1-T_2)/(T_1T_2) \quad . \tag{A5}$$

By substituting eq. (A4) into eq. (A5), the entropy generation S_T becomes:

$$S_T = m^2c_p{}^2[(2D/(k_fNu)) + (t/k_w)][(T_1-T_2)^2/(T_1T_2)][1/(8L)] \quad . \tag{A6}$$

Nomenclature

A	area	Re	Reynolds number
B	plate width	S	entropy
c_1	constant in eq. (14)	t	plate thickness
		T	temperature
c_2	constant in eq. (14)	Δ	difference
		ν	viscosity
c_p	specific heat of gas	ρ	density
D	plate spacing	Subscripts	
f	friction factor		
h	heat transfer coefficient	1	warm end of exchanger
h_{co}	convective heat transfer coefficient	2	cold end of exchanger
		c	wall conduction
k	thermal conductivity	f	fluid
L	heat exchanger length	H	high pressure passage
m	mass	L	low pressure passage
Nu	Nusselt number	P	frictional pressure drop
p	pressure	s	cross section
Pr	Prandtl number	T	gas heat transfer
Q	heat transfer rate	w	wall
R	gas constant		

References

[1] Smith, Jr., J.L., Robinson, Jr., G.Y. and Iwasa Y., Survey of the state of the art of miniature cryocoolers for superconductive devices. Cryog. Eng. Lab. of MIT (Jan. 1984).

[2] Pirtle, F.W. et al., Thermodynamic aspects of small 4.2 K cryocoolers, Adv. in Cryog. Engng. 27, (1982), pp. 595/602.

[3] Kakac, S., Shah, R.K. and London A.L., Low Reynolds number heat exchangers, Hemisphere Publ. Corp., Washington, New York, London (1983).

[4] VDI-Lehrgang, Kryotechnik (1981), VDI Bildungswerk Duesseldorf.

[5] Chowdhury, K. and Sarangi, S., A second law analysis of the concentric tube heat exchanger: optimization of wall conductivity, J. Heat Mass Transfer, Vol 26.,(1983), pp.783-786.

[6] Minta, M. and Smith, Jr., J.L., Helium liquefier cycles with saturated vapor compression, Adv. in Cryog. Engng. 27, (1982), pp. 603/610.

D21

A CLOSED CYCLE CASCADE JOULE THOMSON REFRIGERATOR FOR COOLING JOSEPHSON JUNCTION DEVICES

Emanuel Tward

Jet Propulsion Laboratory
California Institute of Technology
Pasadena, California 91109

and

Raymond Sarwinski

R. G. Hansen and Associates
San Diego, California 92121

A closed cycle cascade Joule Thomson refrigerator designed to cool Josephson Junction magnetometers to liquid helium temperatures is being developed. The refrigerator incorporates 4 stages of cooling using the working fluids CF_4, N_2, H_2 and He. The high pressure gases are provided by a small compressor designed for this purpose. The upper three stages have been operated and performance will be described.

Key words: Cascade Joule Thomson refrigerator; cryocooler.

1. Introduction

The problem of cooling of Josephson junction devices to liquid helium temperatures is becoming increasingly important as systems incorporating such devices are becoming more widespread. Traditionally, experimentalists have preferred the use of liquid helium dewars since, in a laboratory setting where liquid helium is readily available, they are convenient to use. Devices can be cooled and warmed quickly and tests can be made with little attention to the cooler other than replenishment of the liquid helium cryogen. However, once devices are integrated into a system and are to be used for extended periods of time, the use of liquid helium dewars often becomes inconvenient, especially if the system is to be operated remotely from a readily available liquid helium supply or if the system is inaccessible by service personnel.

Under these circumstances, it would be preferable to use a cryocooler. The ideal cryocooler would be one that is convenient to operate (i.e., flick the switch to turn on the power) and it does the job. In addition, the cooler should be efficient, occupy a small volume, be adaptable to cool a wide range of instruments, and have minimal interaction with the instrument (other than cooling it). This latter requirement is especially important for the cooling of Josephson junction magnetometers which are very sensitive to electromagnetic interference (EMI) and to vibration.

Because of this constraint almost all magnetometers are cooled in liquid helium dewars. All commercially available cryocoolers use expansion engines and hence act as sources of both EMI and vibration. Therefore, all such coolers are generally unsuitable for the most demanding applications, unless the instrument is contained in a liquid helium dewar and is being continuously cooled

by a remotely sited refrigerator. Such a refrigerator could be coupled to the instrument, for example, through a continuously flowing liquid helium transfer line. It is often the case that the cooling power required is much less than one watt. The smallest commercially available coolers have cooling powers greater than one watt. In this sense they are also ove-designed for the small cooling power applications.

Attempts have been made to build low cooling power Stirling cycle cryocoolers [1] . These machines incorporate plastic materials in order to reduce EMI from moving conducting materials and require mechanical balancing in order to reduce vibration. In our view, a far better approach is to construct a refrigerator with no cold moving parts. This has been implemented through the use of the cascade Joule Thomson process [2]. Since Joule Thomson refrigerators require a source of very pure high pressure gas, suitable low flow rate large compression ratio compressors are required. We have taken two approaches to this problem. For very long life refrigerators, chiefly for space applications in which no servicing is possible, we have developed non-mechanical adsorption compressors which are thermally driven and incorporate no moving parts [3]. In the second approach we have designed and built a small mechanical compressor which provides very clean high pressure gas to the refrigerator. The compressor can be remotely sited from the refrigerator and connected to it only through long capillaries through which the high pressure room temperature gases are brought to the JT refrigerators and the low pressure room temperature return gases are returned to be recompressed. In this way, EMI is reduced by distance and vibration is greatly reduced because of the weak mechanical coupling to the cold (business) end of the refrigerator.

2. Cascade Joule Thomson refrigerators

The Joule Thomson process is in wide use for cryogenic coolers. For small cooling powers its major application is in the cooling of IR sensors typically to liquid nitrogen temperatures and above. For small cooling powers the JT refrigerators (heat exchanger plus expansion valve) can be implemented in a variety of ways [4, 5]. In our case we have used parallel metal tube heat exchangers with a constricted tube as the expansion valve.

The Joule Thomson process is conceptually simple. High pressure gas of enthalpy H_h enters the inlet of heat exchanger, expands and cools at the JT orifice and returns through the low pressure side of the heat exchanger in order to precool the incoming pressure gas. At the outlet of the heat exchanger the low pressure gas has an enthalpy H_L. The cooling power of the device is given by

$$\dot{Q} = \dot{m}(H_L - H_h) ,$$

where $\dot{m}$ is the mass flow rate. The JT process produces cooling (rather than heating) only if $H_L > H_h$ for the particular gas at the inlet temperature of the heat exchanger. The temperature above which H_L is always less than H_h is called the inversion temperature. Therefore, in order to reach liquid helium temperatures a minimum of three different gases in three cooling loops are required. In the cascade process an upper temperature refrigerator precools the inlet gas to a lower stage refrigerator to a temperature below the inversion temperature of the gas in the lower stage.

In our system we have implemented each JT loop in similar fashion. A schematic of the upper stage loop and the components incorporated is shown in figure 1. The loop incorporates both warm and cold filters as a precaution against contamination resulting in clogging of the refrigerator. The cascaded JT refrigerator which we are reporting on has been implemented with four stages using the working fluids CF_4, N_2, H_2, He. The four stages (rather than three) were used because of increased thermodynamic efficiency and because lower pressures are required from the compressor for the upper stages. The four independent fluid loops are configured as shown in figure 2.

Because of the low gas flows, the eight gas lines to the refrigerator (2 per stage) can be long enough for the compressor to be far from the refrigerator (we have used 3.2 meter lengths) and can be of small diameter (smallest diameter 0.16 cm OD). This provides a very flexible interface to the sensor cryogenics. The refrigerator operates in any orientation which should make the device much easier to use than sensors using liquid helium dewars. The prototype refrigerator shown in figure 3 was specifically designed to cool a SHE biomagnetic probe [6] with a 2nd order gradiometer input coil. A schematic of the cryostat is shown in figure 4. To date, only three of the four stages have been operated. Figures 5 and 6 show cool down curves for the various stages. The

longer than necessary cool down times are due to the fact that these measurements were taken with a leak in one of the loops which resulted in excessive heat leak through the inadequately maintained dewar vacuum. The temperature reached at each stage is determined by the pressure at the liquid reservoir which is in turn determined by the impedance of the J-T orifice, the pressure drop in the low side heat exchanger and the inlet pressure to the compressor. In the experiments to date, gas flows through each of the loops have been in the range of 50 STP cc/sec and are chiefly determined by the impedance of the J-T orifice. With lower gas flows we expect smaller pressure drop in the low side heat exchangers, smaller compressor inlet pressures and hence lower operating temperatures at each stage. The design goal was for flow rates of 15 STP cc/sec in each loop. Once all four stages are operating we intend to reduce the flow rates (and cooling powers) to each stage so that the lowest possible temperatures can be achieved.

3. Conclusions

Closed cycle Joule Thomson coolers appear to be an attractive solution to the problem of cooling low power devices to low temperatures. Their small size, orientation independent performance, and absence of cold moving parts make them particularly useful for application where EMI and vibration are a problem.

The assistance of John Watkins, John Gatewood and James Peterson has contributed greatly to this effort. Support for this research was provided by the Office of Naval Research and the Air Force Medical Research Laboratories.

4. References

[1] Zimmerman, J. E., Davey, D. E. and Sullivan, D. B. In M. Gasser (Ed.), Refrigeration for Cryogenic Sensors, NASA Conference Publication 2287, 95-105.

[2] Tward, E. and Steyert, W. A., In M. Gasser (Ed.), Refrigeration for Cryogenic Sensors, NASA Conference Publication 2287, 419-425.

[3] Chan, C. K., Tward, E. and Elleman, D. D. Proceedings of Cryogenic Engineering Conference, 1983, in press.

[4] Walker, G. Cryocoolers, Plenum Press, New York, 1983.

[5] Little, W. A. Microminiature refrigeration, Rev. Sci. Instrum. 55 (5) 661-680 (1984).

[6] SHE Corporation, San Diego, California.

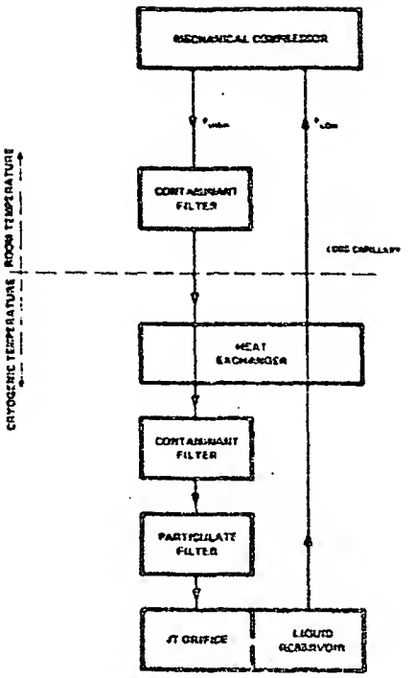

Fig. 1. Schematic of a single stage J-T cooler.

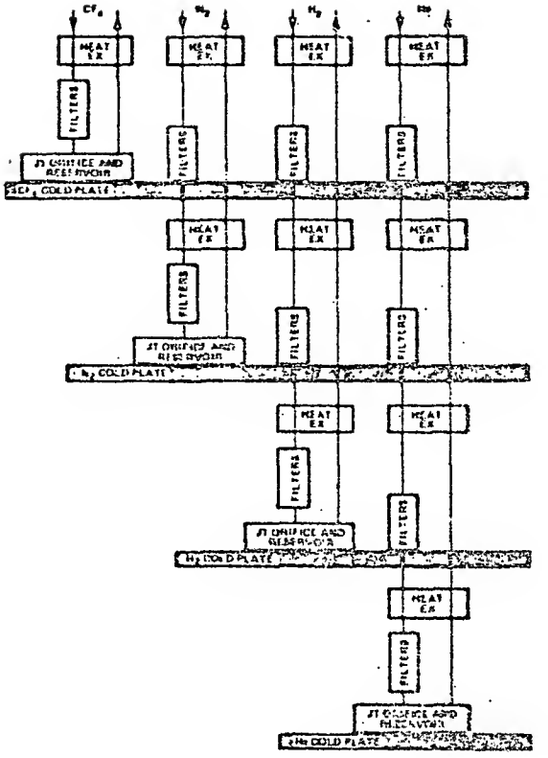

Fig. 2. Schematic of a cascaded four stage J-T cooler.

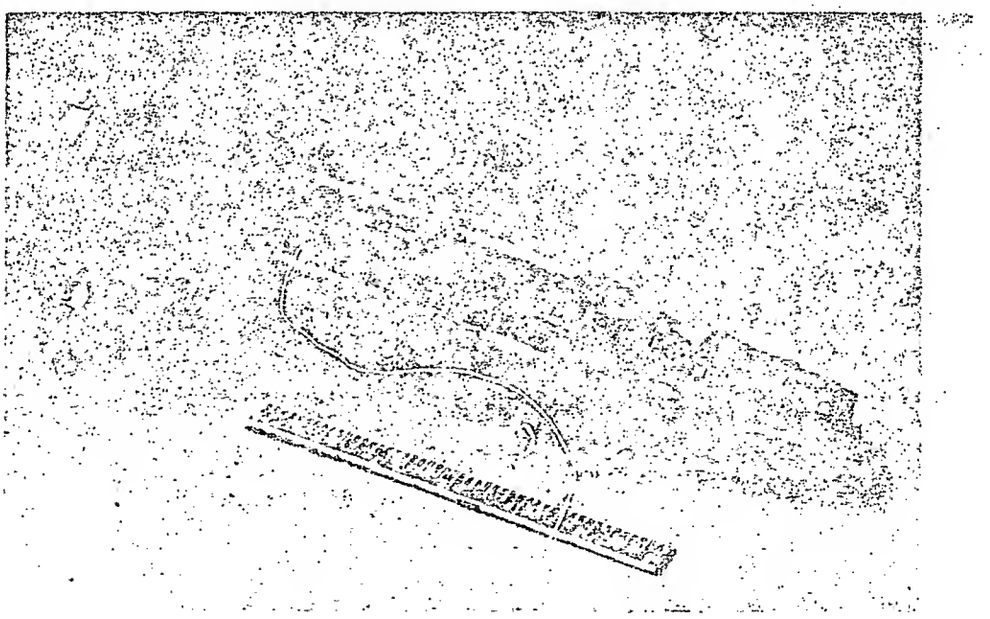

Fig. 3. Four stage cascaded J-T cooler designed to cool biomagnetic probe.

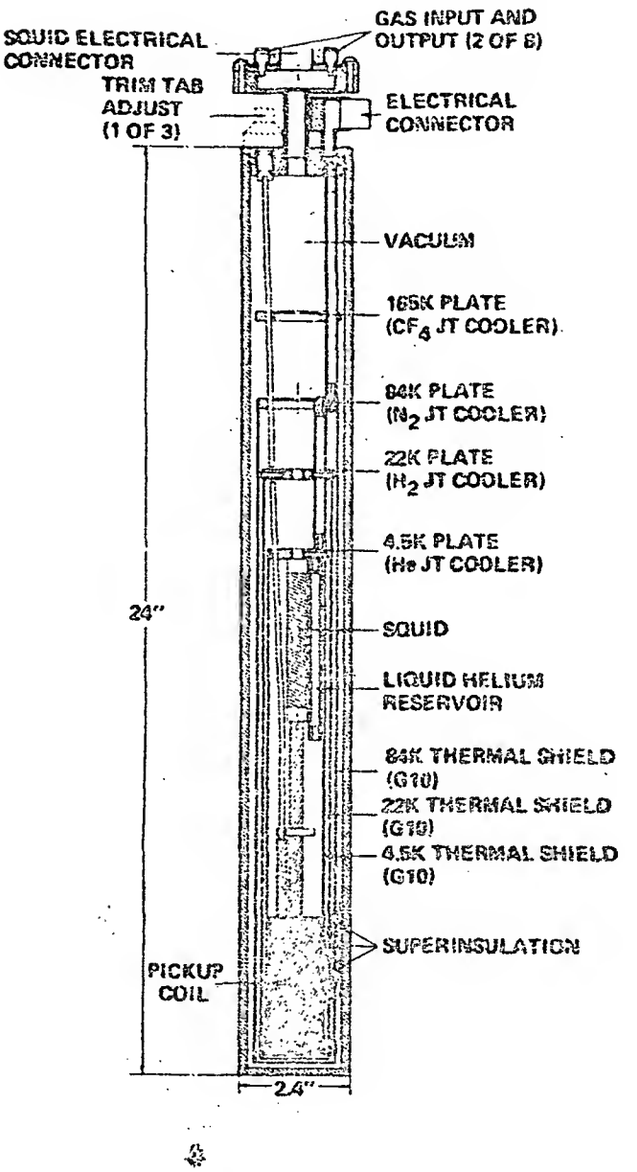

Fig. 4. Schematic of single sensor neuromagnetometer incorporating closed J-T cooler.

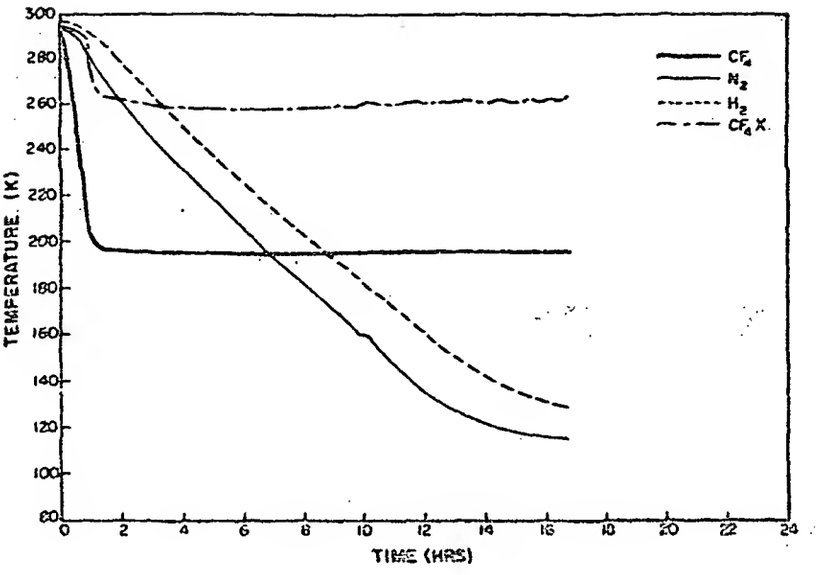

Fig. 5. Cooldown of upper two stages of refrigerator. The H_2 stage is being cooled by conduction. The curve labelled, CF_4X indicates the outlet temperature of the heat exchanger. The low temperature after cooldown is due to excess cooling power.

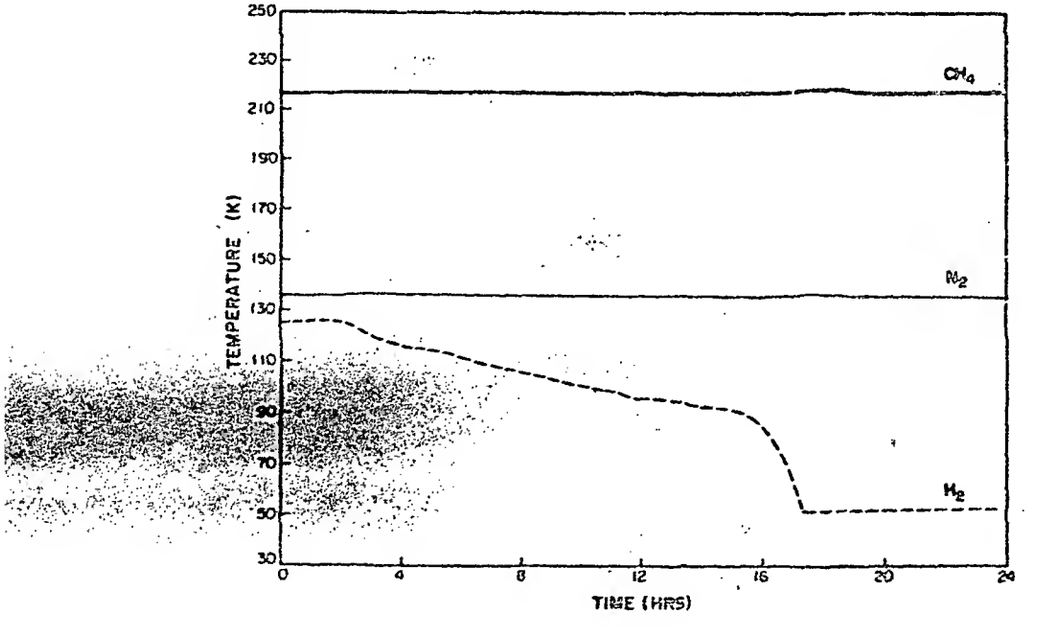

Fig. 6. H_2 stage cool down. Note temperature stability. The rapid cool down below 70 K is due to increased gas flow and cooling power as the impedance of the refrigerator drops with temperature.

D22

A SMALL HELIUM LIQUIFIER WHICH PROVIDES CONTINUOUS COOLING BASED ON CYCLED ISENTROPIC EXPANSION

Calvin Winter, Suso Gygax *, Ken Myrtle and Russel Barton

Quantum Technology Corp.
6237 - 148 ST.
Surrey, B.C., CANADA V3S 3C3

* Simon Fraser University
Department of Physics
Burnaby, B.C., CANADA V5A 1S6

This simple cryocooler provides a small reservoir of liquid helium at a stable temperature of 4.2K. It uses a novel adaptation of the Simon expansion cryocooler to provide continuous cooling. Operation is in a four stage cycle: (1) A closed vessel of helium under high pressure is cooled to 12K using a conventional Gifford-McMahon closed-cycle cryocooler. (2) The pressure is released adiabatically providing cooling to 4.2K. (3) Liquid helium is collected in a second, well insulated, vessel. (4) The first vessel is re-pressurized. The cycle time is 15-30 minutes. In this manner, a pool of liquid helium is continuously maintained in the second vessel, with a temperature stability of 0.03 degrees. The continuous cooling power available is 3mW. This design provides simplicity and reliability through the absence of any orifices or moving parts at cryogenic temperatures except for the conventional Gifford-McMahon cryocooler.

Key words: Cryocoolers; small; liquifiers; helium liquifiers; liquid helium; helium; isentropic expansion; Simon; Gifford-McMahon; refrigerators.

1. Introduction

Historically, the development of low temperature physics and its applications have rapidly followed the development of cryogenic refrigerators, or "cryocoolers". There is now a host of applications of low temperatures, especially those using superconductors, which are not economical, given the high cost of most commercial helium liquifiers. Those applications which are economical generally rely on the presence of a large helium liquifier in their vicinity. Driven by this need for inexpensive helium liquifiers our group has developed a number of different cryocoolers. This paper describes one of our cryocoolers. For a more complete review of our work and that of others in this field the reader is referred to several recent reviews of progress in the field of inexpensive helium liquifiers [1,2,3].

We have built a simple and inexpensive helium liquifier using a commercial two stage Gifford-McMahon cycle cryocooler (of the type used in cryopumps) for the initial stages of cooling. The novelty of our cryocooler is that it is able to provide continuous cooling at liquid helium temperature, by recycling an adiabatic expander. The liquifier is useful for many applications with modest cooling power requirements, i.e. the operation of small superconducting devices, infra-red detectors, laboratory measurements of material properties at low temperatures and neutron diffraction measurements.

2. Principles of operation

2.1 Adiabatic Expansion

Helium is liquified in our cryocooler by adiabatic (isentropic) expansion of previously cooled, high pressure helium gas. This technique was exploited by Simon [4] in 1932 using liquid hydrogen to precool the compressed gas. In our cryocooler, an expansion volume of 10 ml is cooled

to 12K, by the two stage Gifford- McMahon cryocooler, while filling with helium at a pressure of 6.2 MPa (62 bars). Once cooled, the mass or supercritical gas in the expansion volume will be 1.6 g [5]. When an exhaust valve is opened to allow this gas to escape (to the atmosphere) to a pressure of 0.1 MPa cooling is produced in the expansion volume. This process is very nearly adiabatic because at these low temperatures the specific heat of the metal vessel is negligible compared to the specific heat of helium gas. At the 0.1MPa pressure, the expansion volume will contain 1.7 ml of liquid helium with the remainder gaseous for a total of 0.35 g.

2.2 Principle of cycled adiabatic expansion

The liquefaction process described above is of a one-shot nature. After the liquid generated has been boiled off, the temperature rises. In order to recycle the expansion volume it must be filled with compressed helium gas. Since the refill gas comes from outside the apparatus it is initially warm. In addition, the process of compressing the gas adiabatially produces heating. The expansion volume must be cooled to 12K again by the two stage Gifford-McMahon cryocooler before the next expansion and liquefaction cycle may commence. In this manner the adiabatic expansion may be cycled, but the temperature of the expansion volume will oscillate between 4.2K and 20K.

In order to echieve a constant temperature liquid helium bath, a separate, well insulated, container is attached to the bottom of the expansion volume to act as a liquid helium reservoir. This reservoir is replenished with liquid helium at each expansion phase of the cycle. During the compression phase, however, the liquid in this reservoir may be boiled to provide a continuous 4.2K temperature bath.

2.3 Principle of thermal diode

Proper operation of the liquid helium reservoir requires that it be in good thermal contact with the expansion volume during the expansion phase, but that it be thermally isolated during the compression phase. The natural tendency of cold helium to flow to the bottom of a conteiner is used to provide this switching action in our cryocooler. The liquid reservoir is located directly below the expansion vessel. During the expansion phase a slight overpressure in the reservoir allows helium to condense on its cold top surface. This liquid then flows to the bottom of the reservoir. During the compression phase the expansion volume heats up to approximately 20K. This also heats the gas in the upper part of the insulation tube. However, due to the low thermal conductivity of helium and due to the natural stratification of the gas with the warm gas on top, little heat is conducted down to the liquid reservoir.

The function of the long insulation tube at the top of the liquid reservior is analogous to an electrical diode. When the top end is cold it conducts heat, either by natural convection currents or by liquefaction and boiling of helium. When the top end is hot it becomes a thermal insulator. The helium gas stratifies and convection currents cease.

2.4 Operating cycle

The operating cycle is shown in figure 1. There are four phases to the cycle. At (a), helium gas at a pressure of 6.2MPa (62 bars) is cooled to 12K using a conventional two-stage Gifford-McMahon closed cycle refrigerator. At (b), a valve at room temperature is opened allowing the gas to expand. The expansion is essentially adiabatic, since at 12K the specific heat of the stainless steel and copper high pressure expansion vessel is negligible compared to the heat of its gaseous helium contents. The cooling provided by the expansion results in the vessel remaining approximately one-sixth full of liquid helium. At (c), helium gas at a slight overpressure is piped through counterflow heat exchangers and enters the liquid reservoir. Good thermal contact with the bottom of the expansion vessel causes condensation of the incoming helium and evaporation of liquid helium in the expansion vessel. The cold helium produced by evaporation is piped through the counterflow heat exchangers and is vented to the atmosphere. In effect, liquid helium from the expansion vessel is "transferred" to the liquid reservoir, although there is no plumbing connection joining the two vessels. The final step in the cycle, (d), is that high pressure helium gas is forced back into the expansion vessel, figure 1(d). This compression raises the temperature of the expansion vessel to about 20K. At this stage of the cycle, gravity causes stratification to the helium gas - thermally insulating the liquid helium (4.2K) at the bottom of the liquid reservoir, from the relatively hot (20K) expansion vessel.

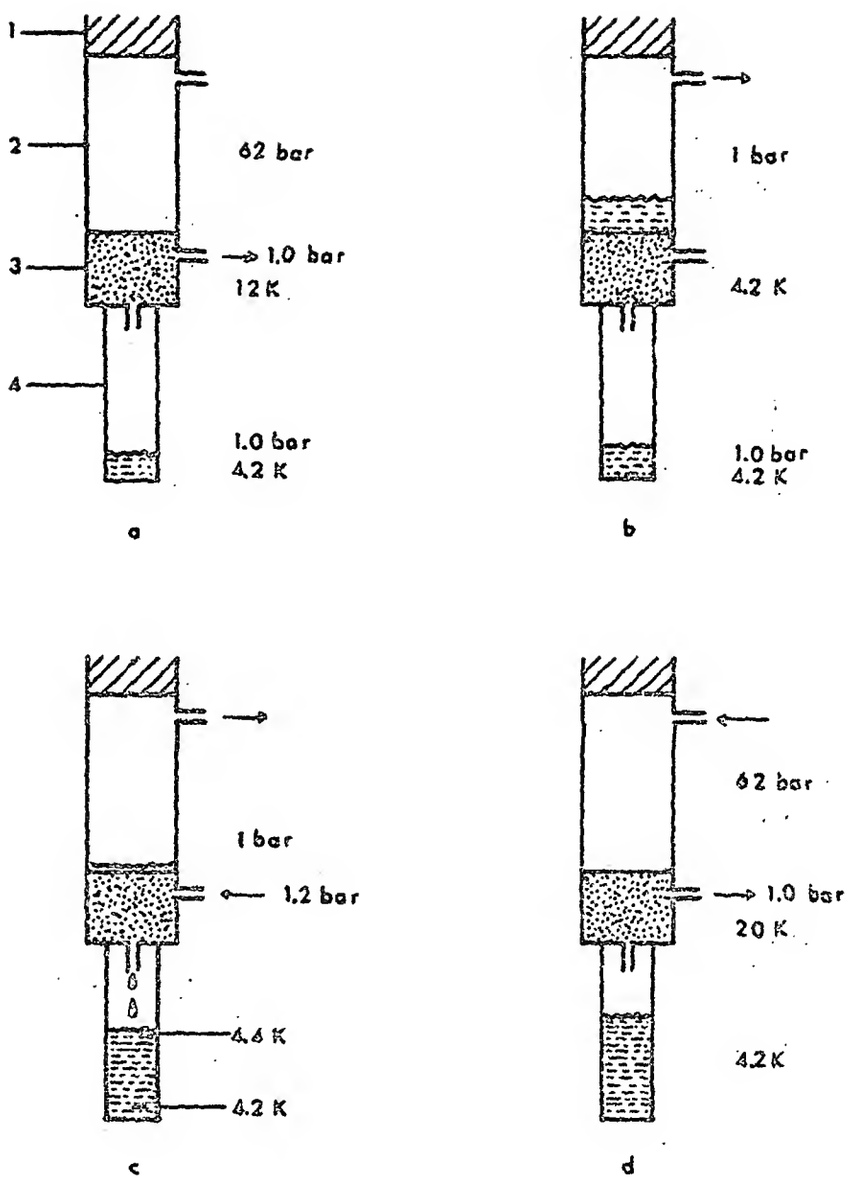

Figure 1 - Cycle of operation

1. 12K Cold finger of Gifford-McMahon cryocooler.
2. High pressure expansion volume.
3. Sintered copper heat exchanger.
4. Low pressure liquid reservoir.

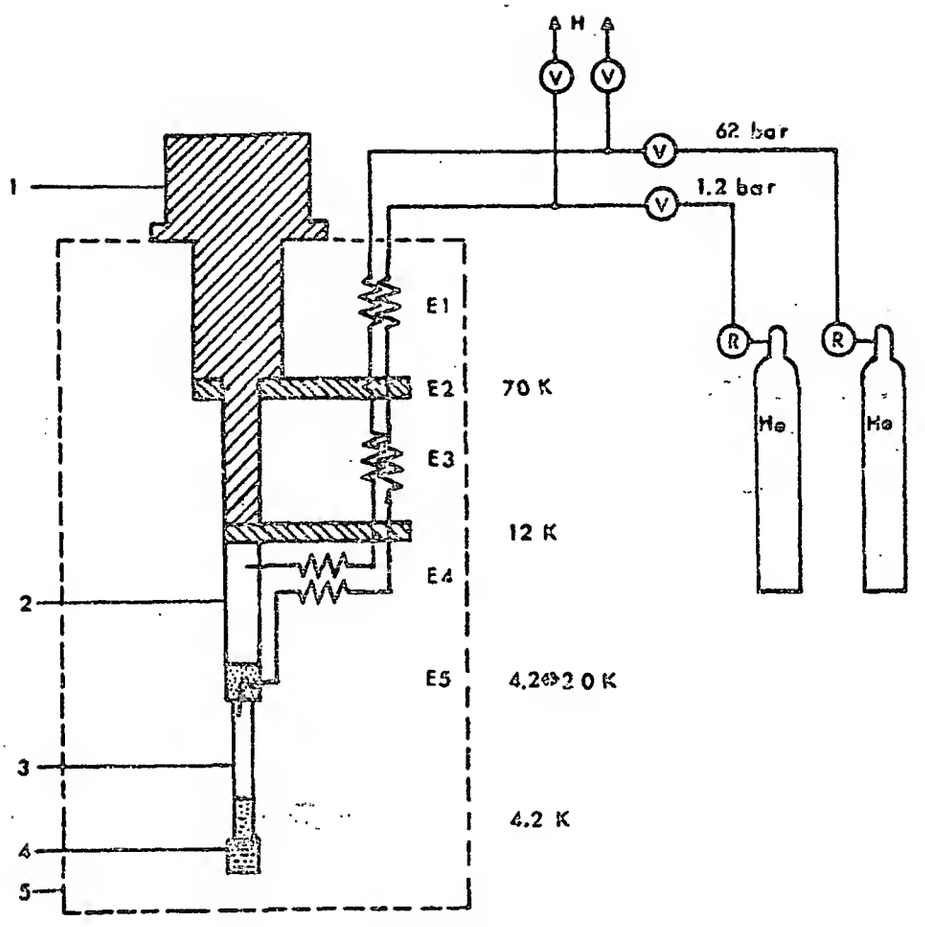

Figure 2 - Schematic diagram of cryocooler

1. 2-Stage, closed-cycle Gifford-McMahon cryocooler.
2. Expansion volume (high pressure).
3. Insulation tube.
4. Liquid helium reservoir (low pressure).
5. Vacuum vessel with heat shields (not shown).

R Pressure regulator valves.
V Electronically driven solenoid valves.
H To helium recovery.
E Heat exchangers.

2.5 Temperature stability in the liquid reservoir

The temperature in the pool of liquid helium in the reservoir is held stable at the boiling point of liquid helium (4.2K). In order to allow helium to condense the pressure in the reservoir is increased to about 0.12MPa (1.2 atmospheres) during the expansion phase. Condensation causes heating of the top layer of liquid helium to its boiling point at this new increased pressure (4.4K). However, the liquid lower down in the reservoir is not heated by condensation. The liquid helium stratifies with a thin warm layer on top. Heating of the liquid at the bottom of the reservoir is by thermal conduction through the liquid and by adiabatic compression of the liquid. The adiabatic compression term is only approximately 20 millidegrees. The thermal conduction term can be much larger. However, the high specific heat of liquid helium and its low thermal conductivity make thermal conduction through the liquid a very slow process. The variation in temperature δT at a depth x due to an abrupt change in temperature of ΔT at the surface is

given by,

$$\frac{\delta T}{\Delta T} = 1 - \mathrm{erf}\left(\frac{x}{2}\sqrt{\frac{\rho\, C_p}{\tau\, K}}\right)$$

where

$$\mathrm{erf}(u) = \frac{2}{\sqrt{\pi}}\int_0^u e^{-y^2}\, dy$$

is Gauss's error integral[6]. The specific heat of liquid helium per unit volume, at constant pressure is ρC_p. The thermal conductivity of liquid helium is K and τ is the time elapsed since the temperature change on the surface.

For example, consider the 0.2 degree change in temperature at the surface of the liquid. The time required for that to cause a temperature change of 0.020 degree is one minute for a liquid helium depth of 0.3cm but is one hour for a depth of only 2.5cm.

In our cryocooler, the liquid reservoir is at a pressure above atmospheric for only 5 minutes during each cycle. Temperature fluctations due to warming of the liquid during this period are therefore substantially dampened once the liquid reservoir starts to accumulate a certain depth of liquid helium.

3. Cryocooler design

A schematic of the four-stage cryocooler is shown in figure 2. The first two stages of cooling, nominally 70K and 12K, are provided by a conventional laboratory Gifford-McMahon cycle crycooler. The third and fourth stage system is thermally connected to the two-stage crycooler. Helium gas lines go from room temperature to the third stage expansion vessel and to the fourth stage liquid helium reservoir. The two gas lines are not interconnected and their helium supplies are independent. Operation of the crycooler is achieved by cycling the pressures at the room temperature ends of the expansion vessel line and the liquid reservoir line.

For simplicity and ease of construction, the pressures are cycled by means of opening and closing electric solenoid valves. The gas lines are alternately charged from compressed gas cylinders and vented to a helium recovery system at one atmosphere pressure. Maximium pressures are set by regulator valves on the gas cylinders. They are set at 6.2MPa (62 bars) for the expansion vessel and 0.12MPa (0.02MPa above atmospheric) for the liquid helium reservoir line. The solenoid valves are controlled by an electronic cycle timing circuit. The rates of charging and venting are quite critical, they are set by manual valves.

The cycle timing is mainly determined by how long it takes the two-stage croycooler to cool the expansion vessel to a threshold temperature of approximately 12K. If the threshold is set too low then it takes a very long time to cool down and the cycle time becomes too long. If the threshold is set too high then very little, or no, liquid helium will be produced during the expansion phase. Typical cycle times are shown in figure 3.

The critical parameter in the design is the length of the time required to complete one cycle. If it takes too long then all the liquid in the reservoir will boil away before the next expansion (cooling) phase commences. During each cycle almost all of the helium gas in the expansion vessel is taken to room remperature then returned to below 12K. The minimum cycle time is mainly determined by how long it takes the two-stage crycooler to cool this mass of helium gas from 300K to 12K. This time is substantially reduced by using effective regenerators to utilize the cooling power of the escaping gasses of one cycle to cool the incoming gasses of the next cycle. The dimensions and masses of the heat exchanger-regenerators are given in table 1. Note that, effective regeneration is assured between 300K and 70K by 500 grams of stainless steel in exchanger E1. Regeneration below 70K is acheived by 850 g of lead shot in exchanger E3. These massive components lengthen the initial cooldown of the crycooler (by about 20 hours) but speed up the operating cycle rate. We have also tested a Simon expander without these regenerators. As expected, its minimum cycle time was too long (over one hour) to maintain a bath of liquid helium.

Another feature worthy of note is the use of the counterflow heat exchanger number E4 (12K-4.2K). This is essential in order for the liquid helium 'transfer', phase (c), to take place. Helium gas entering the liquid reservoir must be cooled to just above its boiling point before passing through the copper powder heat exchanger number E5. If this is not done the cooling power of the boiling liquid in the expansion vessel will be wasted in irreversible heat transfer to hot helium gas and no liquid will be collected in the reservoir.

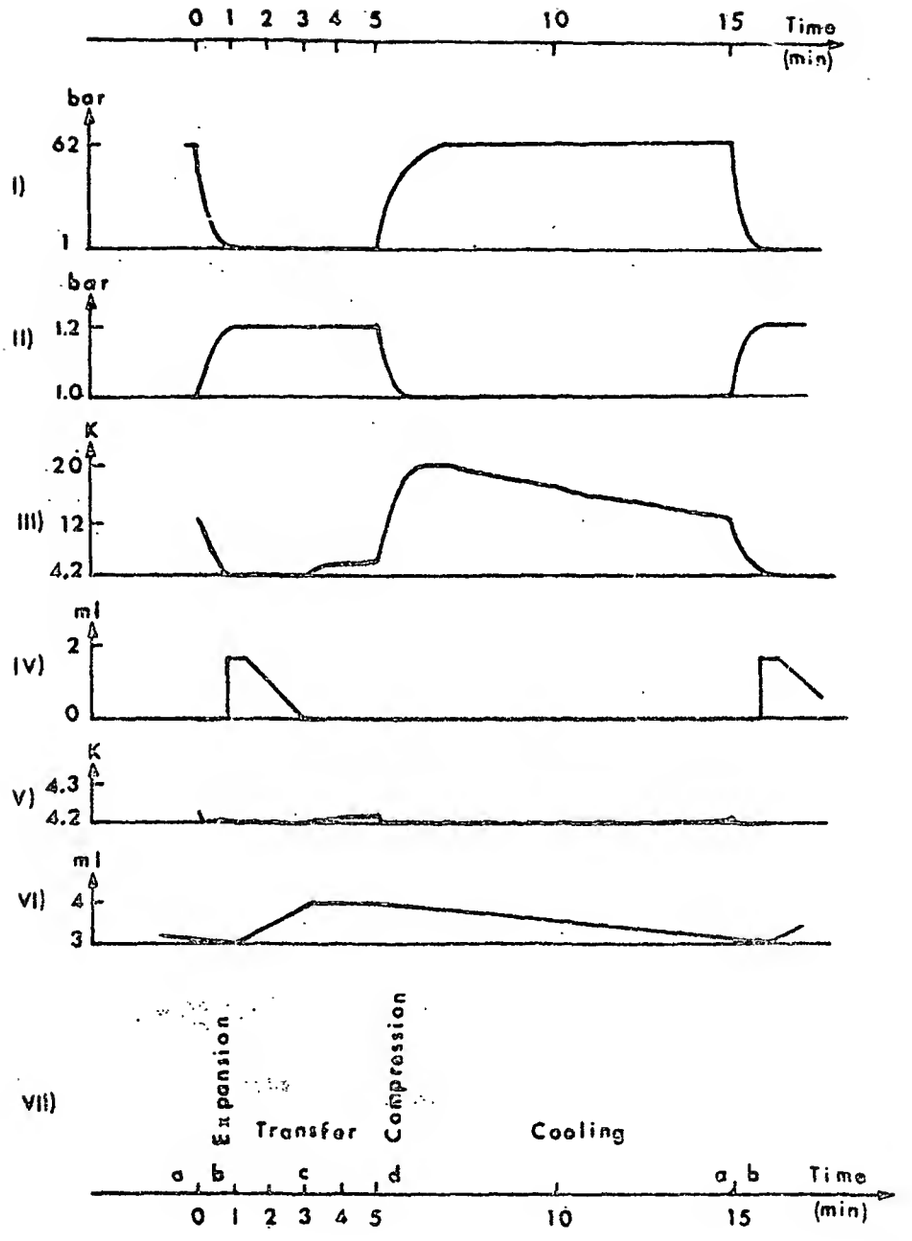

Figure 3 - Cryocooler cycle with no heat load

I) Pressure at the room temperature end of the expansion volume gas line.
II) Pressure at the room temperature end of the liquid reservoir gas line.
III) Measured temperature at the bottom of the expansion volume.
IV) Estimated volume of liquid helium in the expansion volume.
V) Measured temperature at the bottom of the liquid reservoir.
VI) Estimated volume of liquid helium in the liquid reservoir.
VII) Phases of the operating cycle (see also fig. 1).

4. Experimental performance

Figure 3 shows measured cyclic temperature variations at the bottom of the expansion vessel and at the bottom of the liquid reservoir. For convenience, estimated pressure and liquid helium level variations are also shown. The cryocooler provides a good degree of inherent temperature stability. The observed temperature fluctuations at the bottom of the liquid reservoir were only 30 millidegrees, in spite of the 16 degree variation in the temperature of the expansion vessel. This stability is achieved without any electronic temperature regulation.

It was not possible to directly measure the amount of liquid helium in each of the vessels with our apparatus. We have estimated the amount of liquid produced by measuring the time required to boil it off by means of electric heaters. In a series of single expansion experimenta we observed that approximately 2 ml of liquid is produced in the expansion vessel. After a similar expansion followed by a 'transfer' phase approximately 1 ml of liquid had collected in the reservoir. The expansion vessel itself acts as a thermal diode and can retain its charge of liquid for 28 minutes in spite of the fact that its upper surface stays near 12K. That heat leak corresponds to 3 mW which agrees with the value calculated from the thermal conductivity through its thick steel walls. A low thermal conductivity between the top and bottom of the expansion vessel is important so that a pool of liquid may remain at the bottom for long enough to be 'transferred' to the reservoir.

The startup of the cryocooler requires 24 hours of operation of the two stage Gifford-McMahon cycle cryocooler in order to reach 12K. This is due to the massive regenerators which must be cooled. The startup time could be reduced somewhat by providing heat switches to improve the thermal contact to the regenerators. Once the 12K threshold has been reached full operation starts quickly with liquid helium remaining in the reservoir after a couple of cycles. The temperature stability in the reservoir improves dramatically after several additional cycles due to the accumulation of a sufficient depth of liquid helium.

The success of our cryocooler depends on the excellent thermal isolation provided by the thin wall stainless steel insulation tube which separates the expansion vessel from the liquid reservoir. The dimensions of this tube are given in table 1. With one end of the tube at 20K and the other end at 4.2K the theoretical heat leak by conduction through the steel is 0.4 mW and by conduction through the helium is 0.06mW. The liquid reservoir was observed to retain a charge of liquid for over two hours without replenishment. The liquid charge was approximately 2 ml, so this corresponds to a total heat leak of only 0.6 mW.

The cryocooler has been operated with a continuous heat load of 3 mW and it maintains a pool of liquid helium at all times. This power setting agrees with that expected from the latent heat of boiling of 1 ml of liquid every 15 minutes. Naturally, the heat load increases the temperature variation at the liquid reservoir. The maximum temperature variation is nevertheless limited by the boiling point of helium at the pressure applied. Additional temperature regulation could also be incorporated by controlling the pressures in the two gas lines.

The consumption of helium gas from the supply cylinder is such that the cryocooler can be operated for approximately 250 cycles from a laboratory 6 standard cubic meter compressed gas cylinder. With 15 minute cycles this corresponds to 60 hours of continuous operation. If the meximum cooling power is not needed the cycle time may be increased to 30 minutes to extend this period. Another advantage of this design is that cycling can be stopped in the primed state, phase (a), such that liquid helium may be produced at the touch of a button when needed.

5. Conclusions

A cycled adiabatic expansion crycooler which provides continuous cooling at liquid helium temperature has been demonstrated. Temperature stability of the liquid reservoir is very good because it is controlled by the boiling point of liquid helium. Unlike Joule-Thompson cryocoolers, this design does not have any small orifices prone to plugging. It also has no moving parts in the third or fourth stages. These features allow this crycooler to operate even with contaminated helium and make it highly reliable.

The cycled adiabatic cryocooler does not provide as much cooling power at liquid helium temperature as the Quantum Technology Corp. Joule-Thompson cryocoolers using the same two-stage Gifford-McMahon cryocooler. However, it does have its own domain of application where the inherent temperature stability and reliability of the cycled adiabatic cryocooler make it more advantageous.

6. Acknowledgements

The authors thank the Science Council of British Columbia and the National Sciences and Engineering Research Council for their support of this research.

7. References

[1] Winter, C., New approaches to small scale cryogenic facilities, to be published in the Proc. of the 5th World Conference on Biomagnetism, Vancouver, Canada, 1984 Aug. 27; Plenum, NY.

[2] Gygax, S., Cheap helium liquifiers, to be published in LT-17; proceedings of the International Low Temperature Conference-17, Karlsruhe, W. Germany, 1984 August 14.

[3] Zimmerman, J.E., Recent developments in self-contained cryocoolers for SQUIDS and other low-power cryoelectronic devices, to be published in ICEC-10, (Proc. of ICEC-10, Helsinki, Finland, 1984 July 31-August 3).

[4] Simon, F., Phys. Z., 34, 232 (1932).

[5] McCarty, R.D., Thermophysical properties of He-4 from 2 to 1500K with Pressures to 1000 atmospheres, NBS Technical Note 631, (NBS, Boulder, Colorado, 1972).

[6] Jakob, M., Heat Transfer, v. 1, (Wiley, New York, 1962).

Table 1 - Helium liquifier dimensions

STAGE	TEMP. RANGE K	TUBE DIAMETER cm OD	TUBE WALL cm	TUBE LENGTH cm	MATERIAL	MASS gr
(A) EXPANSION VOLUME HIGH PRESSURE TUBING						
E1	300-70	0.48	0.09	500	SS	500
E2	70	0.95	0.15	23	Cu	90
E2	70	copper shot inside copper tube				30
E3	70-12	0.48	0.05	210	SS	130
E3	70-12	lead shot regenerator inside SS tube			Pb	75
E3	70-12	lead shot regenerator outside SS tube			Pb	775
E4	12-4	0.32	0.05	50	SS	20
Expansion volume	4.2	1.6	0.17	8	SS	65
(B) LIQUID RESERVOIR LOW PRESSURE TUBING						
E1	300-70	0.16	0.02	500	SS	50
E3	70-12	1.27	0.09	210	SS	550
E4	12-4.2	0.16	0.02	50	SS	4
E5	4.2	1		0.5	Pressed Cu powder	20
Insulation tube	4.2	0.64	0.02	14	SS	5
Liquid reservoir	4.2	2 ml volume			Cu	10

NOTES: - Expansion chamber volume = 10 ml.

- Low pressure and high pressure tubes are concentric heat exchangers at stages E1, E3 and E4.

VUILLEUMIER CYCLE CRYOCOOLER OPERATING BELOW 8 K

Yoichi Matsubara
Atomic Energy Research Institute
Nihon University
Tokyo 101, Japan

and

Mitsuhiro Kaneko
Cryogenic Department, Suzuki Shokan Co., Ltd.
Saitama 362, Japan

This paper describes the design and development of a Vuilleumier cycle cryocooler (VM cooler) operating below 8 K, for the application of small superconducting devices. Liquid nitrogen has been used as a heat sink of the hot displacer. The annular gap between the phenolic displacer and SUS 304 stainless cylinder has been used as a gap regenerator. In order to obtain the cooling temperature below 8 K, we designed a single stage VM cooler which is precooled to 10 K by another two stage VM cooler. The effect of the mean operating pressure, cycle speed and phase difference between the hot and cold displacer of each VM cooler will be also discussed, including the experimental results.

Key words: Cryocoolers; heat exchangers; helium; low temperature; refrigerators; regenerators; Vuilleumier cycle.

1. Introduction

The requirement of low-power cryocooler investigation for several electronic devices, such as infrared detectors or superconducting devices, has recently increased. This kind of cooler will be used for long term operation with no maintenance. Closed-cycle cryocoolers using gap-regenerators are suitable for these requirements. Zimmerman and Radebaugh have developed a four-stage split-Stirling cryocooler operating at the temperature of about 8.5 K as a SQUID cooler [1]. Myrtle, et al have also demonstrated operation of a split-Stirling cryocooler at 9 K using a single hollow conical displacer [2]. Sager and Paulson have constructed a four stage Gifford-McMahon cycle which achieved an ultimate temperature of 7.1 K [3].

It seems to be difficult to obtain the temperature of below 5 K with these methods, however, Zimmerman and Sullivan have demonstrated the feasibility of operation at the temperature below 4 K using a Stirling cycle cryocooler with the hot end temperature of near 10 K [4]. In our previous work, a Gifford-McMahon cycle cooler anchoring at 10 K also achieved 4.8 K [5]. These results indicate the choice of a cryogenic cycle and the optimized design of regenerators are important in order to achieve the temperature below 8 K. In this paper, we describe the experimental results of two different types of VM cryocooler.

2. Three Stage Vuilleumier Cryocooler

We have built the three stage Vuilleumier cryocooler as a test apparatus. To decrease the mechanical complexity we used liquid nitrogen as a heat rejection stage. A schematic of the VM cooler is shown in figure 1. The expansion and the compression displacers have been driven in sinusoidal motion using a stepping motor with an adjustable eccentric shaft cam. The annular gap between the stainless steel cylinder and the cotton reinforced phenolic displacer was used as a regenerator in each stage. The hot and the three cold displacers were 60, 30, 20, and 10 mm in diameter and about 20 cm in length. The compression part and the expansion part have been operated, respectively, with 15 mm and 20 mm stroke. In the final stage of this cooler, the temperature swing was 7.7 to 8.8 K when the first stage was 33 K and the second was 13 K under the following operating conditions: phase angle of 40 degrees, average pressure of 0.54 MPa, and the

frequency of 70 rpm. Figure 2 shows the cooling capacities at the cold end of this cooler. We have not controlled the quantity of liquid nitrogen flow in its minimum condition, but total LN_2 consumption, including external losses, was 0.5 liter per hour at most.

In order to obtain a lower temperature while reducing the losses in the regenerator, the pressure was decreased. The resulting operation of the cryocooler was not as effective as before. When the phase angle was less than 40 degrees, the temperature difference between the second and final stages increased, despite increasing the temperature of the final stage. We theorized that the changes required an increase in the P-V quantity. To accomplish this it is possible to increase the working mass of the helium gas. However, the losses from the regenerator would simultaneously increase. Another important factor is the second stage temperature. The second stage expansion volume could be increased to optimize the operation when the working pressure is reduced. The cryocooler could be made to produce the same cooling power without increasing the frequency. Consideration of the thermal strain of the thin walled cylinder and the plastic piston during the cool down period shows it is desirable to make the regenerator short. The temperature difference between the warm and the cold end of such a short regenerator must be small in order to reduce the losses in the final stage.

3. The Composite VM Cryocooler

The investigation of the coldest section of the composite VM cryocooler is presented here. Figure 3 shows the schematic diagram. This cooler is made of the two stage pre-cooler and the single stage test cooler. These two coolers have the same driving mechanism in which a variable speed stepping motor and two scotch yokes are used. The working space is separated from atmospheric ambience by two small O-ring seals. The physical dimensions are described in Table I.

Table I. Physical Dimensions of Two VM Coolers

	Pre-cooler			Test Cooler	
	Compression	1st Stage Expansion	2nd Stage Expansion	Compression	Expansion
Cylinder O.D.	48	20	14	48	12
Displacer O.D.	46.8	18.8	12.8	46.8	11.4 *
Displacer L.	136	180	180	136	235 *

All values in millimeters
* - Below pre-cooler 2nd stage (test section)

The test cooler was pre-cooled through a 4 cm width copper band. The radial clearance of the displacer sections were about 0.1 mm. A cotton reinforced phenolic resin rod was used for the displacer. Lead tape 1 mm in width and 0.2 mm thick was wound spirally around the pre-cooler second stage. We used GdRh powder (45 vol. %) with epoxy resin as a regenerative material for the test cooler final stage. The displacer was coated with its material in the thickness of about 0.2 mm.

The pre-cooler was operated without the load of the test cooler. Figure 4 shows its performance under the conditions of 62 degrees in phase angle, 48 rpm and a minimum pressure of 0.25 MPa. The ultimate temperature was 13.4 K. We also obtained about 14 K with the phase angle at about 50 degrees and 65 rpm. Figure 5 shows the test cooler performance with pre-cooler. The minimum pressure of the test cooler was 0.65 MPa and the phase angle was increased by increasing the operating speed until the temperature reached approximately 7 K. This figure shows that the temperature difference of test section is about 11 K under these optimized conditions. It is required to decrease the temperature of pre-cooler 2nd stage in order to obtain the temperature of below 5 K. Table II shows the operating conditions and the results. The temperature swing of the final stage of the test cooler was 5.4 K to 6.5 K without the external heat load. The second stage temperature of the pre-cooler was about 16.1 K with the phase angle of 50 degrees and the minimum pressure of 0.4 MPa. In any other conditions, the temperature of below 16 K was not obtained.

Table II. Test Results of the Composite VM Cooler

I. Pre-cooler
- Phase angle: 50 degrees
- Pressure swing: 0.4 MPa to 0.96 MPa
- Operating speed: 60 rpm
- Stroke of the compression displacer: 18 mm
- Stroke of the expansion displacer: 10 mm
- Temperature of the compression part at cold stage: 81 K
- Temperature of the expansion part at 1st stage: 34.4 K
- Temperature of the expansion part at 2nd stage: 16:1 K

II. Test Cooler
- Phase angle: 53 degrees
- Pressure swing: 0.155 MPa to 0.34 MPa
- Operating speed: 39 rpm
- Stroke of the compression displacer: 18 mm
- Stroke of the expansion displacer: 5 mm
- Temperature of the expansion part at cold stage: 81.4 K
- Temperature of the expansion part at point 1: 41.2 K
- Temperature of the expansion part at point 2: 16.1 K
- Temperature of the expansion part at cold end: 5.4 to 6.5 K

In order to determine the cooling power which the cooler was producing, we measured simultaneously the warm end pressure and the movement of the displacer with the time axis using a pressure transducer and a linear displacement converter. The P-V diagrams are shown in figures 6 and 7. The pre-cooler produced the cooling power of about 250 mW at the second stage. The test cooler produced the cooling power of about 27 mW at the final stage. The effect of the backlash of a scotch yoke appeared at the top and the bottom end in the figures. We estimate that most of the cooling power produced by the pre-cooler was consumed by the regenerator loss. The amount of heat rejection from the test cooler is estimated to be less than 50 mW.

4. Conclusion

We obtained the ultimate temperature of 5.4 K and about 10 mW at 7 K by using the composite VM cryocooler when the temperature of the pre-cooler was about 16 K. However, there remain many problems to be solved such as the regenerator loss analysis including the effect of dead volume and a specific heat of the regenerative materials, phase angle optimization, and the effect of the non-ideality of the helium properties.

The authors would like to thank Professor K. Sekizawa for providing the GdRh powder. Part of this work has been supported by the Science and Technology Agency.

5. References

[1] Zimmerman, J. E., Radebaugh, R., NBS SP-508, Page 59 (1978).

[2] Myrtle, K., Winter, C., and Gygax, S., Cryogenics, 22, Page 139 (1982).

[3] Sager, R. E., Paulson, D. N., NASA CP-2287, Page 81 (1983).

[4] Zimmerman, J. E., Sullivan, D. B., Cryogenics, 19, Page 170-171 (1979).

[5] Matsubara, Y., Yasukochi, K., NASA CP-2287, Page 157 (1983).

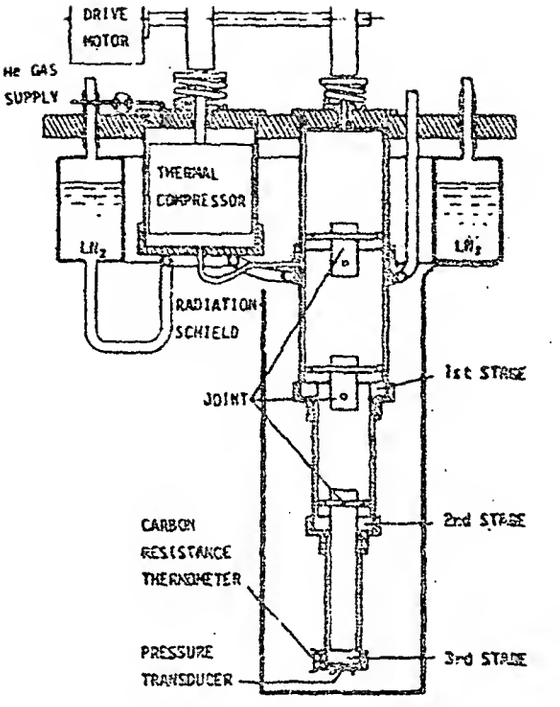

Fig.1. Schematic diagram of three-stage VM cooler

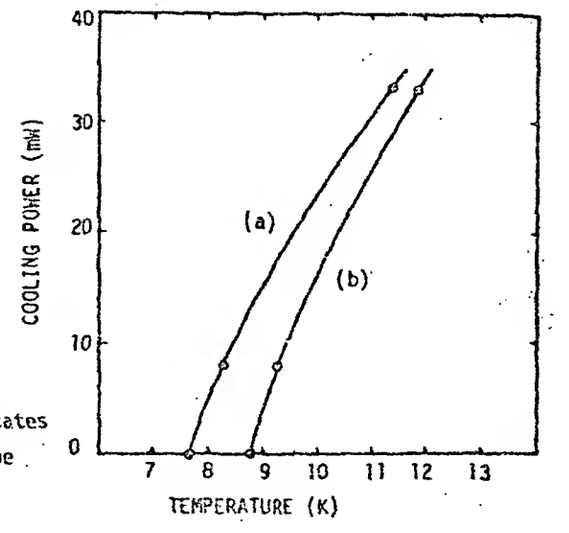

Fig. 2. Three-stage VM cooler cooling capacity of the final stage vs. temperature: (a) and (b) indicates the upper and lower bound of the temperature swing

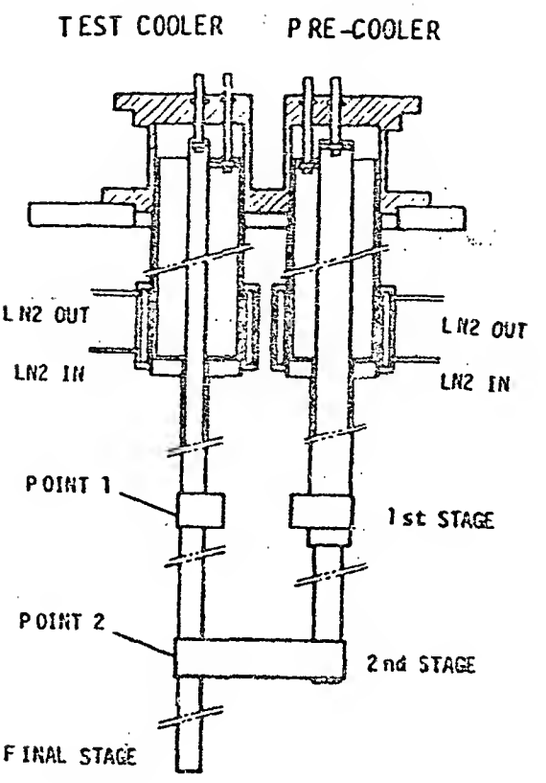

Fig.3. Schematic diagram of the composit VM cooler

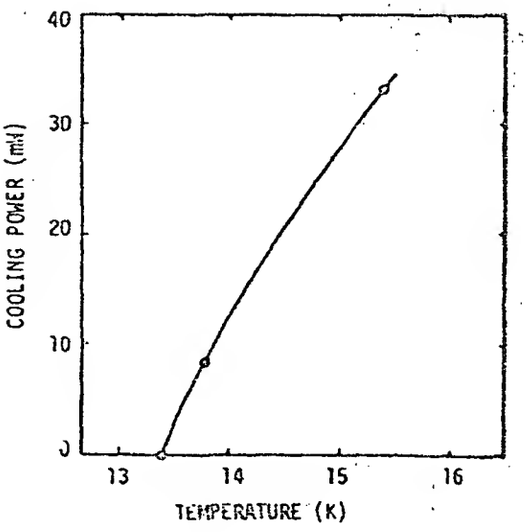

Fig.4. Pre-cooler cooling capacity of the 2nd stage temperature

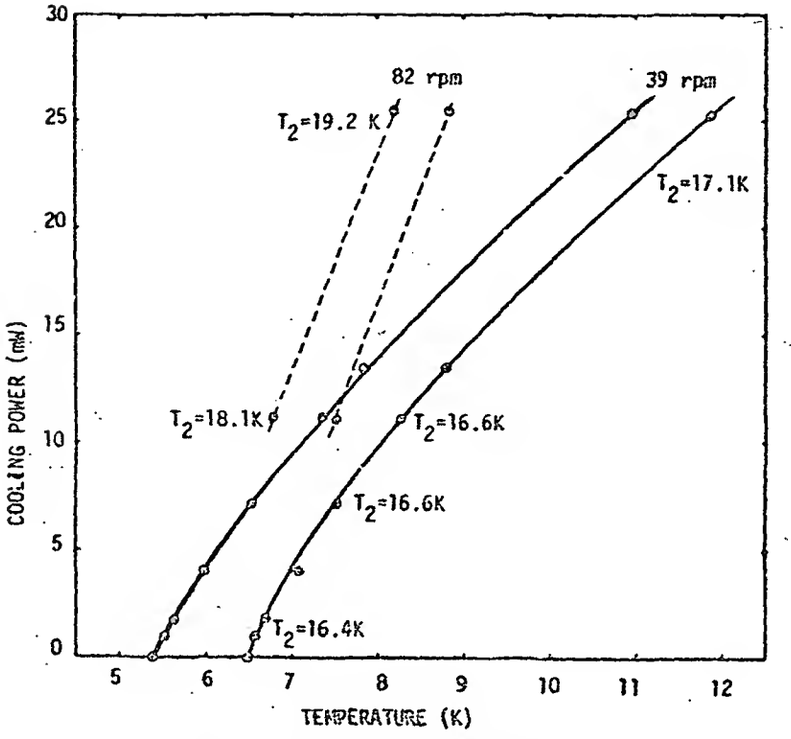

Fig. 5 Test cooler cooling capacity vs temperature
(T_2: Temperature of the precooler 2nd stage)

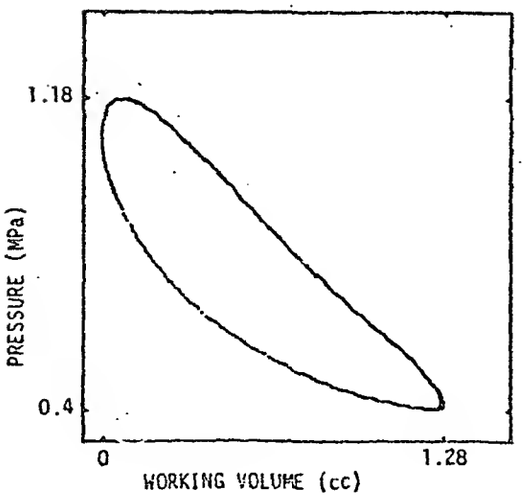

Fig.6. P-V diagram of the 2nd stage of the pre-cooler

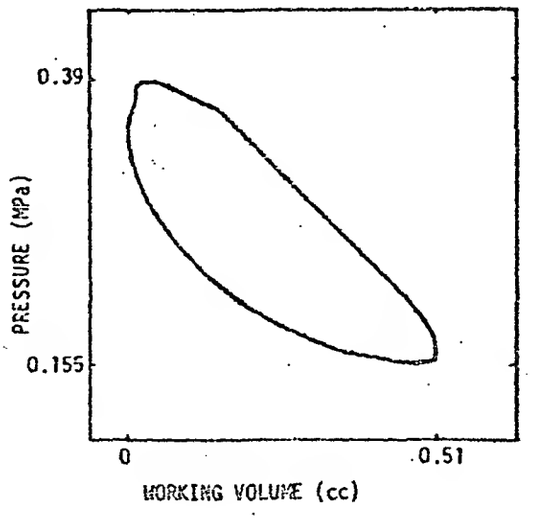

Fig.7. P-V diagram of the final stage of the test cooler

D24

4K REFRIGERATORS WITH A NEW COMPACT HEAT EXCHANGER

R. C. Longsworth

H. A. Steyert

Air Products and Chemicals
Allentown, PA 18105

ABSTRACT

Two refrigerators have been developed which have nominal capacities of 0.25W and 0.5W at 4.2K. These use standard two stage Displex® expanders and compressors combined with a new compact heat exchanger which is concentric with the expander cylinder.

These refrigerators can be used to cool superconducting electronic devices by direct attachment to the 4K heat station, or they can be plugged into the neck of a liquid helium superconducting magnet cryostat where they can cool the radiation shields and reliquefy helium.

Key Words: Compact heat exchanger; cryogenic refrigerator; helium recondenser; superconducting electronics; superconducting magnet

1. Introduction

The use of superconducting magnets for Magnetic Resonance Imaging (MRI) represents the first major commercial application of superconductivity. The magnets presently in use utilize liquid cryogens, helium and nitrogen; however, a number of options for cooling magnets using small refrigerators or liquefiers have been studied [1]. The approach to cooling a superconducting magnet which is the size of an MRI magnet that appears most promising to the authors is to have a multistage refrigerator mounted integrally into the magnet cryostat. This refrigerator will fit into the neck of the cryostat, cool one or two radiation shields, and recondense the helium. This approach has the advantage that heat is removed from the system very close to the point where it enters the system, thus avoiding additional thermal losses associated with transferring refrigeration from a remote liquefier and minimizing temperature drops between the cryostat and refrigerator. The Japanese National Railway in evaluating refrigerators for their magnetically levitated train program recently concluded that multiple Stirling plus J-T cycle coolers are less efficient than one central Claude cycle refrigerator, but the losses in the cryogenic transfer system add so much to the refrigeration requirement of the Claude cycle system that it consumes more power than multiple Stirling plus J-T coolers. They have thus decided to use individual Stirling plus J-T cycle refrigerators mounted in each magnet cyrostat [2].

The most widely used small 4K refrigerators today consist of a two-stage Gifford McMahon type expander with a J-T exchanger [3,4]. These units utilize rather long and bulky finned tube or corrugated tube heat exchangers for the J-T loop, making them difficult to install in the neck of a helium cryostat. These systems would also have thermal losses due to convective heat transfer between the heat exchangers, the expander, and the neck tube.

Recognizing the potential need for a heat exchanger which would fit compactly in the annular space around a two-stage GM type expander cylinder and which would match the temperature gradient in the cylinder, a program was initiated to study heat exchanger designs that would be suitable for this application. This led to an experimental program to test the newly designed heat exchangers by utilizing them in a nominal 0.25 W and a 0.5 W 4K refrigerator. The experimental program also included studies of heat station design, interaction of the refrigerator with magnetic fields, servicing the refrigerator and control of contaminants. This paper describes the results of this work.

2. Design Description

The two units which have been built and tested are designated as a CS302 and a CS304 with nominal capacities at 4K of 0.25 W and 0.5 W, respectively; they consist of standard Displex® refrigerators having 20K capacities of 2 W and 6 W, respectively. A J-T heat exchanger and a second slightly modified standard compressor for the J-T return flow are added to provide the 4K refrigeration.

After studying many heat exchanger designs and experimenting with different fabrication techniques, we elected to utilize a heat exchanger design which consists of multiple high and low pressure tubes in a close contact, coiled configuration. The heat exchanger is continuous from 4K to 300K and is coiled around the expander cylinder in such a way that the temperature in the heat exchanger matches the temperature in the adjacent cylinder. It is thermally bonded to the cylinder at the two heat stations. Adsorbers are installed at the inlet to the heat exchanger and just upstream of the J-T orifice.

Figure 1 shows the essential features of the 0.5 W expander which is designed to fit into the neck of a helium cryostat. A plug at the 20K heat station is designed to fit snugly into a mating receptacle in the neck tube to cool a radiation shield. For cryostats which use liquid nitrogen to cool a shield at 77K, a heat station on the first stage of the refrigerator is unnecessary. The 4K heat station consists of a finned tube which serves to recondense helium boil-off.

The 0.25 W unit which we built is designed to be operated in a vacuum. It has a warm heat station to which a radiation shield can be attached and a 4K heat station for conductively cooling a device and/or instrumentation. This unit has a very small pneumatically actuated J-T valve which permits high J-T flow rates to be maintained during cooldown and adjustment of the operating temperature with maximum capacity when cold.

The adjustable J-T valve is convenient for a research worker who can set it manually but is difficult to automate. A fixed J-T orifice is used in the 0.5W unit. The flow rate is quite low when the helium is warm so cool-down of the 4K heat station is prolonged when the unit is run in a vacuum. This does not matter when the unit is plugged into a cryostat with helium in it because some venting helium cools it quickly. Temperature is set by means of a pressure regulator which controls J-T return pressure. Flow through the fixed orifice is constant so for any pressure above the minimum design pressure, the regulator bypasses the excess flow in the low pressure compressor.

The CS304 unit shown in Figure 1 incorporates several features that facilitate installing and removing it from the neck of a helium cryostat. Guide sleeves are mounted on the valve motor housing which slide over rods that keep the refrigerator centered as it is raised or lowered. A radial "O" ring seal on a short skirt at the warm end allows for axial contraction while maintaining good thermal contact at the 20K heat station. The warm end skirt is also used to tie on an elastomer sleeve which prevents air from getting into the neck tube when the refrigerator is removed to be serviced.

3. Experimental Program

3.1 Refrigeration Capacity

Both size expanders were built with pressure taps just upstream of the orifice in order to monitor contaminant freeze out in the heat exchanger, and temperature sensors on each stage of the refrigerator. Heaters were added as required for specific tests. The capacity of each refrigerator was measured by mounting it in a vacuum pot and wrapping it with six to ten layers of aluminized mylar.

Figure 2 shows the relationship between temperature and heat load applied to the 4K heat station for different settings of the J-T valve in the CS302. This test was run with no heat loads applied to the upper two stages; however, the second stage can carry about 0.5W and the first stage, about 5W without seriously reducing the refrigeration available at the third (4K) stage. Radiation and instrument lead conduction are estimated to impose an additional 100mW heat load on the third stage. A radiation shield attached to the first stage would thus make more refrigeration available at 4K.

Temperature at the 4K heat station is set primarily by the pressure at which the helium leaving the J-T valve is evaporating. Closing the J-T valve reduces the helium flow rate and the compressor return pressure drops. The slight increase in temperature with load is due to an increase in heat transfer between the surface of the heat station and the evaporating liquid as the heat load is increased. At sufficiently high heatloads all of the liquid produced is evaporated and the gas stream itself is heated. A J-T unit has the characteristic that the refrigeration produced drops rapidly when the maximum capacity is exceeded because the flow rate drops as the temperature of the gas flowing through the J-T valve increases.

Figure 3 shows the interrelationship between the refrigeration available at the three heat stations for the CS304 unit. This data was obtained by setting heat loads on the first and second stages and increasing the heat load on the third stage until the unit warmed up. An example of how to interpret Figure 3 is that a load of 15W on the first stage, 3 watts on the second stage and from 0 to 0.5 W on the third stage results in temperatures of 80K and 16K on the first and second stages respectively. The third stage capacity is available over a temperature range of about 3.9 to 4.5K depending on the setting of the pressure regulator.

3.2 Heat Exchanger Performance

Heat exchanger efficiency was measured by adding differential thermocouples (iron doped gold vs. chromel) to the warm ends of each section of the heat exchanger. Figure 4 plots the data in dimensionless heat transfer and pumping energy after Kays and London Fig. 24 [5]. It is seen that the heat exchanger has higher heat transfer efficiency for a given pumping energy than typical plate fin heat exchangers.

3.3 Magnetic Effects

Studies were made of the effect of operating in magnetic fields in terms of the effect of the fields on the refrigerator expander and the effect of the expander on the homogeneity of the field. It was found that the valve motor can only operate satisfactorily in fields of 0.08T and that the 1Kg of iron in the valve motor contributes the only significant amount of inhomogenity to the field [6].

3.4 Test Cryostat

A double-walled cryostat was built for the CS304 which simulates the neck tube of a large liquid helium cryostat and has room to accumulate 1L of liquid. It has an 89mm (3.5") bore and a second stage receptacle to mate with the tapered plug on the second stage of the refrigerator. It has no first stage heat station. This cryostat was used to measure heat transfer characteristics of the second stage thermal coupling, temperature stability, serviceability and long-term operation.

3.5 Cool Down

Figure 5 shows the cool down data collected and plotted on an HP3497/HP87 data acquisition/computer system for the CS304 in the double-walled cryostat. The temperature scale is folded at 30K so the second and third stage temperatures show scale changes at 30K. The first and second stages cool down relatively fast, but the third stage takes a long time because of the thermal mass of the test pot, the cooling of the 1L volume of helium (which is maintained at 1.1 atm pressure), and the low flow rate of helium in the J-T loop during most of the cool down. When operating in a vacuum with no applied heat loads or extra mass attached both refrigerators reach 4.2K in 4 hours.

3.6 Temperature Stability

Despite the lack of a precooling heat exchangers on the CS304 first and second stages the unit condenses 1L of helium overnight. After accumulating liquid in the pot, the feed valve is closed and pressure in the cryostat monitored. Over a period of a week the cryostat pressure is typically maintained in the pressure range of 700 to 720 Torr. Most of the variation is due to changes in barometric pressure which is normally 760 Torr.

3.7 Thermal Coupling

Studies of the heat transfer characteristics of the thermal coupling showed that heat is transferred primarily by gas conduction in the gap and metal-to-metal contact contributes only a small amount. The weight of the refrigerator is sufficient to maintain good contact. A temperature of 1.1K was measured for a heat load of 3W at 16K.

3.8 Serviceability

The refrigerator is designed to be easily serviced. During the testing phases, the refrigerator was removed from the cryostat and reinstalled a number of times to demonstrate that this procedure could be accomplished with no undo problems (such as air inclusion, ice, etc.), as well as to establish service instruction data. On one occasion, for example, the refrigerator was removed using the flexible sleeve to preclude air in-leakage, and warmed to room temperature, a different size J-T orifice was installed, the J-T heat exchanger was purged, and reinstalled in the cryostat in 45 minutes. The unit cooled back to 20K before the last of the 1L liquid helium evaporated.

3.9 Reliability

In order to assure long-term reliability, a considerable effort was expended to determine the most efficient means to clean up the system initially and keep it clean, in order to avoid accumulating contaminants in the gas stream which could have the potential to block the J-T heat exchanger. After initial experimentation, the last 9,000 hours of cumulative operation on several CS304 units, most of it at subatmospheric pressure, have resulted in no indications of contaminant freeze out in these systems.

4. Summary

Compact 4K refrigerators have been developed and tested, primarily to be utilized in superconducting magnet and electronic applications. A simple compact J-T heat exchanger, has been developed which can be mounted on a two-stage G-M type refrigerator, providing a small, efficient, three-stage machine. Extensive testing has been completed on initial prototype and preproduction machines, which has included in-house performance and life testing. Field testing has included the successful cooling of the cold radiation shield and recondensing the helium in an MRI magnet and cooling of a small superconducting electronic device.

References

[1] R. C. Longsworth, "Interfacing Small Closed-Cycle Refrigerators to Liquid Helium Cryostats," Cryogenics, 24, (1984), pg. 175.

[2] T. Ohtsuka, and Y. Kyotani, "Recent Progress on Superconducting Magnetic Levitation in Japan," Plenary Talk at ICEC 10, Helsinki, August 3, 1984.

[3] W. H. Higa and E. Wiebe, "One Million Hours at 4.5 Kelvin," NBS Special Publication 508 V., 1978, pg. 99.

[4] R. C. Longsworth, "Serviceable Refrigerator System for Small Superconducting Devices," NBS Special Publication, 607 V., 1981, pg. 82.

[5] W. M. Kays, and A. L. London, "Compact Heat Exchangers, " Second Ed., McGraw-Hill, New York, 1964, p. 4.

[6] R. C. Longsworth, and W. A. Steyert, "The Use of Small Cryogenic Refrigerators Near High Homogeneity Magnets, " Cryogenics 24, No. 5, (1984), p. 243.

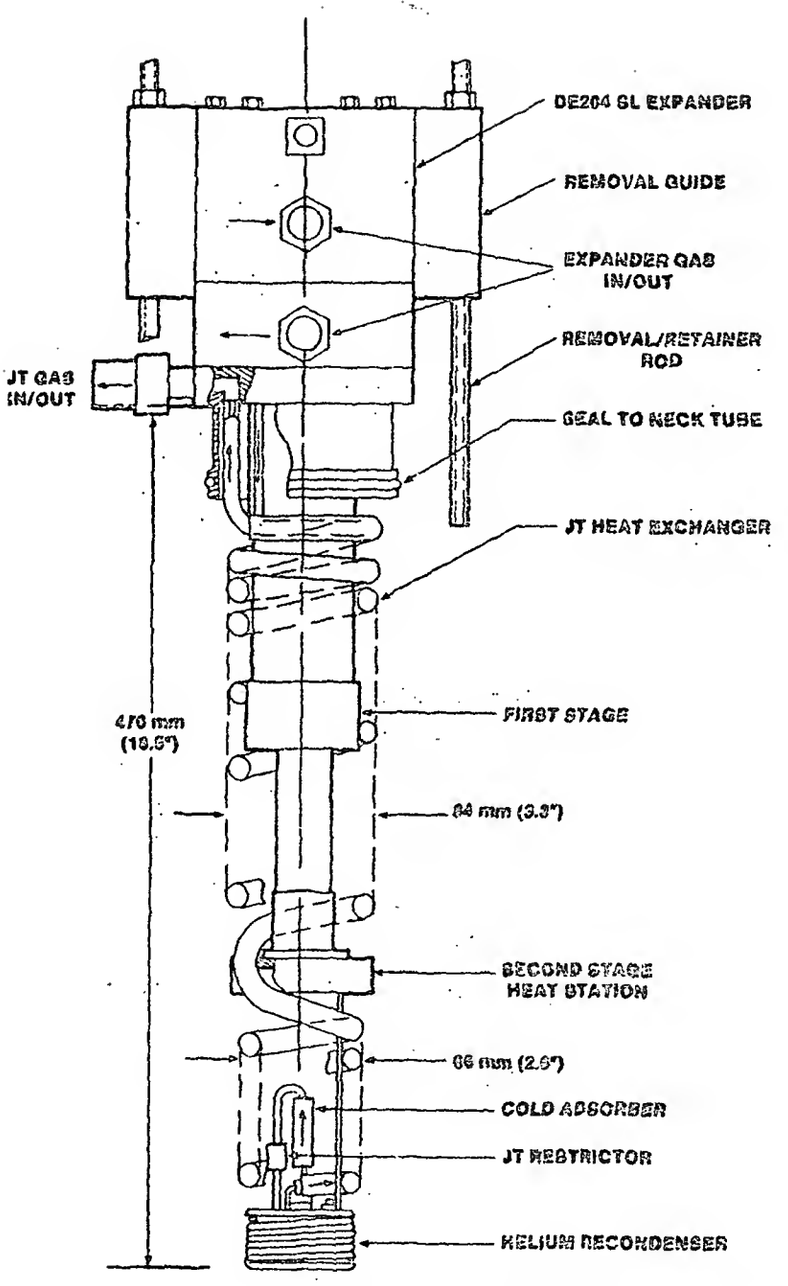

Figure 1. CS304 Refrigerator, Two Stage Expander with Concentric Spiral J-T Heat Exchanger

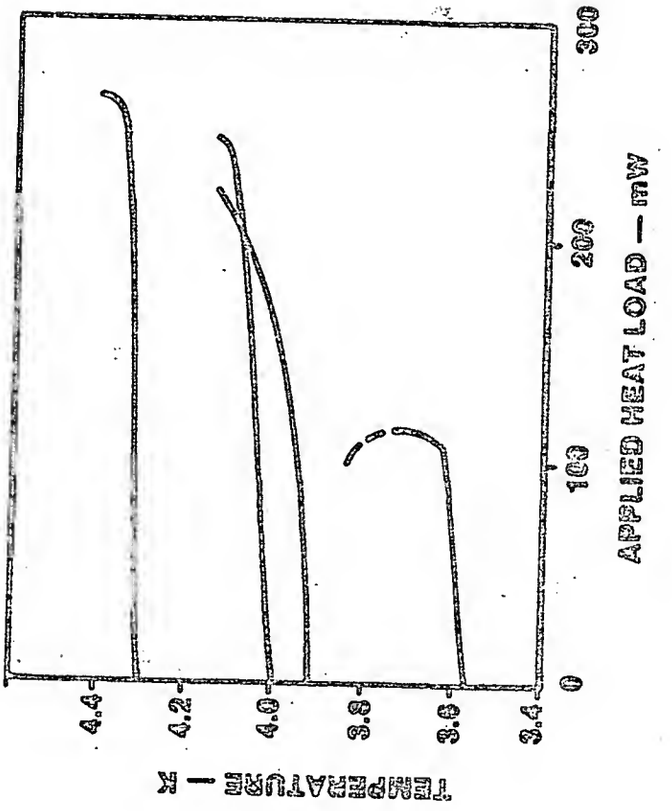

Figure 2. Temperature vs. Applied Load on CS302 for Different Settings of the J-T Valve

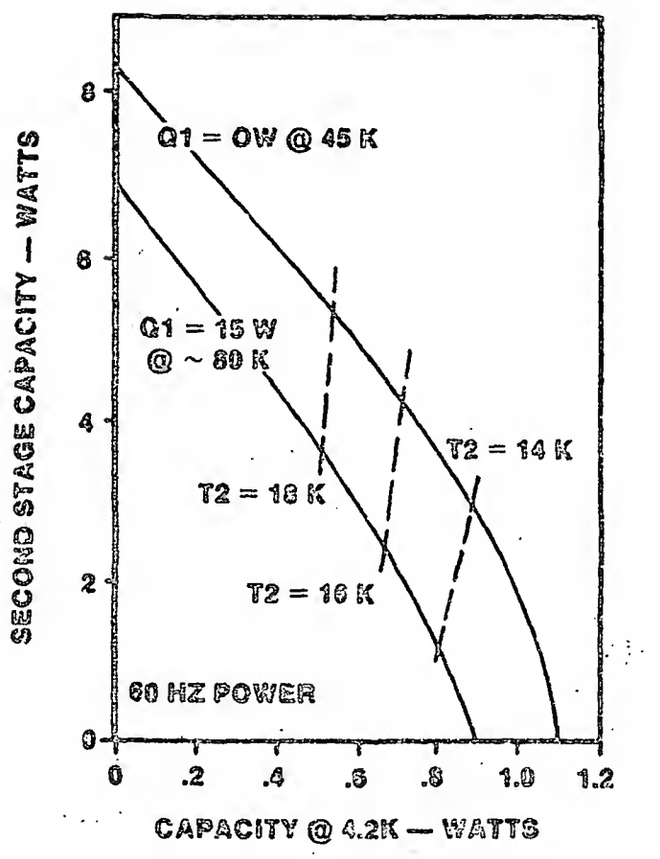

Figure 3. CS304 Maximum Refrigeration Capacity @ 4.2 K vs. First and Second Stage Heat Loads

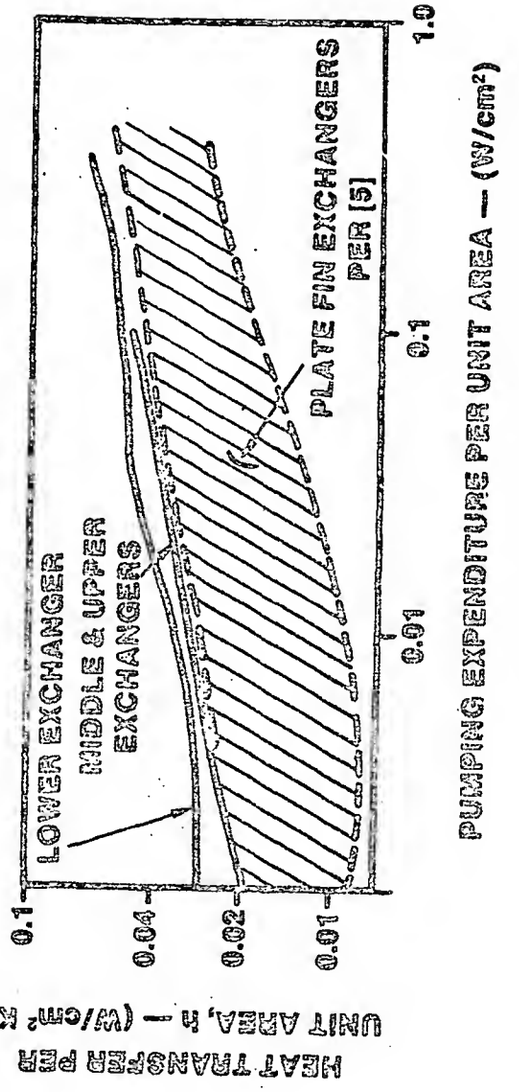

Figure 4. Heat Transfer Coefficient, h. vs. Flow Friction Energy Loss Per Unit Area for APCI Coiled Tube J-T Heat Exchanger and Typical Plate F in Surfaces

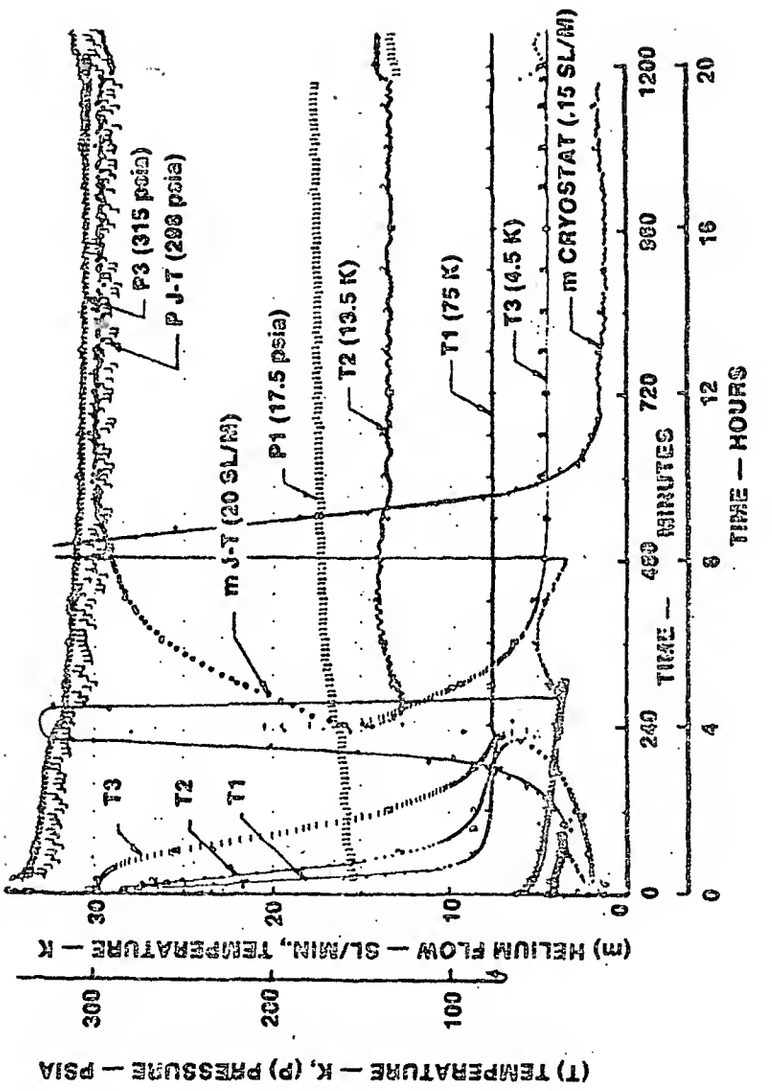

Figure 5. Cooldown of CS304 .5 W 4 K Refrigerator with Experimental Heat Exchanger in Helium Filled Cryostat

D25

THE DESIGN OF A SMALL LINEAR-RESONANT, SPLIT STIRLING CRYOGENIC REFRIGERATOR COMPRESSOR

R.A. Ackermann

MECHANICAL TECHNOLOGY INCORPORATED
968 Albany-Shaker Road
Latham, New York 12110

For the past two years, Mechanical Technology Incorporated (MTI) has been engaged in the development of a small linear-resonant compressor for use in a 1/4-watt, 78K, split Stirling cryogenic refrigerator. The compressor contains the following special features: 1) a permanent-magnet linear motor; 2) resonant dynamics; 3) dynamic balancing; and, 4) a close-clearance seal between the compressor piston and cylinder. This paper describes the design of the compressor, and presents component test data and system test data for the compressor driving a 1/4-watt expander.

Key words: close-clearance seal; compressor; cryogenic refrigerator; dynamic balancing; linear-resonant compressor; permanent-magnet linear motor; resonant dynamics; split Stirling; 1/4-watt expander

1. INTRODUCTION

The objective for this program was to design, fabricate, and test a linear compressor that could be used in the military's 1/4-watt split Stirling cooler. The compressor was designed to demonstrate that it could ultimately meet the existing specifications for size, weight, and input power when driving an existing expander. The important requirements designed for in the compressor are:

1) high reliability, and MTBF's greater than 3000 hours;
2) the elimination of all lubricants;
3) low mechanical vibration; and,
4) the elimination of contacting seals.

Items 1 and 2 were achieved by using a linear drive system that eliminated mechanical linkages and the need for lubricants. Item 3 was achieved by incorporating into the compressor a balancing technique previously developed and patented by MTI, and Item 4 was achieved by using a close-clearance piston/cylinder seal.

2. COMPRESSOR DESCRIPTION

The prototype linear cooler developed is shown in Figure 1, and the design of the compressor is shown in Figure 2. Beginning at the left end, the compressor consists of the piston/cylinder, with the piston connected to the motor plunger through a flexible rod. The plunger, which is made up of radially energized $Sm\ Co_5$ permanent magnets and a back iron, is supported on either end by teflon bearing pads that position the plunger inside the motor stator. The stator contains the electric coils and the end caps rigidly fastened to the stator on either end form the compression cylinder and bearing assemblies described above. On the right end of the compressor is the counterbalance weight, which is connected to the plunger through a mechanical spring and attached to the outer case, along with the stator, through a flexible support configuration. Mechanical springs between the plunger and end caps provide the resonant characteristics. The outer pressure case, gas transfer tube, and displacement sensor located in the center of the plunger complete the design.

Figure 1 MTI Linear 1/4-Watt Split Stirling Breadboard Cooler

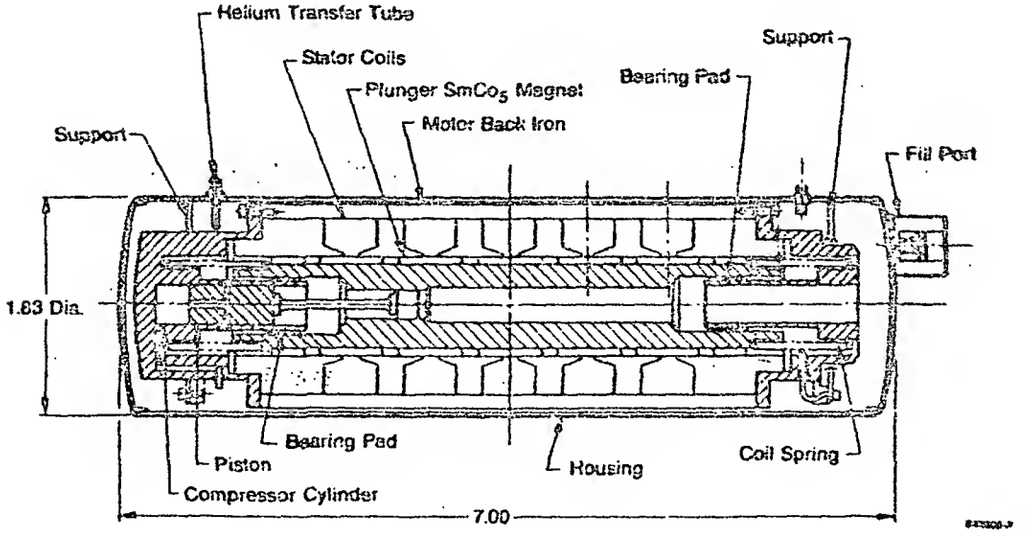

Figure 2 Compressor Layout (Dimensions in inches)

The specifications for the compressor were:

Frequency	22	Hz
Mean Pressure	600	psia
Pressure Differential	400	psia*
Input Power	>30	watts
Weight	>2.5	lb

In the design, it turned out that the critical design trade-off parameters were:

- bore-to-stroke ratio;
- resonant frequency;
- mechanical spring design;
- weight of the motor plunger; and,
- pressure differential.

The bore-to-stroke ratio was important in establishing the size of the motor, the compression-space spring component, the stress in the mechanical springs, and the piston leakage and frictional losses. A trade-off analysis of these parameters with the bore-to-stroke ratio showed (Figure 3) that an upper limit on stroke of 0.6 inch was set by the stress in the mechanical springs, and a lower limit of 0.3 inch was set by the outside diameter of the motor and the amount of gas spring developed in the compression space. The mechanical springs were limited to a stress of 60,000 psi, the gas spring was limited by a maximum plunger weight of 0.5 lb, and the motor size was limited by the maximum diameter specification of 1.750 inch. As for the bore-to-stroke ratio, the other four items also relate to the dynamic operation of the compressor. For this design, the operating frequency of the compressor was specified as 22 Hz. Achieving resonant operation in a high-pressure differential, low-stroke compressor at this low frequency is difficult because of the large spring component derived from the compression space. Balancing this spring with the inertia component of the moving assembly required a large plunger weight. To minimize this weight, a maximum stroke of 0.6 inch was selected.

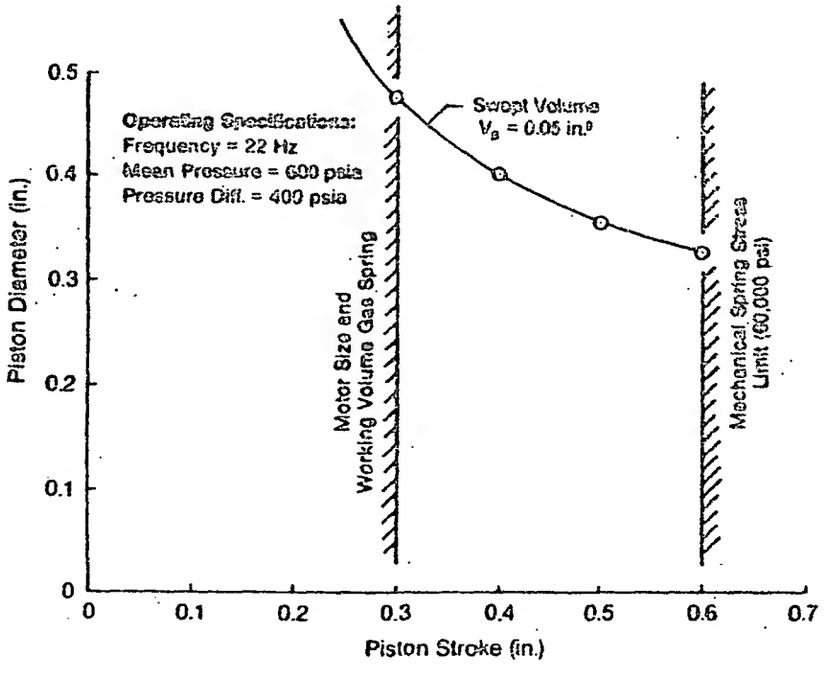

042221

Figure 3 Compressor Bore-Stroke Relationship

*When connected to a 1/4-watt split Stirling cooler expander or equivalent volume.

The final design criteria for the compressor were:

Frequency	-	22 Hz
Swept Volume	-	0.82 cm^3
Stroke	-	15.24 mm
Bore	-	7.9 mm
Motor Diameter	-	44.45 mm
Plunger Weight	-	0.25 kg

2.1. Motor Characteristics

The linear motor used is one of a family of permanent-magnet ($Sm\ Co_5$) linear motors developed at MTI. Figure 4 schematically shows a section of the motor with the plunger in the center position. The motor consists of stationary outer electrical coils wound on a steel bobbin, and an inner permanent-magnet plunger. The magnets are radially magnetized, with alternate magnets having north polarity on the outside diameter and south polarity on the inside diameter. The design characteristics for the motor are:

Frequency	22 Hz
Stroke	15 mm
Static Force	35.6 nt @ 2.0 amp D.C.
Electrical Input Power	<30.0 watts
Voltage	17.5 V.A.C.
Weight	< 1.0 Kg

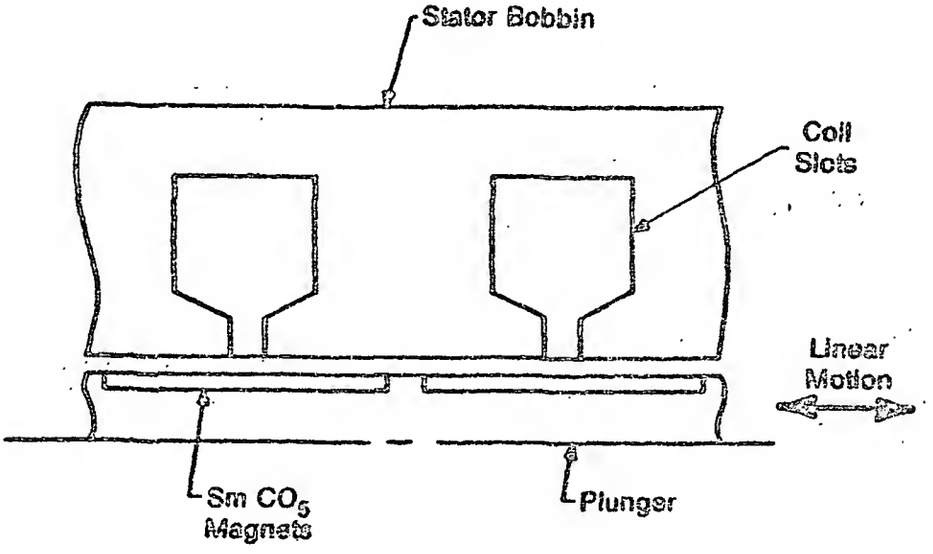

Figure 4 Permanent-Magnet Motor

2.2. Vibration Isolation

Vibration isolation is achieved by employing a counterweight system with the isolation characteristics described in Figure 5. For this isolation technique, the counterweight is attached to the stator through a mechanical spring, and both the stator and counterweight are supported from the housing by mechanical springs. Through the proper design of this spring mass system, the counterweight (M_m) is tuned so that the transmitted force to the case through the two springs (K_3 and K_4) may be designed to cancel one another, producing zero transmissibility. The advantages of this sys-

tem are that the counterweight mass and amplitude are kept small, and good force isolation can be obtained over a broad operating range of frequencies (ω) equal to or near ω_o. The characteristics of the isolation system are:

$K1 = 343$ nt/m
$K2 = 820$ nt/m
$K3 = 491$ nt/m
$M_m = 0.09$ kg
$\omega_n = 18$ Hz
$\omega_o = 22$ Hz

Type of Isolator: Dynamic Two-Degree-of-Freedom

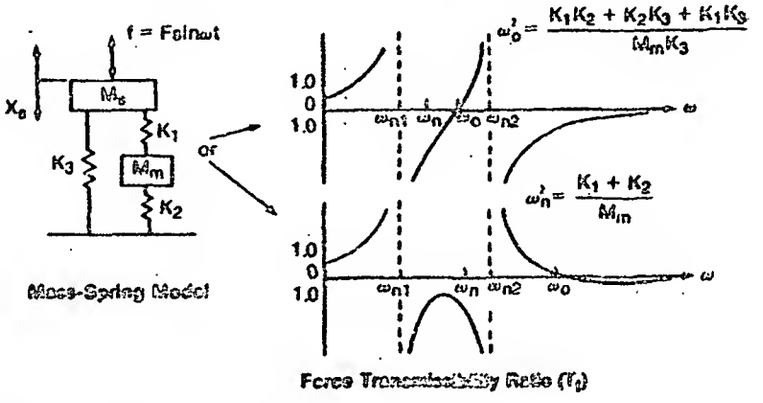

Notes:
$f = F\sin\omega t$ = dynamic exciting force
X_s = dynamic displacement of isolated machine (M_s)
$T_f = 0$ when $\omega = \omega_o$
$X_s = 0$ when $\omega = \omega_n$

$\frac{T_f}{X_s} \to 0$ as $\omega \to \infty$.
Good force isolation can be obtained at (or close to) $\omega = \omega_o$ regardless of the magnitude of X_s

Figure 5 Dynamic Force Transmissibility Characteristics
--Vibration Isolation Technique--

2.3. Test Results

Testing of the compressor was performed using both a 1/4-watt split Stirling cooler expander and a simulated test volume that matches the expander and transfer tube volumes at the design operating point of 80°K. Tests conducted on the compressor showed that the compressor performed better at 30 Hz than at 22 Hz. Rather than change the plunger mass to reduce the operating resonant frequency, it was felt that at this point in the development, testing at the higher frequency should continue, and the inefficiences from the mismatch between the compressor and expander should be accepted.

During the initial checkout tests of the compressor, it took significantly more than 30 watts to develop the required pressure differential of 400 psi. The problem was diagnosed as too large a clearance between the compressor piston and cylinder. By inspecting the hardware, it was found that instead of a radial clearance of .0002 to .0004 inch, the actual clearance was .0006 inch. After refurbishing this hardware and achieving a .0003-inch radial clearance, the machine performed much better. The pressure difference generated by the machine is given in Figure 6. As shown, at the design specification of 400-psi pressure difference, the input power was less than 30 watts.

The cooling capacity of the compressor driving the 1/4-watt expander (shown in Figure 1) is given in Figure 7. The results of these tests showed that the lowest temperature achieved was 35°K; at 77°K, the machine produced 0.35 watts of refrigeration for an input power of 34.5 watts. The cool-down time to 80°K was four minutes.

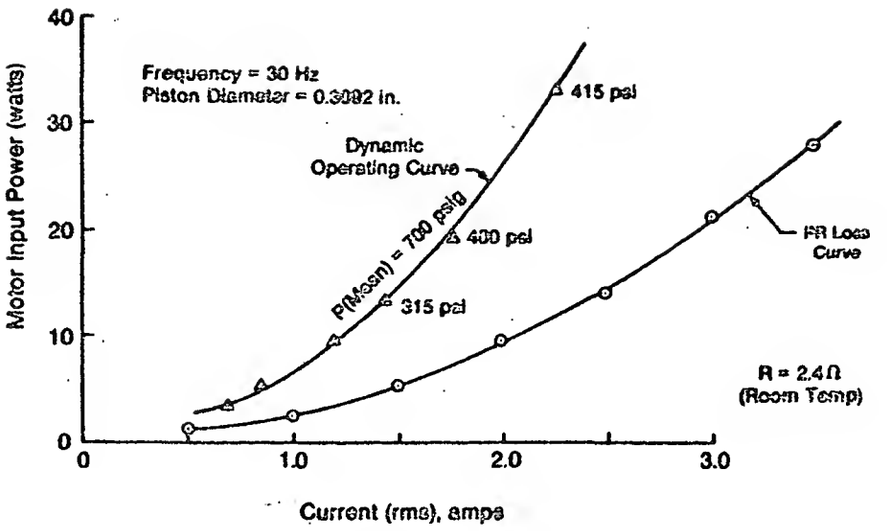

Figure 6 Locked Plunger Power Curve and Dynamic Operating Curve for the Compressor

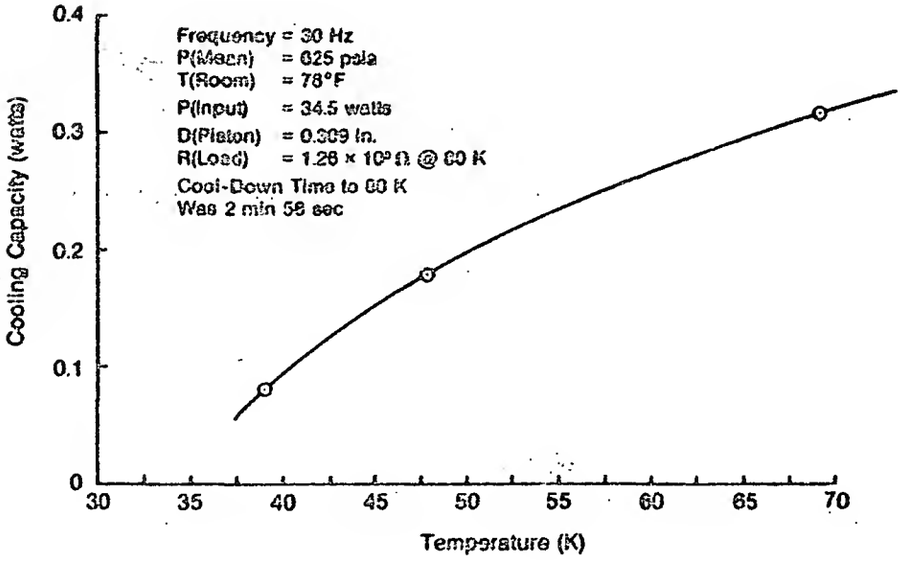

Figure 7 1/4-Watt Cryocooler Cooling Capacity

Another interesting test result was that the number of electrical coils in the stator could be reduced without affecting compressor performance. In the fabrication of this machine, the five coils were wound individually, and separate power leads were brought out of the machine, enabling the coils to be disconnected and the effect studied. The result (shown in Figure 8) was that the two outer coils could be eliminated without a reduction in the pressure differential (the right-hand ordinate), or an increase in input power (the left-hand ordinate). The implication of this is that the motor length can be reduced by two coil segments (1.44 inches), and the overall length of the compressor can be reduced from 7.00 inches (Figure 1) to less than 5.5 inches.

3. CONCLUSION

The concept of using a linear drive for the military 1/4-watt split Stirling cooler compressor is practical, as demonstrated by the program; in particular, the program showed the following:

1. It is difficult to design for a low frequency of 22 Hz and a large pressure difference because of the large spring force produced by the compression space and the large moving weight required to balance the spring component. Increasing the frequency will eliminate this problem.
2. A linear compressor can be developed for the 1/4-watt split Stirling cooler that will meet all of the present cooler specifications.
3. Effective vibration isolation can be incorporated and still meet the design specified envelope.

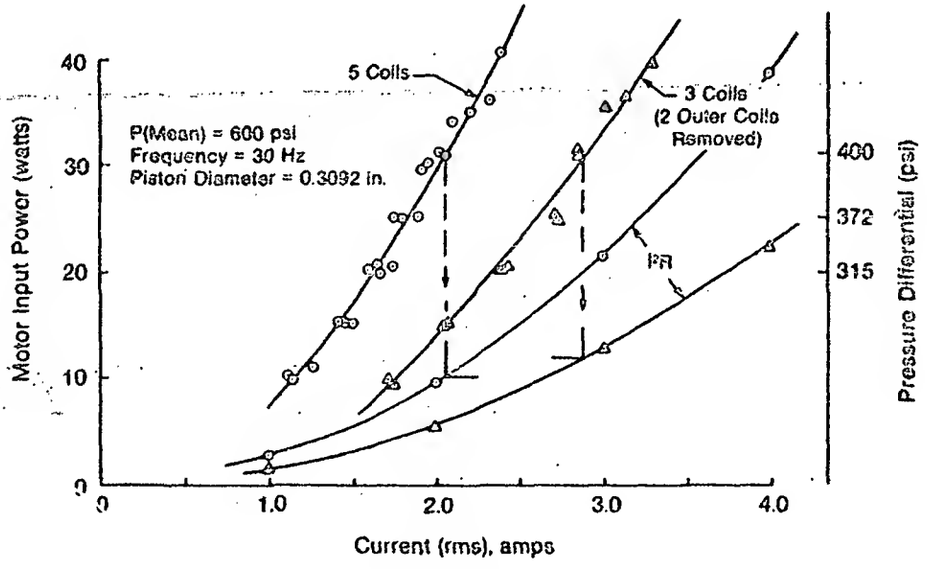

Figure 8 Effect of Eliminating Coils

D26

JOULE-THOMSON VALVES FOR LONG TERM SERVICE IN SPACE CRYOCOOLERS

James M. Lester and Becky Benedict

Cryogenics, Space Systems
Ball Aerospace Systems Division
Boulder, CO 80306

Joule-Thomson valves for small cryocoolers have throttling passages on the order of 0.1 millimeter in diameter. Consequently, they can become plugged easily and stop the operation of the cooler. Plugging can be caused by solid particles, liquids or gases. Plugging is usually caused by the freezing of contaminant gases from the process stream. In small open loop coolers and in closed loop coolers where periodic maintenance is allowed, the problem is overcome by using careful assembly techniques, pure process gases, warm filters and cold adsorbers. A more thorough approach is required for closed loop cryocoolers which must operate unattended for long periods. This paper presents the results of an effort to solve this problem. The causes of plugging are examined, and various ways to eliminate plugging are discussed. Finally, the development of a "J-T defroster" is explained. We conclude that a combination of preventive measures and a defroster will reduce the chance of cooler failure by plugging to such a degree that J-T coolers can be used for long term space missions.

Key words: J-T cryocooler, J-T defroster, J-T valve, long life mechanical refrigerator, space cryocooler

1. Introduction

Typical space cooling applications now being considered are for instruments costing upwards of one hundred million dollars. The required operating lifetime of these instruments is 5 to 10 years without maintenance. One watt of cooling at less than 10K is a typical goal. There is a desire to start these missions in less than 5 years; but, to develop a reasonable chance that such missions can be accomplished, a great deal of successful cooler testing must be done. Ideally, we would like to have many of the coolers operating for longer than ten years before risking huge sums of money on entire instrument systems. Temperatures less than 10K for sufficiently high cooling power have not even been demonstrated for space cooler configurations, much less in any statistically significant way. Realistically, we will not have the luxury of completing statistically significant life testing before a large risk is taken.

In view of this situation, a good design approach is to use the hardware concepts which best avoid the need for extensive life testing and will still do the job. In cryocoolers, machines which do the best job of avoiding the uncertainties of wear, fatigue, critical materials and contamination are favorable at this time. The passive Joule-Thomson (J-T) cold section does this very well except for the plugging problem due to contamination. Test time limitations make it difficult to guarantee that a J-T cooler will not freeze up in 10 years even if traditional purification techniques are applied to the fullest extent possible. This leaves us with an unacceptable risk which must be overcome by some other means.

Fortunately, we can employ a strong countermeasure - namely a defroster, to clean out the J-T valve. Many short duration tests can then be run under severe contaminating conditions in an attempt to show that this cleaning process will always renew the cooler. Then, in flight, under less severe contaminating conditions, the cooler can be "defrosted" on a preset schedule more frequently than the statistically proven safe operating interval. Confidence in the cooler will then be developed on a cycle basis rather than on a total time basis, thus allowing greatly accelerated testing.

We concluded that the plugging problem should be solved prior to refining other components in the J-T system because it is the key to determining if J-T's are usable for long term missions. We are currently developing a J-T valve and defroster with encouraging initial results. This paper describes that work.

2. The plugging problem in J-T coolers

This paper is primarily concerned with small cryocoolers for use in space instruments. Table 1 gives approximate design values which relate to the plugging problem for a 1 watt Helium J-T stage operating between 16 and 1.6 atmospheres.

Table 1 - Approximate cooler characteristics (Example)

• Helium Flow rate	1 Standard ℓ/sec
• Helium Quantity Required to charge the stage	10^2 Standard ℓ
• Cryocooler area which outgasses into the Helium	10^3 cm^2
• Volume of a plug in the J-T valve (Assumes 0.1 mmDia-by0.1mm long plug)	10^{-6} cm^3
• Volume of a plug in the small heat exchanger tubing upstream of the J-T valve (Assumes 2mmDia-by20mm long plug)	10^{-1} cm^3
• Operating time - 10 years-approx.	10^5 hours

The geometry of the J-T valve is assumed to be a short small hole, and this sets the size of its plug. The upstream high pressure side of the heat exchanger is characterized by a single line of small diameter tubing. Plugging by freezing of the mixture of contaminants will be spread over a considerable distance in this tube as dictated by the flow, temperature gradients and freezing points of the various contaminants in the mixture. We suspect that the assumption of a ten diameter freezing zone is a low estimate; but, the point to be considered is that the volume of contaminant required to form a plug is several orders of magnitude greater in the heat exchanger than in the valve itself. The downstream, low pressure side of the heat exchanger is much larger as dictated by the requirement for low pressure drop in the compressor return, so there is much less concern about plugging there.

2.1 Sources of contamination

Potential contaminants are gases, liquids or solid particles. Particles are dirt or chips left in the cooler during construction and dust from adsorbers. Liquids are things like free water or oils, the latter possibly from an oil lubricated compressor. There are three sources of gas: outgassing from the interior surfaces of the entire cooling loop, trace contaminants in the initial charge of Helium, and continuous vaporization of a cooler component. Plastic parts or oil in a compressor fall into this last category. The potential for plugging the example cooler of table 1 was estimated by calculating the sizes of these sources.

2.2 Gaseous contamination

The classical view of metal surface outgassing is given in [1] . This data shows that the outgassing of initially "clean and dry" surfaces at room temperature decreases from a fairly consistent value of

10^{-8} $\frac{\text{STD } cm^3}{cm^2 \text{ Sec}}$ after one hour in vacuum to 10^{-9} $\frac{\text{STD } cm^3}{cm^2 \text{ Sec}}$ after ten hours and continues to decrease by another order of magnitude for each additional order of magnitude span of time. The outgassing of a cooler, at least in the warm areas, will be roughly the same into a charge of pure Helium where the partial pressures of the contaminants are very low.

The outgassing relates to the potential for plugging in a logarithmic manner. In the first logarithmic time interval of outgassing, 1-10 hours, the outgassing will accumulate the equivalent of 160 plugs in the J-T valve and $1.6(0^{-3})$ plugs in the heat exchange tube upstream the J-T valve. The density of the frozen plug is approximately 10^3 times greater than standard density of the gaseous contaminant. Continuing from the second time interval, 10-100 hours, to the last, 10000-100000 hours, the total accumulation is about $8(10^{-4})$ cm^3 of solid, or about 1 milligram. This amount could produce 800 plugs in the J-T valve. (Note that the amount of outgassing by this theory is the same for each time interval. Note also that the heat exchanger is relatively immuno to plugging by gaseous contaminants because of its relatively large size.)

If ultra pure grade Helium is used for the initial charge, the total quantity of contaminants is about the same as the 10 year outgassing. Typical specifications for maximum contaminants in ultra pure Helium and the resultant amounts in the initial charge of 10^2 standard liters include trace amounts of C_2, N_2, Ne, Ar, H_2, CO_2, and H_2O (greatest contaminant listed first). The total amount of solid impurities is about (10^{-3}) cm^3 or about 1 milligram. This amount could produce 1000 valve plugs.

Lastly, the system may have components which vaporize continuously throughout the operating period. Plastic parts or compressor oils are in this category. A good oil will have a vapor pressure of 10^{-10} torr at 300K. The amount of oil vapor (apart from free oil droplets) circulated toward the J-T valve would be that amount which saturates the process gas at the oil vapor pressure. If one standard liter per second of Helium flows in the system and the pressure is 1.6 atm at the oil vapor pickup point, the total amount of oil vapor frozen into solid form would be $3(10^{-5})$ CM^3. This is enough to produce about 30 plugs.

A loaded adsorber can act as a continuous source of contamination if left "wet" from a previous test, and be a large additional source. In summary, over 2000 potential J-T valve plugs can be present in the system due to gaseous contaminants.

2.3 Liquid and solid contamination

Plugging due to free water is possible if the system has been left open to the atmosphere. Oil mist (suspended droplets) from compressors may be present in large quantities. Dirt and chips can be left in the cooler during manufacture. Residue from soldering operating has been known to dislodge and stop at J-T valves. Most J-T coolers use adsorbers which consist of charcoal particles or mol-seive pellets. These adsorbents lose fine dust particles and these are a concern because they are not easily filtered without creating the risk of freezing contaminant gases at the filters.

2.4 The nature of plugging

In spite of the large potential for becoming plugged, J-T coolers usually work. Plugging most often occurs during startup or after a power interruption, when the heat exchangers are warm and will not "cold trap" the contaminant gases. If the initial cool down period is passed, the cooler will usually continue to work. The reason is that the heat exchangers do a very good job of collecting the contaminants before they get to the J-T valve. Then also, the contaminants which do not stick to the heat exchanger walls are mostly in the form of minute ice crystals which are simply blown through the J-T valves. Sometimes coolers will operate at different cooling capacities on separate cooldowns - an indication of partial plugging.

3. Solutions to the plugging problem

Plugging of the J-T valve can be reduced or eliminated by three major techniques: reduction of contamination sources, the use of certain valve geometries, or by methods which counteract the contamination within the system when it is operating. While large improvements can be made with the first two techniques, the potential for plugging still exists. Counteractive measures are necessary. In the final analysis, renewing the valve by defrosting is the surest way to ensure long-term operation.

3.1 Reduction of contamination sources

Initial thorough cleaning and vacuum baking is necessary to reduce massive quantities of contaminants. It is not likely that the outgassing rate can be reduced to below

$10^{-12} \frac{\text{STD } cm^3}{cm^2 \text{ Sec}}$ therefore a significant potential for plugging will still exist in the system.

Research grade gases can be used to charge the cooler instead of ultra pure grade, reducing the potential for plugging by a factor of 5. Careful control of the charging process is necessary to

maintain this improvement. All cooler components should be low vapor pressure materials. Careful design will ensure that the gas produced by these sources is a small fraction of the total contamination. As a general guide, materials with vapor pressure above 10^{-10} Torr should be avoided.

Compressors should either be oil free or should have a very low output of free oil droplets in mist form. The space in and around the J-T valve itself can be treated as a critical component and assembled in the strictest clean room conditions. This will virtually eliminate the chance of plugging by particles in the cooler if the valve capsule is protected by suitable filters.

3.2 Valve geometries

Most J-T valves are simple, short circular holes. Other geometries are possible, but there is little to be gained by these designs and they may be harder to unplug. A long capillary tube could be used as a J-T expansion device, allowing the flow passage to be larger in diameter. The flaw in this idea is that total plugging of the valve is not the only concern. Partial plugging in a long capillary could cause a large change in performance and is not allowable. The idea of using a porous plug suffers from the same flaw. In addition, the very fine pores of the plug will be much more easily plugged by minute ice crystals suspended in the stream.

One attractive compromise geometry is to put a wire through a small hole. This arrangement distributes the orifice into a ring shape which is not sensitive to plugging by a few particles left in the cooler during assembly.

3.3 Counteractive measures

Starting from the warm high pressure end of the system, there are a number of things that can be done to reduce the chance of plugging. In a cooler using oil lubricated compressors, virtually all of the free droplets must be removed by coalescing filters. Fortunately, these filters can be made very long and efficient since they are in the warm areas. Barrier film techniques are also necessary to prevent creep of oil films down the heat exchanger tubing. The more critical problem here is to reduce the mass of free oil to a level lower than that required to saturate downstream gas adsorbers and cause freeze up by that mechanism.

Adsorbers consisting of beds of charcoal, silica-gel, or molecular sieve materials are the most effective way to reduce the flow of contaminants to the J-T valve. Adsorbers in the cold areas just upstream of the J-T valve are very powerful purifiers, possibly eliminating the plugging problem completely, but the problem is in the proof. Several imperfections inherent with adsorbers may allow plugging to occur after a long period of operation. If the beds are made too 'tight' then they themselves may become subject to plugging. Channeling may occur leading to variations in purification efficiency from bed to bed. Adsorbers in flow streams tend to act as chromatograph columns. That is, concentration fronts gradually migrate to the downstream side and eventually a large release of adsorbed contaminants will occur. This effect has been observed in helium liquifiers causing unexpected freeze up after a long period of normal operation.

Particle filters such as screens or porous metals will be needed downstream of adsorbers to trap released dust or particles, but care must be taken to allow sufficient area so that freeze up does not occur in the filters. Chemical getters which combine with the more active gases are useful in reducing those contaminants.

After all of these precautions are taken, it will still be very difficult or impossible to say that a J-T valve will not be plugged in a long mission. Also, if power is interrupted, the entire cooler may become filled with gaseous contaminants. These uncertainties require some sort of valve cleaner which can remove the contamination. Mechanical devices have been used for this purpose, but they are risky because they may not totally remove the contamination and they may become stuck. The safest way to clear a J-T valve is to use a defroster. The design of such a device is described in Section 4.

4. Design of a J-T valve defroster

The J-T valve was arranged as shown in figure 1. Cold, high pressure gas passes through the final adsorber where most of the remaining impurities are trapped. The gas enters the thin wall stainless steel tube whose length is shown as ℓ_1, then it passes into the relatively large diameter entry section of the copper J-T valve. The wire passes through the throat of the valve causing this restriction to be ring shaped which reduces the chance of a few particles forming a plug. After expansion at the valve, the gas-liquid mixture passes through the thin wall stainless steel outlet tube, labeled ℓ_2, to the boiler and from there to the low pressure side of the heat exchanger. A resistance heater is wound around the outer throat of the valve. Figure 2 shows a test model of the device.

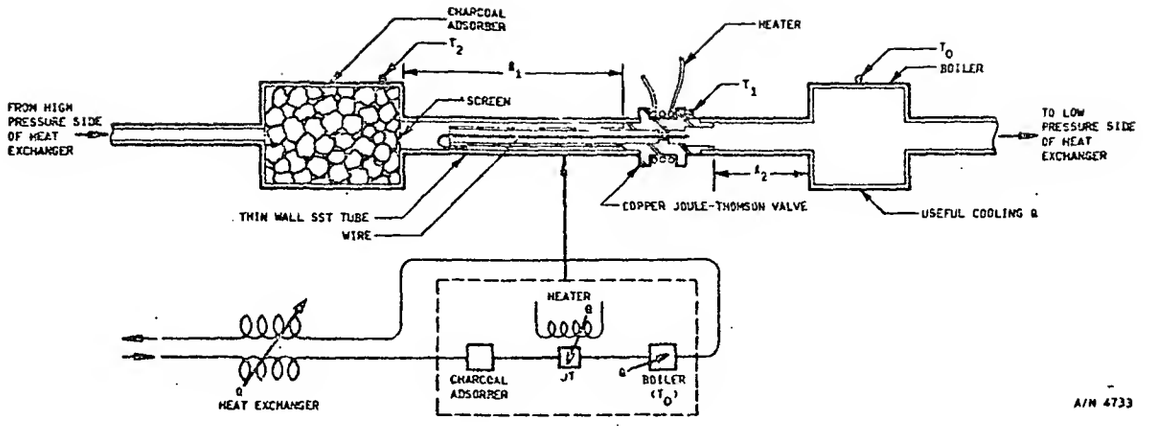

Figure 1 J-T Valve Defrosting Scheme

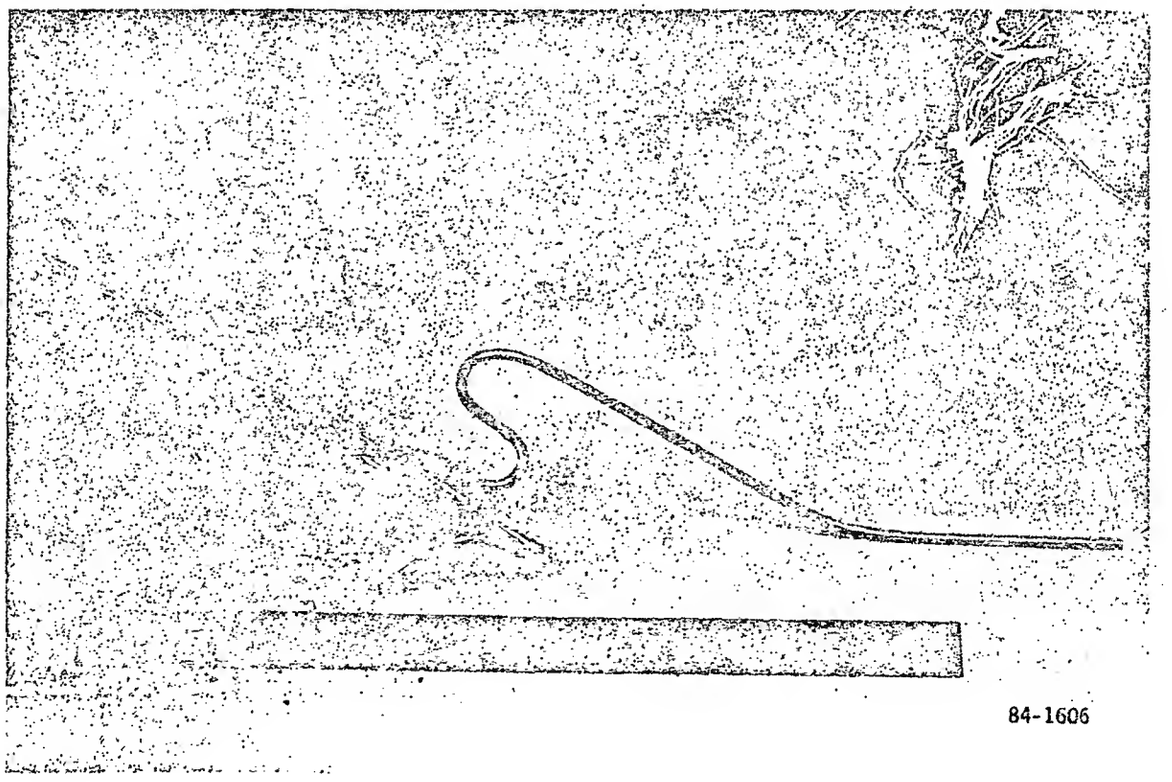

Figure 2 JT-Valve Defroster

The purpose of the arrangement is to allow complete defrosting in a short time period with minimal disturbance to the useful operation of the cooler. The low conductivity stainless steel tubes act as thermal standoffs between the heated copper J-T valve and the adsorber or boiler. This confines most of the heat to the valve where it is needed. Standoff ℓ_1 is also needed to prevent the adsorber from warming up to a temperature where contaminants will be released. The boiler contains a reserve of liquid which maintains constant temperature cooling for the load during the defrosting cycle. The purpose of the copper entry section of the valve is to prevent sudden replugging of the valve after the heater is turned off. This copper part is warmed to room temperature in a few seconds along with the throat of the valve. If the entry section were not there, contaminants from the warm end of the standoff tube ℓ_1 would be immediately available to collect in the valve. As it is, the annular gap between the copper and stainless tubes acts as a cold trap for this temporary source. Further enhancements of this cold trapping scheme are possible but they do not seem to be needed. The heater must be able to raise the valve temperature rapidly to minimize the total heat input to the system and also to the reserve liquid in the boiler.

The heater must also be able to operate over a broad range of heating conditions depending on whether the valve is completely plugged or not plugged at all. This means that the heating power must be several times the steady state cooling power of the cooler because the effective short term cooling power of the stream is high when working against an unplugged warm J-T valve. When the valve is plugged, the same heating power will cause very rapid valve temperature rise because there is no cooling flow, and the heater could burn out. A closed loop heater shut down controlled by valve temperature is needed to handle this range of conditions. Redundancy of heaters and temperature sensors can be provided.

Standoff dimensions, boiler capacity, and heater size are a function of the application. There are considerable differences between 4K Helium valve defrosters and 77K Nitrogen valve defrosters because of the large differences in thermal properties of the materials. To get a feel for the numbers, a 2-watt Nitrogen cooler requires about 20 watts of heating for 10 seconds resulting in a heat input of 200 joules. This consumes about 1 gram of liquid Nitrogen from the reserve in the boiler if precise cooling temperature stability is to be maintained at the load. The heat required to vaporize the plug is negligible and the heat required to warm the copper is only 15 joules. The total heat leak down the standoff tubes is only about 5 joules. Most of the heat goes into the cold gas stream at the valve.

When operated at lower power levels, the defrost heater is also a handy device to control warm up of the system and to aid in initial bakeout. Heating by induction has been suggested as an alternate but this method complicates the power supply for space applications. Section 5 describes the tests performed on the device shown in Figure 2.

5. Defroster testing

Preliminary testing on the J-T defroster (Fig. 2) has been completed for an open-loop Nitrogen J-T system. The results indicate that defrosting can be done in a short time with minimal disturbance to the cooling temperature using low heater input energy. These tests run on our preliminary J-T defroster have been beneficial both in confirming our calculations on the defroster and in defining necessary modifications to the hardware and test methodology.

5.1 Apparatus

The test apparatus, shown in Figure 3, uses K-bottle Nitrogen (ultra high purity) as the source gas. The outer jacket, which houses the coiled tube exchanger and its thermal shroud, is evacuated to 10^{-6} Torr prior to testing. In the 'cold end' of the assembly, there are three thermocouples located and labeled as follows: T_0-potential cooling load (on the downstream mol seive trap), T_1-J-T defroster, T_2-upstream mol sieve trap. The contamination loop inlet is also located in the cold section just upstream of the J-T valve and defroster. A flow meter, temperature scanner, contamination cylinder (H_2O), power supply, voltmeter, ammeter, and pressure controller complete the apparatus.

Note that the system shown in figure 3 makes provisions for the addition of a useful cooling load where the downstream mol sieve trap is currently located. The only load that was applied during these tests was conductive and radiative heat leak.

5.2 Test methodology

In order to develop a J-T defroster that will be able to recover from a variety of worst-case conditions, two concepts required testing. The defroster heater design was tested in order to determine its effect on the overall cooler thermal stability. After sufficient testing and mapping of the defroster's operating characteristics using the pure (ultra high purity) Nitrogen gas source, additional tests were done with a contaminated Nitrogen source. The pure Nitrogen tests are discussed first.

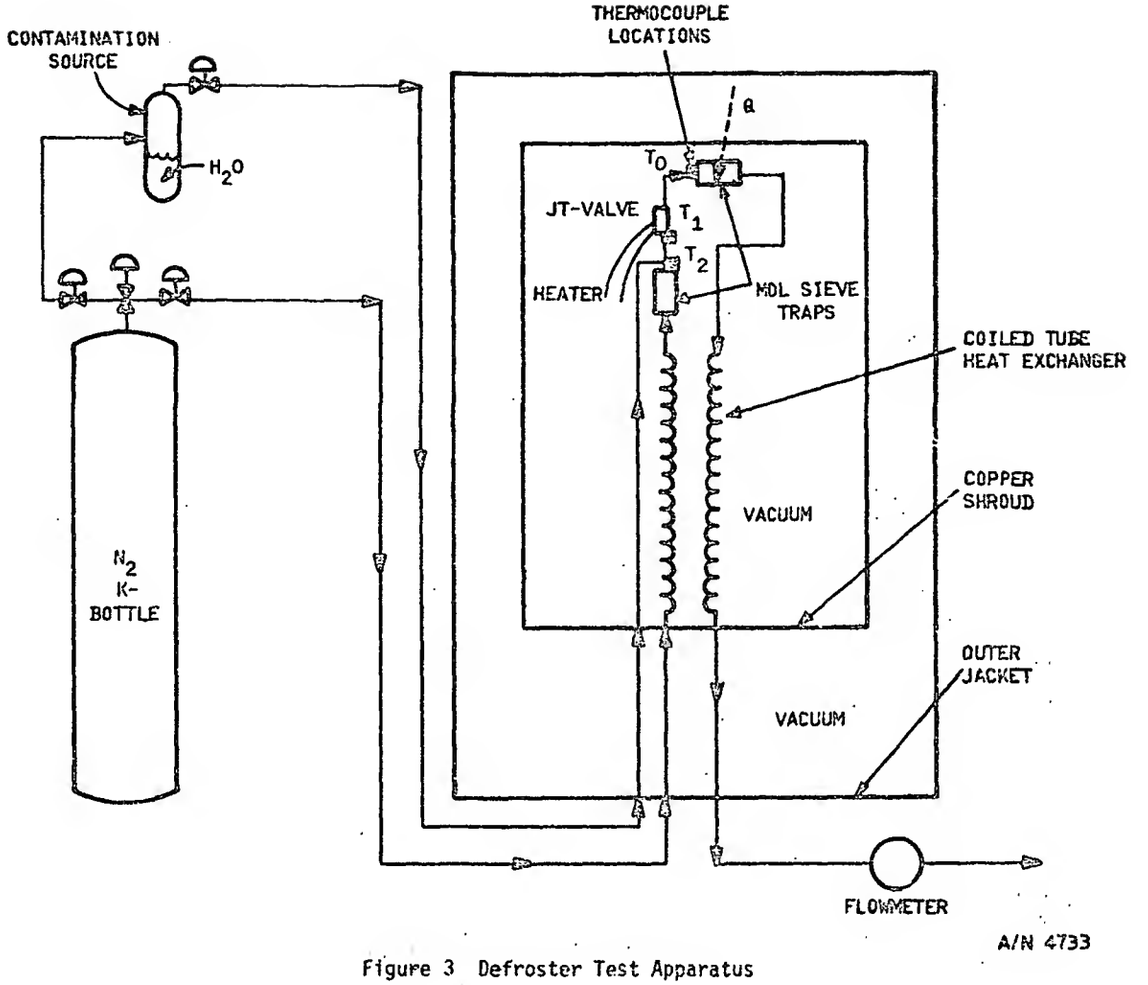

Figure 3 Defroster Test Apparatus

To assure consistency in the pure Nitrogen tests, two variables, the operating pressure (high pressure source) and the time interval between the defrosting, were specified. During the current tests, a source operating pressure of 450 psia provided sufficiently low temperatures at the J-T valve to test the defroster, while still providing the cooling necessary to recover from the defrost. The time interval between defrosting was always less than 2 hours.

When starting a test run, we used a Nitrogen operating pressure of 2000 psia to expedite the equipment cool down by producing high pressure (and relatively high temperature) liquid Nitrogen. Then, over a period of one and a half hours, we gradually decreased the operating pressure until the system was stabilized at 450 psia. Under these conditions the 'cold end' of the apparatus was usually operating under partially flooded conditions. This was apparent when the temperature gradient between the three thermocouples (Fig. 3) was 10K or less. When these conditions were met we tested the defroster.

We powered the defroster heater with a measured voltage while watching the thermocouple attached to the valve, T_1. When the high temperature limit, approximately 20°C, was reached we manually shut off the power supply and recorded the highest temperature observed on the J-T valve. Then we recorded the system response for all thermocouples, flow and vacuum level. The temperature scanner recorded the three temperatures continuously for analysis after completion of the tests.

The contamination loop shown in Figure 3 was used to provide a water saturated Nitrogen source. The contamination loop was used either to provide 100 percent water saturated or partially saturated Nitrogen by using only flow through the contamination source or through the exchanger and the contamination source. When using the contamination source, the source cylinder was heated to

approximately 100°C, in order to fully saturate the Nitrogen. The water was expected to freeze out in the J-T valve in a short period of time, as indicated by a reduction in flow rate. Once the flow slowed enough to indicate that the valve was plugged the J-T defroster testing was carried out in the same manner as described for the pure Nitrogen source tests.

5.3 Results

The results for testing done at 450 psia are shown in figure 4, for four separate defrosting tests, case I, case II, case III, and case IV. These tests on the apparatus were done consecutively, during one cool down period. For this reason, we feel that these are the most representative results out of all the tests completed to date. The defrost in case I required 7.6 W and the cooler required 40 minutes before it had stabilized to the conditions prior to the defrost. In case IV, the defrost required 15 W and the cooler returned to the conditions prior to defrosting in only 4 minutes. The heater input power for case I disturbed the thermal stability of the entire cooler ten times longer than the heater input power in case IV. Note that in case I the total energy input is 718 W•s and it decreases to 285 W•s in case IV. The trend can be traced from case I to case IV (Fig. 4).

When the valve is heated, the mass flow is substantially reduced because of the large change in fluid conditions there. This effect reduces the pressure downstream of the valve and results in a lower temperature in the boiler for a short time. This effect would be less noticeable in a cooler with more open downstream plumbing as would be the case for a more refined cooler. There would still be a substantial decrease in flow in a more refined cooler and this would tend to minimize the heat addition due to the defrosting pulse.

The data plotted in figure 5 compare the defroster's requirements in W•s and in equivalent grams of L-N2. This plot is particularly useful design information for the valve tested here, but is only characteristic of this valve. Knowledge of the equivalent grams L-N2 boiled off during defrost cycle allows for the design of a L-N2 reservoir with enough capacity to absorb the entire heat input of the defrost cycle without allowing a change in load temperature.

Defrosting tests run using the contamination loop to simulate a wet Nitrogen source show that the device is effective, but the tests were not entirely conclusive. The loop (Fig. 3) supplies contaminated Nitrogen directly to the system upstream of the J-T valve. However, the valving on the current apparatus allows wet Nitrogen to remain in the contamination tube. Consequently some recontamination would occur before we could take adequate flow measurements to prove that the valve had been totally cleared.

5.4 Conclusions

The tests done using pure Nitrogen confirm that the J-T defroster can be operated with little effect on the thermal stability of the cooler. The current testing equipment must be refined in order to conduct conclusive testing of the J-T defrosting action.

One additional testing problem encountered was the need for better control on the defroster power supply. To protect against heater burnout, the power supply must be automated to shut off the power before the J-T valve temperature exceeds 20°C. An additional thermocouple must be added to the heater very close to (if not toughing) the heater wire in order to more accurately measure the heater temperature.

6. Additional work

Further refinements of the defroster scheme will be tested in the remainder of 1984 and in 1985. In 1985 we will operate a closed-loop 4K helium J-T cooler employing the defroster and pressurized by a long-life oil lubricated compressor.

The authors are grateful for the ongoing expert consultation of Dr. Tom M. Flynn on various purification concepts and thermodynamic aspects of the J-T cyrocoolers. In addition, Dr. Thomas R. Strobridge has greatly added to our understanding of J-T cyrocoolers by drawing on his 20 years experience with helium liquifiers.

7. References

[1] Santeler, D. J., Holkeboer, D. H., Jones, D. W., Pagano, F., Vacuum Technology and Space Simulation, NASA SP-105 (1966).

CASE I: 7.6W APPLIED FOR 1 MIN 35 SEC (718 W-S)

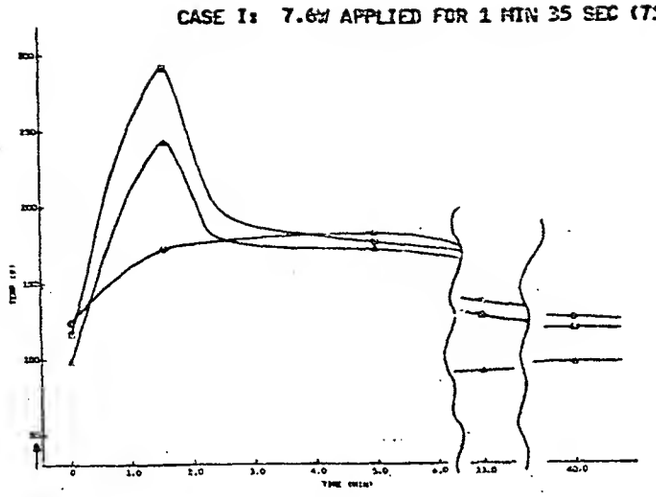

ΔT_0: POTENTIAL COOLING LOAD LOCATION $\square T_1$: J-T DEFROSTER $O T_2$: UPSTREAM TRAP

CASE II: 9.8 W APPLIED FOR 52 SEC (509 W-S)

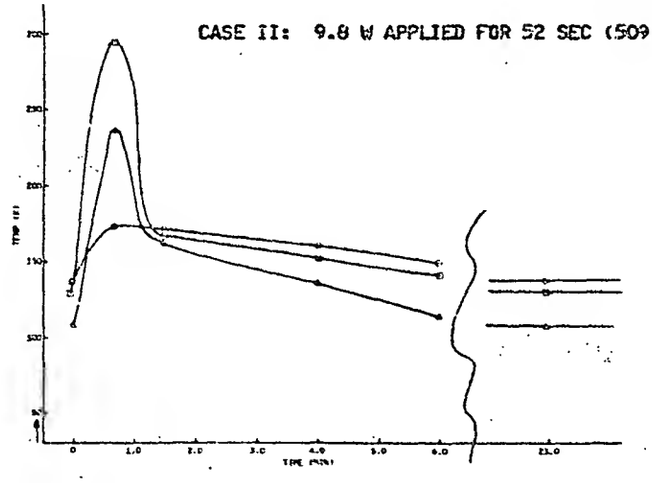

CASE III: 11.9 APPLIED FOR 41 SEC (490 W-S)

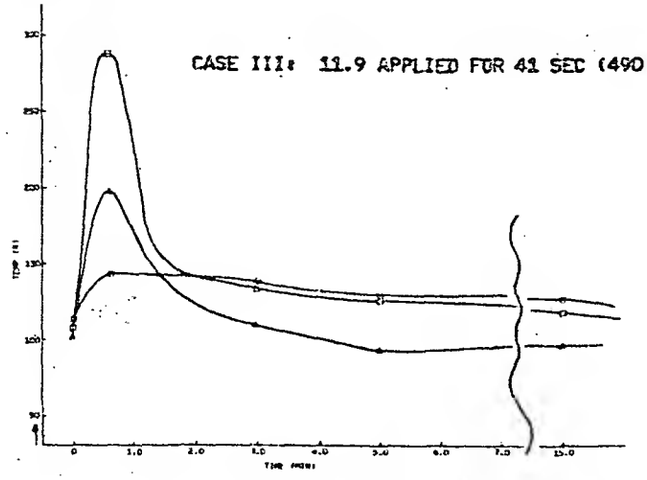

Figure 4 Pulsed Heating of the J-T Cooler (Continued on next page)

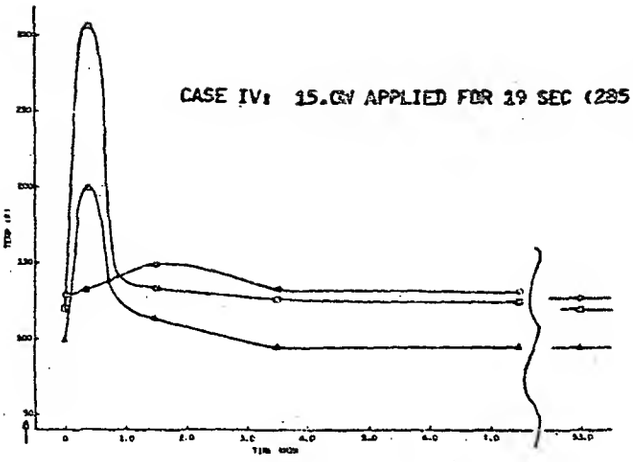

ΔT_0: POTENTIAL COOLING LOAD LOCATION $\square T_1$: J-T DEFROSTER OT_2: UPSTREAM TRAP

Figure 4 Pulsed Heating of the J-T Cooler

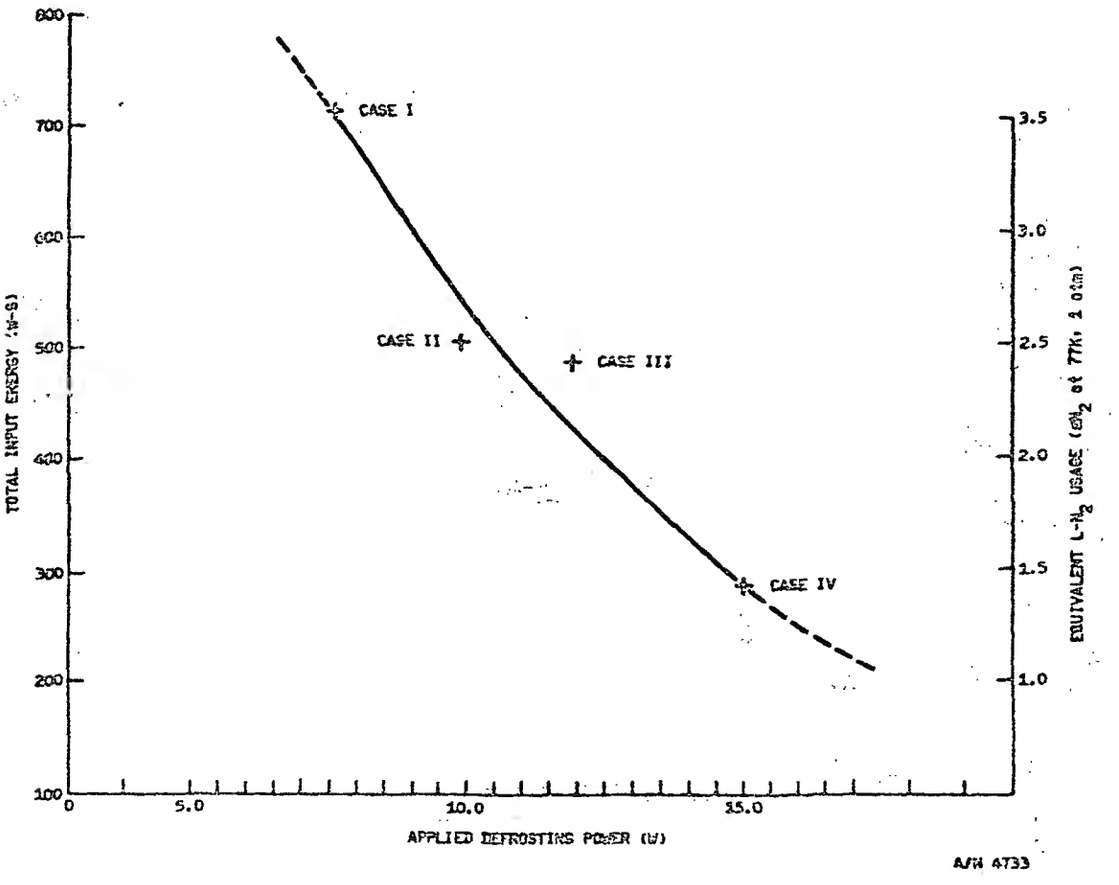

Figure 5 Energy Requirements for Defrosting the J-T Valve (to ~20°C)

ATTENDANCE LIST
3rd Cryocooler Conference on Refrigeration for
Cryogenic Sensors and Electronic Systems
National Bureau of Standards
September 17 & 18, 1984
Boulder, Colorado 80303

Robert A. Ackerman
Mechanical Technology, Inc.
Stirling Engine Systems Division
968 Albany-Shaker Road
Lathan, NY 12110
518-785-2255

John Barclay
Los Alamos National Lab.
Group P-10
M. S. K764
Los Alamos, NM 87544
505-667-6431

Becky Benedict
Ball Aerospace Systems Division
P. O. Box 1062 - M. S. TT-5
Boulder, CO 80306
303-939-4000

Nel Bello
Aerospace Corporation
El Segundo, CA 90501
213-648-7277

Bascom H. Birmingham
Birmingham Associates
5440 White Place
Boulder, CO 80303
303-442-1248

Leon Bledjian
Aerospace Corporation
2350 East El Segundo Blvd.
Mail Stop 4906
El Segundo, CA 90245
213-648-6895

Richard Bocchicchio
M. S. A24-05
Grumman Aerospace Corp.
Bethpage, NY 11714
516-575-0988

Guenther Bogner
Siemens AG Research Labs.
8520 Erlangen
West Germany
9131-731228

Thomas H. Bradshaw
Rutherford Appleton Laboratory
Bldg. R65
Chilton, Didcot, Oxon
England
Abingdon 21900 ext. 6149

R. Warren Breckenridge
Arthur D. Little, Inc.
20 Acorn Park
Cambridge, MA 02140
617-864-5770

Michael T. Brown
Hughes Aircraft Company
E1/C102
El Segundo, CA 90245
213-616-9651

Jim Breuel
Ball Aerospace Systems Division
P. O. Box 1062 - M.S. TT-4
Boulder, CO 80306
303-939-4000

Robert Buzerak
Ford Aerospace & Communications Corp.
One Ford Road
Newport Beach, CA 92660
714-720-4956

Chung K. Chan
Jet Propulsion Laboratory
California Institute of Technology
4800 Oak Grove Drive
Pasadena, CA 91109

Yen H. Chen
Aerojet Electro Systems Company
1100 W. Hollyvale St.
P. O. Box 296
Bldg. 160 - Dept. 4323
Azusa, CA 91702
818-812-1877

James E. Chenoweth
Air Force Wright Aeronautical Labs.
AFWAL/FIEE
Wright-Patterson AFB
Ohio 45433
513-255-4853

David E. Daney
National Bureau of Standards
Division 773.10
325 Broadway
Boulder, CO 80303
303-497-3595

Ken H. Davies
U. K. Science & Engineering
Research Council
Rutherford Appleton Laboratory
Chilton, Didcot,
England
0235-21900

Axel Dehne
Hughes Aircraft
6155 El Camino Real
Carlsbad, CA 92008
619-438-9191

Andre DeVilliers
Riverside Research Institute
1701 North Fort Myer Drive #700
Arlington, VA 22202
703-522-2310

Bernard Dewanckel
Centre D'Etudes Nucleaires de Grenoble
Service des Basses Temperatures
85 X 38041
Grenoble Cedex
FRANCE
76-974111

R. Dittrich
Univ. of Giessen
Institut fur Angewandte Physik
Heinrich-Buff-Ring 16
D6300 Giessen
Germany
0641 702 2791

Alan C. Eckert
Analytic Decisions, Inc.
1401 Wilson Blvd.
Arlington, VA 22209
703-528-3337

Edgar A. Edelsack
Office of Naval Research
Code 414
800 North Quincy Street
Arlington, VA 22217
202-696-4218

Alain Faure
L'Air Liquide
B15 Sassenage 38360
France
76 268131

A. A. Fife
CTF Systems Inc.
#15-1750 McLean Ave.
Port Loquitlam
B. C. V3C1M9
Canada
604-941-8561

Ephrain B. Flint
IBM - T. J. Watson Research Center
P. O. Box 218
Yorktown Heights, NY 10598
914-945-2470

Tom Flynn, Consultant
Ball Aerospace Systems Division
3445 Longwood Ave.
Boulder, CO 80303
303-494-0245

John M. Gary
National Bureau of Standards
Division 713 - Room 4059
325 Broadway
Boulder, CO 80303
303-497-3369

Max G. Gasser
NASA - Code 713
Goddard Space Flight Center
Greenbelt, MD 20771
301-344-8378

Peter E. Gifford
President, Cryomech, Inc.
1630 Erie Blvd. East
Syracuse, NY 13210
315-475-9692

David B. Giguere
Hughes Aircraft Co.
3100 W. Lomita Blvd.
P. O. Box 2999
Torrance, CA 90274
213-517-6200

Richard M. Grabow
Ford Aerospace Corporation
1 Ford Road - Bldg. 5K208
Newport Beach, CA 92660
714-720-7108

Geoffrey Green
U. S. Navy - DTNSRDC
Code 2712
Annapolis, Maryland 21402
301-267-3632

Chen Guobang
Cryogenic Engineering Lab.
Zhejiang University
Hangzhou
China
21701-2427

Gene A. Jaeger
Naval Weapons Center
Missile Systems Branch
Code 3621
China Lake, CA 93555
619-939-2283

Jack E. Jensen
CVI Incorporated
P. O. Box 2138
Columbus, OH 43216
614-876-7381

Alfred L. Johnson
Aerospace Corporation
2350 East El Segundo Blvd.
M4/929 - P. O. Box 92957
Los Angeles, CA 90009
213-648-5295

Dean L. Johnson
Jet Propulsion Laboratory
MS 238-737
4800 Oak Grove Drive
Pasadena, CA 91109
818-354-4942

Mark Johnson
Ball Aerospace Systems Division
P. O. Box 1062
Boulder, CO 80306
303-939-4000

Jack A. Jones
Applied Mechanics Division
Jet Propulsion Laboratory
California Institute of Technology
Pasadena, CA 91109
818-354-4717

Frank J. Kadi
Air Products & Chemicals, Inc.
1833 Vultee Street
Allentown, PA 18103
215-481-3706

Robert A. Kamper
Director, National Bureau of
Standards -Boulder Laboratories
325 Broadway
Boulder, CO 80303
303-497-3535

Mitsuhiro Kaneko
Cryogenic Department
Suzuki Shokan Co., Ltd.
No. 73 Hiratsuka
Ageo, Saitama-Ken
Japan 362
0487-21-5225

Peter J. Kerney
CTI Cryogenics
266 Second Avenue
Waltham, MA 02154
617-890-9400

Chi-Sing Keung
Philips Laboratories
345 Scarborough Road
Briarcliff Manor, NY 10510
914-945-6124

J. F. Keville
Aerojet Electro Systems
P. O. Box 296
Azusa, CA 91702
818-812-1430

Hui K. Kim
TRW
One Space Park
Redondo Beach, CA 90278
213-535-5678

Jerry King
13627 N. 23rd Ave.
Phoenix, AZ 85029
602-863-2459

Peter Kittel
NASA
M/S 244-7
Moffett Field, CA 94035
415-965-6525

Lawrence D. Knox
Philips Laboratories
345 Scarborough Road
Briarcliff Manor, NY 10510
914-945-6357

Herbert Korf
AEG Telefunken
IM Margstall 4
7100 Heilbronn
Germany
7131 621220

Nick Lambert
Delft University of Technology
Department of Applied Physics
Lorentzweg 1
2645 NE Delfgauw
The Netherlands

William Lang
Singer Kearfott
M. S. 12B10
150 Totowa Road
Wayne, NJ 07470
201-785-6555

Edward Lax
Rockwell International
5637 Wilhelmina Ave.
Woodland Hills, CA 91367
714-632-1146

Jean G. Leclerc
Commissariat a'l'Energie Atomique
C.E.S.T.A.
33830 Belin-Beliet
France
56 23.10.50

Daniel Lehrfeld
Magnavox
46 Industrial Avenue
Mahwah, NJ 07430
201-529-1700

James M. Lester
Ball Aerospace Systems Division
P. O. Box 1062 - M. S. TT-5
Boulder, CO 80306
303-939-4000

Shimo Li
Cryogenic Engineering Lab.
Zhejiang University
Hangzhou
China
21701-2427

Paul Lindquist
U. S. Air Force
Code AFWAL/FIEE
Wright-Patterson AFB
Ohio 45433

Del Linenberger
Ball Aerospace Systems Division
P. O. Box 1062 - M. S. M&P-2
Boulder, CO 80306
303-939-4000

Richard C. Lins
HR Textron Inc.
25200 W. Rye Canyon Road
Valencia, CA 91355
805-259-4030, ext. 5512

L. Lombardini
Officine Galileo, S. P. A.
Florence
Italy 50013
055/8350455

Ralph C. Longsworth
Air Products & Chemicals, Inc.
1833 Vultee St.
Allentown, PA 18103
215-481-3708

Beverly Louie
National Bureau of Standards
Division 773.10
325 Broadway
Boulder, CO 80303
303-497-3190

Ronald Mahler
Sperry Corp.
P. O. Box 64525 - M. S. U1K14
Sperry Park
St. Paul, MN 55164
612-456-3846

W. R. Martini
Martini Engineering
2303 Harris
Richland, WA 99352
509-375-0115

Yoichi Matsubara
Atomic Energy Research Institute
Nihon University
7-24-1 Narashinodai
Funabashi-Shi
Chiba-Ken
JAPAN 274
0474-66-1111, ext. 374

Frank E. McCrea
Jet Propulsion Laboratory
4800 Oak Grove Drive
M.S. 238/737
Pasadena, CA 91109
818-354-3129

Larry Meehan
Amdahl Corp.
P. O. Box 3470 MS 197
Sunnyvale, CA 94088

Lawrence Miller
Philips Laboratories
345 Scarborough Road
Briarcliff Manor, NY 10510
914-945-6128

A. S. Mitchell
Westinghouse Electric Corporation
P. O. Box 1521 - M. S. 3642
Baltimore, MD 21203
301-765-7228

Robert A. Mohling
Beech Aircraft Corp.
P. O. Box 9531
Engineering Dept. 690
Boulder, CO 80301
303-443-1650

Ronald N. Morris
CTI-Cryogenics
266 Second Avenue
Waltham, MA 02254
617-890-9400, ext. 384

Ken Myrtle
Quantum Technology Corp.
6237-148 St.
Surrey, B. C.
Canada V5A 3C3

Ram Narayan
Magnavox
46 Industrial Avenue
Mahwah, NJ 07430
201-529-1700

Martin Nisenoff
Naval Research Laboratory
Code 6854
Washington, D. C. 20375
202-767-3099

Neil A. Olien
National Bureau of Standards
Division 773.30
325 Broadway
Boulder, CO 80303
303-497-3257

Rodney Oonk
Ball Aerospace Systems Division
P. O. Box 1062 - M. S. TT-4
Boulder, CO 80306
303-939-4000

Hal C. Parish
CVI Incorporated
P. O. Box 2138
Columbus, OH 43216
614-876-7381

Paul J. Patt
Philips Laboratories
345 Scarborough Road
Briarcliff Manor, NY 10510
914-945-6285

George Patton
David Taylor Ship R & D Center
Annapolis, MD 21146
301-267-3632

Douglas N. Paulson
S.H.E. Corporation
4174 Sorrento Valley Blvd.
San Diego, CA 92121
619-453-6300

Steven Pergament
RCA Astro
P. O. Box 800
Princeton, NJ 08520
609-420-3388

Hans Pfister
Siemens AG, ZFE TPH 1
Paul-Gossen-Str. 100
D-8520 Erlangen
Erlangen
West Germany
9131/731060

Nachman Pundak
Ricor Ltd.
En-Harold Ihud 18960
Israel
972-65-31703

Ray Radebaugh
National Bureau of Standards
Division 773.30
325 Broadway
Boulder, CO 80303
303-497-3710

Jean-Claude Renard
Laboratoires de Marcoussis-CR-CGE
Route de Noxay
91460 - Marcoussis
France
33 (6) 449 1172

Philipp B. Rudolf von Rohr
Massachusetts Institute of Technology
Cryogenic Engineering Laboratory
Room 41-211D
Cambridge, MA 02139
617-253-2420

Samuel Russo
Hughes Aircraft Company
E1/C102 - P. O. Box 902
El Segundo, CA 90245
213-616-9651

Rudy S. Saenz
Hughes Aircraft Company
6155 El Camino Real
Carlsbad, CA 92008
619-438-9191

Frank M. Salvatore, Jr.
CTI - Cryogenics
266 Second Avenue
Waltham, MA 02254
617-895-1312

Raymond E. Sarwinski
R. G. Hansen & Associates
C/O GWR Instruments
11404 Sorrento Valley Road
Suite 117
San Diego, CA 92121
619-455-0913

William Schelar
Clifton Precision
I & LS Division
P. O. Box 4508
Davenport, IA 52808
319-383-6340

Peter Seyfert
Centre D'Etudes Nucleaires De Grenoble
Service des Basses Temperatures
85X 38041 Greenoble, Cedex
France
76-974111

Allan Sherman
NASA - Code 713
Goddard Space Flight Center
Greenbelt, MD 20771
301-344-5405

Arnold H. Silver
TRW Space & Technology Group
One Space Park
Mail Stop R1/2170
Redondo Beach, CA 90278
213-535-2500

Herbert Sixsmith
Creare R & D Inc.
P. O. Box 71, Great Hollow Road
Hanover, NH 03755
603-643-3800

Joseph L. Smith, Jr.
MIT Cryogenic Engineering Lab.
MIT, Room 41-204
Cambridge, MA 01742
617-253-2296

W. Dodd Stacy
Creare R & D Inc.
P. O. Box 71, Great Hollow Road
Hanover, NH 03755
603-643-3800

George R. Stecker
Military Vision Inc.
12 Oak Park Drive
Bedford, MA 01730
617-275-9390

William A. Steyert
Air Products & Chemicals, Inc.
1833 Vultee Street
Allentown, PA 18103
215-481-3700

Fred R. Stolfi
Philips Laboratories
345 Scarborough Road
Briarcliff Manor, NY 10510
914-945-6334

Stephen W. Sumner
Air Force Space Technology Center
Kirtland AFB
NM 87117
505-846-9750

T. H. Sun
Hughes Aircraft Company
P. O. Box 2999
Torrance, CA 90509
213-517-5280

Walter L. Swift
Creare R & D Inc.
P. O. Box 71, Great Hollow Road
Hanover, NH 03755
603-643-3800

John Talbourdet
Honeywell Electro Optics Division
2 Forbes Road
M.S. 345
Lexington, MA 02173
617-863-3698

William A. Thompson
Rockwell International
2600 Westminster Blvd.
Seal Beach, CA
213-594-3802

K. D. Timmerhaus
University of Colorado
Engineering Center AD1-25
Boulder, CO 80309
303-492-7427

Emanual Tward
Jet Propulsion Laboratory
MS 183-901
4800 Oak Grove Drive
Pasadena, CA 91109
818-354-6581

Graham Walker
General Pneumatics Corp.
225 8256 Arabian Tr.
Scottsdale, AZ 85260
602-998-1856

Wan Weiwu
Xian Jiaotong University
Department of Power Machinery Engineer
Xian Jiaotong University
The People's Republic of China

Stephen Werrett
Oxford University
Department of Atmospheric Physics
Parks Road, Oxford
England

Ronald White
U.S.A.F.- AFWAL/FIEE
Wright-Patterson A.F.B.
Ohio 45433
513-255-4853

Scott Willen
Ball Aerospace Systems Division
P. O. Box 1062 - M. S. TT-4
Boulder, CO 80306
303-939-4000

David P. Williams
P. O. Box 2
National Radio Astronomy Observatory
Green Bank, WV 24944
304-456-2011

Calvin Winter
Quantum Technology Corp.
6237-148 St.
Surrey, B. C.
Canada V3S 3C3

B. Woensdregt
nv Optische Industrie De Oude Delft
Van Hiereveltlaan 9
Delft
Holland
015-145949

Masayoshi Yanai
Osaka Sanso Kogyo Ltd.
Moriyama Factory
1095,Katsube-cho, Moriyama-city
Shiga Prefecture 524
Japan
0775-82-3773

Herbert Yanowitz
Perkin-Elmer Corp.
100 Wooster Heights Road
Danbury, CT 06810
203-796-7477

James E. Zimmerman
National Bureau of Standards
Division 724.03
325 Broadway
Boulder, CO 80303
303-497-3901

NBS Technical Publications

Periodical

Journal of Research- The Journal of Research of the National Bureau of Standards reports NBS research and development in those disciplines of the physical and engineering sciences in which the Bureau is active. These include physics, chemistry, engineering, mathematics, and computer sciences. Papers cover a broad range of subjects, with major emphasis on measurement methodology and the basic technology underlying standardization. Also included from time to time are survey articles on topics closely related to the Bureau's technical and scientific programs. Issued six times a year.

Nonperiodicals

Monographs—Major contributions to the technical literature on various subjects related to the Bureau's scientific and technical activities.

Handbooks—Recommended codes of engineering and industrial practice (including safety codes) developed in cooperation with interested industries, professional organizations, and regulatory bodies.

Special Publications—Include proceedings of conferences sponsored by NBS, NBS annual reports, and other special publications appropriate to this grouping such as wall charts, pocket cards, and bibliographies.

Applied Mathematics Series—Mathematical tables, manuals, and studies of special interest to physicists, engineers, chemists, biologists, mathematicians, computer programmers, and others engaged in scientific and technical work.

National Standard Reference Data Series—Provides quantitative data on the physical and chemical properties of materials, compiled from the world's literature and critically evaluated. Developed under a worldwide program coordinated by NBS under the authority of the National Standard Data Act (Public Law 90-396).
NOTE: The Journal of Physical and Chemical Reference Data (JPCRD) is published quarterly for NBS by the American Chemical Society (ACS) and the American Institute of Physics (AIP). Subscriptions, reprints, and supplements are available from ACS, 1155 Sixteenth St., NW, Washington, DC 20056.

Building Science Series—Disseminates technical information developed at the Bureau on building materials, components, systems, and whole structures. The series presents research results, test methods, and performance criteria related to the structural and environmental functions and the durability and safety characteristics of building elements and systems.

Technical Notes—Studies or reports which are complete in themselves but restrictive in their treatment of a subject. Analogous to monographs but not so comprehensive in scope or definitive in treatment of the subject area. Often serve as a vehicle for final reports of work performed at NBS under the sponsorship of other government agencies.

Voluntary Product Standards—Developed under procedures published by the Department of Commerce in Part 10, Title 15, of the Code of Federal Regulations. The standards establish nationally recognized requirements for products, and provide all concerned interests with a basis for common understanding of the characteristics of the products. NBS administers this program as a supplement to the activities of the private sector standardizing organizations.

Consumer Information Series—Practical information, based on NBS research and experience, covering areas of interest to the consumer. Easily understandable language and illustrations provide useful background knowledge for shopping in today's technological marketplace.
Order the **above** *NBS publications from: Superintendent of Documents, Government Printing Office, Washington, DC 20402.*
Order the **following** *NBS publications—FIPS and NBSIR's—from the National Technical Information Service, Springfield, VA 22161.*

Federal Information Processing Standards Publications (FIPS PUB)—Publications in this series collectively constitute the Federal Information Processing Standards Register. The Register serves as the official source of information in the Federal Government regarding standards issued by NBS pursuant to the Federal Property and Administrative Services Act of 1949 as amended, Public Law 89-306 (79 Stat. 1127), and as implemented by Executive Order 11717 (38 FR 12315, dated May 11, 1973) and Part 6 of Title 15 CFR (Code of Federal Regulations).

NBS Interagency Reports (NBSIR)—A special series of interim or final reports on work performed by NBS for outside sponsors (both government and non-government). In general, initial distribution is handled by the sponsor; public distribution is by the National Technical Information Service, Springfield, VA 22161, in paper copy or microfiche form.